

Modelling and simulation techniques to investigate
pharmacokinetics, pharmacodynamics, and drug-drug
interactions

Dissertation

zur Erlangung des Grades der Doktorin der Naturwissenschaften der
Naturwissenschaftlich-Technischen Fakultät
der Universität des Saarlandes

Anke-Katrin Volz

Saarbrücken

2020

Die vorliegende Arbeit wurde von Oktober 2013 bis April 2020 unter Anleitung von Herrn Professor Dr. rer. nat. Thorsten Lehr in der Fachrichtung Klinische Pharmazie der Naturwissenschaftlich-Technischen Fakultät der Universität des Saarlandes angefertigt.

Datum der Disputation: 06 Januar 2021

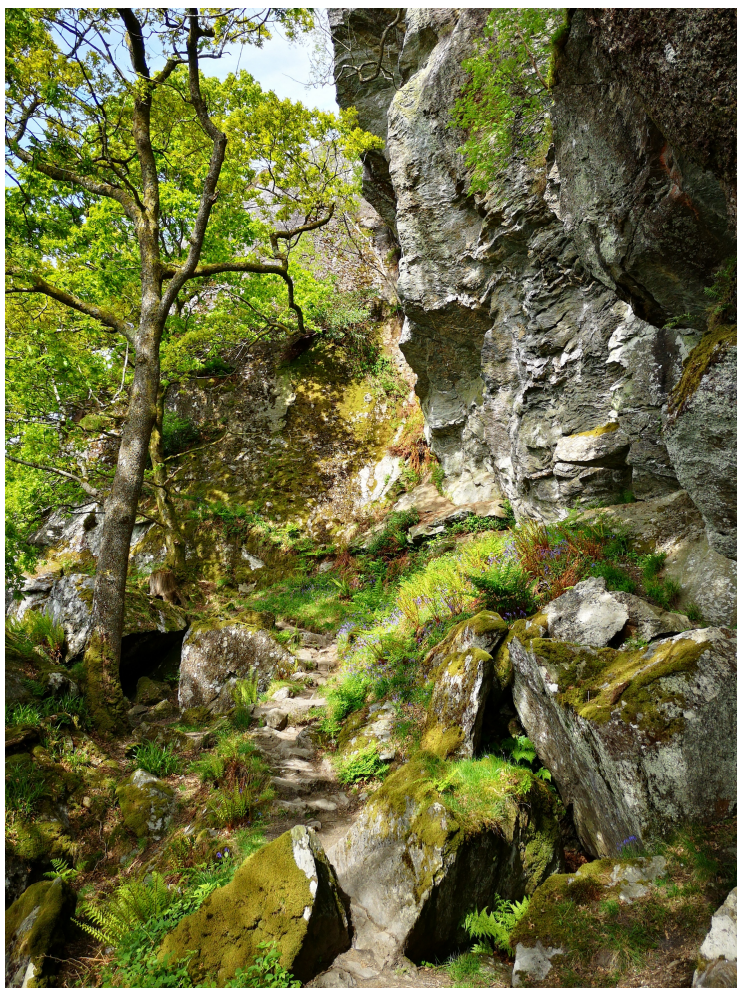
Dekan: Prof. Dr. Jörn Walter

Vorsitz: Prof. Dr. Andriy Lutzhetsky

Berichterstatter: Prof. Dr. Thorsten Lehr

Prof. Dr. Claus Jacob

Akademischer Beisitzer: Dr. Michael Ring



Gehen. Weiter gehen

Erling Kagge

Für Rainer

Acknowledgements

I express my sincere gratitude to Professor Thorsten Lehr for giving me the opportunity for this work, for sharing his knowledge. Thank you for the many scientific discussions that drove my scientific and personal development. Thank you, Professor Hans Maurer, for accompanying this work.

Professor Walter Emil Haefeli, with this I express my sincere gratitude for continuously supporting me scientifically and personally, and for motivating me through all the years. You've convinced me that it's worth continuing. Without your support, I would certainly have given up.

I express my sincere gratitude to Professor Charlotte Kloft, Professor Wilhelm Huisinga and the PharMetriX graduate research training program for giving me the opportunity of being part of this unique program, providing education, scientific discussion and a nice atmosphere where to meet many great people. I express my sincere gratitude to Jasper Dingemans and Andreas Krause for their support and for sharing their scientific knowledge. I thank the Saarland University for supporting this work with a doctoral scholarship, which enabled me to focus on this scientific work for quite some time.

I express my lovely thanks to Miro, Lisa, Imke, Mohammed, Sulav, and Niklas. It was wonderful to meet you. I wouldn't want to miss a minute with you. Niklas, I will never forget you.

Thank you Norbert, for standing up for me. Thank you Thomas for designing the infographics. I thank my yoga teachers and my mediation trainer, Patric and my doctors, who all showed me how to get back on my feet when nothing seems to go on. Thank you Troy for which and that despite this and that. Thank you Dada Jadranka for sharing your knowledge and experience with me. Thank you Katrin, Carina, Steffi, Nathalie, Ingrid, Jochen, Anne, Jens, Vroni, Viola, Phillipp, Lisa, Sebastian, Ann-Kristin, Petra, Gaby, Kirsten, and all the other nice people I met over these years. Each of you accompanied and supported me with its own spirit and its own unique way.

Tim, thank you so much for just still being here. Uli, there are not many coincidences in life that give you such wonderful encounters. Thanks for always being here, walking with me each road, the low and the high ones.

I express my infinite gratitude for my family. You encourage me and push me forward, you criticise me, discuss with me, you suffer with me and celebrate with me, and you support me unconditionally. Thank you my sisters, Anne-Kristin and Antje-Karola. Thank you, my mother Sigrun. Thank you my father Rainer, you should have stayed much longer – this work is for you.

Contents

Acknowledgements.....	9
Contents	10
Abbreviations	12
Graphical abstract.....	15
List of publications.....	16
Contribution report.....	17
1 Introduction.....	18
1.1 Model-informed drug development	18
1.2 Pulmonary arterial hypertension.....	20
1.3 Endothelin and endothelin receptors.....	24
1.4 Endothelin receptor antagonists.....	26
1.4.1 Bosentan	27
1.4.2 Clazosentan.....	31
1.4.3 Tezosentan	31
1.5 Fluvoxamine	33
1.6 Cytochrome P450 isozymes and genetic polymorphisms.....	34
1.7 Drug-drug interaction.....	35
1.7.1 Drug-drug interaction potential of bosentan, clazosentan, and tezosentan.....	35
1.7.2 Physiologically-based pharmacokinetic modelling for drug-drug interaction.....	37
1.8 Endogenous rhythms and chronopharmacology.....	38
2 Objectives.....	40
2.1 Project I – Pharmacometric analyses of bosentan and endothelin-1.....	40
2.2 Project II – Population target-mediated drug disposition modelling of bosentan, clazosentan, and tezosentan	40
2.3 Project III – The influence of CYP2D6 polymorphism and smoking on pharmacokinetics of fluvoxamine	40
3 Methods.....	41

3.1	Population modelling	41
3.1.1	Naïve average data approach	41
3.1.2	Two-stage approach	41
3.1.3	Nonlinear mixed-effects modelling approach	41
3.1.3.1	Structural model	43
3.1.3.2	Stochastical model	44
3.1.3.3	Covariate model	45
3.1.3.4	Model evaluation and simulations	45
3.2	Target-mediated drug disposition models	47
4	Results	49
4.1	Publication I	49
4.2	Publication II	49
4.3	Publication III	49
5	Conclusion	50
6	Limitations	52
7	Future perspectives	53
8	Summary	55
9	Zusammenfassung	56
10	References	57
	Images	66
	Appendix	68

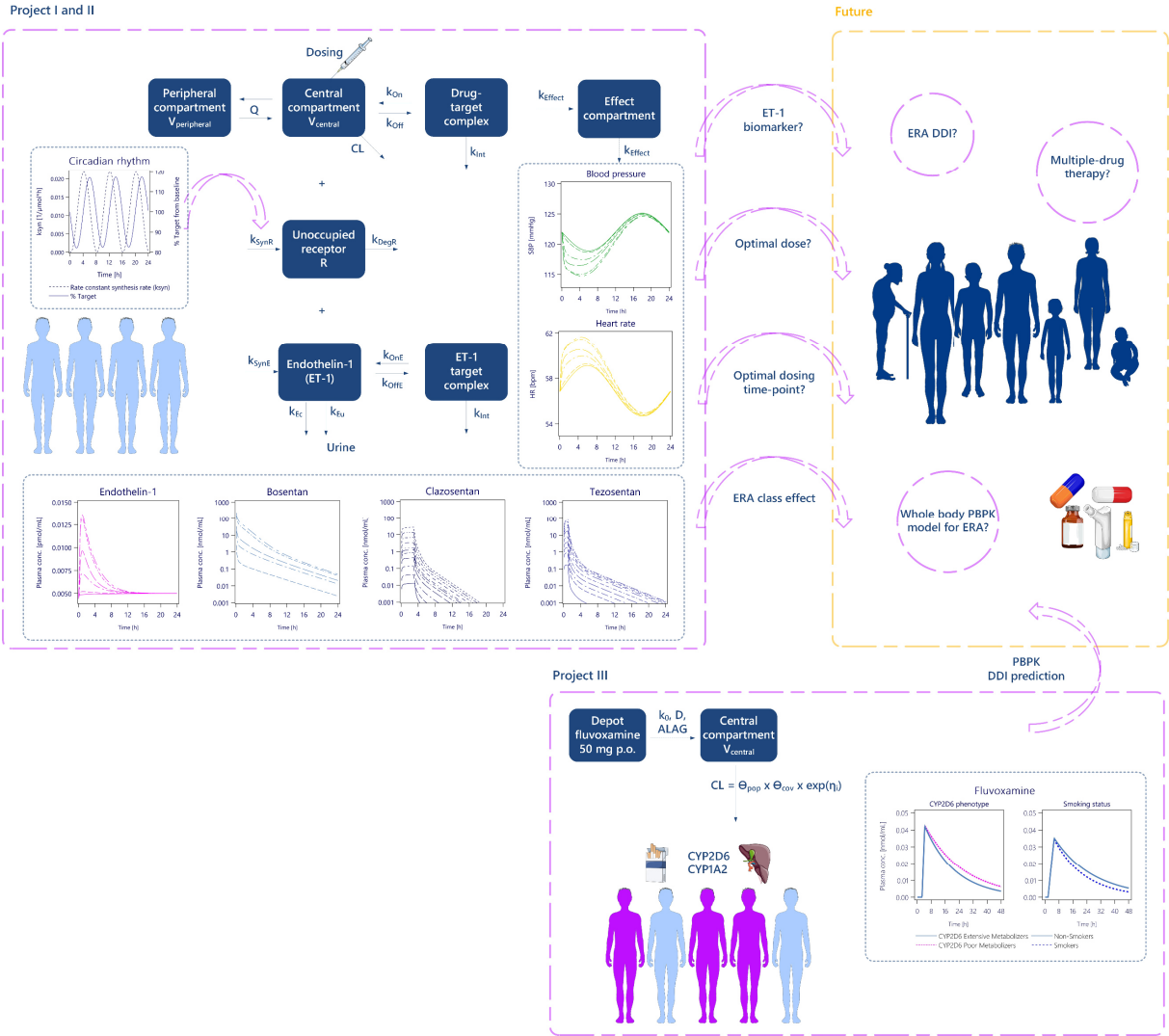
Abbreviations

-2LL	Minus twice the logarithm of the likelihood function
6MWD	6-minute walking distance
6MWT	6-minute walking test
ADME	Absorption, distribution, metabolism, and excretion
AC	Adenylate cyclase
ALT	Alanine aminotransferase
AST	Aspartate aminotransferase
ATP	Adenosine triphosphate
AUC	Area under the concentration-time curve
BMPR2	Bone morphogenetic protein receptor 2
BSEP	Bile salt export pump
cAMP	Cyclic adenosine monophosphate
cGMP	Cyclic guanosine monophosphate
CL	Clearance
C_{max}	Maximum plasma concentration
CYP enzyme	Cytochrome P450 enzyme
DDI	Drug-drug interaction
ECE-1	Endothelin-converting enzyme-1
EIF2AK4	Eukaryotic Translation Initiation Factor 2 Alpha Kinase 4
ERA	Endothelin receptor antagonist
ESC	European Society of Cardiology
ET	Endothelin
ET _A / ET _B	Endothelin receptor A / B
F	Bioavailability
FDA	US Food and Drug Administration

GMP	Guanosine monophosphate
GTP	Guanosine triphosphate
HIV	Human immunodeficiency virus
IIV	Inter-individual variability
IOV	Intra-individual variability
IP	Prostacyclin receptor
IP3	Inositol triphosphate
k_0	Zero-order rate constant of drug infusion
k_a	First-order absorption rate constant
K_d	Dissociation constant
k_{deg}	Rate constant degradation free / unoccupied receptor
k_{el}	Elimination rate constant
k_m	Rate constant complex internalisation
k_{off}	Rate constant complex dissociation drug
k_{on}	Rate constant complex building drug
k_{syn}	Rate constant receptor synthesis
M&S	Modelling and simulations
MIDD	Model-informed drug development
NLME modelling	Nonlinear mixed-effects modelling
NO	Nitric oxide
OCC	Occasion
OATP	Organic anion transporting polypeptide
OFV	Objective function value
PAH	Pulmonary arterial hypertension
PAP	Pulmonary arterial blood pressure
PAPm	Mean pulmonary arterial pressure
PBPK modelling	Physiologically-based pharmacokinetic modelling

pc-VPC	Prediction-corrected visual predictive check
PD	Pharmacodynamics
PDE5	Phosphodiesterase type 5
PGI ₂	Prostacyclin
P-gp	P-glycoprotein
PH	Pulmonary hypertension
PK	Pharmacokinetics
PLC	Phospholipase C
PVR	Pulmonary vascular resistance
QSP	Quantitative systems pharmacology
RSE	Relative standard error
sGC	Soluble guanylate cyclase
TMDD	Target-mediated drug disposition
V	Volume of distribution
V _{Central}	Volume of distribution central compartment
VPC	Visual predictive check
V _{Peripheral}	Volume of distribution peripheral compartment
WHO-FC	World Health Organisation functional class
WU	Wood units

Graphical abstract



List of publications

- I. A.-K. Volz, A. Krause, W.E. Haefeli, J. Dingemans, T. Lehr, Target-Mediated Drug Disposition Pharmacokinetic–Pharmacodynamic Model of Bosentan and Endothelin-1, *Clin. Pharmacokinet.* 56 (2017) 1499–1511. doi:10.1007/s40262-017-0534-4.
- II. A.-K. Volz, J. Dingemans, A. Krause, T. Lehr, Target-Mediated Population Pharmacokinetic Modeling of Endothelin Receptor Antagonists., *Pharm. Res.* 37 (2019) 2. doi:10.1007/s11095-019-2723-3.
- III. H. Britz, N. Hanke, A.-K. Volz, O. Spigset, M. Schwab, T. Eissing, et al., Physiologically-Based Pharmacokinetic Models for CYP1A2 Drug–Drug Interaction Prediction: A Modeling Network of Fluvoxamine, Theophylline, Caffeine, Rifampicin, and Midazolam, *CPT Pharmacometrics Syst. Pharmacol.* 8 (2019) 296–307. doi:10.1002/psp4.12397.

Contribution report

Herewith, the author Anke-Katrin Volz declares her contributions and the co-authors contributions to the publications I - III included in this thesis.

- I. Anke-Katrin Volz created the datasets, performed the analyses, created the graphics, and wrote the manuscript.

Andreas Krause and Jasper Dingemanse supported this publication by providing data, sharing scientific experience, proofreading, and making suggestions for rewording of individual text sections.

Walter Emil Haefeli supported this publication by sharing scientific experience, proofreading, and making suggestions for rewording of individual text sections.

Thorsten Lehr as supervisor supported this publication by sharing scientific experience, proofreading, and making suggestions for rewording of individual text sections.

- II. Anke-Katrin Volz created the datasets, performed the analyses, created the graphics, and wrote the manuscript.

Andreas Krause and Jasper Dingemanse supported this publication by providing data, sharing scientific experience, proofreading, and making suggestions for rewording of individual text sections.

Thorsten Lehr as supervisor supported this publication by sharing scientific experience, proofreading, and making suggestions for rewording of individual text sections.

- III. Anke-Katrin Volz contributed to this project as a co-author with conducting the population pharmacokinetic analysis. She created the dataset, performed the analysis, and wrote the text of the supplementary S1, regarding the population pharmacokinetic analysis.

Hannah Britz edited and created the datasets for PBPK modeling, performed the PBPK modeling and simulation analyses, created the graphics and tables, and wrote the manuscript.

Nina Hanke supported the PBPK model development, discussed the modelling results, co-authored the manuscript and accompanied the peer-review process.

Olav Spigset provided plasma concentration-time profiles of fluvoxamine, discussed the modelling results and proofread the manuscript.

Matthias Schwab discussed the modelling results and proofread the manuscript.

Thomas Eissing discussed the modelling results and proofread the manuscript.

Thomas Wendl discussed the modelling results and proofread the manuscript.

Sebastian Frechen discussed the modelling results and proofread the manuscript.

Thorsten Lehr supervised and supported the modelling and simulation analyses and co-authored the manuscript.

1 Introduction

1.1 Model-informed drug development

A mathematical model might be defined as an abstraction of reality describing a system with mathematical languages in order to study and explain it, and enable predictions on patterns of behaviour. However, a model is typically a simplification of a system and thus should not be judged of being “right” or “wrong”, but by its fit for purpose, as George Box stated: “Essentially, all models are wrong, but some are useful” (1,2).

Drug development extends to various stages from early pre-clinical development to post-marketing authorisation management (Figure 1). It is a continuous process where a vast amount of data from *in vitro* and animal studies, as well as human clinical trials is collected and needs to be considered to inform decision-making. This is not only a challenging process but also time-consuming and expensive (3). The number of late clinical development failure in phase 2 and 3 stages is high due to insufficient efficacy, and only less than 10 % of new compounds finally receive marketing authorisation (4).

Model-informed drug development (MIDD) approaches, also known as model-based drug development, or modelling and simulations (M&S) techniques, provide a framework to integrate and analyse various data with relevant prior knowledge to drive industrial and regulatory decision-making through all stages of the drug development process (Figure 1) (4–6). In addition, good practice in MIDD can reduce costs and increase the success rates in late-stage clinical phases (5). From a regulatory perspective, the degree of impact of M&S exercises on the regulatory decision depends on the intended purpose of the model. A framework of three main categories has been proposed; related to the purpose of the model, it can be of low, medium, or high impact, where M&S is used to describe, justify, or replace the available or usual evidence, respectively (4).

Overall, MIDD approaches facilitate understanding and predicting the pharmacokinetics (PK) and pharmacodynamics (PD) of a drug candidate. They can for instance be used to inform clinical trial designs, inform on disease progression, guide optimal dosing strategies (e.g. initial dose selection in first-in-human trials), perform (paediatric) extrapolations (7), guide dosing recommendations in product labelling, or support evidence for efficacy and safety (6).

MIDD encompasses several quantitative mathematical / statistical approaches, such as pharmacometrics, Physiologically-based Pharmacokinetic (PBPK) modelling, or Quantitative Systems Pharmacology (QSP). More specifically, pharmacometrics can be defined as the science of quantitative pharmacology that enables the characterisation, understanding and prediction of the PK and PD of a drug candidate, including the quantification of uncertainty, by applying mathematical and statistical methods (8,9). Under the umbrella of pharmacometrics, in particular population PK, PD, and PKPD M&S, including exposure-response analyses, are of special interest and increasingly applied in drug development (8). The different types of population

approaches, i.e. naïve average data approach, the two-stage approach, and the nonlinear mixed-effects modelling (NLME) approach, are described later in this work.

Another important approach is the PBPK (or PBPK/PD) modelling, where the models include knowledge of the physiology and physicochemical information, as well as information on the target population, enabling to distinguish between drug parameters and systems' parameters (i.e. physiological and anatomical or organ parameters). Knowledge on the concentration-time behaviour in blood and tissue(s) can be obtained taking into consideration organs that are most relevant to absorption, distribution, metabolism, and excretion (ADME) (10,11). PBPK models are increasingly used to predict a drug's exposure for a given population or for instance, to extrapolate exposure from adults to children (12) or even from animals to humans. Moreover, it is used to predict drug-drug interaction (DDIs) qualitatively and quantitatively *in silico* (10,13). However, in European Regulation, applications of PBPK models are so far predominantly limited to DDIs (6). In QSP, all relevant processes are considered even more detailed; as an example, PBPK models are combined with *in vitro-in vivo* correlations of ADME processes, the complex underlying biology of the system, and information on the pathophysiology, and they include details of the disease process. However, overall, these three mentioned approaches (pharmacometrics, PBPK, and QSP), should not necessarily be considered separately, but may rather be considered as a network of different approaches that may inform each other.

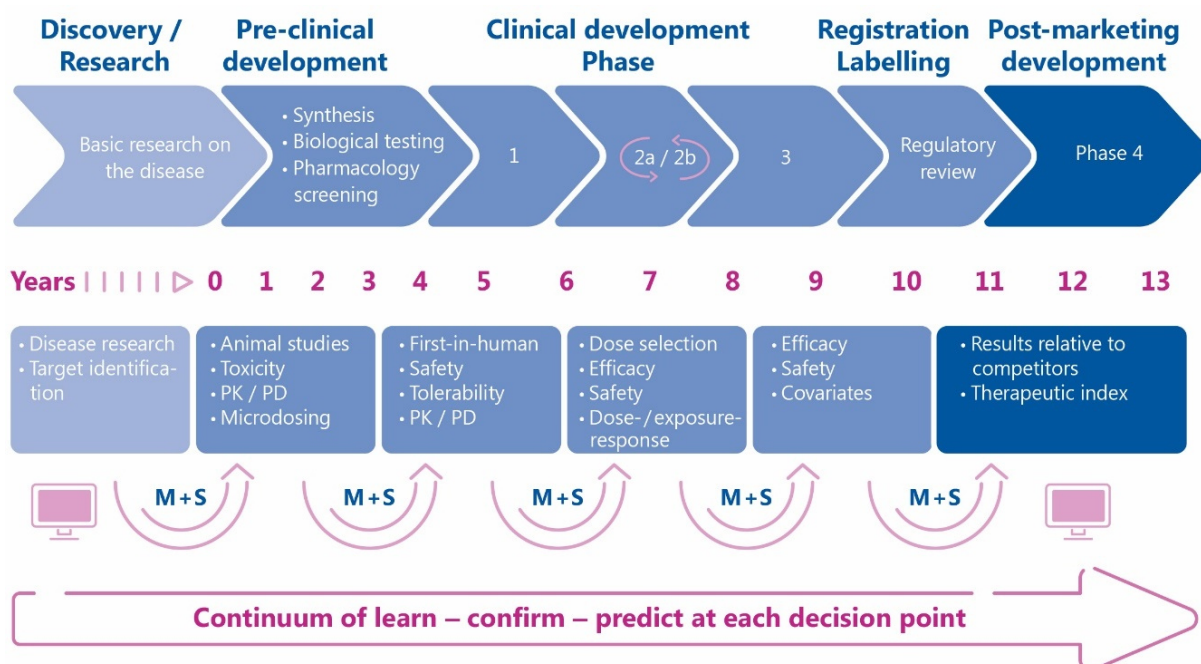


Figure 1 Stages of drug development as continuous process from drug discovery to post-marketing development. Modelling and Simulation (M&S) techniques (indicated by pink arrows) are used at each step to support decision-making. [Modified from (4,5)]

1.2 Pulmonary arterial hypertension

Pulmonary hypertension (PH) is a pathophysiological disorder that encompasses a number of diseases that are characterised by elevated pulmonary vascular resistance (PVR) and pulmonary arterial blood pressure (PAP). PH is currently classified in five groups of diseases according to their similar clinical presentation, pathological findings, haemodynamic characteristics, and treatment strategy (14). Further subcategories allow to distinguish between diverse origins of the diseases within each classification, leading to various forms of PH (Table 1) (14).

Pulmonary arterial hypertension (PAH, group 1) is a rare disease with a prevalence of about 15 to 60 patients per million and an incidence of 5 to 10 cases per million per year in Europe (15). In 2014, the incidence was about 3.9 per million adults and the prevalence 25.9 per million adults in Germany (16). PAH is more frequently diagnosed in elderly patients between 50 and 65 years of age compared to younger ages (14), however, it affects every age, including the new-born. It is a progressive, currently incurable disease and the mean survival after diagnosis is approximately 3 years (17). The patient status can be categorised according to a classification system (World Health Organisation functional class, WHO-FC), and is based on a complex disease assessment (14,18). Patients are classified in low-risk (WHO-FC I), medium-risk (WHO-FC II), or high-risk (WHO-FC III or IV) groups. The estimated 1-year mortality varies depending on the class between < 5 % (low risk) and > 10 % (high risk) (14).

Overall, PAH is recognised as a very heterogeneous disease. As such, besides the idiopathic form, PAH can, for instance, occur due to genetic mutations (e.g. mutation in the bone morphogenetic protein receptor 2, BMPR2) or intake of drugs or toxins, and it can be associated with autoimmune diseases, human immunodeficiency virus (HIV) infection, or congenital heart disease (Table 1).

Table 1 Pulmonary hypertension (PH) classification system

Pulmonary hypertension (PH)		
<p style="text-align: center;">Group I</p> <p style="text-align: center;">Pulmonary arterial hypertension (PAH)</p> <p>I.1 Idiopathic I.2 Heritable I.2.1 BMPR2 mutation I.2.2 Other mutations I.3 Drugs and toxins induced I.4 Associated with: I.4.1 Connective tissue disease I.4.2 Human immune deficiency virus (HIV) infection I.4.3 Portal Hypertension I.4.4 Congenital heart disease I.4.5 Schistosomiasis</p>	<p style="text-align: center;">Group I.1</p> <p style="text-align: center;">Pulmonary veno-occlusive disease and/or pulmonary capillary haemangiomas</p> <p>I.1.1 Idiopathic I.1.2 Heritable I.1.2.1 EIF2AK4 mutation I.1.2.2 Other mutations I.1.3 Drugs, toxins and radiation induced I.1.4 Associated with: I.1.4.1 Connective tissue disease I.1.4.2 HIV infection</p>	<p style="text-align: center;">Group II</p> <p style="text-align: center;">PH due to left heart disease</p> <p>II.1 Left ventricular systolic dysfunction II.2 Left ventricular diastolic dysfunction II.3 Valvular disease II.4 Congenital / acquired left heart inflow/outflow tract obstruction and congenital cardiomyopathies II.5 Congenital / acquired pulmonary veins stenosis</p>
	<p>Group I.2</p> <p>Persistent PH of the new-born</p>	
<p style="text-align: center;">Group III</p> <p style="text-align: center;">PH due to lung disease and/or hypoxia</p> <p>III.1 Chronic obstructive pulmonary disease III.2 Interstitial lung disease III.3 Other pulmonary diseases with mixed restrictive and obstructive pattern III.4 Sleep-disordered breathing III.5 Alveolar hypoventilation disorders III.6 Chronic exposure to high altitude III.7 Developmental lung disease</p>	<p style="text-align: center;">Group IV</p> <p style="text-align: center;">Chronic thromboembolic hypertension and other pulmonary obstructions</p> <p>IV.1 Chronic thromboembolic pulmonary hypertension IV.2 Other pulmonary artery obstruction IV.2.1 Angiosarcoma IV.2.2 Other intravascular tumours IV.2.3 Arteritis IV.2.4 Congenital pulmonary arteries stenosis IV.2.5 Parasites (hydatidosis)</p>	<p style="text-align: center;">Group V</p> <p style="text-align: center;">PH with unclear and/or multifactorial mechanism</p> <p>V.1 Haematological disorders: chronic haemolytic anaemia, myeloproliferative disorders, splenectomy V.2 Systemic disorders: sarcoidosis, pulmonary histiocytosis, lymphangioleiomyomatosis, neurofibromatosis V.3 Metabolic disorders: glycogen storage disease, Gaucher disease, thyroid disorders V.4 Others: pulmonary tumoral thrombotic microangiopathy, fibrosing mediastinitis, chronic renal failure (with / without dialysis), segmental pulmonary hypertension</p>

Modified from (14,19)

PAH is a pre-capillary PH form (Figure 2) with an increase in mean PAP (PAPm) ≥ 25 mmHg at rest as assessed by right heart catheterisation. In the absence of other causes of precapillary PH, such as PH due to lung diseases, or chronic thromboembolic PH, it is defined by a pulmonary arterial wedge pressure of ≤ 15 mmHg and a PVR > 3 Wood units (WU) (14). In healthy persons, the normal PAPm at rest is at about 14 ± 3 mmHg with an upper limit of 20 mmHg and a PVR of ≤ 3 WU (14,20).

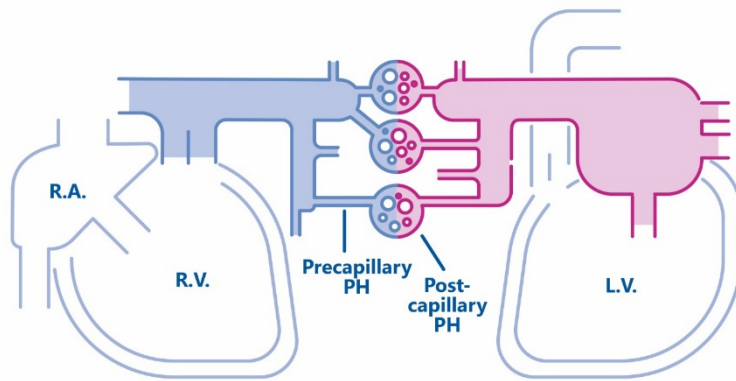


Figure 2 Schematic representation of pulmonary hypertension (PH). Illustration of site of initiation of elevated pulmonary arterial pressure of precapillary pulmonary hypertension, and postcapillary pulmonary hypertension. L.V., left ventricle; R.A., right atrium; R.V., right ventricle. [Modified from (21)]

Since symptoms of P(A)H are initially non-specific (e.g. exertion, shortness of breath, fatigue, weakness, or angina) (14), diagnosis is difficult and should be assessed by experts only, according to a complex algorithm, as suggested by the guideline from the European Society of Cardiology (ESC) (14). Overall, diagnostics of PH include a number of tests such as electrocardiogram, pulmonary function tests, arterial blood gases, right heart catheterisation, and vasoreactivity testing. The 6-minute walking test (6MWT) is a popular procedure to assess the exercise capacity of PAH patients (22,23). However, the 6-minute walking distance (6MWD) is influenced by a number of factors, such as demographics (e.g. age, weight, height, and sex) or the need for oxygen and comorbidities that need to be considered (14). Furthermore, the cardiopulmonary exercise testing provides information on exercise capacity, gas exchange, ventilator efficacy, and cardiac function during exercise (14). So far, the only biochemical markers used in clinical practice are markers of myocardial stress, i.e. b-type natriuretic peptide and N-terminal-pro b-type natriuretic peptide, which are not specific for PH but can provide information on the prognosis in patients with P(A)H (14). A continuous risk assessment of patients with PAH should be performed according to the ESC guideline (14) and regular laboratory tests (e.g. including aspartate aminotransferase [AST] and alanine aminotransferase [ALT]) should be conducted during follow-up assessment and under drug treatment.

Key elements of the pathogenesis of PAH involve vasoconstriction of the small pulmonary arteries and vascular remodelling and proliferation due to a variety of cellular and molecular factors, leading to a progressive increase in vascular resistance. An increase in right ventricular afterload finally leads to right-sided heart failure. In all forms of PAH, thickening of the vascular walls as a consequence of proliferation of smooth muscular cells in the small peripheral arteries and neovascularisation can be observed (24). Vasoconstriction of the pulmonary arteries due to endothelial dysfunction is a common mechanism that is associated with a decreased production of the vasodilators nitric oxide (NO) and prostacyclin. Overexpression of the potent and long-acting

vasoconstrictor endothelin-1 (ET-1), which also promotes vascular remodelling, occurs concurrently (Figure 3) (25). Further explanation of the pathophysiology is provided in the next chapter.

The current treatment options for patients with PAH are limited. Besides general interventions and measures such as physical activity, infection prevention, or psychosocial support, a comprehensive pharmacological treatment strategy includes for instance supportive therapy with oral anticoagulants, diuretics, oxygen, and digoxin in the first step (14). Calcium channel blockers (e.g. nifedipine, diltiazem, amlodipine) can be administered to some patients with response to acute vasodilator testing at the time of right heart catheterisation (14). Further specific drug treatment options include single or combination therapy with phosphodiesterase type 5 (PDE5) inhibitors (sildenafil, tadalafil, vardenafil), the soluble guanylate cyclase (sGC) stimulator riociguat, prostacyclin analogues (beraprost, epoprostenol, iloprost, treprostinil), the prostacyclin receptor (IP) agonist selexipag, or endothelin receptor antagonists (ERAs; ambrisentan, bosentan, macitentan) (Figure 3). The ESC guideline gives comprehensive recommendations for efficacy of drug monotherapy, combination therapy, and sequential drug combination therapy depending on the different WHO-FC levels (14).

1.3 Endothelin and endothelin receptors

ET-1 is an endothelium-derived peptide and a member of a ET-gene family that comprises three isoforms, i.e. ET-1, ET-2, and ET-3 (26). The ET mRNA encodes the precursor protein prepro-ET-1, which is cleaved to big-ET-1. Proteolytic cleavage of big-ET-1 through endothelin-converting enzyme (ECE-1) yields the mature peptide (Figure 3) (26–28). ET-1 is synthesised by almost every cell type, but in particular in vascular endothelial and smooth muscle cells, airway epithelial and smooth muscle cells, macrophages, fibroblasts, cardiac myocytes, mesangial cells, podocytes, and neurons (29). ET-2 is synthesised in the ovary and intestinal epithelial cells. It contributes to ovulation, thermoregulation, lung alveolarisation and intestinal contraction, while ET-3 mainly mediates release of vasodilator and anti-inflammatory molecules such as NO and prostacyclin (29). Furthermore, it may promote growth of cells such as melanocytes (29). ET-3 is mainly expressed in the placenta, brain neurons, melanocytes, renal tubular epithelial cells, and intestinal epithelial cells (29).

ET peptides are bound to the two endothelin receptors A and B (ET_A and ET_B). ET_A binds ET-1 and ET-2 with high affinity (ET-1 ≥ ET-2), and ET-3 with a 100-fold lower affinity (29,30). Binding to ET_B is similar for all three ETs (30), however, a selective binding of ET-3 to ET_B has also been suggested (29). ET_A and ET_B are G-protein coupled receptors that are expressed in almost every cell of the body (28) and extensively in the kidneys (30). However, ET_A are predominately expressed in vascular smooth muscle cells, myocytes, and fibroblasts, while ET_B is mainly located in endothelial cells and renal tubuli and less on smooth muscle cells, fibroblasts, and macrophages (28,31,32) (Figure 3). ET-1 binding to its G-protein coupled receptors Gi, Gq, Gs, and G_{α12/13}, regulates a variety of signalling cascades (28). ET_A and ET_B show opposite action in normal physiological conditions. ET_A predominately promotes strong vasoconstriction, cell proliferation, inflammation, fibrosis, and hypertrophy in vascular smooth muscle cells (28,29,32) (Figure 3). The activation of ET_B causes vasodilatation, at least initially, via production of NO and vasodilator prostanoids and eicosanoids, with anti-proliferative and anti-apoptotic properties (28,30–32). Furthermore, endothelial ET_B can be considered as physiological antagonist when activated by ET-3, as it inhibits ET-1-mediated effects (29). However, ET_A and ET_B seem to form heterodimers. As such, ET_B on smooth muscle cells are coupled with ET_A exhibiting vasoconstrictive effects (32).

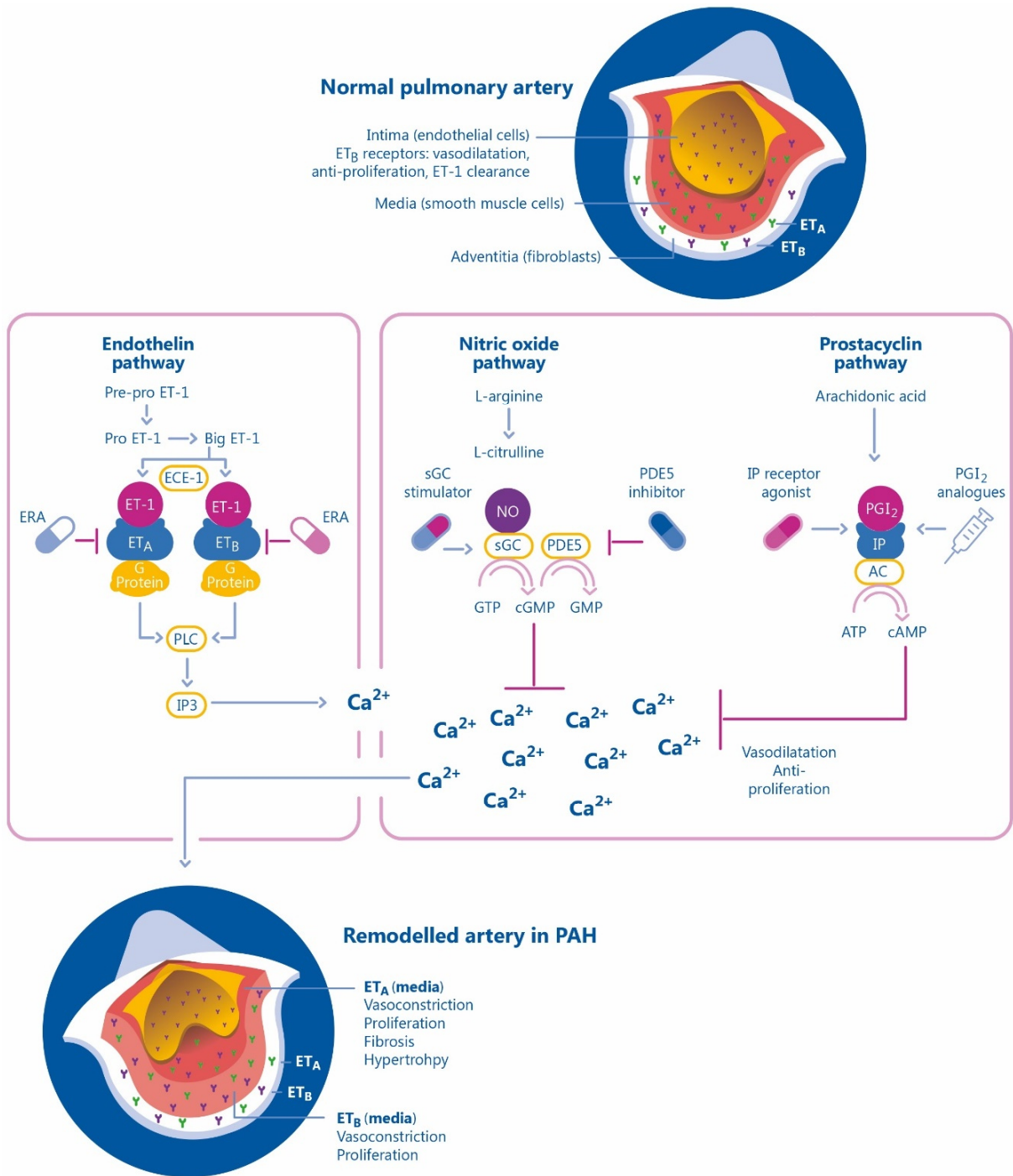


Figure 3 Endothelin (ET), nitric oxide (NO), and prostacyclin (PGI₂) pathway involved in cell proliferation and contraction of smooth-muscle cells in patients with PAH and the respective targets for therapeutic intervention. Current drug treatment options shown here include endothelin receptor A and B (ET_A and ET_B) antagonists (ERA; ambrisentan, bosentan, macitentan), phosphodiesterase type 5 (PDE5) inhibitors (sildenafil, tadalafil, vardenafil), the soluble guanylate cyclase (sGC) stimulator riociguat, prostacyclin analogues (beraprost, epoprostenol, iloprost, treprostinil), and the prostacyclin receptor (IP) agonist selexipag. AC: adenylate cyclase, ATP: adenosine triphosphate, cAMP: cyclic adenosine monophosphate, cGMP: cyclic guanosine monophosphate, ECE-1: endothelin-converting enzyme-1, ET-1: endothelin-1, GMP: guanosine monophosphate, GTP: guanosine triphosphate, IP3: inositol triphosphate, PLC: phospholipase C [Modified from (32,33)]

ET-1 binding to ET_A is almost irreversible and binding lasts almost 2 h after internalisation of the receptor-complex followed by recycling of the ET_A receptors (34). This leads to continuously activated signal transduction followed by prolonged biological effects, such as vasoconstriction and long-lasting increase in blood pressure (34,35). ET-1 clearance is mediated by an ET_B receptor-linked mechanism in the pulmonary circulation (36). ET_B are degraded by lysosomes and therefore serve as a clearance receptor for ET-1, which is removed from the systemic circulation within seconds (29,35). ET-1 uptake into lungs is markedly decreased and clearance is shifted towards liver and kidney after acute treatment of the non-selective ET_A and ET_B receptor antagonist bosentan (36). Furthermore, clearance is disabled after acute blockade of ET_A and ET_B (36). After long-term treatment with selective ET_A antagonists, a potential interaction (i.e. cross-talk) between ET_A and ET_B may cause a partial reduction in ET_B-mediated clearance from the pulmonary circulation. This results in a compensatory increase of ET-1 in the liver and kidneys, similarly as observed after non-selective ET_A/ET_B blockage (36).

Overall, the ET system is involved in the pathogenesis of various disease conditions such as PAH, cardiovascular diseases, coronary artery disease, cardiac arrhythmias, heart failure, idiopathic pulmonary fibrosis, renal diseases, cancer, autoimmune diseases, neurological diseases, or age-related eye diseases (29).

1.4 Endothelin receptor antagonists

The family of ERAs currently comprises three oral compounds that are approved for the treatment of PAH; the selective ET_A antagonist ambrisentan, and the two non-selective ET_A / ET_B antagonists bosentan and macitentan. Sitaxsentan was another selective ET_A antagonist also approved for the treatment of PAH, but withdrawn from the market in 2010 due to its hepatotoxicity.

A number of additional ERAs for oral use have been developed for the treatment of various disease conditions associated with involvement of the ET system. A selection of different selective ET_A antagonists is listed in Table 2. The selective ET_A antagonist clazosentan and the non-selective ET_A / ET_B antagonist tezosentan have both been developed for parenteral use in emergency indications. In project I and project II, the ERAs bosentan, clazosentan, and tezosentan were investigated. A detailed description of their PK and PD characteristics is given below.

Table 2 Endothelin receptor antagonists in development for the treatment of various diseases.

Compound	Proposed effect
Aprocitentan (active metabolite of macitentan)	Antihypertensive effect
Darusentan	Treatment of resistant hypertension, essential hypertension (37), improved endothelium-dependent vasodilation, attenuated progression of experimental atherosclerosis in mice (38), and mitigation of myocardial ischemia has been observed in mice (39). It reversed proteinuria, caused regression of established glomerulosclerosis, and restored podocyte structure and function in a model of normotensive focal segmental glomerulosclerosis (40).
Zibotentan	Inhibits pro-carcinogenic behaviour such as inhibition of apoptosis and cellular proliferation and has been developed as an antineoplastic drug candidate (41).
Atrasentan	Reduced blood pressure and seem to have favourable effect on metabolic parameters such as glucose metabolism (42); it reduced atherosclerotic plaque volume (43), has been studied in patients with diabetic nephropathy to reduce doubling of serum creatinine (44), and appears to have a protective effect on renal function (44).
Avosentan	Anti-proteinuric effects have been reported (45).
Sparsentan (dual oral ERA and angiotensin receptor antagonist)	Compound currently under investigation in patients with primary focal segmental glomerulosclerosis; an antihypertensive effect has been reported in patients with essential hypertension (29).

1.4.1 Bosentan

The non-selective ET_A / ET_B antagonist bosentan has been developed in the 1990s and is the first approved ERA, commonly prescribed for the treatment of PAH. In 2001 orphan designation has been granted by the European Commission for the treatment of PAH and chronic thromboembolic PH (EU/3/01/019). It has been authorised in the European Union in 2002 as Tracleer™. The period of market exclusivity ended in 2012 (46,47) and a couple of generic products are now available on the market.

Bosentan (Tracleer™) is currently approved for the treatment of patients with PAH WHO-FC III. Efficacy has been shown in primary (idiopathic and heritable) PAH, PAH secondary to scleroderma without significant interstitial pulmonary disease, and PAH associated with congenital systemic-to-pulmonary shunts and Eisenmenger's physiology (48). Bosentan is approved for use in adults and children aged one year and older.

Treatment in adults should be started with the oral application of 62.5 mg twice daily. After four weeks, the dose should be increased to 125 mg twice daily. For children aged one year and older, the recommended dose is 2 mg/kg body weight twice daily. Bosentan is contraindicated in patients with moderate to severe liver impairment (i.e. Child-Pugh class B and C) but no dose adjustments is recommended in patients with mild hepatic impairment (i.e. Child-Pugh class A). Dose adjustments are neither warranted in renal dysfunction, advanced age (elderly above the age of 65 years), or other patient characteristics (e.g. sex, ethnicity). Very common adverse reactions are hepatobiliary disorders. Elevated levels of liver AST and ALT are associated

with bosentan administration in a dose-dependent manner, which may be partly due to inhibition of the bile salt export pump (BSEP), leading to accumulation of bile salts in the hepatocytes.

Bosentan is a competitive antagonist binding tightly to ET_A and ET_B (dissociation constant K_d about 7.7 and 67 nM, respectively) displacing ET-1 from its binding site. PK, efficacy, and safety of bosentan have been investigated over the last decades in various trials in healthy volunteers, adults, and paediatric patients. A brief overview of PD effects of bosentan observed in different clinical trials is given in Table 3. The PK characteristics of bosentan are provided in the following section and key points are summarised in the three boxes below.

Table 3 Pharmacodynamic effects of bosentan observed in different clinical trials

Study name, population, treatment	Pharmacodynamic effect
<p>BREATHE-1 and study AC-052-351 (48)</p> <ul style="list-style-type: none"> ➤ Adult PAH patients with WHO-FC III-IV 	<ul style="list-style-type: none"> ➤ Increase in exercise capacity measured by 6MWT ➤ Improvement in WHO-FC ➤ Improvement in haemodynamic measures
<p>EARLY trial (study AC-052-364) (48,49)</p> <ul style="list-style-type: none"> ➤ Adult PAH patients with WHO-FC II ➤ 6 months treatment 	<ul style="list-style-type: none"> ➤ Improved PVR and 6MWT ➤ Reduced clinical worsening
<p>BREATHE-5 (study AC-052-405)(48)</p> <ul style="list-style-type: none"> ➤ Adult PAH patients with WHO-FC III and Eisenmenger physiology associated with congenital heart disease ➤ 16 weeks treatment 	<p>Bosentan:</p> <ul style="list-style-type: none"> ➤ Did not worsen hypoxaemia, ➤ Reduced the mean PVR, ➤ Improved exercise capacity
<p>BREATHE-4 (study AC-052-362)(48)</p> <ul style="list-style-type: none"> ➤ PAH patients with WHO-FC III associated with HIV infection ➤ 16 weeks treatment 	<ul style="list-style-type: none"> ➤ Improved exercise capacity
<p>COMPASS-3 (50)</p> <ul style="list-style-type: none"> ➤ Adult PAH patients ➤ 28 weeks treatment with bosentan monotherapy or in combination with sildenafil 	<ul style="list-style-type: none"> ➤ Improvement of 6MWD of ≥ 380 meters has been achieved

In addition to the studies mentioned in Table 3, the acute PD effect of sildenafil in patients with PAH, treated with bosentan has been investigated (study COMPASS-1) (51), as well as the effect of bosentan combined with sildenafil compared to sildenafil monotherapy (study COMPASS-2) (52). BREATHE-3 (study AC-052-356) and FUTURE 1 / 2 / 3 (studies AC-052-365 / AC-052-367 / AC-052-373) assessed primarily the PK of bosentan film-coated or dispersible tablet in children between 0.2 to 15 years of age (48,53–55). BREATHE-4 was a study performed in term or pre-term neonates (48,56).

After intravenous or oral administration, bosentan uptake into hepatocytes occurs via the two organic anion transporting polypeptides OATP1B1 and OATP1B3. Furthermore, bosentan is a substrate and possibly an inducer of P-glycoprotein (P-gp). Bosentan is primarily eliminated through the bile into the intestine and excreted with the faeces, whereof about 30.2 % of the administered dose are eliminated unchanged after oral administration, and 3.7 % after intravenous administration (57). Bosentan is catalysed by Cytochrome P450 (CYP) isozymes 3A4, 2C9, and 2C19 (57) yielding two metabolites, i.e. hydroxy-bosentan (RO48-5033) and desmethyl-bosentan (RO47-8634) that account for about 8.3 % and 3.1 %, in plasma, respectively (58). Both metabolites are further catalysed by CYP2C9 and/or 3A4 to hydroxy-desmethyl-bosentan (RO64-1056) (57). The affinity of hydroxy-bosentan to ET receptors is about 2-fold lower compared to bosentan and it contributes to the overall efficacy with approximately 20 % (57). By inducing the CYP isozymes CYP3A4, 2C9, and possibly 2C19, bosentan induces its own metabolism and causes many DDIs with other substrates of these isozymes (Table 4).

After multiple dose administration of bosentan over 10 days to healthy volunteers, exposure at steady-state has been reduced to 57 % and apparent oral clearance increased by 73 % (autoinduction) (59). Exposure of the three metabolites also decreased by 71 to 80 % (59).

Bosentan has a blood/plasma distribution ratio of 0.6 and it is highly bound to albumin (≥ 98 %) (57). The fraction unbound of the main metabolite hydroxy-bosentan is about 3-fold greater compared to bosentan, however, the two other metabolites show a higher plasma protein binding with a free fraction of 0.4 – 1.2 % (57). After oral administration, the half-life of

the main metabolite hydroxy-bosentan is longer compared to bosentan (10-14 h vs. 5.4 h), whereas the other metabolites show similar half-lives as bosentan (57).

Intravenously administered bosentan has been investigated in healthy volunteers over a dose range from 10 to 750 mg with varying infusion rates (60). A dose-dependent decrease in clearance, volume of distribution, and elimination half-life has been observed (57,60). A nonlinear tissue binding (saturation of widespread ET receptors) resulting in an apparent decrease in volume of distribution has been proposed (57).

Single oral doses of an oral suspension formulation ranging from 3 – 2400 mg have been investigated in healthy volunteers (60). Maximum plasma concentrations (C_{max}) and area under the concentration-time curve

Key points

Metabolism, elimination, and excretion of bosentan

Elimination and excretion

- ✘ Primarily eliminated through the bile into intestine
- ✘ Excretion with faeces: about 30 % unchanged after oral administration, and 4 % after intravenous administration
- ✘ Liver uptake via OATP1B1 and OATP1B3
- ✘ Inhibits the BSEP
- ✘ Substrate and possibly inhibitor of P-gp

Metabolism

- ✘ CYP isozymes 3A4, 2C9, and 2C19
- ✘ Three metabolites
 - ✘ hydroxy-bosentan (RO48-5033): main metabolite, about 8.3 % in plasma, contribution to efficacy about 20 %
 - ✘ desmethyl-bosentan (RO47-8634): about 3.1 % in plasma
 - ✘ hydroxy-desmethyl-bosentan (RO64-1056): secondary metabolite through metabolism of hydroxy-bosentan and desmethyl-bosentan
- ✘ Autoinduction of CYP3A4, 2C9 and possibly 2C19

from zero to infinity (AUC_{∞}) increased almost proportionally for doses up to 600 mg, while higher doses showed a trend to a less proportional increase in exposure metrics with a prolonged terminal half-life, maybe due to limited absorption with increasing doses (flip-flop kinetics) (57,60).

Absolute bioavailability has been investigated in two-way crossover studies. The total availability was approximately 50 % and was similar after single and multiple dose administration (57,61).

Doses from 100 mg to 1000 mg bosentan have orally been given as tablet formulation over 8 days to healthy volunteers assessing steady-state PK, which was reached within 3 to 5 days (61). Plasma concentrations increased dose-proportional for doses up to 500 mg, but exposure (AUC) decreased about 37 to 60 % on day 8 compared to day 1 (61,62), which is likely caused by autoinduction of the metabolising enzymes (62). After multiple oral dosing of therapeutic doses of 62.5 mg bosentan, a slightly smaller decrease in exposure of only about 33 % has been observed (62).

Key points

Pharmacokinetic parameters for bosentan

- ✘ Absolute bioavailability (oral administration) about 50 %
- ✘ Protein binding: albumin (≥ 98 %)
- ✘ Distribution blood/plasma ratio 0.6

Volume of distribution at steady-state

- ✘ Single intravenous 10 – 750 mg, healthy volunteers: mean 9.3 – 46.4 L

Clearance

- ✘ Single intravenous 10 – 750 mg, healthy volunteers: mean 4.8 – 10.7 L/h
- ✘ Single oral 3 - 2400 mg, healthy volunteers: mean 12.2 to 32.1 L/h
- ✘ Multiple oral 62.5 and 125 mg, PAH patients: mean 3.7 L/h

Terminal elimination half-life

- ✘ Single intravenous 10 – 750 mg, healthy volunteers: mean 2.8 – 4.3 h
- ✘ Single oral 3 - 2400 mg, healthy volunteers: mean 3.6 – 6.7 h
- ✘ Multiple oral 100 - 1000 mg, healthy volunteers: mean 4.8 – 19 h

Key points

Bosentan mean exposure after single and multiple, intravenous and oral administration

Route of administration and dose	C_{max}	AUC
Single intravenous 10 – 750 mg * (57)	1.08 – 137 mg/L	0.95 – 179 mg*h/L
Single oral 3 - 2400 mg * (57)	0.034 – 16.5 mg/L	0.26 – 77.3 mg*h/L
Multiple oral 100 - 1000 mg * (57)		
day 1	0.99 – 5.52 mg/L	5.03 – 28.9 mg*h/L
day 8	0.69 – 3.21 mg/L	3.38 – 12.9 mg*h/L
Multiple oral 62.5 and 125 mg * (57)	1190 – 2290 μ g/L	6230 – 8910 μ g*h/L

* healthy volunteers + PAH patients

Results of studies investigating the PK of therapeutic doses of bosentan in adult patients with PAH reveal that exposure is dose-disproportional and about 2-fold higher compared to healthy volunteers, while clearance is about 2-fold lower (57).

After twice daily administration of 62.5 mg and 125 mg bosentan, exposure of the metabolites hydroxy-bosentan, desmethyl-

bosentan and hydroxy-desmethyl-bosentan relative to bosentan has been higher (62.5 mg: 3.8 %, 39 %, and 27 %, and 125 mg with 3.3 %, 29 %, and 21 %) (57,58).

1.4.2 Clazosentan

Clazosentan is an intravenous administered successor compound of bosentan, currently not approved (63). It is a highly selective ET_A antagonist with only low affinity to ET_B (K_d about 0.2 and 11 nM, respectively). It has been developed for the treatment of emergency indications like aneurysmal subarachnoid haemorrhage, brain cerebral vasospasm and cerebral infraction. As such, clazosentan prevented and reversed cerebral vasospasm in a canine model of subarachnoid haemorrhage (64). Since cerebral vasospasm is one of the major causes of morbidity and mortality after subarachnoid haemorrhage (63,64), clazosentan has been investigated in patients with aneurysmal subarachnoid haemorrhage (65–69).

Clazosentan PK has been investigated in healthy volunteers over a broad dose range from and 3 – 60 mg/h and with varying infusion durations of up to 12 h, and 0.1 mg/kg/h to 0.05 mg/kg/h over 72 h (64,70). Non-compartmental as well as compartmental PK analyses indicated a dose-proportional behaviour of C_{max} and AUC (64,70). Mean clearance ranged from 35.5 to 43.9 L/h (64,70) and the volume of distribution at steady-state from 23 to 32.4 L for doses up to 60 mg/h and infusion durations up to 12 h (64). Both parameters decreased with higher doses (64). A compartmental PK analysis in patients with aneurysmal subarachnoid haemorrhage revealed similar parameter values for clearance (34.4 L/h) and volume of distribution (volume of distribution central compartment: 14.5 L and for the peripheral compartment 20.4 L) (71).

Clazosentan is highly bound to plasma proteins (> 98 %). After uptake into hepatocytes via OATP1B1 / OATP1B3 (72), clazosentan is primarily eliminated via bile and excreted unchanged with the faeces (64,71). The formation of one minor metabolite is catalysed by CYP2C9 (70,73).

1.4.3 Tezosentan

Tezosentan is another successor compound of bosentan currently under investigations. It shows high affinity to both receptors, ET_A and ET_B (K_d about 0.26 and 0.5 nM, respectively (74)), and has been developed for parenteral use thus allowing its use in emergency indications such as ischemic renal failure. Tezosentan increases cardiac output and renal blood flow, while decreasing peripheral and pulmonary pressures and pulmonary oedema. It induces coronary vasodilation and showed efficacy in acute renal failure complicating rhabdomyolysis (75–77).

The PK has been investigated after single-dose administration to healthy volunteers over broad dose ranges from 5 – 600 mg as 1 h infusion (75), 100 mg/h over 6 h, and 5 mg/h over 72 h (76). Exposure (C_{max} and AUC) proportionally increases with single doses of tezosentan, while clearance and volume of distribution decreased with increasing doses (mean clearance 26 – 49 L/h and mean volume of distribution at steady-state of 10 – 22 L) (75,76).

Tezosentan is highly bound to plasma proteins, mainly albumin with 74 – 96 % and has a blood/plasma distribution ratio of 0.6. It is a substrate for OATP, and predominantly eliminated via bile followed by

unchanged excretion with the faeces (78,79). Three minor metabolites have been identified, whereof the formation of hydroxy-tezosentan may be catalysed by CYP2C9 and has been detected only in some samples (75,78). Hydroxy-tezosentan is active with 10 – 20-fold lower potency than tezosentan (75). Tezosentan is an inhibitor of CYP2C9 (78).

1.5 Fluvoxamine

Fluvoxamine is a serotonin-selective reuptake inhibitor and therapeutically used for the treatment of depressive disorders including episodes of major depressions, and obsessive compulsive disorder. The recommended dose in adults varies between 50 mg to a maximum of 300 mg daily divided into two or three oral single doses.

After oral administration, fluvoxamine is fully absorbed from the gastrointestinal tract (80). C_{max} after administration of single and multiple doses of 50 mg to young healthy female and male volunteers, is achieved within about 3 to 12 h (81). After single doses of 50 mg mean C_{max} values of about 30 ng/mL were reached, while after multiple doses C_{max} varied between 32 to 300 ng/mL (81). Due to a first-pass effect, absolute bioavailability is about 50 %. Fluvoxamine is bound to plasma proteins with about 80 % and the mean volume of distribution is approximately 25 L/kg. Clearance varied between 1.1 to 3 L/min after single dose administration of 50 mg (82). Fluvoxamine metabolism in the liver occurs almost completely leading to a number of inactive metabolites predominantly excreted with urine (80). The main enzyme involved in the metabolism of fluvoxamine is CYP isoenzyme 2D6 (83), and the involvement of CYP1A2 is likely (82,84).

Fluvoxamine is a strong inhibitor of CYP1A2 and 2C19, as well as moderate inhibitor of the isozymes CYP2C9, 2D6, and 3A4. Therefore, co-administration with fluvoxamine can affect exposure of a number of substances like tricyclic antidepressants (e.g. clomipramine, imipramine, and amitriptyline), neuroleptic agents (e.g. clozapine, olanzapine), theophylline, caffeine, methadone, propranolol, or ropinirole, due to an increase in exposure through inhibition of CYP1A2 by fluvoxamine. Further, exposure of warfarin increases when administered with fluvoxamine mainly because of its CYP2C9 inhibiting effect. Moreover, PK DDIs are known for compounds metabolised by CYP3A4 leading to an increase in exposure (e.g. terfenadine, cisaprid, carbamazepine, ciclosporin, midazolam, alprazolam, or diazepam). Due to its CYP1A2 and 2C19 inhibiting property, fluvoxamine has been assigned a lead compound status for DDI with CYP1A2 and 2C19 by the US Food and Drug Administration (FDA) (83).

1.6 Cytochrome P450 isozymes and genetic polymorphisms

Metabolic transformation of xenobiotics is achieved in phase I reactions (oxidation, reduction, or hydrolysis), phase II reactions (e.g. conjugation with glucuronic acid), or both. A key role in phase I metabolism is oxidation by monooxygenases that contain haem as a cofactor (i.e. haemoproteins), the CYP isozymes. CYP isozymes are classified by their gene sequence into families, assigned by numbers (e.g. CYP1, CYP2, CYP3), subfamilies, assigned by letters (e.g. CYP1A, CYP2D, CYP3A), and isozymes, again assigned by numbers (e.g. CYP2D6, CYP3A4). In addition, a frequent spelling includes the allelic variants, assigned by an asterisk and numbers (e.g. CYP1C19*2, CYP2C9*3). The main families involved in drug metabolism are CYP1, CYP2, and CYP3 (85,86). CYP isozymes are predominantly expressed in the liver, but also in the gastrointestinal tract or the lungs.

The activity of many CYP isozymes can be altered by genetic mutations that are predominantly single-nucleotide polymorphisms (85). Genetic polymorphisms can lead to increased and decreased enzyme activity or even loss of enzyme activity. Accordingly, populations are classified by their genetic polymorphism status as ultrarapid, intermediate, poor metabolisers, and extensive metabolisers with “normal” enzyme activity (wild type) (85). Genetic polymorphisms for CYP2A6, 2C9, 2C19, and 2D6 are very common and of particular interest in drug therapy (85), and a ethnicity-related polymorphism in CYP3A4, was described (87). Reduction or loss of enzyme activity can lead to significantly higher drug exposure and consequently affect drug safety. In contrast, exposure of a drug can be significantly lower in ultrarapid metabolisers and thus reduce efficacy. However, the opposite case may occur for compounds where active metabolites strongly contribute to the drug effect or drive safety risks. Implications for drug treatment can be even more complex for compounds catalysed by two or more CYP isozymes exhibiting genetic polymorphisms. The relative enzyme abundances of different CYP isozymes can vary extensively between individuals, shifting exposure of the parent compound and the metabolites, and thus leading to distinct variability in PK within the same target population. Dose adjustments may be required for certain subpopulations based on their genetic polymorphisms. However, identifying the optimal dose for patients based on their genetic polymorphisms can be challenging, because PK data for the different subpopulations may be limited or even lacking.

1.7 Drug-drug interaction

The big issue of DDIs comes into play in case of multiple-drug treatment with compounds that are substrates, inhibitors, or inducers of the same CYP isozymes, other metabolic enzymes, or transporters, such as OATP, BSEP, or P-gP. As a consequence, reduction or loss of efficacy, increase in side effects, serious or fatal adverse events, or hospitalisation may occur. In such cases, dose adjustments may be required or the co-administration can be contraindicated.

1.7.1 Drug-drug interaction potential of bosentan, clazosentan, and tezosentan

Three of the most common CYP isozymes (2C9, 2C19, and 3A4), which also exhibit genetic polymorphisms (85,87), are involved in bosentan metabolism. Because bosentan is an inducer of CYP3A4, 2C9, and possibly 2C19, an inhibitor of BSEP, a substrate of OATP, as well as a possibly inducer of P-gp, co-administration with a numerous other compounds can lead to clinically meaningful changes in PK of either bosentan, the co-medication, or both. A selection of important DDIs with bosentan is listed in Table 4.

For Clazosentan, DDI due to inhibition of OATP uptake can substantially increase exposure and decrease clearance and volume of distribution of clazosentan, which may be of clinical relevance (72). A substantial increase in tezosentan exposure as well as decrease in clearance and volume of distribution occur after co-administration with cyclosporine, likely due to inhibition of transport proteins in the liver (72,79).

Table 4 Selection of important drug-drug interactions with bosentan

Compound	Effect on enzymes or transporters	Effect on exposure
Clarithromycin	Inhibitor of CYP3A4, OATP, and P-gp	Increase in peak plasma concentrations and AUC of bosentan by 282 % and 273 %, respectively (59). Increase in exposure (i.e. AUC) of hydroxy-bosentan, desmethyl-bosentan, and hydroxy-desmethyl-bosentan by 204 %, 44 %, and 52 %, respectively (59).
Ketoconazole, itraconazole, ritonavir	Strong inhibitors of CYP3A4	C_{max} and AUC of bosentan increase 2.1- and 2.3-fold (mean), respectively with ketoconazole (62). 48-fold increase in bosentan concentration with ritonavir during the first 4 days (88). Treatment is not recommended due to meaningful increase of exposure of bosentan (48). Co-administration of strong CYP3A4 inhibitors is expected to particularly increase bosentan plasma concentrations in CYP2C9 poor metabolisers, which may lead to harmful adverse events (48,58).
Voriconazole	CYP2C9, CYP2C19, and CYP3A inhibitor	Combination not recommended due to expected substantial increase in bosentan plasma concentration (48).
Fluconazole	CYP2C9 / CYP3A4 inhibitor	Combination not recommended due to expected substantial increase in bosentan plasma concentration (48).
Rifampicin	Strong inducer of CYP2C9 / CYP3A4	Bosentan plasma concentrations are expected to decrease by up to 90 % (48).

Compound	Effect on enzymes or transporters	Effect on exposure
Carbamazepine, phenobarbital, phenytoin, St. John's wort	Inducers of CYP3A4	Expected decrease in systemic exposure of bosentan: caution is required (48)
Sildenafil, tadalafil	Substrates of CYP3A4	Exposure of the PDE5 inhibitors is expected to decrease in a meaningful manner about 40 to 63 % (sildenafil) and 41.5 % (tadalafil) (48,89,90). concurrently, bosentan plasma concentrations increase (50) and are significantly higher compared to ambrisentan, when given with sildenafil (59).
Simvastatin	Substrate of CYP3A4	Decreased exposure to simvastatin and β -hydroxyacid simvastatin by 34 and 46 %, respectively (91).
Lopinavir / Ritonavir	Substrate and inducer of CYP3A4 (lopinavir) Strong inhibitor of CYP3A4 and inhibitor of OATP1B1 (ritonavir)	Increase in AUC and C_{max} of bosentan and hydroxy-bosentan by 5.2-fold and 4.3-fold, and 6.1- and 5.3-fold, respectively (48,88). Initial trough plasma concentrations of bosentan have been approximately 48-fold higher than those measured after bosentan administered alone (48).
Digoxin	Substrate of P-gP	Decrease in exposure of digoxin (48,92).
Warfarin	Substrate of CYP3A4 (R-warfarin) and CYP2C9 (S-warfarin)	Reduction in mean AUC of 38 % for R-warfarin and 29 % for S-warfarin (48,93).
Glibenclamide	Substrate of CYP3A4, Inhibitor of BSEP	Decrease in C_{max} and AUC of glibenclamide by about 22 % and 40 %, respectively. Exposure (AUC) of bosentan and its three metabolites decreased by about 29%, 26 %, 25 %, and 22 %, respectively. Combination causes elevated liver aminotransferase (48,94). Co-administration with glibenclamide is not recommended (48).
Cyclosporine	Substrate and inhibitor of CYP3A4, Inhibitor of P-gp and OATP	Concomitant use is contraindicated (48), and an increase in plasma concentration of bosentan can be expected when co-administered with tacrolimus or sirolimus (48,57). Steady-state plasma concentrations increase 3-fold to 4-fold compared with bosentan alone. Decrease in blood concentrations of cyclosporine A by approximately 50% (48,95).

1.7.2 Physiologically-based pharmacokinetic modelling for drug-drug interaction

The risk of potential PK DDIs should generally be assessed *in vitro* using human enzymes and transporters, and *in vivo* (13) to ensure safe and effective drug therapies. However, the use of *in silico* methods such as PBPK modelling methods is an emerging technique to assess potential DDIs qualitatively and quantitatively (10,13).

PBPK models are developed using specialised software platforms (i.e. collection of computer programs and included system data) that need to be qualified for the intended use (10). The platform needs to be able to adequately perform simulations for the intended scenario (10). Moreover, the predictive performance of the specific drug models needs to be satisfactorily based on pre-defined decision criteria (10,96). The predictive performance of compound files (e.g. inhibitor, inducer, or probe drug) in the PBPK platform need to be confirmed, for instance by comparison with *in vivo* PK studies for this drug (10).

The model development process generally follows a common cycle of “predict, learn, confirm” (96). A base model is typically developed based on experimental or *in silico* predicted physicochemical data, as well as *in vitro* ADME parameters. The obtained predictions are then compared with *in vivo* single and multiple dose clinical PK data. Model parameters may be adjusted and the refined model compared, and ideally confirmed, using additional PK data from other studies, such as DDI studies.

The FDA provides information on index victim drugs (drugs affected by the DDI) or perpetrator drugs (drugs affecting the PK of other drugs) suitable for clinical DDI studies. These compounds are (almost exclusive) substrates of a certain metabolic pathway or are inhibitors or inducers of specific enzymes (i.e. clinical index substrates, inhibitors or inducers). For instance, theophylline and caffeine are substrates for CYP1A2. Rifampicin is a strong inducer of CYP1A2, 2C19, 3A, and moderate inducer of CYP2B6, 2C8, 2C9, and therefore frequently used for DDI studies. Midazolam is a compound that is exclusively metabolised by CYP3A4, and thus commonly used to investigate DDIs regarding CYP3A4. Fluvoxamine as a strong CYP1A2 inhibitor has been assigned a lead compound status for DDI with this isoenzyme (83). Due to their CYP enzyme related properties, these compounds can be used as compound files in a PBPK platform, when sufficiently qualified PBPK models are available. As such, PBPK models for fluvoxamine, theophylline, caffeine, rifampicin, and midazolam, forming a network for CYP1A2 DDI prediction, have been built (97). In addition, a population PK model was developed aiming to confirm and substantiate the results of the PBPK model for fluvoxamine (project III). The PK of fluvoxamine was investigated using the NLME approach. Data from two studies were used, where the PK was assessed after administration of single oral doses of 50 mg fluvoxamine to healthy volunteers. In study one, all volunteers were phenotyped according to their CYP2D6 status (extensive and poor metabolisers)(98), and in study two, the smoking status of all participants was recorded (82). The population PK model development followed a commonly used strategy of sequential testing of a variety of model structures, investigations of random, as well as covariate effects, as described in chapter 3.

1.8 Endogenous rhythms and chronopharmacology

"Circadian time keeping allows appropriate temporal regulation of an organism's internal metabolism to anticipate and respond to recurrent daily changes in the environment." (99). Endogenous rhythms are typically called circadian rhythms, as suggested by Halberg, and are commonly characterised by a mean period length of 24 h (daily rhythm) (100,101). It is driven by clock genes (101,102), expressed in the suprachiasmatic nucleus (103).

The first clock gene *period* has been identified by Seymour Benzer and Ronald Konopka in 1971 (104) and has been isolated and further investigated by Jeffrey Hall, Michael Rosbash, Michael Young and others (105–111). Briefly, *period* influences the circadian rhythm by encoding the protein *PER*, that accumulates during the night and is degraded during the day, oscillating over a 24 h cycle. After binding to the protein *TIM*, which is encoded by another clock gene called *timeless* (112), the two proteins enter the nucleus and block the activity of the *period* gene, thus regulating the synthesis of *PER* in a cyclic manner through an negative feedback loop (111). Over the years, a number of additional clock genes such as *doubletime* (113), *clock*, *cycle*, and *cryptochrome*, have been identified, all contributing to an overall very complex system regulating the circadian rhythm (99,102).

The phenomenon of endogenous rhythms influences life on different scales, reaching from milliseconds (e.g. neuronal discharge) to seasonal (circa-annual) rhythms (101). They can vary on a daily basis (circadian rhythm), several times within one day (ultradian rhythm), or be longer than 24 h (infradian rhythm) (103). For instance, it is known that body temperature, organ functions, or concentrations of endogenous compounds (e.g. cortisol, thyroid hormones, melatonin, epinephrine) underlie cyclic rhythms (103,114–116). A daytime-dependent variation in production of ET and its receptors has also been suggested (117–119). The sleep-wakening rhythm as well as many other processes such as regulation of blood pressure, heart rate, or menstrual cycle follow time-dependent rhythms (116). Furthermore, it has been observed that the occurrence of disease onsets (e.g. asthma or heart attacks, ischemic strokes), as well as birth and death can predominantly occur at specific times of a day or during a specific season (101,120,121). Desynchronisation of the internal clock can lead to meaningful disturbances of the endogenous rhythm by affecting the underlying physiological process and can consequently cause diseases (e.g. metabolic diseases or depressive disorders due to chronic sleep disturbances) (99,122).

Since many physiological processes underlie endogenous rhythms, this can consequently also hamper pharmacotherapy and the field of chronopharmacology is emerging (99). It is increasingly recognised that the time point of drug administration can be of special interest. For instance, it is widely accepted that antihypertensive drugs in dippers or therapy with thyroid hormones should be given in the morning due to circadian rhythm in blood pressure (120,121) and peak in endogenous hormone production in the morning,

respectively. On the other hand, non-dippers should preferably receive their antihypertensive drugs in the evening (121) and likewise, statins should be administered in the evening, because HMG-CoA-reductase production underlies a circadian rhythm with peaks around midnight (101). In addition, optimal dosing time points may also reduce drug-induced toxicity (103).

Moreover, endogenous rhythms also affect ADME processes in the body, therewith affecting PK (121). Time to and extent of C_{max} reached, can vary meaningful when a drug is administered in the morning or in the evening. For example, absorption (by passive diffusion) occurs faster in the morning, which can lead to a significant increase in C_{max} (121). In addition, a circadian rhythm in renal blood flow and glomerular filtration rate have been observed in humans, resulting in variation of renal elimination processes depending on time (101,123). Moreover, hepatic clearance in rats has been observed to be faster during night time and a possible rhythm in CYP3A4 activity in human liver have been presumed (101), overall suggesting the existence of periodical patterns in elimination processes.

2 Objectives

2.1 Project I – Pharmacometric analyses of bosentan and endothelin-1

Bosentan is still one of the most frequently used therapeutic options to treat patients with PAH. However, it exhibits nonlinear PK and shows distinct variability. In order to better characterise and understand its PK behaviour, the first goal of this project was to develop a PK model for bosentan after intravenous administration to healthy volunteers, including the competitive antagonism with ET-1. Furthermore, a PKPD model for blood pressure and heart rate aimed to describe the influence of bosentan on cardiovascular effects. In addition, an analysis was conducted investigating covariates that possibly affect PK and PD.

2.2 Project II – Population target-mediated drug disposition modelling of bosentan, clazosentan, and tezosentan

Although target-mediated drug disposition (TMDD) is a behaviour that is predominantly known for large molecule drugs such as peptides and proteins, the numbers of small molecule drugs that exhibit TMDD and thus nonlinear PK behaviour due to their pronounced target (i.e. receptor or enzyme) selectivity and activity, are increasing. Since for the small molecule bosentan TMDD was found to explain the nonlinearity in PK (project I), the primary aim of this project was to investigate whether the concept of TMDD could be applied for bosentan's follow-up compounds, clazosentan, and tezosentan, hypothesising a class effect for ERAs. Secondly, the hypothesis of diurnal receptor expression, as put forward in project I, was further investigated.

2.3 Project III – The influence of CYP2D6 polymorphism and smoking on pharmacokinetics of fluvoxamine

The occurrence of DDI during multiple-drug therapy is a very important topic, due to either higher risks of safety issues or possibly loss in efficacy on the other hand. PBPK models can be used to predict a drug's exposure and can allow to identify important interactions with metabolising enzymes and drugs concomitantly used. CYP1A2 is an important enzyme frequently involved in drug metabolism, thus highly likely involved in DDIs. Fluvoxamine is a strong inhibitor for CYP1A2 and an important compound used for investigations of DDIs with CYP1A2. As part of the development of a PBPK DDI network for CYP1A2 with fluvoxamine, theophylline, caffeine, rifampicin, and midazolam, project III aimed, to investigate the influence of CYP2D6 polymorphisms and smoking on the PK of fluvoxamine, by developing a population PK model using the NLME approach.

3 Methods

3.1 Population modelling

The PK and PD properties of a drug candidates need to be adequately investigated during drug development to ensure that treatments are safe and efficacious. Every drug however, exhibits variability in exposure and response to a certain extent. The population modelling approach allows to estimate parameters (i.e. PK or PD parameters) including their variability at a population level, where data from all individuals are considered simultaneously, thus identifying the relationship between patient's characteristics and drug exposure and response. Three common population approaches are the naïve average data approach, the two-stage approach and the NLME approach.

3.1.1 Naïve average data approach

The naïve average data approach is a relatively simple method of analysing population PK data; after pooling the data from all individuals the average value of each sampling time is computed and a model is fitted to the mean data. Although such models allow to describe a general trend of the mean data, which can also be sparse, the identification of variability in exposure is hampered, as all sources of variability data are masked (9).

3.1.2 Two-stage approach

The two-stage approach is a traditional procedure used to analyse PK data. In a first stage, model parameters are fitted to each individual separately, while in the second stage the distribution of these parameters is described by calculating the mean or median values, the variance and percentiles. Although this method is somehow attractive due to its simplicity, it requires data rich situation and well-balanced studies, which can be considered a big disadvantage.

3.1.3 Nonlinear mixed-effects modelling approach

In 1972 Sheiner and co-workers (124) first described the usage of a population PK model that commonly means today a NLME model. Such population models can also be used to analyse PD data or for instance to exhibit exposure-response analyses for efficacy and safety.

NLME models can be used to describe, understand, and predict the concentration-time profiles and PD responses for efficacy and safety of a given compound for an intended target population. They allow the simultaneous estimation of population mean parameters, inter-individual (IIV) and intra-individual variability (IOV), and to quantify the extent of covariates (e.g. patient factors, disease state, or co-medication) influencing a certain parameter. This can be done using pooled data of different origins and properties (e.g. data from phase 1, 2, and 3 clinical trials, data obtained from adult and paediatric patients, or data from healthy

volunteers and patients). Pooling such data can be much more informative for the analysis of covariates because the diversity of patient factors increases and thus the range of a particular covariate expands. For instance, pooling data from volunteers with varying degrees of renal dysfunction (mild, moderate, severe, or end-stage renal disease) can allow to better predict their influence on PK. Furthermore, only few data points are necessary to conduct an NLME analysis, which is a great advantage in situations when only sparse sampling can be conducted (e.g. paediatric / vulnerable patients). Nonetheless, pooling data from different sources should be performed carefully and its results may need cautious interpretation, if data from a certain population are underrepresented with relatively little data contributing to the overall dataset (e.g. children vs. adult, patients with end-stage renal disease or hepatic impairment vs. volunteers with normal organ function, poor metabolisers with rare genetic polymorphisms of a certain enzyme such as CYP2C9*3/*3 vs. extensive metabolisers CYP2C9*1/*1).

In a NLME model, the dependent variable (e.g. plasma concentration) is related to the independent variable (e.g. time point, dose) in a nonlinear way ("nonlinear"). The term "mixed-effects" is related to the model parametrisation, that consist of "fixed effects", i.e. population mean parameters (structural model), and "random effects" (IIV, IOV, residual variability) that differ between individuals (stochastical model). As such, the general three components of a NLME model are the structural model, the stochastical model, and the covariate model (Figure 4). In general, model development starts with evaluation of the structural model, followed by the stochastical model, and finally the covariate analysis is conducted to identify factors influencing PK or PD parameters.

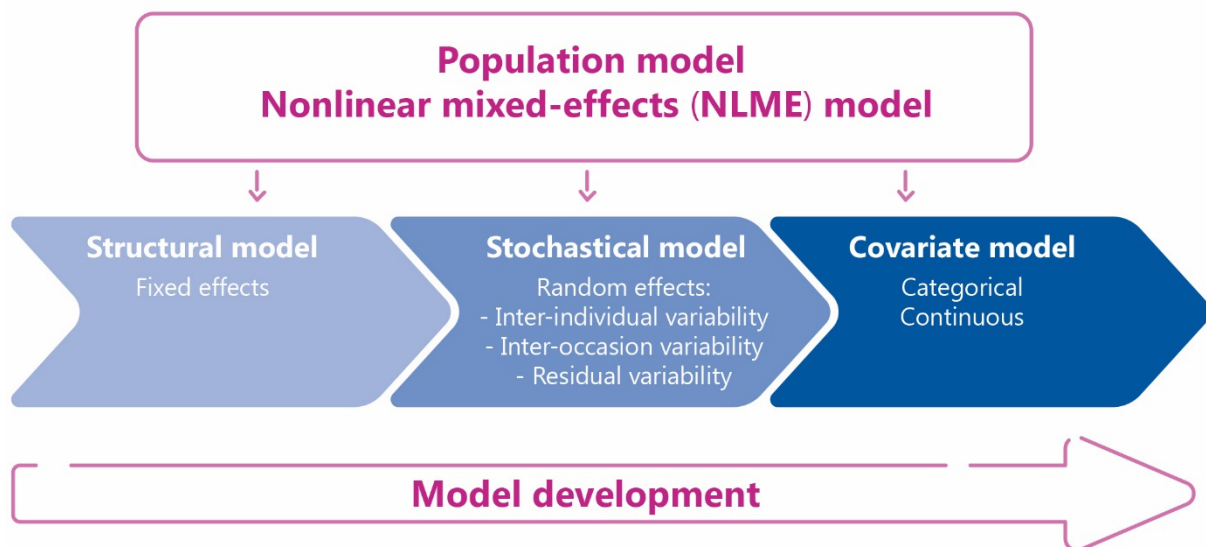


Figure 4 Nonlinear mixed-effects (NLME) models consist of three main pillars, the structural, the stochastical, and the covariate model, which are usually developed sequentially.

3.1.3.1 Structural model

The structural model describes the general trend of the observed data (e.g. plasma concentration) as a function of (PK) parameters and dose.

The mathematical model can be expressed as algebraic equations (Equation 1), or differential equation (Equation 2) if the system is getting more complex. A differential equation describes the rate of change of a variable over time. An example for the simplest case, a one-compartment model for single intravenous administration of a drug, is given in Equation 1 (algebraic equation) and Equation 2 (differential equation):

$$C_{(t)} = \frac{Dose}{V} e^{-\frac{CL}{V} \cdot t} \quad (\text{Equation 1})$$

In this model (Equation 1) the dependent variable C (concentration) is related to time (t) and depends on t . The constant parameters dose, clearance (CL), and volume of distribution (V) do not change with different values of t .

$$\frac{dC}{dt} = -\frac{CL}{V} \times C, C_0 = \frac{Dose}{V} \quad (\text{Equation 2})$$

In Equation 2, the rate of change of the concentration (C) is related to time and expressed by $\frac{dC}{dt}$. The initial value at time point zero of the dependent variable (C_0) is specified by $\frac{Dose}{V}$.

In a more general way, the function $f()$ describes the observed plasma concentration Y_{ij} of a plasma concentration j from patient i with a function of the individual parameter θ_i and a fixed or measured component x_{ij} (e.g. dose, time) (Equation 3).

$$Y_{ij} = f(\theta_i, x_{ij}) \quad (\text{Equation 3})$$

The evaluation of the structural PK model usually includes testing of various types of models, such as one-, two-, or three-compartment models, where additionally different absorption, distribution, or elimination behaviours (e.g. nonlinear elimination described by Michaelis-Menten kinetics) may be tested. However, also other, more complex model structures, such as TMDD models, should be tested, depending on the characteristics of the drug.

Commonly, PD structural model evaluation includes linear, log-linear, E_{max} , or sigmoidal E_{max} functions, which can be linked directly (using plasma concentrations) or indirectly to PK. A delay in actual effect mostly requires the usage of indirect models, such as indirect-link models (i.e. linking with tissue concentrations), using effect-compartments as an interface between PK and PD, or indirect-response models, where the PD effect or biomarker is described as a function of time (e.g. endogenous substances that underlie synthesis and degradation processes).

3.1.3.2 Stochastic model

The stochastic model describes and quantifies the observed variability in the population and allows to parse it into IIV, IOV, and residual variability. The variability can be implemented as additive, proportional, or exponential model.

The IIV reflects the variability in fixed-effects parameters between each individual compared to the population typical (mean) values and is usually described as exponential model (Equation 4).

$$\theta_i = \theta_{pop} \times \exp(\eta_i) \quad (\text{Equation 4})$$

where θ_i is the individual parameter for the individual i , and η_i is the deviation from the population typical value (θ_{pop}) for the individual i , and assumed to be normally distributed with mean 0 and variance ω^2 (125). The variability is usually reported as relative coefficient of variation (CV [%] or %CV), which is calculated as follows:

$$CV[\%] = \sqrt{\exp(\omega^2) - 1} \times 100 \quad (\text{Equation 5})$$

IOV, accounts for the variability within an individual, for instance observed after multiple dose administration or different periods in a cross-over study (i.e. observation at different occasions). Equation 6 gives the general exponential model form where κ is the deviation from the population typical value at different occasions (OCC), and is assumed to be normally distributed with mean 0 and variance π_{κ}^2 .

$$\theta_i = \theta_{pop} \times \exp(\eta_i + \kappa_1 OCC_1 + \kappa_2 OCC_2 + \dots + \kappa_0 OCC_0) \quad (\text{Equation 6})$$

Residual variability (ε) addresses all variability that cannot be characterised by IIV or IOV. This may be variability in analytical assays, in time of drug administration, or differences in actual sampling time points. They characterise the deviation of measured values from predicted values that are based on individual model parameters. Residual variability (ε_{ij}) is assumed to be normally distributed with mean 0 and variance σ^2 . It can be modelled as additive (σ^2 is a constant for the range of observed data; Equation 7), proportional (σ^2 increases with larger values; Equation 8), a combined (proportional and additive; Equation 9), exponential (Equation 10), or a power model (Equation 11).

$$Y_{obs,ij} = Y_{pred,ij} + \varepsilon_{ij} \quad (\text{Equation 7})$$

$$Y_{obs,ij} = Y_{pred,ij} + Y_{pred,ij} \times \varepsilon_{ij} \quad (\text{Equation 8})$$

$$Y_{obs,ij} = Y_{pred,ij} + Y_{pred,ij} \times \varepsilon_{1ij} + \varepsilon_{2ij} \quad (\text{Equation 9})$$

$$Y_{obs,ij} = Y_{pred,ij} \times \exp(\varepsilon_{ij}) \quad (\text{Equation 10})$$

$$Y_{obs,ij} = Y_{pred,ij} + Y_{pred,ij}^{\varepsilon_{ij}} \quad (\text{Equation 11})$$

where $Y_{pred,ij}$ is the individual model-predicted concentration.

3.1.3.3 Covariate model

In order to investigate, understand, and evaluate why PK or PD differ between individuals of a population, a covariate analysis studying patient-related and / or study-specific characteristics can be conducted. Covariates are usually categorised into continuous (e.g. age, weight, clinical laboratory parameters) and categorical (e.g. race, sex, smoking status, CYP isoenzyme phenotype).

The investigation of covariates is often conducted graphically in a first step (e.g. plotting the individual PK parameter versus a covariate) evaluating potential systematic relationships. The statistical testing of selected covariates is then usually performed applying a forward inclusion and backward elimination procedure. Firstly, all covariates are tested separately in a univariate manner on each parameter of interest and added to the model if considered statistically significant at a pre-defined significance level (e.g. $p < 0.05$, with 1 degree of freedom, difference in objective function value between two models $[\Delta\text{OFV}] < -3.84$) to build the full covariate model. Afterwards, covariates are removed sequentially (backward elimination) applying more stringent criteria (e.g. $p < 0.001$, with 1 degree of freedom, $\Delta\text{OFV} < -10.83$) until the final covariate model is built.

Covariates can be included in a model in many different ways. In this work, in project III, the impact of CYP2D6 phenotype (poor vs. extensive metabolisers) and smoking status on the clearance (CL) of fluvoxamine were modelled as categorical covariates. A factor for CYP2D6 poor metabolisers ($\theta_{PM/EM}$) as compared to extensive metabolisers ($\theta_{PM/EM} = 1$), was estimated and multiplied by the typical population parameter value for CL (θ_{pop}) and the IIV ($\exp(\eta_i)$) (Equation 12).

$$CL = \theta_{pop} \times \theta_{PM/EM} \times \exp(\eta_i) \quad (\text{Equation 12})$$

3.1.3.4 Model evaluation and simulations

In order to assess which model is most suitable to describe the PK or PD data, during model development, several diagnostic methods are used for decision-making. Typically, numerical analyses include the assessment of OFV, precision, and plausibility of parameter estimates, and graphical methods such as goodness-of-fit plots and visual predictive checks (VPCs) are used.

A key element of the modelling approach is to derive model parameters that describe the observed data best. This is commonly done using the likelihood function, which is a probability function for the occurrence of the measured data depending on the respective parameter estimates. Minus twice the logarithm of the likelihood function (-2LL) is used to assess the alignment of the observed data and the model-prediction for a set of parameters. The OFV is equal to -2LL. The difference of the OFV can be used to discriminate between models with the lowest OFV indicating the best model fit. The OFV approximately follows the chi-square χ^2 distribution. As such, for instance a level of significance of $p < 0.05$ is achieved if OFV is decreased by ≥ 3.84 points for one degree of freedom, where the degree of freedom is the numerical difference of estimated parameters between a full model compared to a reduced model. This test is also called ratio likelihood test and is only

valid for models where the reduced model is nested within the full model and has one estimated parameter less than the full model (i.e. nested model).

Furthermore, the reliability of a model is assessed by considering the precision of the parameter estimates based on the relative standard error (RSE [%]) of the estimated parameter, which ideally is as low as possible (and commonly should be below 50 %).

Goodness-of-fit plots are used for graphical model evaluation. Variables of interest are plotted against each other (e.g. observed data versus population prediction or individual prediction) allowing to visually assess the model performance and identify model misspecifications (e.g. systematic over-predictions or under-predictions of the observed data).

VPCs are generally produced to graphically assess the predictive performance of a model including the variability. The final model is used to simulate a large number (e.g. 1000) of datasets that are a subset of the original data (internal validation) or a new dataset (external validation), and are plotted against the observed data. The observed and model-predicted 5th, 50th, and 95th percentiles are plotted together with the 90 % prediction interval (or different widths of the prediction interval and percentiles), evaluating whether the observed data are lying within the prediction interval. Different types of VPCs exist, however, the prediction-corrected VPC (pc-VPC) (126) is one of the most commonly used methods to assess the predictive performance of a model.

The final model can also be used to simulate data other than the original data for interpolation (non-observed data within the bounds of the original data) or extrapolation (non-observed data outside the original data) purpose. Moreover, simulations can be conducted to understand the behaviour of the system under different scenarios. They can be carried out to assess the effect of covariates of certain subpopulations on drug exposure (e.g. how the exposure changes for patients with different degrees of renal impaired compared to patients with normal renal functions receiving the same dose). Furthermore, they can guide recommendation for dose adjustments and labelling. However, it should be kept in mind that simulations require confidence in the underlying model with a clear understanding of its limitations (1).

3.2 Target-mediated drug disposition models

The development of drugs that bind with high specificity and potency to a target are of increasing interest because they enable targeted therapies. Such compounds are bound with distinct affinity to their target, e.g. receptors or enzymes that are only of low capacity. Therefore, a substantial fraction of the dose is often rapidly bound to the target site, which can be observed in the PK profile that exhibits disproportional behaviour (127,128). However, such nonlinearity may only be observed in total clearance and volume of distribution (127) and not distinctly in exposure (e.g. C_{max} or AUC). Dose-normalised concentration-time profiles (concentration/dose vs. time) may show apparent dose-proportionality at relatively high concentrations (superimposition), but not at lower concentrations, in the terminal elimination phase (127). Such a behaviour is known as TMDD. However, since the binding capacity of non-specific tissues is larger than the low capacity of receptors or enzymes, saturable target binding is often masked, in particular for small molecules. The phenomenon of drugs exhibiting TMDD has been predominately reported for large molecules such as peptides and proteins (128). Nevertheless, the development of small molecule compounds with extensive target selectivity and potency is emerging. When applying M&S techniques, like population modelling, to investigate the PK behaviour of substances exhibiting TMDD, concentration-time profiles can most likely not be sufficiently described using linear models. For instance, a one-compartment model with linear elimination process, as used to analyse the PK of fluvoxamine, will not be applicable in most cases to compounds that show distinct nonlinear PK due to their high target affinity (e.g. bosentan). Thus, more complex models are required and the application of the TMDD concepts to small molecules is of increasing interest. As such, the development of PK models reflecting TMDD are emerging. A general PK TMDD model as proposed by Mager and Jusko (129) was used and adjusted in project I and project II of this work. Figure 5 illustrates a general TMDD model for a drug that is orally or intravenously administered, bound to a receptor (k_{on}) from which it can dissociate again (k_{off}). The drug can distribute from the plasma to a non-specific tissue in the periphery (k_{tp} , k_{pt}) and be eliminated either from the central compartment (k_{el}) or via an internalisation process after binding to the target site (k_m). The receptors are synthesised (k_{syn}) and degraded (k_{deg}).

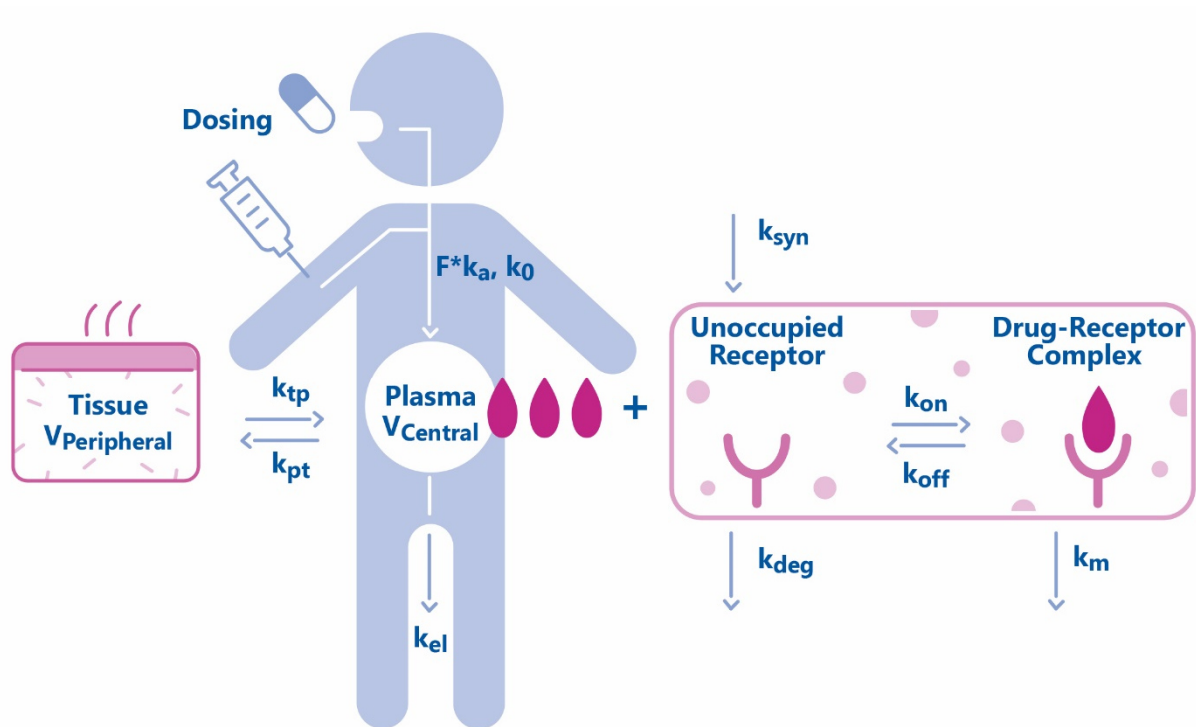


Figure 5 Illustration of a PK target-mediated drug disposition (TMDD) model. Dosing compartment: the drug may be administered orally or intravenously and is absorbed with first-order absorption rate constant (k_a) and bioavailability (F) or zero-order rate constant of drug infusion (k_0), respectively. The drug in the central compartment (plasma, V_{Central}) can distribute to non-specific tissue sites ($V_{\text{Peripheral}}$), be eliminated from the system (k_{el}), or bind with rate constant k_{on} to a pharmacologic target, e.g. the unoccupied receptor to form a drug-receptor complex. This complex may then either dissociate (k_{off}) or be internalised and degraded (k_m). The free target (e.g. receptors) are synthesised (k_{syn}) and degraded (k_{deg}). [Modified from (129)]

4 Results

The three projects were published in scientific journals and are presented with their supplementary material in the Appendix.

4.1 Publication I

A.-K. Volz, A. Krause, W.E. Haefeli, J. Dingemans, T. Lehr, Target-Mediated Drug Disposition Pharmacokinetic–Pharmacodynamic Model of Bosentan and Endothelin-1, *Clin. Pharmacokinet.* 56 (2017) 1499–1511. doi:10.1007/s40262-017-0534-4.

4.2 Publication II

A.-K. Volz, J. Dingemans, A. Krause, T. Lehr, Target-Mediated Population Pharmacokinetic Modeling of Endothelin Receptor Antagonists., *Pharm. Res.* 37 (2019) 2. doi:10.1007/s11095-019-2723-3.

4.3 Publication III

H. Britz, N. Hanke, A.-K. Volz, O. Spigset, M. Schwab, T. Eissing, et al., Physiologically-Based Pharmacokinetic Models for CYP1A2 Drug–Drug Interaction Prediction: A Modeling Network of Fluvoxamine, Theophylline, Caffeine, Rifampicin, and Midazolam, *CPT Pharmacometrics Syst. Pharmacol.* 8 (2019) 296–307. doi:10.1002/psp4.12397.

5 Conclusion

M&S techniques provide helpful methods to characterise and understand the PK and PD behaviour of drugs. The knowledge obtained from pharmacometric analyses can consequently facilitate optimal dosing recommendations for the intended use and across subgroups of a target population, and therefore support industrial and regulatory decision-making.

In this context, the investigation of DDI is of special interest. Because DDIs for instance due to CYP isozyme activation or inhibition can alter a drug's exposure in a meaningful way, comprehensive knowledge on the DDI potential of compounds of interest is essential. *In silico* methods, such as PBPK modelling, can be used to qualitatively and quantitatively predict the DDI potential of a certain combination. However, this requires well informed, qualified model networks. Fluvoxamine as a lead substance for DDI with CYP1A2 was used to develop a network for CYP1A2 DDI prediction with theophylline, caffeine, rifampicin, and midazolam, using PBPK modelling techniques. As part of this work (project III), in addition a NLME model was developed to characterise the PK of fluvoxamine after single oral administration to healthy volunteers, aiming to confirm and support the results from the PBPK model. The influence of CYP2D6 phenotype and cigarette smoking (induction of CYP1A2) on fluvoxamine PK was successfully described by a one-compartment model with linear absorption and elimination processes, confirming the results from the developed PBPK model network, which now contributes to the library of publicly available PBPK models for DDI prediction (www.open-systems-pharmacology.org). The results of this project also confirmed previous observations obtained in clinical trials (130,131) and showed that both, CYP2D6 phenotype and cigarette smoking, influence the clearance of fluvoxamine, leading to increased exposures in CYP2D6 poor metabolisers and decreased exposures in smokers compared to non-smokers.

Although the characteristics of bosentan, the first ERA approved for the treatment of PAH, have been already studied during its development in the 1990s, plasma concentration-time profiles over broad dose ranges in healthy volunteers and after therapeutic doses in patients revealed that bosentan PK follows a distinct nonlinear behaviour and bosentan showed pronounced IIV in PK and PD, which deserves more attention.

The NLME approach, was used to characterise and better understand the PK behaviour of bosentan after intravenous administration, and to discover sources of the observed nonlinearity and variability (project I). Moreover, in this project the influence of bosentan on endogenous ET-1 levels as well as its effects on blood pressure and heart rate were investigated in healthy volunteers. It was suggested, that the observed nonlinearity in PK is caused by the strong receptor binding affinity and that the usage of relatively simple linear compartment models (with or without implementation of Michaelis-Menten kinetics), may not be appropriate to describe the plasma concentration-time profiles of bosentan over broad dose ranges. A more complex approach was necessary. Finally a competitive TMDD PKPD model was successfully developed confirming the

hypothesis of a distinct nonlinearity caused by the strong receptor binding affinity. The developed two-compartment TMDD model enables to simultaneously describe the nonlinear plasma concentration-time data of bosentan through its strong ET receptor binding, leading to a displacement of ET-1 from the binding sites, and consequently decreasing blood pressure with simultaneously increasing heart rate.

The application of the TMDD concept to small molecules such as bosentan was further investigated for the two intravenous administered successor compounds, clazosentan and tezosentan (project II). Because both compounds exhibit dose-dependent nonlinearity in clearance and volume of distribution, their strong receptor binding affinities were suggested to be the reason for this observation, necessitating and justifying the application of a complex TMDD model to adequately describe the observed plasma concentration-time profiles in healthy volunteers. Furthermore, the developed models were able to distinguish between selective antagonism on ET_A (clazosentan) and non-selective ET_A/ET_B antagonism (bosentan and tezosentan), which was in addition reflected in the occurrence of a drug clearance process through internalisation of the drug - ET_B - complex only for the non-selective antagonists.

Since endogenous rhythms as internal timekeepers influence almost every cell and each process, a diurnal variation of the receptor synthesis was integrated in the TMDD PK models, reflecting a daytime-dependent change in receptor expression. This could be observed in a multiple peak phenomenon in the observed plasma concentration-time profiles.

6 Limitations

The TMDD models developed in project I and project II confirmed the hypothesis that the nonlinear PK observed for the three investigated ERAs is caused by their distinct receptor binding activity. The firstly developed model (project I) allowed to describe the competitive antagonism with endogenous ET-1 and it was possible to differentiate several clearance processes. Further, the model included a description of the delayed effect in haemodynamics. However, a disadvantage of the first model was that the internalisation processes for the target complexes could not be estimated separately for bosentan and ET-1 due to the limited data on ET-1 measures. Furthermore, in all TMDD models developed in project I and project II, the target was implemented as a mixture of both receptor subtypes, ET_A and ET_B. This is considered the major limitation. Because of the complexity of the model and lack of more informative data, it was not possible to estimate the receptors and their individual drug binding affinity separately. Therefore, some of the estimated parameters (receptor baseline values and rate constants of the target synthesis and degradation) were only approximations which ideally would be further investigated and adopted in future *in vitro* and *in silico* studies.

The diurnal receptor synthesis or reappearance was successfully described in all TMDD models by implementing a cosine function on the (lumped) receptor synthesis rate. However, the 8-h variation with peaks in receptor production around morning, afternoon, and midnight is only an approximation and it is likely, that ET_A and ET_B receptors in different tissues do not underlie identical endogenous rhythms.

In project III, the PK of fluvoxamine was described using NLME modelling. The model was further used to investigate the influence of CYP2D6 phenotype and cigarette smoking on fluvoxamine's clearance and thus on exposure. A model was successfully developed and confirmed the results from the PBPK analysis, as well as previous clinical studies on fluvoxamine. In addition, the analysis showed, that PK in fluvoxamine is variable and pronounced differences in plasma concentrations in the absorption phase could be observed. An influence of cigarette smoking on the absorption of fluvoxamine after oral administration can be assumed, as reflected by the prolonged absorption rate constants, estimated by model. However, only very limited data from 10 and 24 young and healthy volunteers, respectively, after single oral doses of 50 mg fluvoxamine were available for this analysis. To obtain even more reliable information on the PK characteristics of fluvoxamine the usage of a larger, more heterogeneous dataset could be helpful. Ideally such data should contain PK measures after intravenous administration, allowing a more precise analysis of the absorption phase. A larger dataset with a wider range of covariates could be useful to gain further information on the impact of different patient characteristics of interest on exposure of fluvoxamine under certain conditions. This may then also include DDI analyses for various subpopulations.

7 Future perspectives

The population PK analysis for fluvoxamine conducted in project III, underlined the observation that CYP2D6 poor metabolisers are expected to have higher exposure and that cigarette smoking induces the clearance of fluvoxamine, yielding lower systemic exposure. This knowledge itself should be considered in clinical practice to provide optimal treatment to patients receiving fluvoxamine therapy. Beyond this, fluvoxamine as a strong inhibitor of CYP1A2 and 2C19, as well as a moderate inhibitor of the isozymes CYP2C9, 2D6, and 3A4, is involved in DDIs when co-administered with substances that are substrates of these isoenzymes, which needs to be considered during multiple-drug treatment with fluvoxamine.

Furthermore, fluvoxamine as a lead compound for DDI with CYP1A2 now contributes to a network of PBPK models for DDIs with this isoenzyme. However, fluvoxamine is also a lead substance for DDI with CYP2C19. Therefore, the developed PBPK model may further be extended by the strong CYP2C19 inhibitory effect of fluvoxamine allowing future *in silico* investigations for DDI with drugs metabolised by CYP1A2 and / or CYP2C19. A well informed and sufficiently qualified model for CYP2C19 could then be used to predict the influence on a drug's exposure for patients with different CYP2C19 phenotype status, and finally be used to guide optimal dosing strategies for a compound of interest.

Overall, results from the modelling exercises in project I and project II showed that the strong receptor binding affinity of three intravenous administered ERAs is reflected in the concentration-time profiles revealing TMDD as a class phenomenon for ERA PK. In addition, these findings suggested that the PK of ERAs is modulated to a certain extent by an endogenous rhythm of receptor expression or reoccurrence.

The developed TMDD models describing and predicting the PK of the three investigated ERAs build a useful basis to further investigate the characteristics of these compounds after single and multiple oral administration (bosentan) or multiple intravenous administration (clazosentan, tezosentan). The models can be applied to patient data to further investigate covariate effects between patient subgroups. One may then raise the question whether the developed TMDD models may help optimising current dosing recommendations, e.g. for bosentan, to overcome the observed variability in PK and PD in PAH patients. Furthermore, the introduction of a therapeutic drug monitoring concept based on the TMDD model could be considered to individualise dosing strategies for subgroups of the target population. The incorporation of competitive antagonism by endogenous ET-1, as successfully performed for bosentan, may be a helpful tool to use ET-1 as a biochemical marker for PKPD predictions and the significance of such a marker for the prediction of effectiveness should be evaluated. For the two follow-up compounds, clazosentan and tezosentan, the models may be used to guide optimal dosing strategies in clinical trials. Further investigations on the time-dependent receptor expression could be conducted and results could be easily integrated into the model to possibly discover an optimal timing of ERA doses.

In addition, the knowledge gained from these projects can be used to develop a mechanistic whole-body PBPK model for bosentan and other ERAs to reflect the different binding affinities to ET_A and ET_B in more detail. Provided the availability of data, in such a model, systems parameter could ideally be integrated separately for each receptor subtype allowing a more precise description of the binding and elimination processes for each compound, including the endogenous ET-1. This would allow to differentiate between non-selective ET_A / ET_B antagonists as opposed to selective ERAs, characterise substance specific PK within the group of ERAs, quantify expected drug specific PD effect, and identify optimal dosing regimens. The model may be extended by incorporation of the metabolites to more comprehensively assess their PD contribution and also the impact of metabolic DDI changing metabolic ratios, as often observed. Moreover, a PBPK model would allow to additionally account for the OATP transporter-mediated uptake into the liver, the inhibition of BSEP, and the interaction with the various CYP isozymes. Such an approach may also allow to develop a PBPK DDI model for the different ERAs which then may be used to predict optimal dosing regimen under combined drug treatment for various patient populations.

8 Summary

Modelling and simulation techniques (M&S) can be used to characterise and understand a drug's pharmacokinetic (PK) and pharmacodynamic (PD) behaviour, and therewith support dosing strategies and decision-making during drug development and for regulatory purposes.

Endothelin receptor antagonists (ERAs) are a class of compounds that displace endogenous endothelin-1 (ET-1) from its receptor binding sites. Because ET-1 plays a key role in the pathogenesis of various diseases, ERAs are interesting compounds for the treatment of the numerous diseases in whose pathogenesis the ET system is involved.

Bosentan, was the first ERA approved for the treatment of pulmonary arterial hypertension (PAH), a fatal and rare disease. Because bosentan exhibits distinct PK nonlinearity and considerable variability in PK and PD, a population model was developed to better characterise and understand the drug's properties. A target-mediated drug disposition (TMDD) model best described the nonlinear PK of bosentan, reflecting its strong receptor binding affinity and simultaneously describing the replacement of the endogenous ET-1 from its binding sites as well as bosentan's effect on blood pressure and heart rate. Additionally, the TMDD model structure, as developed for bosentan, was successfully applied to its successor compounds clazosentan and tezosentan. The model allowed to distinguish between selective ET_A and non-selective ET_A / ET_B antagonists as reflected by the absence of (indirect) evidence of drug-receptor internalisation by clazosentan. In addition, a diurnal receptor expression was integrated in the models, reflecting the observed multiple peak phenomenon in the PK profiles.

Furthermore, a population PK model for fluvoxamine was developed evaluating the effect of CYP2D6 phenotype and smoking on clearance and exposure of fluvoxamine. A one-compartment model with combined linear zero- and first order absorption and linear elimination was successfully applied to the data. The model showed, that CYP2C6 poor metabolisers are expected to have higher fluvoxamine plasma concentrations, because metabolisation of fluvoxamine through CYP2D6 is reduced. At the same time, it was shown that cigarette smoking induces the CYP1A2 metabolism of fluvoxamine and also leads to a decrease in oral absorption. Consequently exposure in smokers is expected to decrease compared to non-smokers. The population model underlined and confirmed the results of a fluvoxamine PBPK model as part of a DDI network with theophylline, caffeine, rifampicin, and midazolam, which can now be used for DDI predictions with CYP1A2.

9 Zusammenfassung

Modellierungs- und Simulationstechniken (M&S) können zur Charakterisierung und zum Verständnis des pharmakokinetischen (PK) und pharmakodynamischen (PD) Verhaltens eines Arzneimittels eingesetzt werden und damit Dosierungsstrategien und Entscheidungsfindung während der Arzneimittelentwicklung und für regulatorische Zwecke unterstützen.

Endothelin-Rezeptor-Antagonisten (ERAs) sind eine Klasse von kleinen Molekülen, die endogenes Endothelin-1 (ET-1) von seinen Rezeptor-Bindungsstellen verdrängen. Da ET-1 in der Pathogenese verschiedener Erkrankungen eine Rolle spielt, sind ERAs interessante Verbindungen für die Behandlung von Erkrankungen, in denen das ET-1-System involviert ist.

Bosentan war der erste ERA, der für die Behandlung der pulmonalen arteriellen Hypertonie (PAH), einer tödlichen und seltenen Krankheit, zugelassen wurde. Da Bosentan eine ausgeprägte nichtlineare PK und Variabilität in der PK und PD aufweist, wurde ein Populationsmodell entwickelt, um die Eigenschaften des Medikaments besser zu charakterisieren und zu verstehen. Ein sogenanntes target-mediated drug disposition (TMDD) PKPD-Modell beschrieb die nichtlineare PK von Bosentan am besten. So gelang es, die starke Rezeptor-Bindungsaffinität von Bosentan abzubilden und gleichzeitig die Verdrängung des natürlichen ET-1 aus diesen Bindungsstellen, sowie die Wirkung auf Blutdruck und Herzfrequenz zu beschreiben. Die für Bosentan entwickelte Modellstruktur, das TMDD-Modell, wurde erfolgreich auf dessen Nachfolgeprodukte Clazosentan und Tezosentan angewandt. Das Modell ermöglichte die Unterscheidung zwischen selektiven ET_A - und nicht-selektiven ET_A - / ET_B -Rezeptorantagonisten, was sich in der fehlenden Internalisierung des Wirkstoff-Rezeptor-Komplexes für Clazosentan widerspiegelt. Darüber hinaus wurde eine zeitlich schwankende Rezeptorexpression in das Modell integriert, die das beobachtete Phänomen mehrfacher Spitzen in den Plasmakonzentrationen der PK Profile beschreiben kann.

Zusätzliche wurde ein PK-Populationsmodell für Fluvoxamin entwickelt, um den Einfluß des CYP2D6-Phänotyps und des Rauchens auf die Clearance und die Fluvoxamin-Exposition zu untersuchen. Ein Ein-Kompartiment-Modell mit kombinierter linearer Absorption nullter und erster Ordnung sowie linearer Elimination wurde erfolgreich auf die Daten angewendet. Das Modell zeigte, dass bei schlechten CYP2C6 Metabolisierern höhere Fluvoxamin-Plasmakonzentrationen zu erwarten sind, da die Metabolisierung von Fluvoxamin durch CYP2D6 reduziert ist. Gleichzeitig wurde gezeigt, dass das Rauchen von Zigaretten den CYP1A2-Stoffwechsel von Fluvoxamin induziert und zusätzlich zu einer Abnahme der oralen Absorption führt. Folglich wird erwartet, dass die Exposition bei Rauchern im Vergleich zu Nichtrauchern abnimmt. Das Modell unterstrich und bestätigte die Ergebnisse eines physiologiebasierten PK (PBPK) Modells von Fluvoxamin als Teil eines Netzwerks für Arzneimittelwechselwirkungen mit Theophyllin, Koffein, Rifampicin und Midazolam, welches nun für Vorhersagen von Arzneimittelwechselwirkungen mit CYP1A2 verwendet werden kann.

10 References

1. Mould DR, Upton RN. Basic concepts in population modeling, simulation, and model-based drug development. *CPT Pharmacometrics Syst Pharmacol*. 2012 Sep;1, e6(9):1–12.
2. Box GEP, Draper NR. Empirical model-building and response surfaces. John Wiley & Sons, Inc. New York, 1986;
3. Lalonde RL, Kowalski KG, Hutmacher MM, Ewy W, Nichols DJ, Milligan PA, et al. Model-based drug development. *Clin Pharmacol Ther*. 2007;82(1):21–32.
4. Manolis E, Rohou S, Hemmings R, Salmonson T, Karlsson M, Milligan PA. The role of modeling and simulation in development and registration of medicinal products: output from the EFPIA/EMA modeling and simulation workshop. *CPT Pharmacometrics Syst Pharmacol*. 2013;2(2):e31.
5. Marshall S, Burghaus R, Cosson V, Cheung S, Chenel M, DellaPasqua O, et al. Good practices in model-informed drug discovery and development: practice, application, and documentation. *CPT Pharmacometrics Syst Pharmacol*. 2016;5(3):93–122.
6. Wang Y, Zhu H, Madabushi R, Liu Q, Huang S, Zineh I. Model-Informed Drug Development: Current US Regulatory Practice and Future Considerations. *Clin Pharmacol Ther*. 2019 Apr;105(4):899–911.
7. European Medicines Agency (EMA). Reflection paper on the use of extrapolation in the development of medicines for paediatrics. EMA/189724/2018. 2018;1–20. Available from: https://www.ema.europa.eu/en/documents/scientific-guideline/adopted-reflection-paper-use-extrapolation-development-medicines-paediatrics-revision-1_en.pdf
8. van der Graaf PH. CPT: pharmacometrics and systems pharmacology. *CPT Pharmacometrics Syst Pharmacol*. 2012 Sep;1(9):e8.
9. Ette, E.I. & Williams PJ. Pharmacometrics: the science of quantitative pharmacology. John Wiley & Sons, Inc., Hoboken, New Jersey, 2007;
10. European Medicines Agency (EMA), Committee for Human Medicinal Products (CHMP). Guideline on the reporting of physiologically based pharmacokinetic (PBPK) modelling and simulation - EMA/CHMP/458101/2016. 2018;1–16. Available from: http://www.ema.europa.eu/docs/en_GB/document_library/Scientific_guideline/2016/07/WC500211315.pdf%0Awww.elsevier.com/locate/apsb%0Awww.sciencedirect.com%0Ahttp://dx.doi.org/10.1016/j.apsb.2016.04.004
11. Kuepfer L, Niederalt C, Wendl T, Schlender J-F, Willmann S, Lippert J, et al. Applied concepts in PBPK modeling: how to build a PBPK/PD model. *CPT Pharmacometrics Syst Pharmacol*. 2016 Oct;5(10):516–31.
12. Yellepeddi V, Rower J, Liu X, Kumar S, Rashid J, Sherwin CMT. State-of-the-art review on physiologically based pharmacokinetic modeling in pediatric drug development. *Clin Pharmacokinet*. 2019 Jan 18;58(1):1–13.
13. European Medicines Agency (EMA), Committee for Human Medicinal Products (CHMP). Guideline on the investigation of drug interactions CPMP/EWP/560/95/Rev. 1 Corr. 2**. 2012;44(June):1–59. Available from: http://www.ema.europa.eu/docs/en_GB/document_library/Scientific_guideline/2012/07/WC50012960

14. Galiè N, Humbert M, Vachiery J-L, Gibbs S, Lang I, Torbicki A, et al. 2015 ESC/ERS guidelines for the diagnosis and treatment of pulmonary hypertension. *Eur Heart J*. 2015;1–58.
15. Peacock AJ, Murphy NF, Caballero L, Stewart S. An epidemiological study of pulmonary arterial hypertension. *Eur Respir J*. 2007;30:104–9.
16. Hoepfer MM, Huscher D, Pittrow D. Incidence and prevalence of pulmonary arterial hypertension in Germany. *Int J Cardiol*. 2016;203:612–3.
17. Girerd B, Montani D. Pulmonary arterial hypertension [Internet]. 2015 [cited 2019 Nov 12]. Available from: [https://www.orpha.net/consor/cgi-bin/Disease_Search.php?lng=EN&data_id=18210&Disease_Disease_Search_diseaseGroup=PAH&Disease_Disease_Search_diseaseType=Pat&Disease\(s\)/group_of_diseases=Pulmonary-arterial-hypertension&title=Pulmonary arterial hypertension&](https://www.orpha.net/consor/cgi-bin/Disease_Search.php?lng=EN&data_id=18210&Disease_Disease_Search_diseaseGroup=PAH&Disease_Disease_Search_diseaseType=Pat&Disease(s)/group_of_diseases=Pulmonary-arterial-hypertension&title=Pulmonary%20arterial%20hypertension&)
18. Galiè N, Humbert M, Vachiery JL, Gibbs S, Lang I, Torbicki A, et al. 2015 ESC / ERS guidelines for the diagnosis and treatment of pulmonary hypertension – web addenda the joint task force for the diagnosis and treatment of pulmonary hypertension of the European Society of Cardiology (ESC) and of the european respiratory. *Eur Heart J*. 2015;
19. Hoepfer MM, Ghofrani H, Grünig E, Klose H, Olschewski H, Rosenkranz S. Pulmonary hypertension. *Dtsch Arztebl Int*. 2017;114:73–84.
20. Rosenkranz S, Preston IR. Right heart catheterisation: best practice and pitfalls in pulmonary hypertension. *Eur Respir Rev*. 2015;24:642–52.
21. Sysol JR, Machado RF. Classification and pathophysiology of pulmonary hypertension. *Contin Cardiol Educ*. 2018;4(1):2–12.
22. Enright PL. The six-minute walk test. *Respir Care*. 2003;48(8):783–5.
23. Crapo RO, Casaburi R, Coates AL, Enright PL, MacIntyre NR. American Thoracic Society ATS Statement : Guidelines for the six-minute walk test. *Am J Respir Crit Care Med*. 2002;166:111–7.
24. Montani D, Günther S, Dorfmueller P, Perros F, Girerd B, Garcia G, et al. Pulmonary arterial hypertension. *Orphanet J Rare Dis*. 2013;8:1–28.
25. Humbert M, Morrell NW, Archer SL, Stenmark KR, Maclean MR, Sc B, et al. Cellular and molecular pathobiology of pulmonary arterial hypertension. *J Am Coll Cardiol*. 2004;43(12):S13–24.
26. Webb DJ. Endothelin: from molecule to man. *Br J Clin Pharmacol*. 1997;44(1):9–20.
27. D'Orléans-Juste P, Plante M, Honoré JC, Carrier E, Labonté J. Synthesis and degradation of endothelin-1. *Can J Physiol Pharmacol*. 2003;81(6):503–10.
28. Kohan DE, Rossi NF, Inscho EW, Pollock DM. Regulation of blood pressure and salt homeostasis by endothelin. *Physiol Rev*. 2011;91(1):1–77.
29. Barton M, Yanagisawa M. Endothelin: 30 years from discovery to therapy. *Hypertension*. 2019;1:1232–65.
30. Boesen E. Endothelin receptors, renal effects and blood pressure. *Curr Opin Pharmacol*. 2015;21:25–

- 34.
31. Haynes WG, Webb DJ. Endothelin as a regulator of cardiovascular function in health and disease. *J Hypertens*. 1998;16(8):1081–98.
 32. Opitz CF, Ewert R, Kirch W, Pittrow D. Inhibition of endothelin receptors in the treatment of pulmonary arterial hypertension: does selectivity matter? *Eur Heart J*. 2008;29(16):1936–48.
 33. Humbert M, Sitbon O, Simonneau G. Drug treatment of pulmonary arterial hypertension. *N Engl J Med*. 2004;(351):1426–36.
 34. Chun M, Lin HY, Henis YI, Lodish HF. Endothelin-induced endocytosis of cell surface ETA receptors: endothelin remains intact and bound to the ETA receptor. *J Biol Chem*. 1995;270(18):10855–60.
 35. Bremnes T, Paasche JD, Mehlum A, Sandberg C, Bremnes B, Attramadal H. Regulation and intracellular trafficking pathways of the endothelin receptors. *J Biol Chem*. 2000;275(23):17596–604.
 36. Burkhardt M, Barton M, Shaw SG. Receptor- and non-receptor-mediated clearance of big-endothelin and endothelin-1: differential effects of acute and chronic ETA receptor blockade. *J Hypertens*. 2000;18(3):273–9.
 37. Nakov R, Pfarr E, Eberle S. Darusentan: an effective endothelin A receptor antagonist for treatment of hypertension. *Am J Hypertens*. 2002;15(7):583–9.
 38. Barton M, Haudenschild CC, D’Uscio L V., Shaw S, Münter K, Lüscher TF. Endothelin ETA receptor blockade restores NO-mediated endothelial function and inhibits atherosclerosis in apolipoprotein E-deficient mice. *Proc Natl Acad Sci U S A*. 1998;95(24):14367–72.
 39. Caligiuri G, Levy B, Pernow J, Thorén P, Hansson GK. Myocardial infarction mediated by endothelin receptor signaling in hypercholesterolemic mice. *Proc Natl Acad Sci U S A*. 1999;96(12):6920–4.
 40. Ortmann J, Amann K, Brandes RP, Kretzler M, Münter K, Parekh N, et al. Role of podocytes for reversal of glomerulosclerosis and proteinuria in the aging kidney after endothelin inhibition. *Hypertension*. 2004;44(6):974–81.
 41. Astra Zeneca. Zibotentan (ZD4054) mechanism of action: endothelin receptor A (ETA) antagonist [Internet]. 2020 [cited 2020 Jan 27]. Available from: <https://openinnovation.astrazeneca.com/Zibotentan-ZD4054.html>
 42. Raichlin E, Prasad A, Mathew V, Kent B, Holmes DR, Pumper GM, et al. Efficacy and safety of atrasentan in patients with cardiovascular risk and early atherosclerosis. *Hypertension*. 2008;52(3):522–8.
 43. Yoon MH, Reriani M, Mario G, Rihal C, Gulati R, Lennon R, et al. Long-term endothelin receptor antagonism attenuates coronary plaque progression in patients with early atherosclerosis. *Int J Cardiol*. 2013;168(2):1316–21.
 44. AbbVie closes SONAR study evaluating investigational compound atrasentan on renal outcomes in patients with diabetic nephropathy. 2017 [cited 2020 Jan 28]; Available from: <https://news.abbvie.com/news/press-releases/therapeutic-area/general-medicine/abbvie-statement-on-sonar-study-closure.htm>
 45. Wenzel RR, Littke T, Kuranoff S, Jürgens C, Bruck H, Ritz E, et al. Avosentan reduces albumin excretion in diabetics with macroalbuminuria. *J Am Soc Nephrol*. 2009;20(3):655–64.

46. European Medicines Agency (EMA), Committee for Human Medicinal Products (CHMP). Bosentan for treatment of pulmonary arterial hypertension and chronic thromboembolic pulmonary hypertension Orphan designation EU/3/01/019. 2001 [cited 2020 Jan 27]; Available from: <https://www.ema.europa.eu/en/medicines/human/orphan-designations/eu301019>
47. European Medicines Agency (EMA), Committee for Human Medicinal Products (CHMP). Public summary of opinion on orphan designation bosentan for the treatment of pulmonary arterial hypertension and chronic thromboembolic pulmonary EMA/COMP/1280/2003 Rev.4 hypertension [Internet]. 2013 [cited 2020 Jan 27]. Available from: https://www.ema.europa.eu/en/documents/orphan-designation/eu/3/01/019-public-summary-positive-opinion-orphan-designation-bosentan-treatment-pulmonary-arterial_en.pdf
48. European Medicines Agency (EMA). Summary of product characteristics Tracleer. 2019 [cited 2020 Jan 27]; Available from: https://www.ema.europa.eu/en/documents/product-information/tracleer-epar-product-information_en.pdf
49. Galiè N, Rubin L, Hoeper M, Jansa P, Al-Hiti H, Meyer G, et al. Treatment of patients with mildly symptomatic pulmonary arterial hypertension with bosentan (EARLY study): a double-blind, randomised controlled trial. *Lancet*. 2008;371:2093–100.
50. Benza RL, Raina A, Gupta H, Murali S, Burden A, Zastrow MS, et al. Bosentan-based, treat-to-target therapy in patients with pulmonary arterial hypertension: Results from the COMPASS-3 study. *Pulm Circ*. 2018;8(1):1–13.
51. Gruenig E, Michelakis E, Vachiéry JL, Vizza CD, Meyer FJ, Doelberg M, et al. Acute hemodynamic effects of single-dose sildenafil when added to established bosentan therapy in patients with pulmonary arterial hypertension: Results of the COMPASS-1 study. *J Clin Pharmacol*. 2009;49(11):1343–52.
52. McLaughlin V, Channick RN, Ghofrani HA, Lemarié JC, Naeije R, Packer M, et al. Bosentan added to sildenafil therapy in patients with pulmonary arterial hypertension. *Eur Respir J*. 2015;46(2):405–13.
53. Carter NJ, Keating GM. Bosentan: in pediatric patients with pulmonary arterial hypertension. *Pediatr Drugs*. 2010;12(1):63–73.
54. Berger RMF, Haworth SG, Bonnet D, Dulac Y, Fraisse A, Galiè N, et al. FUTURE-2: results from an open-label, long-term safety and tolerability extension study using the pediatric formulation of bosentan in pulmonary arterial hypertension. *Int J Cardiol*. 2016;202:52–8.
55. Berger RMF, Gehin M, Beghetti M, Ivy D, Kusic-Pajic A, Cornelisse P, et al. A bosentan pharmacokinetic study to investigate dosing regimens in paediatric patients with pulmonary arterial hypertension: FUTURE-3. *Br J Clin Pharmacol*. 2017;83(8):1734–44.
56. Steinhorn RH, Fineman J, Kusic-Pajic A, Cornelisse P, Gehin M, Nowbakht P, et al. Bosentan as adjunctive therapy for persistent pulmonary hypertension of the newborn: results of the randomized multicenter placebo-controlled exploratory trial. *J Pediatr*. 2016;177:90–96.e3.
57. Dingemans J, van Giersbergen PLM. Clinical pharmacology of bosentan, a dual endothelin receptor antagonist. *Clin Pharmacokinet*. 2004;43(15):1089–115.
58. European Medicines Agency (EMA). Scientific discussion. 2005 [cited 2020 Jan 27];1–38. Available from: https://www.ema.europa.eu/en/documents/scientific-discussion/tracleer-epar-scientific-discussion_en.pdf
59. Markert C, Schweizer Y, Hellwig R, Wirsching T, Riedel KD, Burhenne J, et al. Clarithromycin substantially

- increases steady-state bosentan exposure in healthy volunteers. *Br J Clin Pharmacol.* 2013;77(1):141–8.
60. Weber C, Schmitt R, Birnboeck H, Hopfgartner G, van Marle SP, Peeters PAM, et al. Pharmacokinetics and pharmacodynamics of the endothelin-receptor antagonist bosentan in healthy human subjects. *Clin Pharmacol Ther.* 1996;60(2):124–37.
 61. Weber C, Schmitt R, Birnboeck H, Hopfgartner G, Eggert H, Meyer J, et al. Multiple-dose pharmacokinetics, safety, and tolerability of bosentan, an endothelin receptor antagonist, in healthy male volunteers. *J Clin Pharmacol.* 1999;39(7):703–14.
 62. van Giersbergen PLM, Halabi A, Dingemans J. Single- and multiple-dose pharmacokinetics of bosentan and its interaction with ketoconazole. *Br J Clin Pharmacol.* 2002;53(6):589–95.
 63. Roux S, Breu V, Giller T, Neidhart W, Ramuz H, Coassolo P, et al. Ro 61-1790, a new hydrosoluble endothelin antagonist: general pharmacology and effects on experimental cerebral vasospasm. *J Pharmacol Exp Ther.* 1997;283(3):1110–8.
 64. van Giersbergen PLM, Dingemans J. Tolerability, pharmacokinetics, and pharmacodynamics of clazosentan, a parenteral endothelin receptor antagonist. *Eur J Clin Pharmacol.* 2007;63(2):151–8.
 65. Vajkoczy P, Meyer B, Weidauer S, Raabe A, Thome C, Ringel F, et al. Clazosentan (AXV-034343), a selective endothelin A receptor antagonist, in the prevention of cerebral vasospasm following severe aneurysmal subarachnoid hemorrhage: results of a randomized, double-blind, placebo-controlled, multicenter Phase IIa study. *J Neurosurg.* 2005;103(1):9–17.
 66. Mayer SA, Aldrich EF, Bruder N, Hmissi A, Macdonald RL, Viarasilpa T, et al. Thick and diffuse subarachnoid blood as a treatment effect modifier of clazosentan after subarachnoid hemorrhage. *Stroke.* 2019;50(10):2738–44.
 67. MacDonald RL, Kassell NF, Mayer S, Ruefenacht D, Schmiedek P, Weidauer S, et al. Clazosentan to overcome neurological ischemia and infarction occurring after subarachnoid hemorrhage (CONSCIOUS-1): randomized, double-blind, placebo-controlled phase 2 dose-finding trial. *Stroke.* 2008;39(11):3015–21.
 68. Macdonald RL, Higashida RT, Keller E, Mayer SA, Molyneux A, Raabe A, et al. Clazosentan, an endothelin receptor antagonist, in patients with aneurysmal subarachnoid haemorrhage undergoing surgical clipping: a randomised, double-blind, placebo-controlled phase 3 trial (CONSCIOUS-2). *Lancet Neurol.* 2011;10(7):618–25.
 69. MacDonald RL, Higashida RT, Keller E, Mayer SA, Molyneux A, Raabe A, et al. Randomized trial of clazosentan in patients with aneurysmal subarachnoid hemorrhage undergoing endovascular coiling. *Stroke.* 2012;43(6):1463–9.
 70. van Giersbergen PLM, Dingemans J. Effect of gender on the tolerability, safety and pharmacokinetics of clazosentan following long-term infusion. *Clin Drug Investig.* 2007;27(11):797–802.
 71. Zisowsky J, Fuseau E, Bruderer S, Krause A, Dingemans J. Challenges in collecting pharmacokinetic and pharmacodynamic information in an intensive care setting: PK/PD modelling of clazosentan in patients with aneurysmal subarachnoid haemorrhage. *Eur J Clin Pharmacol.* 2014;70(4):409–19.
 72. Juif PE, Voors-Pette C, Ufer M, Dogterom P, Dingemans J. Influence of rifampin-mediated organic anion-transporting polypeptide 1B1/1B3 inhibition on the pharmacokinetics of clazosentan. *Clin Transl Sci.* 2019;12(5):440–4.

73. van Giersbergen PLM, Treiber A, Dingemans J. In vitro and in vivo pharmacokinetic characteristics of clazosentan, an intravenous endothelin receptor antagonist, in humans. *Int J Clin Pharmacol Ther.* 2009;47(3):169–77.
74. Gatfield J, Mueller Grandjean C, Sasse T, Clozel M, Nayler O. Slow receptor dissociation kinetics differentiate macitentan from other endothelin receptor antagonists in pulmonary arterial smooth muscle cells. *PLoS One.* 2012;7(10):e47662.
75. Dingemans J, Clozel M, van Giersbergen PLM. Entry-into-humans study with tezosentan, an intravenous dual endothelin receptor antagonist. *J Cardiovasc Pharmacol.* 2002;39(6):795–802.
76. Dingemans J, Clozel M, van Giersbergen PLM. Pharmacokinetics and pharmacodynamics of tezosentan, an intravenous dual endothelin receptor antagonist, following chronic infusion in healthy subjects. *Br J Clin Pharmacol.* 2002;53(4):355–62.
77. Clozel M, Ramuz H, Clozel JP, Breu V, Hess P, Löffler BM, et al. Pharmacology of tezosentan, new endothelin receptor antagonist designed for parenteral use. *J Pharmacol Exp Ther.* 1999;290(2):840–6.
78. Treiber A, van Giersbergen PLM, Dingemans J. In vivo and in vitro disposition profile of tezosentan, an intravenous dual endothelin receptor antagonist, in humans. *Xenobiotica.* 2003;33(4):399–414.
79. van Giersbergen PLM. Cyclosporin increases the exposure to tezosentan, an intravenous dual endothelin receptor antagonist. 2002;58:243–5.
80. de Vries MH, van Harten J, van Bommel P, Raghoobar M. Pharmacokinetics of fluvoxamine maleate after increasing single oral doses in healthy subjects. *Biopharm Drug Dispos.* 1993;14(4):291–6.
81. de Vries MH, Raghoobar M, Mathlener S, van Harten J. Single and multiple oral dose fluvoxamine kinetics in young and elderly subjects. *Ther Drug Monit.* 1992;14:493–8.
82. Spigset O, Carlborg L, Hedenmalm K, Dahlqvist R. Effect of cigarette smoking on fluvoxamine pharmacokinetics in humans. *Clin Pharmacol Ther.* 1995;58(4):399–403.
83. FDA. Drug development and drug interactions: table of substrates , inhibitors and inducers. 2019 [cited 2020 Jan 7]; Available from: <https://www.fda.gov/drugs/drug-interactions-labeling/drug-development-and-drug-interactions-table-substrates-inhibitors-and-inducers#table2-1>
84. Carrillo JA, Dahl ML, Svensson JO, Alm C, Rodríguez I, Bertilsson L. Disposition of fluvoxamine in humans is determined by the polymorphic CYP2D6 and also by the CYP1A2 activity. *Clin Pharmacol Ther.* 1996;60(2):183–90.
85. Zhou SF, Liu JP, Chowbay B. Polymorphism of human cytochrome P450 enzymes and its clinical impact. *Drug Metab Rev.* 2009;41(2):89–295.
86. Zanger UM, Turpeinen M, Klein K, Schwab M. Functional pharmacogenetics/genomics of human cytochromes P450 involved in drug biotransformation. *Anal Bioanal Chem.* 2008;392(6):1093–108.
87. Guttman Y, Nudel A, Kerem Z. Polymorphism in cytochrome P450 3A4 is ethnicity related. *Front Genet.* 2019 Mar;10:Article 224.
88. Dingemans J, van Giersbergen PLM, Patat A, Nilsson PN. Mutual pharmacokinetic interactions between bosentan and lopinavir/ritonavir in healthy participants. *Antivir Ther.* 2010;15(2):157–63.
89. Paul GA, Gibbs JSR, Boobis AR, Abbas A, Wilkins MR. Bosentan decreases the plasma concentration of

- sildenafil when coprescribed in pulmonary hypertension. *Br J Clin Pharmacol*. 2005;60(1):107–12.
90. Wrishko RE, Dingemans J, Yu A, Darstein C, Phillips DL, Mitchell MI. Pharmacokinetic interaction between tadalafil and bosentan in healthy male subjects. *J Clin Pharmacol*. 2008;48(5):610–8.
 91. Dingemans J, Schaarschmidt D, van Giersbergen PLM. Investigation of the mutual pharmacokinetic interactions between bosentan, a dual endothelin receptor antagonist, and simvastatin. *Clin Pharmacokinet*. 2003;42(3):293–301.
 92. Weber C, Banken L, Birnboeck H, Nave S, Schulz R. The effect of bosentan on the pharmacokinetics of digoxin in healthy male subjects. *Br J Clin Pharmacol*. 1999;47(6):701–6.
 93. Weber C, Banken L, Birnboeck H, Schulz R. Effect of the endothelin-receptor antagonist bosentan on the pharmacokinetics and pharmacodynamics of warfarin. *J Clin Pharmacol*. 1999;39:847–54.
 94. van Giersbergen PLM, Treiber A, Clozel M, Bodin F, Dingemans J. In vivo and in vitro studies exploring the pharmacokinetic interaction between bosentan, a dual endothelin receptor antagonist, and glyburide. *Clin Pharmacol Ther*. 2002;71(4):253–62.
 95. Binet I, Wallnöfer A, Weber C, Jones R, Thiel G. Renal hemodynamics and pharmacokinetics of bosentan with and without cyclosporine A. *Kidney Int*. 2000;57(1):224–31.
 96. Shebley M, Sandhu P, Emami Riedmaier A, Jamei M, Narayanan R, Patel A, et al. Physiologically based pharmacokinetic model qualification and reporting procedures for regulatory submissions: a consortium perspective. *Clin Pharmacol Ther*. 2018 Jul;104(1):88–110.
 97. Britz H, Hanke N, Volz A-K, Spigset O, Schwab M, Eissing T, et al. Physiologically-Based Pharmacokinetic Models for CYP1A2 Drug–Drug Interaction Prediction: A Modeling Network of Fluvoxamine, Theophylline, Caffeine, Rifampicin, and Midazolam. *CPT Pharmacometrics Syst Pharmacol*. 2019 May 13;8(5):296–307.
 98. Spigset O, Granberg K, Hägg S, Norström Å, Dahlqvist R. Relationship between fluvoxamine pharmacokinetics and CYP2D6/CYP2C19 phenotype polymorphisms. *Eur J Clin Pharmacol*. 1997;52(2):129–33.
 99. Maury E. Off the clock: from circadian disruption to metabolic disease. *Int J Mol Sci*. 2019;20(7):1–25.
 100. Halberg F. Circadian (about twenty-four-hour) rhythms in experimental medicine [Abridged]. *Proc R Soc Med*. 1963 Apr;56(4):253–7.
 101. Lemmer B. *Chronopharmakologie*. 4th ed. Wissenschaftliche Verlagsgesellschaft Stuttgart; 2012.
 102. Albrecht U. Functional genomics of sleep and circadian rhythm invited review: regulation of mammalian circadian clock genes. *J Appl Physiol*. 2002;92:1348–55.
 103. Kalafatakis K. Rhythmicity as an important regulatory factor in complex biological systems: introduction to chronopharmacology. *Ann Res Hosp*. 2018;2(14):1–7.
 104. Konopka RJ, Benzer S. Clock mutants of *Drosophila melanogaster*. *Proc Natl Acad Sci U S A*. 1971;68(9):2112–6.
 105. The Nobel Prize in Physiology or Medicine 2017. [cited 2020 Jan 28]; Available from: <https://www.nobelprize.org/prizes/medicine/2017/press-release/>

106. Zehring WA, Wheeler DA, Reddy P, Konopka RJ, Kyriascou CP, Rosbash M, et al. P-element transformation with period locus DNA restores rhythmicity to mutant, arrhythmic drosophila melanogaster. *Cell*. 1984;39(Part 1):369–76.
107. Siwicki KK, Eastman C, Petersen G, Rosbash M, Hall JC. Antibodies to the period gene product of drosophila reveal diverse tissue distribution and rhythmic changes in the visual system. *Neuron*. 1988;1(2):141–50.
108. Hall J, Rosbash M. Mutations and molecules influencing biological rhythms. *Annu Rev Neurosci*. 1988;11:373–93.
109. Rosbash M, Hall JC. The molecular biology of circadian rhythms. *Neuron*. 1989;3:387–98.
110. Bargiello TA, Jackson FR, Young MW. Restoration of circadian behavioural rhythms by gene transfer in drosophila. *Nature*. 1984;312:752–4.
111. Hardin PE, Hall JC, Rosbash M. Feedback of the drosophila period gene product on circadian cycling of its messenger RNA levels. *Nature*. 1990;343:536–40.
112. Vosshall LB, Price JL, Sehgal A, Saez L, Young MW. Block in nuclear localization of period protein by a second clock mutation, timeless. *Science*. 1994;263:1606–9.
113. Price JL, Blau J, Rothenfluh A, Abodeely M, Kloss B, Young MW. Double-time is a novel drosophila clock gene that regulates period protein accumulation. *Cell*. 1998;94(1):83–95.
114. Linsell CR, Lightman SL, Mullen PE, Brown MJ, Causon RC. Circadian rhythms of epinephrine and norepinephrine in man. *J Clin Endocrinol Metab*. 1985;60(6):1210–5.
115. Naafs MA. Glucocorticoid chronotherapy: a mini-review. *Endocrinol Int J*. 2018;6(2):118–22.
116. Baker FC, Driver HS. Circadian rhythms , sleep , and the menstrual cycle. *Sleep Med*. 2007;8:613–22.
117. Richards J, Welch AK, Barilovits SJ, All S, Cheng KY, Wingo CS, et al. Tissue-specific and time-dependent regulation of the endothelin axis by the circadian clock protein Per1. *Life Sci*. 2014;118(2):255–62.
118. Herold M, Cornélissen G, Loeckinger A, Koeberle D, Koenig P, Halberg F. About 8-hour variation of circulating human endothelin-1. *Peptides*. 1998;19(5):821–5.
119. Loeckinger A, Herold M, Cornelissen G, Halberg F, Fiser B. Circaoctohoran (about 8-hourly) chronome component of circulating human endothelin-1 in health. *Scr Medica Fac Medicae Univ Brun Masaryk*. 1998;71(4):199–207.
120. Lemmer B. Wie innere Uhren die Wirksamkeit von Medikamenten beeinflussen: Chronopharmakologie. *Biol Unserer Zeit*. 2013;43(4):220–7.
121. Lemmer B. Chronopharmacokinetics: implications for drug treatment. *J Pharm Pharmacol*. 1999;51(8):887–90.
122. Germain A, Kupfer DJ. Circadian rhythm disturbances in depression. *Hum Psychopharmacol*. 2008;23(7):571–85.
123. De Lavallaz L, Musso CG. Chronobiology in nephrology: the influence of circadian rhythms on renal handling of drugs and renal disease treatment. *Int Urol Nephrol*. 2018;50(12):2221–8.

124. Sheiner LB, Rosenberg B, Melmon KL. Modelling of individual pharmacokinetics for computer-aided drug dosage. *Comput Biomed Res.* 1972 Oct;5(5):441–59.
125. Karlsson MO, Jonsson EN, Wiltse CG, Wade JR. Assumption testing in population pharmacokinetic models: illustrated with an analysis of moxonidine data from congestive heart failure patients. *J Pharmacokinet Biopharm.* 1998;26(2):207–46.
126. Bergstrand M, Hooker AC, Wallin JE, Karlsson MO. Prediction-corrected visual predictive checks for diagnosing nonlinear mixed-effects models. *AAPS J.* 2011 Jun 8;13(2):143–51.
127. Levy G. Pharmacologic target-mediated drug disposition. *Clin Pharmacol Ther.* 1994;56(3):248–52.
128. An G. Small-molecule compounds exhibiting target-mediated drug disposition (TMDD): a minireview. *J Clin Pharmacol.* 2017;57(2):137–50.
129. Mager DE, Jusko WJ. General pharmacokinetic model for drugs exhibiting target-mediated drug disposition. *J Pharmacokinet Pharmacodyn.* 2001;28(6):507–32.
130. Suzuki Y, Sugai T, Fukui N, Watanabe J, Ono S, Inoue Y, et al. CYP2D6 genotype and smoking influence fluvoxamine steady-state concentration in Japanese psychiatric patients: Lessons for genotype-phenotype association study design in translational pharmacogenetics. *J Psychopharmacol.* 2011;25(7):908–14.
131. Oliveira P, Ribeiro J, Donato H, Madeira N. Smoking and antidepressants pharmacokinetics: a systematic review. *Ann Gen Psychiatry.* 2017;16(1):1–8.

Images

I took the photos on the pages 3 and 67 during my walk through the Scottish Lowlands and Highlands in 2019. For me, the photos symbolise that the stoniest paths can often be the most beautiful and exciting ones and that it is always worthwhile to go on and risk a look around the corner.

The illustrations of drugs and people in the graphical abstract were taken from <https://smart.servier.com>.

The Figures 1 to 5 were stylistically revised and illustrated by Thomas Gronle (www.gronle-legron.de).



Appendix

- I. A.-K. Volz, A. Krause, W.E. Haefeli, J. Dingemanse, T. Lehr, Target-Mediated Drug Disposition Pharmacokinetic–Pharmacodynamic Model of Bosentan and Endothelin-1, *Clin. Pharmacokinet.* 56 (2017) 1499–1511. doi:10.1007/s40262-017-0534-4.
- II. A.-K. Volz, J. Dingemanse, A. Krause, T. Lehr, Target-Mediated Population Pharmacokinetic Modeling of Endothelin Receptor Antagonists., *Pharm. Res.* 37 (2019) 2. doi:10.1007/s11095-019-2723-3.
- III. H. Britz, N. Hanke, A.-K. Volz, O. Spigset, M. Schwab, T. Eissing, et al., Physiologically-Based Pharmacokinetic Models for CYP1A2 Drug–Drug Interaction Prediction: A Modeling Network of Fluvoxamine, Theophylline, Caffeine, Rifampicin, and Midazolam, *CPT Pharmacometrics Syst. Pharmacol.* 8 (2019) 296–307. doi:10.1002/psp4.12397.

Target-Mediated Drug Disposition Pharmacokinetic–Pharmacodynamic Model of Bosentan and Endothelin-1

Anke-Katrin Volz¹ · Andreas Krause² · Walter Emil Haefeli³ · Jasper Dingemans² · Thorsten Lehr¹

Published online: 11 April 2017
© Springer International Publishing Switzerland 2017

Abstract

Background and Objectives Bosentan is a competitive antagonist on endothelin receptor A and B (ET_A and ET_B), displacing the endogenous binding partner endothelin-1 (ET-1) from its binding sites. After administration of escalating single doses of 10–750 mg as an intravenous (i.v.) infusion, bosentan showed dose-dependent pharmacokinetics (PK). The aim of this analysis was to develop a PK model of bosentan after i.v. administration including competitive antagonism with ET-1 and to analyze its influence on blood pressure and heart rate with a combined pharmacokinetic/pharmacodynamic (PK/PD) model.

Methods PK/PD data from 70 young male Caucasian subjects were analyzed after single i.v. administration of 10, 50, 250, 500, and 750 mg of bosentan. Population analyses, simulations, and evaluation were performed using a non-linear mixed-effects modeling approach.

Results The PK of bosentan was best described by a two-compartment, target-mediated drug disposition (TMDD)

model. ET-1 plasma and urine profiles were successfully integrated into the bosentan two-compartment, TMDD model encompassing competition for the same receptor. A multiple-peak phenomenon of bosentan plasma concentrations after i.v. administration was best described by a diurnal expression or reappearance of ET receptors on the cell surface. Blood pressure was best described by an E_{\max} model; heart rate was modeled as a compensatory effect of changes in blood pressure.

Conclusion The developed competitive PK/PD model of bosentan and ET-1 after i.v. administration provides a first step towards understanding the complex PK properties of bosentan and offers a valuable tool for future PK/PD research.

Key Points

Based on data from a single i.v. administration across a wide dose range (10–750 mg), for the first time, a TMDD model was developed for bosentan explaining the non-linearity in PK and its effect on ET-1 in plasma and urine.

The model proposes a new hypothesis that a circadian expression of ET receptor(s) explains a multiple-peak phenomenon in the profile of bosentan.

The effect of bosentan on blood pressure was best described by the amount of bosentan bound to the receptor and modeled by an E_{\max} model, whereas the increase in heart rate was modeled as a compensatory effect of changes in blood pressure.

Electronic supplementary material The online version of this article (doi:10.1007/s40262-017-0534-4) contains supplementary material, which is available to authorized users.

✉ Thorsten Lehr
thorsten.lehr@mx.uni-saarland.de

¹ Clinical Pharmacy, Saarland University, Campus C2 2, 66123 Saarbrücken, Germany

² Department of Clinical Pharmacology, Actelion Pharmaceuticals Ltd, Allschwil, Switzerland

³ Department of Clinical Pharmacology and Pharmacoepidemiology, Heidelberg University, Heidelberg, Germany

1 Background and Objectives

Bosentan is one of the most frequently used drugs in the therapy of pulmonary arterial hypertension (PAH). Bosentan is a dual endothelin receptor A and B (ET_A, ET_B) antagonist displacing endothelin-1 (ET-1) from its binding site, causing vasodilatation and blood pressure reduction preferentially in the pulmonary but also in the systemic circulation.

Bosentan is highly bound to albumin ($\geq 98\%$) [1], eliminated via the bile into the intestine, and mainly excreted with feces [2]. After uptake into the hepatocytes via organic anion transporting polypeptides (OATP1B1 and OATP1B3), bosentan is metabolized by cytochrome P450 (CYP) isozymes CYP3A4, CYP2C9, and CYP2C19 [1]. Three metabolites are formed of which the main metabolite, hydroxybosentan, actively contributes to the overall efficacy with 10–20% [1]. Bosentan exhibits auto-induction by inducing the metabolizing enzymes CYP3A4, CYP2C9, and possibly CYP2C19 [1]. It is a substrate and possibly an inducer of P-glycoprotein (P-gp) and also an inhibitor of the bile salt export pump (BSEP) [3].

Bosentan is administered as a tablet in a dose-escalating manner, starting with 62.5 mg up to 125 mg twice daily [1, 3]. When administered in a wide and off-label dose range of 10–750 mg as an intravenous (i.v.) infusion, bosentan showed a marked inter-individual variability (IIV) and dose-dependent pharmacokinetics (PK) up to 500 mg [4]; the area under the plasma concentration-time curve (AUC) increased disproportionately while clearance and volume of distribution decreased with higher doses [4]. Although bosentan is frequently applied in the treatment of PAH, its PK is still not completely understood and, to our knowledge, no PK or PD model is publically available describing bosentan plasma concentrations and their influence on blood pressure neither with nor without taking into account the competitive antagonism with ET-1.

The aims of these analyses were (1) the development of a PK model of bosentan after i.v. administration including competitive antagonism with ET-1, (2) the development of PK/PD models for the effects on blood pressure and heart rate, and (3) to perform a covariate identification on the final PK/PD model.

2 Methods

2.1 Study Design

Data from the first-in-human study of bosentan in healthy subjects were used for analyses. A brief summary of the

study design is outlined below [4]. Bosentan was administered as an i.v. infusion of 10, 50, 250, 500, or 750 mg with varying infusion rates and combinations resulting in nine different dosing groups (Supplementary Table S1). In each dosing group, six participants were treated with bosentan and two received a 5% dextrose placebo infusion. In dosing group 8, bosentan was administered without a placebo control (i.v. vs. oral administration). Treatment was administered between 8 and 9 a.m. after fasting overnight. Blood samples for bosentan plasma concentrations were taken pre-dose and 5, 10, 20, and 30 min and 1, 1.25, 2.5, 4, 6, 8, 10, 12, and 24 h after dosing. ET-1 plasma levels were taken pre-dose, and after 35 min, 2.5, 6, and 24 h. ET-1 urine samples were taken over the following intervals: pre-dose, 0–4, 4–8, 8–12, and 12–24 h. Systolic and diastolic blood pressure (SBP and DBP) as well as heart rate were measured nine times between the pre-dose and 24 h after dosing.

Plasma concentrations of bosentan were determined either by HPLC-UV or narrow-bore HPLC with tandem mass spectrometry detection using ion spray, depending on the drug concentration. The lower limit of quantification for HPLC-UV was 50 ng/mL (0.088 nmol/mL) and for the HPLC-MS method was 500 pg/mL (8.8×10^{-4} nmol/mL). Plasma and urine levels of ET-1 were analyzed by a radioimmunological assay [5]. ET-1 in plasma was determined in dose groups 1–7 and 9. Urine levels of ET-1 were determined for dose groups 1–5. Total circulating bosentan and ET-1 levels, i.e., unbound (free) compounds and those bound to plasma proteins were determined, but not those bound to the receptor because the receptor is not soluble.

2.2 Model Development and Evaluation

Population analyses, simulations, and model evaluations were performed using non-linear mixed-effects modeling techniques (NONMEM, Version 7.3; ICON Development Solutions, Ellicott City, MD, USA). These allowed estimation of population means (medians) for PK and PK/PD model parameters and quantification of IIV and residual (unexplained) variability. Model selection was based on visual inspection of goodness-of-fit plots, precision of parameter estimates, and the objective function value (OFV) provided by NONMEM. A nested model was considered superior to another when the OFV was reduced by 3.84 units [χ^2 test statistic, $p < 0.05$, 1 degree of freedom (DF)]. All pre-dose values (PK and PD) were set to time zero. SAS, Version 9.4 (SAS Institute Inc., Cary, NC, USA) was used for statistical analyses and generation of graphics.

Model development was performed sequentially. First, a PK model for bosentan plasma concentrations was developed. Subsequently, ET-1 measurements in plasma and urine were included. One-, two-, and three-compartment models with linear or non-linear distribution and elimination processes (e.g., Michaelis–Menten) were evaluated. As binding of bosentan to its receptors is tight and might influence the PK, additionally, various target-mediated drug disposition (TMDD) models [6] were explored. Binding kinetics of TMDD models are usually not easy to identify; therefore, model exploration was performed sequentially by fixing some parameter values alternately and estimating them in the next steps. The final PK model was used as a basis for the PK/PD model, linking blood pressure and heart rate to the PK model. PK parameter values were fixed to their estimates and SBP, DBP, and heart rate were modeled simultaneously, but not linked to each other. Different linear, exponential, and E_{\max} models were evaluated. Direct links to plasma concentration, indirect link models, indirect response models, and effect compartment models were explored. Further, the circadian rhythm of blood pressure was included in the model and the model was simplified by linking heart rate increase as a result of the change in blood pressure.

For the final PK and PK/PD model, the following pre-specified covariates were investigated: age, weight, height, body mass index, creatinine clearance, serum creatinine, bilirubin, serum glutamate pyruvate transaminase, serum glutamic-oxaloacetic transaminase, alkaline phosphatase, gamma-glutamyl transpeptidase, albumin, protein, cholesterol, hemoglobin, and hematocrit. Continuous covariate effects were modeled as exponential terms centered on the median.

Covariate analysis was performed on the PK and PK/PD model in a stepwise procedure. Covariates were tested one by one (univariate) for statistical significance ($p < 0.01$), added to the model using a forward inclusion, and eliminated in a backward elimination procedure with significance levels of 1 and 0.1%, respectively. A visual predictive check (VPC) based on 1000 simulations using the final PK and PK/PD model was performed stratified by dose group. Median values and corresponding 5th and 95th percentiles were plotted against time and the observed data superimposed. Perl-speaks-NONMEM (PsN), Version 4.6.0 was used for prediction-corrected VPC across all dose groups.

3 Results

3.1 Study Population and Dataset

The population consisted of 70 young, healthy male Caucasian subjects, mean ages were 22 years and the

bodyweight ranged from 56.8 to 101.1 kg (mean 77.5 kg) [Supplementary Table S2]. Overall, 706 bosentan plasma, 320 ET-1 plasma, and 115 ET-1 urine levels, and in total 630 measurements of heart rate and blood pressure were available for analyses. All post-dose bioanalytical measurements available were above the lower limit of quantification.

3.2 Population PK/PD Model

The bosentan PK and the final competitive TMDD PK model (each without diurnal receptor synthesis) were linked to blood pressure and heart rate (Fig. 1) and described the data very well. The results of both PK/PD models were comparable, parameter estimates did not differ remarkably (Supplementary Table S3, Table 1); all parameters were estimated precisely. Goodness-of-fit plots (Fig. 2, Supplementary Figures S1 and S2) showed that the data were well described by the final model. VPC stratified by dose and prediction corrected showed a good descriptive performance with neither bias nor under- or over-estimation of the model variability (Fig. 3, Supplementary Figures S3–S5). None of the investigated covariates had a significant impact on the PK/PD model. Furthermore, no correlation was observed between baseline levels of ET-1 and the PD parameters. Model stability was confirmed by changing the initial parameter $\pm 10\%$, which did not result in different estimates. The NONMEM code of the final model is provided in the Supplementary Material.

3.2.1 Bosentan PK Model

Bosentan PK was best described by a two-compartment TMDD model. The TMDD model was statistically significantly superior to the linear one-, two-, or three-compartment models ($\Delta\text{OFV} -1300$, $\Delta\text{DF} 7$, $p < 0.001$). Bosentan is distributed from the central compartment to the periphery (Q), eliminated with a first-order rate (k_{EB}) or bound (k_{ONB}) to its binding partner, probably the ET_A and ET_B receptors, by a second-order process. The binding partner was best described by a turnover model with a zero-order production (k_{SynR}) and a first-order degradation rate (k_{DegR}). The formed bosentan-binding partner complex was cleared by a first-order rate process (k_{Int}) or by dissociation of the complex (k_{OffB}). The estimated central (4.14 L) and peripheral volumes of distribution (5.7 L) were small. The elimination rate constant of bosentan from the central compartment ($k_{\text{EB}} = \text{CL}/V_{\text{central}}$) was estimated as 1.24/h, about nine times higher than the elimination rate constant of the bosentan-binding partner complex ($k_{\text{Int}} = 0.134/\text{h}$). A low to moderate IIV [coefficient of variation (%CV) 17–37] was observed for bosentan clearance, both volumes

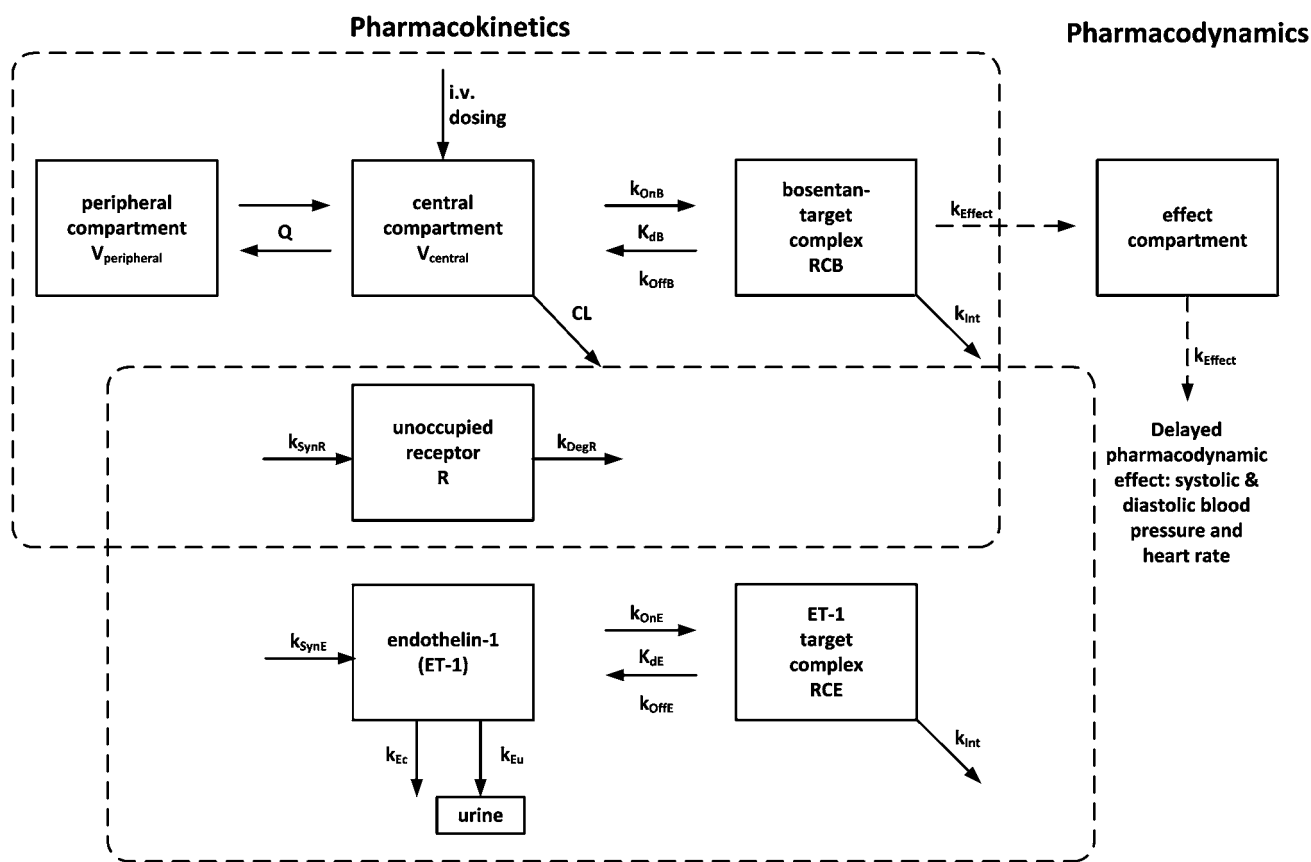


Fig. 1 Competitive TMDD, PK/PD model illustration. CL total body clearance of bosentan, K_{dB} dissociation rate constant bosentan, K_{dE} dissociation rate constant of ET-1, k_{DegR} degradation rate constant of free receptor, k_{Ec} second elimination/degradation rate constant of ET-1, k_{Effect} rate constant effect compartment, k_{Eu} elimination rate constant of ET-1 into urine, k_{Int} internalization rate constant of the bosentan-complex and ET-1-complex, k_{OffB} dissociation rate constant of the bosentan-complex, k_{OffE} dissociation rate constant of the ET-1-

complex, k_{OnB} building rate constant of bosentan-complex, k_{OnE} building rate constant of the ET-1-complex, k_{SynE} synthesis rate constant of ET-1, k_{SynR} synthesis rate constant of free receptor, Q inter-compartmental clearance, RCB bosentan-target complex, RCE ET-1 target complex, $V_{central}$ volume of distribution of the central compartment, $V_{peripheral}$ volume of distribution of the peripheral compartment. Model description: see text

of distribution, and the internalization process of the bosentan-binding partner complex (k_{Int}).

Although the bosentan TMDD model described the plasma concentration-time profiles very well, a systematic time-dependent wave pattern was observed in the conditional weighted residuals (CWRes), caused by a systematic multiple-peak phenomenon within individual plasma concentration-time profiles (Fig. 4a, c). As an improvement, an enterohepatic recycling model (EHC) [7] was tested as well as cosine functions (F_{Cos}) for the synthesis rate of the binding partner (the ET receptors) and the synthesis rate of endogenous ET-1. For the cosine functions, periods with 24, 12, 8, and 6 h (Ω) were tested while the amplitude (α) was fixed to 1 and the shift from the origin was estimated by the model. The cosine function (F_{Cos}) was coded as follows, varying around the mean 1, and multiplied by the synthesis rate:

$$F_{Cos} = 1 + a * \cos((2\pi/\Omega) * (\text{time} - \text{shift})),$$

$$k_{SynR} = k_{DegR} * R_{Base} * F_{Cos},$$

where shift is the time of occurrence of the maximum and k_{DegR} is the degradation rate of the unoccupied receptors with a baseline R_{Base} at time zero. Overall, the cosine function F_{Cos} of the synthesis rate of the binding partner (k_{SynR}) improved the model significantly ($p < 0.001$) and better than the other two options tested. The best period was found to be 8 h and the time shift was estimated to be 4.33 h. Figure 4 shows that the model misspecification decreased significantly; CWRes profiles showed almost no trend over time (Fig. 4d) and the multiple peak phenomenon was captured in individual profiles (Fig. 4b). Whereas all parameters from the TMDD model were estimated in similar dimensions for all models evaluated, the introduction of the cosine function caused numerical model instabilities when linking the PK model to the PD.

Table 1 Estimated parameter values for the final competitive PK/PD model

Parameter	Value	RSE, %	Description
Pharmacokinetics			
<i>Fixed effects</i>			
V_{central} , L	4.14	7	Volume of distribution of central compartment
$V_{\text{peripheral}}$, L	5.71	9	Volume of distribution of peripheral compartment
Q , L/h	11.3	14	Inter-compartmental clearance
R_{Base} , μmol	0.112	12	Receptor baseline at timepoint zero
k_{DegR} , h^{-1}	0.105	17	Rate constant degradation free receptor
K_{dB} , nM	1.93	14	Dissociation rate constant bosentan
k_{OnB} , $\mu\text{mol}^{-1} * \text{h}^{-1}$	48.7	15	Rate constant complex building bosentan
k_{Int} , h^{-1}	0.134	7	Rate constant internalization of the complex
CL , L/h	5.15	6	Total body clearance
ET_{Base} , μmol	$5 * 10^{-6}$	3	ET-1 baseline at timepoint zero
k_{Eu} , h^{-1}	0.229	7	Rate constant elimination ET-1 into urine
k_{Ec} , h^{-1}	0.295	10	Rate constant second elimination/degradation ET-1
K_{dE} , nM	9.66	15	Dissociation rate constant ET-1
k_{OnE} , $\mu\text{mol}^{-1} * \text{h}^{-1}$	62.7	17	Rate constant complex building ET-1
<i>Random effects: IIV</i>			
IIV V_{c} , %CV	37	10	IIV in volume of distribution, central compartment
IIV V_{p} , %CV	19	20	IIV in volume of distribution, peripheral compartment
IIV k_{Int} , %CV	17	18	IIV in internalization of the (two) complexes
IIV CL , %CV	31	14	IIV in total body clearance
IIV ET_{Base} , %CV	13	12	IIV in ET-1 baseline
IIV k_{Eu} , %CV	37	12	IIV in elimination ET-1 into urine
IIV k_{Ec} , %CV	27	28	IIV in second elimination/degradation ET-1
<i>Residual variability, %</i>			
Proportional plasma _B	24	6	Proportional residual error plasma bosentan
Proportional plasma _E	16	5	Proportional residual error plasma ET-1
Proportional urine	44	7	Proportional residual error urine ET-1
Pharmacodynamics			
<i>Fixed effects</i>			
$SBP_{(0)}$, mmHg	122	2	Baseline SBP
$DBP_{(0)}$, mmHg	59.3	1	Baseline DBP
$HR_{(0)}$, bpm	56.8	1	Baseline heart rate
k_{Effect} , h^{-1}	4.32	1	Rate constant effect compartment
S_{Max}	0.513	17	Maximum effect in SBP
D_{Max}	(0.726)	–	Maximum effect in DBP
EC_{50} , nmol/mL	1.13	41	Concentration at which effect is half maximum
α	0.817	13	Amplitude cosine function blood pressure
Ω , h	(24)	–	Period cosine function blood pressure
Shift, h	12	2	Phase shift cosine function blood pressure
<i>Random effects: IIV</i>			
IIV $SBP_{(0)}$, %CV	6	9	IIV in baseline of SBP
IIV $DBP_{(0)}$, %CV	11	9	IIV in baseline of DBP
IIV $HR_{(0)}$, %CV	11	9	IIV in baseline of HR
<i>Residual variability</i>			
Additive SBP, mmHg	33	7	Additive residual error SBP
Additive DBP, mmHg	27	6	Additive residual error DBP
Additive HR, bpm	24	8	Additive residual error HR

Parameter values in parentheses were not estimated but fixed

bpm beats per minute, CL clearance, CV coefficient of variation, DBP diastolic blood pressure, $ET-1$ endothelin-1, HR heart rate, IIV inter-individual variability, RSE relative standard error, SBP systolic blood pressure

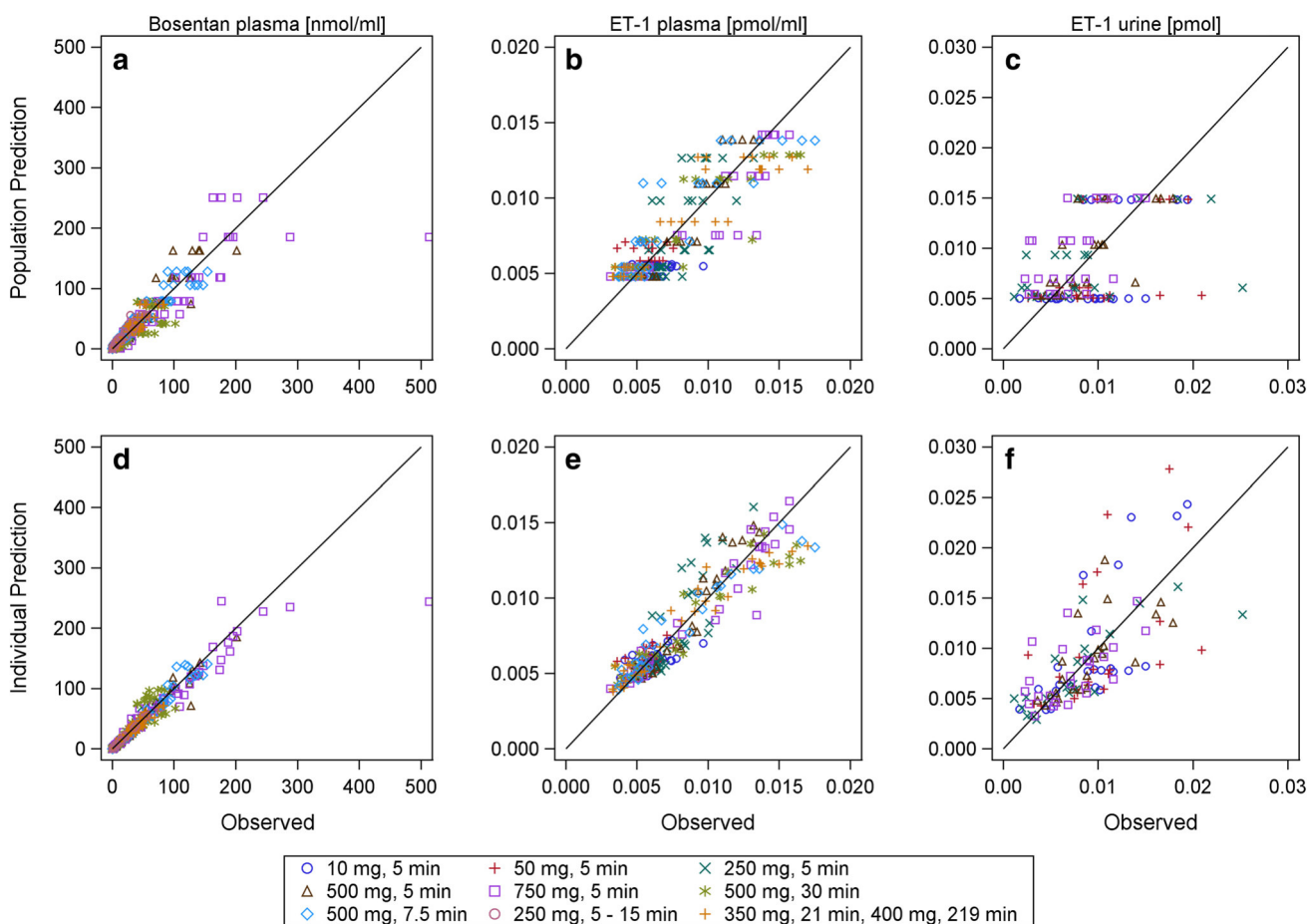


Fig. 2 Goodness-of-fit plot (linear scale) of the final competitive PK/PD model. Observed vs. model population predicted (*upper panels*) or individual predicted (*lower panels*) data of the final competitive, TMDD model (linear scale): bosentan plasma concentration (nmol/

mL) (**a, d**), ET-1 level (pmol/mL) in plasma (**b, e**), ET-1 amount in urine (pmol) at the end of each collection interval of 0–4, 4–8, 8–12, and 12–24 h (**c, f**). Colors/symbols denote dosing groups. The black solid line indicates the line of identity

Therefore, the cosine function was not kept for the final PK/PD model.

3.2.2 ET-1 PK Model

Concentration-time profiles of the endogenous ET-1 were best described by a TMDD model, which was integrated into the bosentan TMDD model; the resulting model had two ligands competing for the same binding partner. Endogenous ET-1 was synthesized by a zero-order production rate (k_{SynE}) and eliminated by a first-order process into urine (k_{Eu}) or catabolized (k_{Ec}). Bound ET-1 was internalized by a first-order rate constant (k_{Int}), where the rate was assumed to be identical to the elimination rate of the bosentan-binding partner complex. The steady-state levels of circulating ET-1 at baseline ($\text{ET}_{(0)}$) and the amount of ET-1 bound to the target at baseline ($\text{RCE}_{(0)}$) were estimated according to the following equations adapted from the literature [8]:

$$\text{ET}_{(0)} = (k_{\text{Int}} * k_{\text{OnE}} * R_{\text{Base}} * \text{ET}_{\text{Base}}) / (k_{\text{Int}} + k_{\text{OffE}}) + (k_{\text{Eu}} * \text{ET}_{\text{Base}} + k_{\text{Ec}} * \text{ET}_{\text{Base}}),$$

$$\text{RCE}_{(0)} = (k_{\text{OnE}} * \text{ET}_{\text{Base}} * R_{\text{Base}}) / (k_{\text{Int}} + k_{\text{OffE}}),$$

where k_{Int} is the rate constant for internalization of the ET-1-binding partner complex, k_{OnE} is the rate constant for the complex building, k_{OffE} is the complex dissociation rate constant, and R_{Base} and ET_{Base} are the initial estimates of the target and ET-1 baseline values, respectively, at time-point zero.

The urinary excretion (k_{Eu}) and the catabolic metabolism rate (k_{Ec}) contributed equally to the elimination of circulating ET-1 from the central compartment (k_{Eu} : 0.229 1/h vs. k_{Ec} : 0.296 1/h). Overall, the total elimination of circulating ET-1 from the central compartment ($k_{\text{Eu}} + k_{\text{Ec}}$) was about four times higher than ET-1 elimination via the binding partner complex (k_{Int}). The dissociation rate constant ($K_{\text{d}} = \frac{k_{\text{OffE}}}{k_{\text{OnE}}}$) value of ET-1 (K_{dE}) to the binding partner

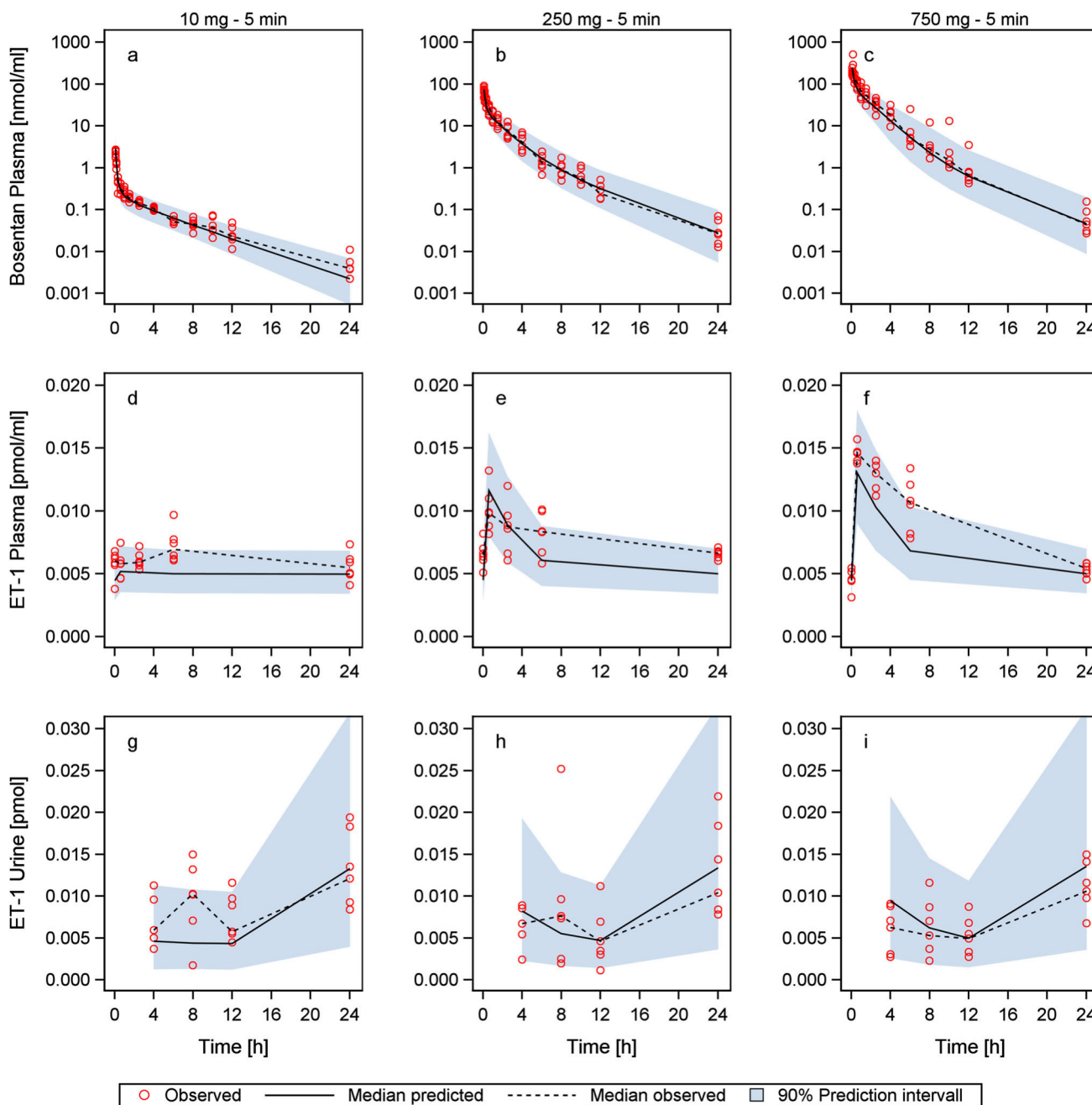


Fig. 3 Visual predictive check of the final competitive PK/PD model. Three selected doses (low, medium, and high) of the final competitive, TMDD model. *Open circles* indicate observed concentrations, the *solid line* indicates the median predicted concentration, the *dashed line* indicates the median observed concentration, the *shaded area*

indicates the 5th to 95th percentile of simulated concentrations in 1000 simulated subjects. Bosentan concentration in plasma (nmol/mL) (**a, b, c**), ET-1 level in plasma (pmol/mL) (**d, e, f**) and ET-1 amount in urine (pmol) at the end of each collection interval of 0–4, 4–8, 8–12, and 12–24 h (**g, h, i**)

was estimated to be about five times higher than the value of bosentan (K_{dB}) [9.66 vs. 1.93 nM], indicating that bosentan displaces endogenous ET-1 from its binding site. A low-to-moderate IIV (%CV 13–37) was established on the urinary excretion (k_{Eu}), the catabolic metabolism (k_{Ec}), and the ET-1 baseline levels (ET_{Base}).

3.2.3 PD Model

SBP and BDP under bosentan treatment were best described by E_{max} functions decreasing the estimated baseline values in a proportional manner. The amount of bound bosentan-binding partner complex was the best descriptor

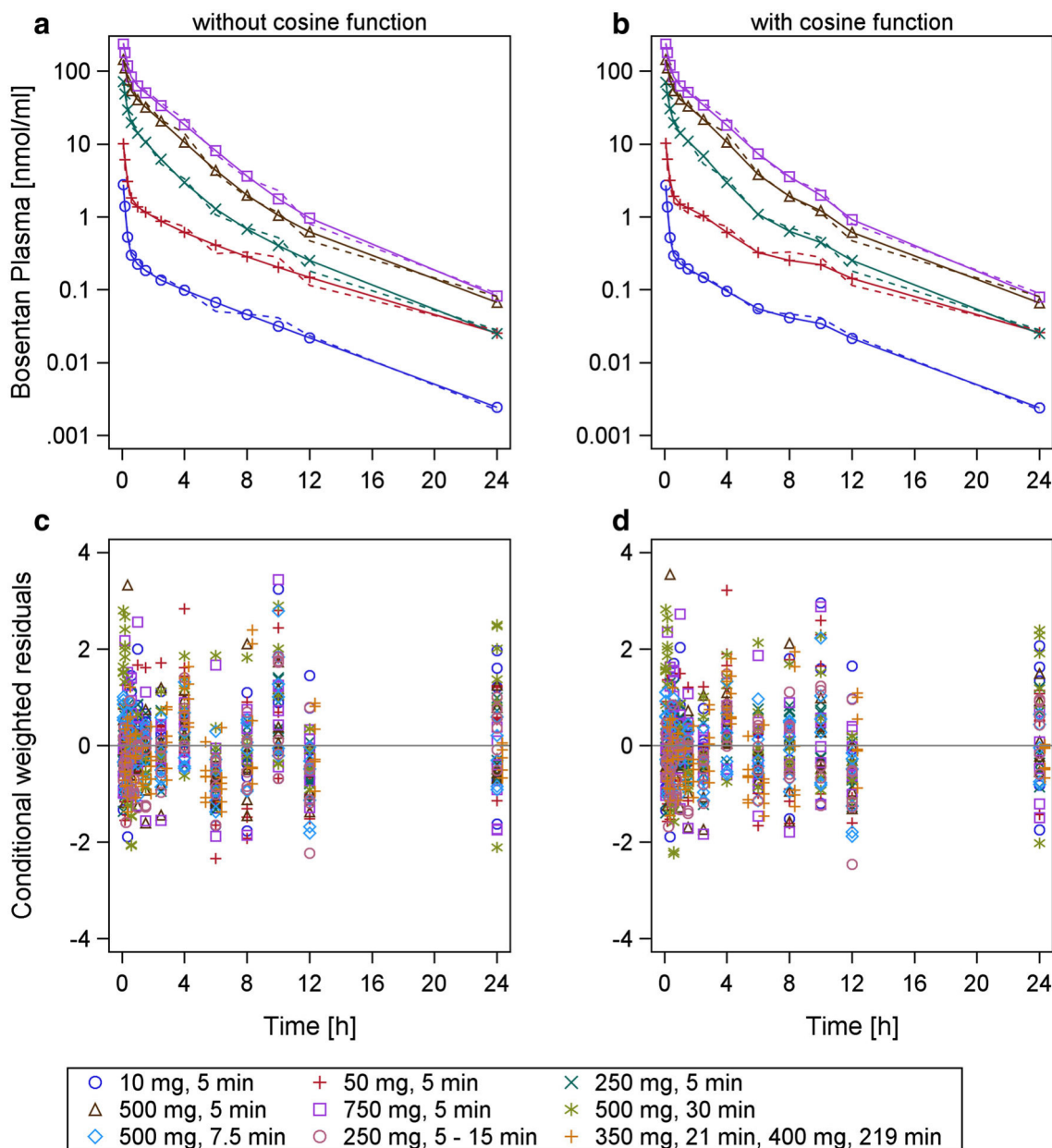


Fig. 4 Randomly selected individual profiles (*upper panel*) and conditional weighted residuals over time (*lower panel*) without (*left panel*) and with (*right panel*) cosine function on receptor synthesis. *Upper panel* Randomly selected individual PK profiles after i.v. administration of 10, 50, 250, 500, or 750 mg of bosentan over 5 min, **a** without and **b** with cosine function on receptor synthesis. *Dashed*

lines indicate observed concentrations, *solid lines* and *symbols* represent individual predicted concentrations. *Lower panel* Conditional weighted residuals over time for the bosentan pharmacokinetic, TMDD model **c** without and **d** with cosine function on receptor synthesis separated for all dosing groups

of the PD effect, and an effect compartment improved the descriptive performance significantly ($\Delta\text{OFV} -32$, $\Delta\text{DF} 1$, $p < 0.001$). Because blood pressure underlies a circadian rhythm [9, 10], a sine function was introduced varying the systolic and diastolic baseline values ($\text{SBP}_{(0)}$, $\text{DBP}_{(0)}$) and this improved the model significantly ($\Delta\text{OFV} -41$, $\Delta\text{DF} 2$, $p < 0.001$). The final SBP and DBP models are described in the following equations:

$$\begin{aligned} \text{SBP} &= (\text{SBP}_{(0)} + a * \sin((2\pi/\Omega) * (\text{time} - \text{shift}))) \\ &\quad * (1 - (S_{\text{max}} * A_{\text{Effect}} / (\text{EC}_{50} + A_{\text{Effect}}))), \\ \text{DBP} &= (\text{DBP}_{(0)} + a * \sin((2\pi/\Omega) * (\text{time} - \text{shift}))) \\ &\quad * (1 - (D_{\text{max}} * A_{\text{Effect}} / (\text{EC}_{50} + A_{\text{Effect}}))), \end{aligned}$$

where $\text{SBP}_{(0)}$ and $\text{DBP}_{(0)}$ reflect the SBP and DBP, respectively, at baseline, and S_{max} and D_{max} are the

maximum effects on SBP and DBP. A_{Effect} is the amount of the bosentan-binding partner complex in the effect compartment. In the sine function, Ω describes the period, α the amplitude, and shift the time shift from the origin. The baseline values for SBP and DBP were estimated at 122 and 60 mmHg, with a small IIV (%CV 6 and 11%, respectively). The equilibrium rate constant was estimated at 4.32/h, indicating a rapid adjustment of the equilibrium concentration in the effect compartment ($t_{0.5} = 0.165$ h).

Initially, heart rate was modeled independently from the change in blood pressure. However, as heart rate increased compensatorily with decreasing blood pressure, heart rate was modeled in dependence of the blood pressure. The mean arterial blood pressure (MAP) and its baseline value ($\text{MAP}_{(0)}$) were calculated based on SBP and DBP and their baseline values. The compensatory increase in heart rate as a result of blood pressure reduction was described as follows:

$$\text{MAP}_{(0)} = \text{DBP}_{(0)} + 1/3 * (\text{SBP}_{(0)} - \text{DBP}_{(0)}),$$

$$\text{MAP} = \text{DBP} + 1/3 * (\text{SBP} - \text{DBP}),$$

$$\text{Heart rate} = \text{HR}_{(0)} * (\text{MAP}_{(0)}/\text{MAP}).$$

The population typical heart rate at baseline ($\text{HR}_{(0)}$) was estimated as 57 beats per min (bpm) with an IIV of %CV 11. Modeling heart rate in dependence of MAP improved the descriptive performance of the model ($\Delta\text{OFV} -66$, $\Delta\text{DF} 1$, $p < 0.001$) and the parameter estimates did not change markedly.

3.3 Simulations

Simulations were performed to visualize the complex PK/PD model. Six different, single i.v. bosentan doses were administered and median concentration and effect profiles over time are shown in Fig. 5. The bosentan concentration-time profiles showed the typical non-linear and dose-dependent behavior, which is triggered by the TMDD processes. Once bosentan is administered, endogenous ET-1 is displaced immediately from the binding partner; at bosentan doses of >500 mg, ET-1 levels increase almost three times and return to baseline after 12 h for all doses investigated. The SBP is reduced under bosentan treatment. At the highest dose group (750 mg), a reduction of 7 mmHg was observed with a compensatory increase in heart rate of 5 bpm.

4 Discussion

In the present study assessing a wide dose range, bosentan PK was non-linear with clearance and volume of distribution decreasing dose dependently and a less than

proportional increase in the AUC. This phenomenon was best described by a TMDD model. Such models are often applied to describe non-linear PK behavior of drugs with substantial and high affinity binding to a binding site, thus markedly influencing the temporal profile of drug plasma concentrations. TMDD has received considerable interest in explaining non-linear PK of specific peptide [11] and protein pharmaceuticals [12], but it also plays a role for small molecules, e.g., linagliptin [13], imirestat [14], or warfarin [15].

In our analysis, the binding partner was not pre-specified. Based on preclinical findings, it can be assumed that binding to ET_A receptors, which are predominantly expressed in vascular smooth muscle cells, and ET_B receptors, which are the major ET receptors found in endothelial cells and renal tubules [16], influenced the PK of bosentan and probably represents the high affinity binding partner for bosentan. In the present model assessing a non-selective endothelin antagonist, ET_A and ET_B receptors were not considered separately, but taken together as one binding partner for bosentan and ET-1, respectively. The TMDD concept is further supported by the dose-dependent increase of endogenous ET-1 levels, which is probably displaced from ET receptors by bosentan, which binds with a much higher affinity. With the present model, a dissociation rate constant for bosentan of 1.93 nM was estimated, which is in the order of magnitude of measured binding constant (Kb) values of 0.79–1.1 nM [17]. The Kd value of ET-1 was estimated five times higher at 9.66 nM, reflecting the lower binding affinity to ET receptors compared with bosentan.

ET-1 binding to its receptors is tight and causes long biological effects, particularly after binding to ET_A [16]. One reason for its long-lasting effect is that ET-1 remains bound to ET_A after internalization for up to 2 h before the ET_A receptors enter the recycling pathway [16, 18, 19] and are again presented at the cell surface [18]. In contrast, the ET_B -ET-1 receptor complex is degraded by lysosomes in the cells [20]. Therefore, ET_B is recognized as a ‘clearance’ receptor removing ET-1 from the systemic circulation via internalization and degradation [16, 20–23]. Investigations of the internalization process of other compounds binding to the ET_A receptor suggest that not only binding of the natural agonist ET-1 to ET_A leads to endocytosis but also of ET-1 receptor antagonists, e.g., BQ123 can promote receptor internalization [24]. This is similar to the behavior towards other receptor blockers, such as of GnRH antagonists [25] or cholecystokinin antagonists [26], which are also able to initiate endocytosis.

In our model, we also identified that a degradation component of the bosentan-binding partner improved the model significantly. It is conceivable that bosentan is also able to initiate endocytosis, possibly leading to

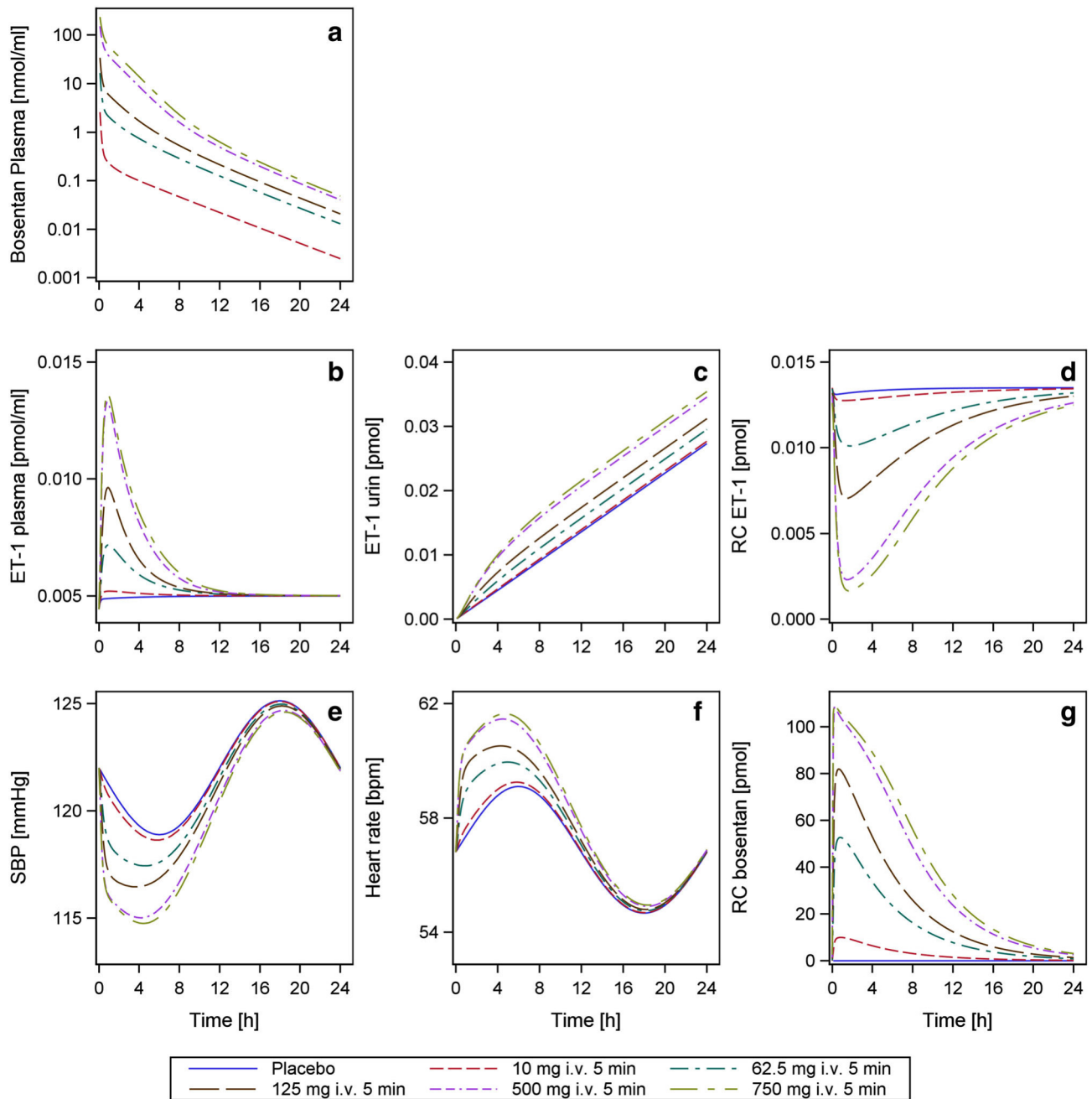


Fig. 5 Simulations of the final PK/PD model after single-dose i.v. administration of placebo, 10, 62.5, 125, 500, or 750 mg of bosentan (a). Free endothelin-1 (ET-1) level in plasma over time increases with higher doses of bosentan (b); cumulated ET-1 amount excreted into

urine (c); formed receptor complex of ET-1 by time (d); systolic blood pressure (SBP) change (mmHg) [e]; compensatory heart rate (HR) change (bpm) (f); and formed receptor complex of bosentan by time (g). RC receptor complex

internalization of bosentan; the subsequent intracellular clearance process is currently not entirely understood. Although the estimated degradation constant was about nine times smaller than the elimination constant of total plasma bosentan, it should be considered that at low doses (<50 mg i.v.), the majority of bosentan is bound and consequently degradation may play a pronounced role.

The presented model includes two simplifications. First, the assumption was made that the degradation process of bound bosentan and bound ET-1 occurs at the same rate. Because of the lack of available data, it was not possible to differentiate these two kinetic processes. Second, with the available data it was neither possible to differentiate the binding of bosentan and ET-1 to the two ET receptors. Hence, the model used a lumped ET receptor as binding

partner, which is a mixture of both ET receptors. This appeared justified because bosentan is a non-selective ET receptor antagonist.

Bosentan binding to ET receptors occurred with high affinity ($K_d \sim 1.9$ nM). Low doses of bosentan (10–50 mg i.v.) were almost completely bound and primarily removed from the system via an internalization process. With ascending doses (>50 mg i.v.), the amount of bosentan eliminated from the central compartment, i.e., via the liver and bile, increased, suggesting saturable receptor-binding capacity. The bosentan TMDD model was extended with endogenous ET-1 plasma and urine levels where the K_d value of ET-1 for the binding partner was estimated five times lower at 9.7 nM. Because of the higher affinity of bosentan to the binding partner, bound ET-1 was displaced from the binding site, resulting in a significant increase of free ET-1 in plasma after administration of high bosentan doses (Fig. 5). Plasma ET-1 could serve as a potential biomarker to determine the receptor occupancy of bosentan.

Incorporation of ET-1 urine excretion allowed the identification of two elimination processes of free ET-1. Approximately 44% of free ET-1 eliminated from plasma is excreted into urine and this amount shows a marginal dose-dependent increase (Fig. 5). Approximately 56% of free ET-1 is eliminated by a second elimination pathway. It might be speculated that this process is at least in part receptor-mediated via ET_B from the lung, kidney, or liver [22, 23]. Incorporation of the latter elimination pathway improved the model significantly ($p < 0.001$).

Bosentan is a competitive antagonist of ET-1 at its receptors [17]. Therefore, its action will depend on its concentration at the target site and the level of the natural agonist (ET-1). It appears possible that patients with high circulating ET-1 levels and concurrently low exposure to the antagonist might differ compared with patients with low ET-1 levels in their response to the antagonist, whereas such differences are less important if plateau effects of the antagonist are reached. ET-1 was included in the model for the following reasons: (1) In patients, ET-1 levels can be up to five times the levels in healthy subjects [27], indicating that circulating amounts can be substantially increased. (2) Given the fact that most of the circulating ET-1 is released by the lung in a paracrine fashion [28], local ET-1 release is obviously considerable and slight changes in circulating ET-1 levels likely reflect pronounced changes in the target organ (lung). (3) The currently approved therapeutic bosentan dosing regimen (125 mg twice daily) does not appear to fully block ET receptors because higher doses give rise to even higher ET-1 levels [4], indicating that plateau effects are not reached. However, it should be considered that the presented model can be applied also without restrictions in the

absence of ET-1 measurements (see Supplementary Table S3).

Bosentan plasma concentration-time profiles showed a multiple-peak phenomenon after i.v. administration (Fig. 4a) and diagnostic plots showed a wave-like pattern in the CWRes over time (Fig. 4c). A multiple-peak phenomenon can occur as a consequence of a number of different mechanisms, such as the presence of gastrointestinal absorption windows or EHC [7, 29]. In our analysis, bosentan was administered i.v., which eliminates a majority of potential reasons caused by absorption processes. Although no EHC was yet described for bosentan, we investigated a basic EHC model [7]. Compared with the other options tested, the EHC model was not superior, but further investigations such as co-administration of an absorbent agent (e.g., charcoal) would be required to definitely reject the EHC hypothesis.

Recent studies revealed that the ET-1 system underlies circadian variability; ET-1, ET_A , and ET_B showed a clock time-dependent mRNA expression regulated by Per1 in the liver, heart, kidney, and lung [30]. Expression of the ET-1 clearance receptor (ET_B) has been shown to be lowest at noon and highest at midnight. Further, circadian variability of ET-1 plasma levels has been reported in chronic kidney disease and, based on the impact of treatment with an ET-receptor antagonist, related to clinical endpoints such as blood pressure and dipping [31]. Hence, these findings suggest that short-lived changes are indeed possible. In-vitro internalization of the receptors occurs within minutes [32] and short exposure (30–120 min) profoundly down-regulates ET_B receptors (for details, please refer to De Mey et al. [33]). To the best of our knowledge, it is currently unknown whether receptors also internalize after antagonist exposure.

We tested the circadian hypothesis in our model by incorporating a cosine function, which modulates either ET-1 production or synthesis/reappearance of the receptors at the cell surface. Consideration of diurnal modulation of the synthesis of the binding partner (ET receptor) significantly improved the model, accurately described the multiple-peak phenomenon, and removed the model misspecification in the diagnostic plots almost completely (Fig. 4d). For the synthesis or receptor reappearance at the cell surface, a period of 8 h was estimated, which is in perfect agreement with in-vitro findings [34]. To our knowledge, there is no published evidence describing the period of ET receptor expression in humans in vivo. In addition, it should be acknowledged that the analytes were less frequently measured beyond 12 h after dosing, which may lead to an only approximate estimate of the period, owing to a lack of data over a full 24-h period. While this may be less relevant for bosentan, which is dosed twice daily, this should be more thoroughly assessed for ET

antagonists with once-daily dosing such as ambrisentan and macitentan. To our knowledge, this is the first report of a circadian PK variation caused by expression changes of a binding partner/receptor.

To confirm the hypothesis experimentally, bosentan PK might be compared in animals with and without Per1 clock protein and by relating these findings to receptor expression in the tissue [30]. Another option would be to measure circadian ET_B receptor expression in human platelets (e.g., at the RNA or protein level) and to assess the impact of desynchronizing the internal clock (e.g., in a sleep-deprivation experiment).

The bosentan PK and the final competitive TMDD PK model were linked to blood pressure and heart rate and described the data very well. The results of both PK/PD models were comparable, parameter estimates did not differ remarkably (Table 1 and Supplementary Table S3). The circadian variation of the cardiovascular markers was reflected in the model by a cosine function. The estimates and the diurnal effect size were comparable to other reports [9, 10]. The best linkage between PK and PD was achieved if the bosentan-binding partner complex was considered, which reflects the amount of bound bosentan, thus further supporting the physiological basis of the TMDD model. The effect of this complex on the PD was slightly delayed and best described by an effect compartment. This delay is probably caused by the downstream cascade processes induced after formation of the drug-receptor complex.

The effect of bosentan on heart rate was successfully modeled as a compensatory effect for blood pressure changes (baroreceptor reflex). This approach is novel and elegant because it reflects the physiology very well and reduced the number of model parameters; to describe heart rate, no additional parameter was required besides the estimation of a baseline value. The overall acute cardiovascular effects of bosentan were mild. Simulation studies revealed that at the highest dose (750 mg), a drop in blood pressure of 7 mmHg and a heart rate increase by 5 bpm was observed.

These findings suggest that after single-dose administration of bosentan, blood pressure reduction is associated with adequate baroreflex activation and thereby a compensatory increase in heart rate. After administration of ascending oral doses (once or twice daily) of bosentan for 4 weeks in 293 patients with mild-to-moderate essential hypertension, DBP was significantly reduced with an absolute reduction of 5.7 mmHg at each dose (daily dose 500 or 2000 mg), while heart rate was not increased significantly [35]. It is expected that after long-term use of bosentan, no sympathetic reflex activation and no heart rate increases occur compared with the short-term intake of a single dose owing to the resetting of the baroreflex. Observations with nicardipine and nifedipine, which effectively reduce blood pressure, showed similar behavior after short- and long-term treatment

[36, 37]. Based on these findings with respect to baroreflex activation with nicardipine and nifedipine, the changes observed in blood pressure and heart rate with bosentan could be expected and a heart rate increase might vanish after multiple dosing of the drug [38].

5 Conclusion

In a comprehensive and mechanistic TMDD PK/PD model, we successfully described the competitive relationship between bosentan and ET-1 and the cardiovascular effects of the drug on heart rate and blood pressure. The model suggests that a strong binding to the target (presumed to be ET receptors) is responsible for the non-linearity in the PK of bosentan, a cause of PK variability not reported previously. Furthermore, the model suggests that circadian expression of ET receptors explains the multiple-peak phenomenon of bosentan plasma concentrations after i.v. administration. The model provides a first step towards understanding the complex PK properties of bosentan and offers a valuable tool for future PK/PD research on bosentan.

Acknowledgments We thank Saarland University for enabling this work with the support of a doctoral scholarship.

Compliance with Ethical Standards

Funding The clinical study used for modeling was funded by Actelion Pharmaceuticals Ltd. For modeling analysis no funding was provided.

Conflict of interest Anke-Katrin Volz and Thorsten Lehr report no potential conflicts of interest. Jasper Dingemans and Andreas Krause are employees of Actelion Pharmaceuticals Ltd. Walter E. Haefeli received research grants from Actelion Pharmaceuticals Ltd.

Ethics Approval All procedures performed in studies involving human participants were in accordance with the ethical standards of the institutional and/or national research committee and with the 1964 Helsinki Declaration and its later amendments or comparable ethical standards.

Consent to Participate Informed consent was obtained from all individual participants included.

References

1. Dingemans J, van Giersbergen PLM. Clinical pharmacology of bosentan, a dual endothelin receptor antagonist. *Clin Pharmacokinet.* 2004;43:1089–115.
2. Weber C, Gasser R, Hopfgartner G. Absorption, excretion, and metabolism of the endothelin receptor antagonist bosentan in healthy male subjects. *Drug Metab Dispos.* 1999;27:810–5.
3. Venitz J, Zack J, Gillies H, et al. Clinical pharmacokinetics and drug-drug interactions of endothelin receptor antagonists in

- pulmonary arterial hypertension. *J Clin Pharmacol.* 2012;52:1784–805.
4. Weber C, Schmitt R, Brinboeck H, et al. Pharmacokinetics and pharmacodynamics of the endothelin-receptor antagonist bosentan in healthy human subjects. *Clin Pharmacol Ther.* 1996;60:124–37.
 5. Löffler B-M, Maire J-P. Radioimmunological determination of endothelin peptides in human plasma: a methodological approach. *Endothelium.* 1994;1:273–86.
 6. Dua P, Hawkins E, van der Graaf P. A tutorial on target-mediated drug disposition (TMDD) models. *CPT Pharmacomet Syst Pharmacol.* 2015;4:324–37.
 7. Lehr T, Staab A, Tillmann C, et al. A quantitative enterohepatic circulation model: development and evaluation with tesofensine and meloxicam. *Clin Pharmacokinet.* 2009;48:529–42.
 8. Yan X, Chen Y, Krzyzanski W. Methods of solving rapid binding target-mediated drug disposition model for two drugs competing for the same receptor. *J Pharmacokinet Pharmacodyn.* 2012;39:543–60.
 9. Taylor KS, Heneghan CJ, Stevens RJ, et al. Heterogeneity of prognostic studies of 24-hour blood pressure variability: systematic review and meta-analysis. *PLoS One.* 2015;10:e0126375.
 10. Middeke M. Chronopathologie und Chronotherapie. *Kompend Herz-Kreislauf.* 2007;3:17–21.
 11. Blank A, Markert C, Hohmann N, et al. First-in-human application of the first-in-class hepatitis B and hepatitis D virus entry inhibitor myrcludex B. *J Hepatol.* 2016;65:483–9.
 12. Tang L, Persky AM, Hochhaus G, Meibohm B. Pharmacokinetic aspects of biotechnology products. *J Pharm Sci.* 2004;93:2184–204.
 13. Retlich S, Withopf B, Greischel A, et al. Binding to dipeptidyl peptidase-4 determines the disposition of linagliptin (BI 1356): investigations in DPP-4 deficient and wildtype rats. *Biopharm Drug Dispos.* 2009;30:422–36.
 14. Brazzell RK, Mayer PR, Dobbs R, et al. Dose-dependent pharmacokinetics of the aldose reductase inhibitor imirestat in man. *Pharm Res.* 1991;8:112–8.
 15. Cheung WK, Levy G. Comparative pharmacokinetics of coumarin anticoagulants. XLIX: nonlinear tissue distribution of S-warfarin in rats. *J Pharm Sci.* 1989;78:541–6.
 16. Kohan DE, Rossi NF, Inscho EW, Pollock DM. Regulation of blood pressure and salt homeostasis by endothelin. *Physiol Rev.* 2011;91:1–77.
 17. Gatfield J, Mueller Grandjean C, Sasse T, et al. Slow receptor dissociation kinetics differentiate macitentan from other endothelin receptor antagonists in pulmonary arterial smooth muscle cells. *PLoS One.* 2012;7:e47662.
 18. Paasche JD, Attramadala T, Sandberg C, et al. Mechanisms of endothelin receptor subtype-specific targeting to distinct intracellular trafficking pathways. *J Biol Chem.* 2001;276:34041–50.
 19. Chun M, Lin HY, Henis YI, Lodish HF. Endothelin-induced endocytosis of cell surface ETA receptors: endothelin remains intact and bound to the ETA receptor. *J Biol Chem.* 1995;270:10855–60.
 20. Bremnes T, Paasche JD, Mehlum A, et al. Regulation and intracellular trafficking pathways of the endothelin receptors. *J Biol Chem.* 2000;275:17596–604.
 21. Boesen E. Endothelin receptors, renal effects and blood pressure. *Curr Opin Pharmacol.* 2015;21:25–34.
 22. Fukuroda T, Fujikawa T, Ozaki S, et al. Clearance of circulating endothelin-1 by ETB receptors in rats. *Biochem Biophys Res Commun.* 1994;199:1461–5.
 23. de Nucci G, Thomas R, D’Orleans-Juste P, et al. Pressor effects of circulating endothelin are limited by its removal in the pulmonary circulation and by the release of prostacyclin and endothelium-derived relaxing factor. *Proc Natl Acad Sci USA.* 1988;85:9797–800.
 24. Bhowmick N, Narayan P, Puett D. The endothelin subtype A receptor undergoes agonist- and antagonist-mediated internalization in the absence of signaling. *Endocrinology.* 1998;139:3185–92.
 25. Jennes L, Stumpf WE, Conn PM. Receptor-mediated binding and uptake of GnRH agonist and antagonist by pituitary cells. *Pep-tides.* 1984;5:215–20.
 26. Roettger BF, Ghanekar D, Rao R, et al. Antagonist-stimulated internalization of the G protein-coupled cholecystokinin receptor. *Mol Pharmacol.* 1997;51:357–62.
 27. Stewart DJ, Cernacek P, Costello KB, Rouleau JL. Elevated endothelin-1 in heart failure and loss of normal response to postural change. *Circulation.* 1992;85:510–7.
 28. Tsutamoto T, Wada A, Maeda Y, et al. Relation between endothelin-1 spillover in the lungs and pulmonary vascular resistance in patients with chronic heart failure. *Am Coll Cardiol.* 1994;23:1427–33.
 29. Davies NM, Takemoto JK, Brocks DR, Yáñez AJ. Multiple peaking phenomena in pharmacokinetic disposition. *Clin Pharmacokinet.* 2010;49:351–77.
 30. Richards J, Welch AK, Barilovits SJ, et al. Tissue-specific and time-dependent regulation of the endothelin axis by the circadian clock protein Per1. *Life Sci.* 2014;118:255–62.
 31. Dhaun N, Moorhouse R, MacIntyre IM, et al. Diurnal variation in blood pressure and arterial stiffness in chronic kidney disease: the role of endothelin-1. *Hypertension.* 2014;64:296–304.
 32. Evans NJ, Walker JW. Sustained Ca²⁺ signaling and delayed internalization associated with endothelin receptor heterodimers linked through a PDZ finger 1. *Can J Physiol Pharmacol.* 2008;86:526–35.
 33. De Mey JGR, Compeer MG, Lemkens P, Meens MJPM. ETA-receptor antagonists or allosteric modulators? *Trends Pharmacol Sci.* 2011;32:345–51.
 34. Terada K, Horinouchi T, Fujioka Y, et al. Agonist-promoted ubiquitination differentially regulates receptor trafficking of endothelin type A and type B receptors. *J Biol Chem.* 2014;289:35283–95.
 35. Krum H, Viskoper RJ, Lacourciere Y, et al. The effect of an endothelin-receptor antagonist, bosentan, on blood pressure in patients with essential hypertension. *N Engl J Med.* 1998;338:784–90.
 36. Young MA, Watson RD, Littler WA. Baroreflex setting and sensitivity after acute and chronic nicardipine therapy. *Clin Sci.* 1984;66:233–5.
 37. Kiowski W, Erne P, Bertel O, et al. Acute and chronic sympathetic reflex activation and antihypertensive response to nifedipine. *J Am Coll Cardiol.* 1986;7:344–8.
 38. Weber C, Schmitt R, Brinboeck H, et al. Multiple-dose pharmacokinetics, safety, and tolerability of bosentan, an endothelin receptor antagonist, in healthy male volunteers. *J Clin Pharmacol.* 1999;39:703–14.

Clinical Pharmacokinetics

A target-mediated drug disposition pharmacokinetic-pharmacodynamic model of bosentan and endothelin-1

Anke-Katrin Volz, Andreas Krause, Walter Emil Haefeli, Jasper Dingemanse, Thorsten Lehr

Author for correspondence:

Thorsten Lehr, Clinical Pharmacy, Saarland University, 66123 Saarbrücken, Germany

E-mail: HYPERLINK "mailto:thorsten.lehr@mx.uni-saarland.de" thorsten.lehr@mx.uni-saarland.de

Electronic supplementary material - figures and tables

Supplementary Table S1 Treatment regimens studied

Dose group	Bosentan single dose [mg]	Duration of intravenous administration [min]
1	10	5
2	50	5
3	250	5
4	500	5
5	750	5
6	500	30
7	500	15
8	250	5 or 15
9	750	350 mg over 21 minutes followed by 400 mg over 219 minutes

Supplementary Table S2 Summary statistics of subjects' characteristics at baseline

Covariate	Min	P5*	Mean	SD*	Median	P95*	Max
Age [years]	19	19	22.2	2.33	22	26	31
Weight [kg]	56.8	65.2	77.5	8.43	76.5	90.3	101.1
Height [cm]	167	176	184.4	6.27	184	195	201
Body mass index [kg/m ²]	19.5	20	22.8	1.91	22.7	26.8	27.2
Bilirubin [μ mol/L]	4	5	11.6	4.74	11	22	29
Serum glutamate pyruvate transferase [U/L]	5	8	15.6	7.12	14	28	45
Akaline phosphatase [U/L]	28	38	56.7	13.45	56	80	93
Serum glutamate oxalacetate transferase [U/L]	1	5	10.5	4.72	10	23	25
Gamma glutamyl transpeptidase [U/L]	6	8	12.7	3.85	11.5	21	25
Albumin [g/L]	46	47	50.9	2.26	50.5	55	58
Protein [g/L]	60	64	69.3	3.23	69	74	80
Cholesterol [mmol/L]	3.1	3.3	4.38	0.77	4.4	5.8	6.4
Hemoglobin [mmol/L]	13.2	13.4	14.6	0.75	14.5	15.8	16.4
Hematocrit [L/L]	0.39	0.41	0.44	0.023	0.44	0.48	0.51
Serum Creatinine [μ mol/L]	66	70	83.5	7.91	84	99	103
Creatinine clearance [ml/min]	83.2	88.5	115.1	17.28	113	142.8	162.8

* P5: 5th percentile, P95: 95th percentile, SD: standard deviation

Supplementary Table S3 Parameter estimates of key interim models

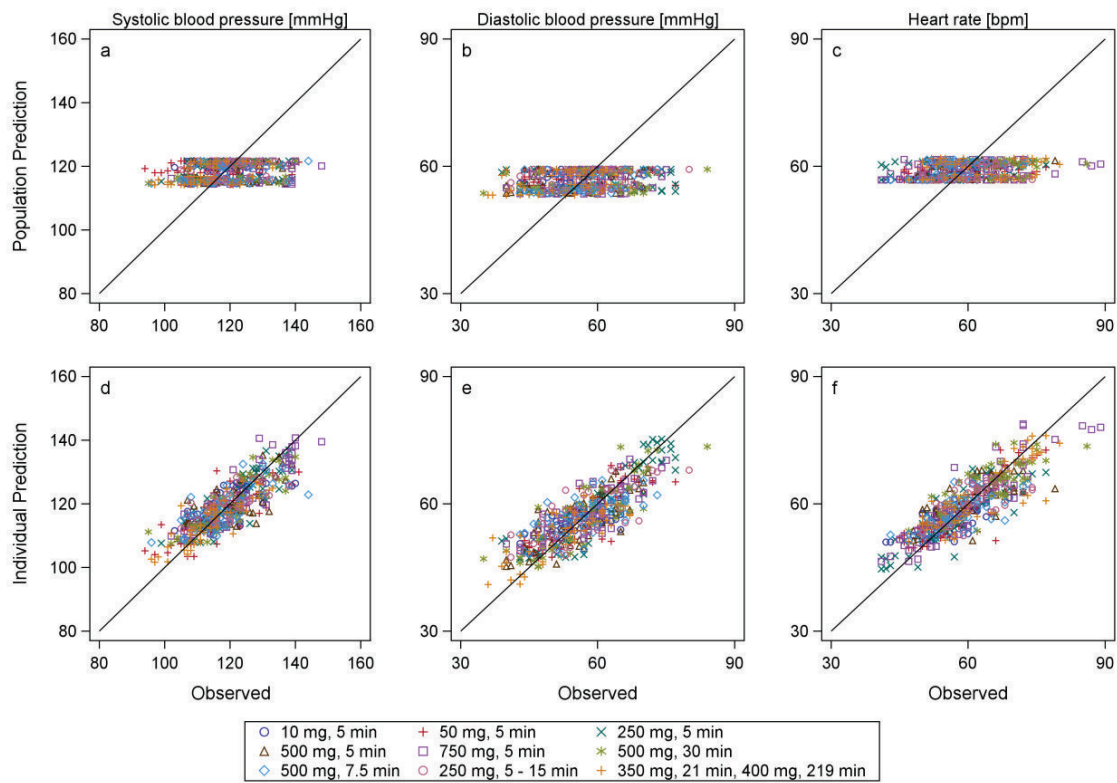
Pharmacokinetics							
	PK model of bosentan		PKPD model of bosentan		Competitive PK model of bosentan and ET-1		
Parameter	Value	RSE [%]	Value	RSE [%]	Value	RSE [%]	Description
Fixed Effects							
V _{central} (L)	4.2	7	(4.2)	-	4.14	6	Volume of distribution of central compartment
V _{peripheral} (L)	5.88	8	(5.88)	-	5.73	6	Volume of distribution of peripheral compartment
Q (L/h)	11.9	12	(11.9)	-	11.3	11	Intercompartmental clearance
R _{Base} (μmol)	0.092	16	(0.092)	-	0.111	5	Receptor baseline at time point zero
k _{DegR} (h ⁻¹)	0.085	33	(0.085)	-	0.101	14	Rate constant degradation free receptor
K _{dB} (nM)	1.66	14	(0.007)	-	(1.93)	-	Dissociation rate constant bosentan
k _{OnB} (μmol ⁻¹ *h ⁻¹)	58.6	17	(58.6)	-	48.3	11	Rate constant complex building bosentan
k _{Int} (h ⁻¹)	0.118	12	(0.118)	-	0.133	5	Rate constant internalisation of the complex
CL (L/h)	5.52	6	(5.52)	-	5.18	5	Total body clearance
ET _{Base} (μmol)	N/A	N/A	N/A	N/A	5*10 ⁻⁶	2	ET-1 baseline at time point zero
k _{En} (h ⁻¹)	N/A	N/A	N/A	N/A	0.229	6	Rate constant elimination ET-1 into urine
k _{Ec} (h ⁻¹)	N/A	N/A	N/A	N/A	0.297	10	Rate constant second elimination / degradation ET-1
K _{dE} (nM)	N/A	N/A	N/A	N/A	(9.66)	-	Dissociation rate constant ET-1
k _{OnE} (μmol ⁻¹ *h ⁻¹)	N/A	N/A	N/A	N/A	63.1	14	Rate constant complex building ET-1
Random Effects: Interindividual variability (IIV)							
IIV V _c (%CV)	30	10	(30)	-	37	10	IIV in volume of distribution, central compartment
IIV V _p (%CV)	20	17	(20)	-	19	20	IIV in volume of distribution, peripheral compartment
IIV k _{Int} (%CV)	19	19	(19)	-	17	19	IIV in internalization of the (two) complexes
IIV CL (%CV)	29	14	(29)	-	31	13	IIV in total body clearance
IIV ET _{Base} (%CV)	N/A	N/A	N/A	N/A	13	12	IIV in ET-1 baseline
IIV k _{En} (%CV)	N/A	N/A	N/A	N/A	37	12	IIV in elimination ET-1 into urine
IIV k _{Ec} (%CV)	N/A	N/A	N/A	N/A	27	28	IIV in second elimination / degradation ET-1
Residual variability							
proportional plasma _B (%)	24	12	(24)	-	24	6	Proportional residual error plasma bosentan
proportional plasma _E (%)	N/A	N/A	N/A	N/A	16	5	Proportional residual error plasma ET-1
proportional urine (%)	N/A	N/A	N/A	N/A	44	7	Proportional residual error urine ET-1
Pharmacodynamics							
	PK model of bosentan		PKPD model of bosentan		Competitive PK model of bosentan and ET-1		
Parameter	Value	RSE [%]	Value	RSE [%]	Value	RSE [%]	Description
Fixed Effects							
SBP ₍₀₎ (mmHg)	N/A	N/A	122	1	N/A	N/A	Baseline systolic blood pressure
DBP ₍₀₎ (mmHg)	N/A	N/A	59.5	1	N/A	N/A	Baseline diastolic blood pressure
HR ₍₀₎ (bpm)	N/A	N/A	56.7	1	N/A	N/A	Baseline heart rate
k _{Effect} (h ⁻¹)	N/A	N/A	4.37	6	N/A	N/A	Rate constant effect compartment
S _{Max}	N/A	N/A	0.512	49	N/A	N/A	Maximum effect in systolic blood pressure
D _{Max}	N/A	N/A	0.726	45	N/A	N/A	Maximum effect in diastolic blood pressure
EC50 (nmol/ml)	N/A	N/A	0.93	50	N/A	N/A	Concentration at which effect is half max
α	N/A	N/A	0.836	2	N/A	N/A	Amplitude cosine function blood pressure
Ω (h)	N/A	N/A	(24)	-	N/A	N/A	Period cosine function blood pressure
Shift (h)	N/A	N/A	12	2	N/A	N/A	Phase shift cosine function blood pressure
Random Effects: Interindividual variability (IIV)							
IIV SBP ₍₀₎ (%CV)	N/A	N/A	6	9	N/A	N/A	IIV in baseline of systolic blood pressure
IIV DBP ₍₀₎ (%CV)	N/A	N/A	11	9	N/A	N/A	IIV in baseline of diastolic blood pressure
IIV HR ₍₀₎ (%CV)	N/A	N/A	11	9	N/A	N/A	IIV in baseline of heart rate
Residual variability							
additive SBP (mmHg)	N/A	N/A	33	7	N/A	N/A	Additive residual error systolic blood pressure
additive DBP (mmHg)	N/A	N/A	26	6	N/A	N/A	Additive residual error diastolic blood pressure
additive HR (bpm)	N/A	N/A	23	8	N/A	N/A	Additive residual error heart rate

*RSE relative standard error,

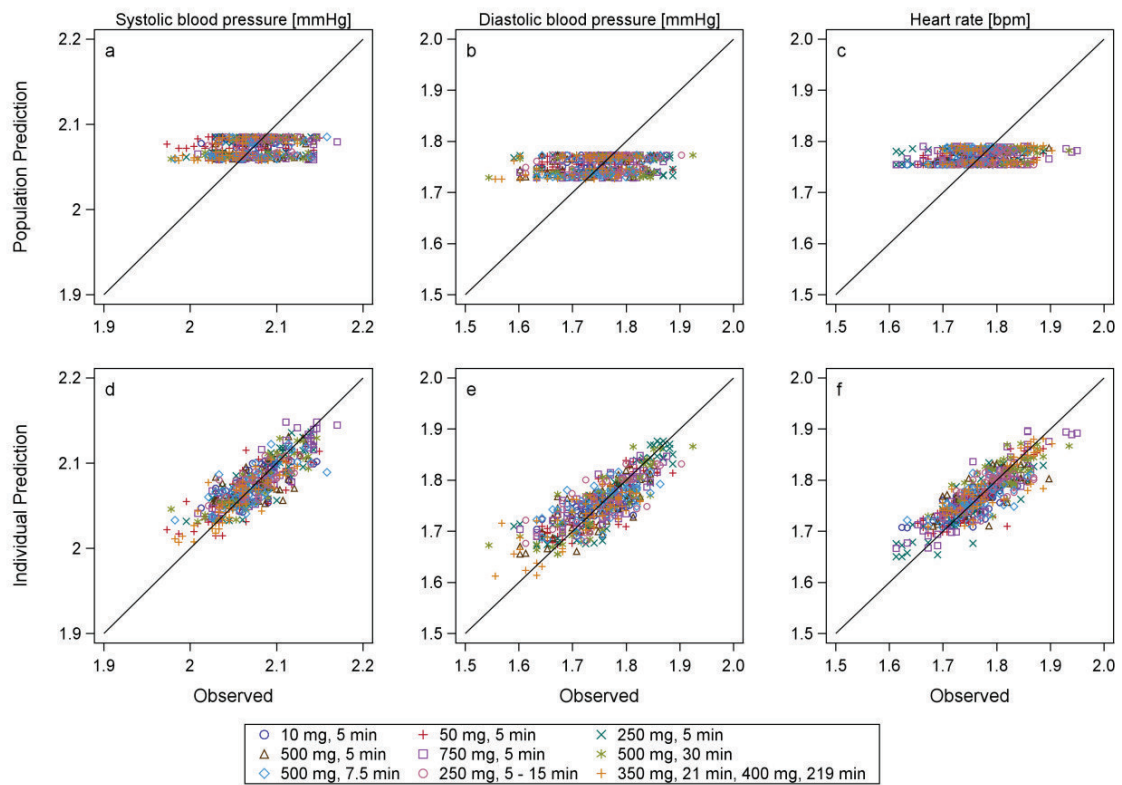
N/A: not applicable

Parameter values in parentheses were not estimated but fixed.

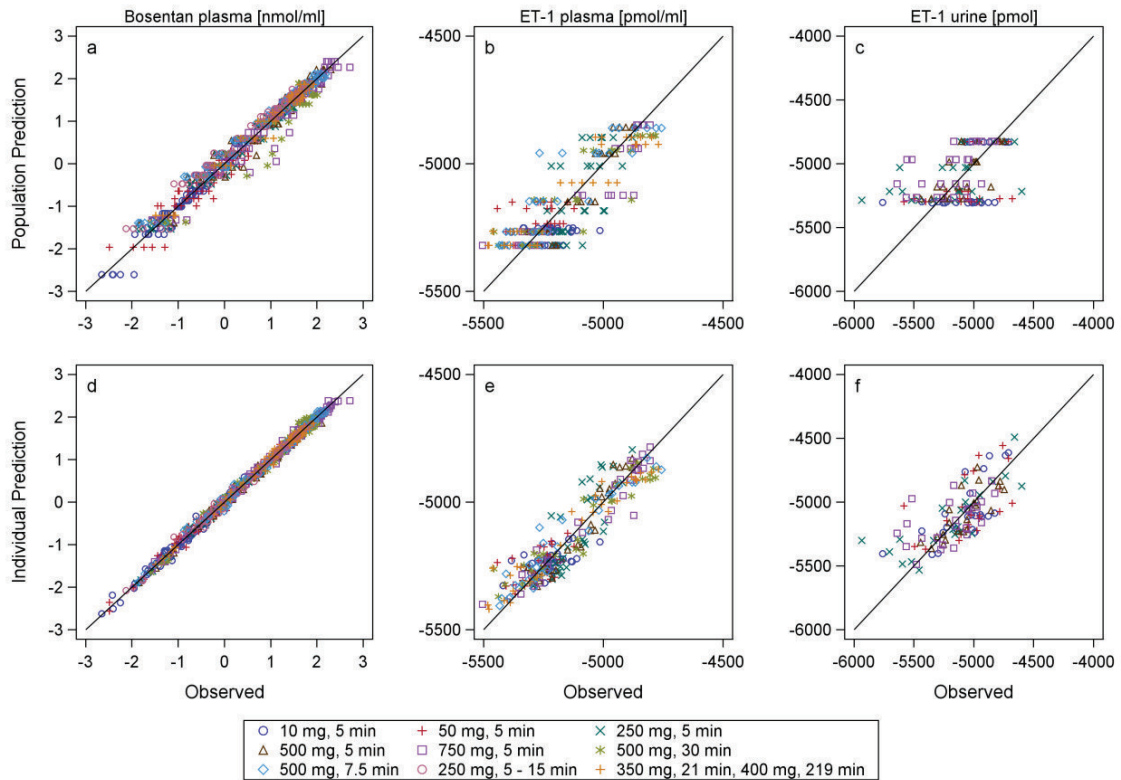
Supplementary Figure S1a Goodness-of-fit plots (**linear scale**) of pharmacodynamics with observed vs. population predicted (upper panels) or individual predicted (lower panels): systolic blood pressure (BP) [mmHg] (a, d), diastolic BP [mmHg] (b, e), heart rate [bpm] (c, f)



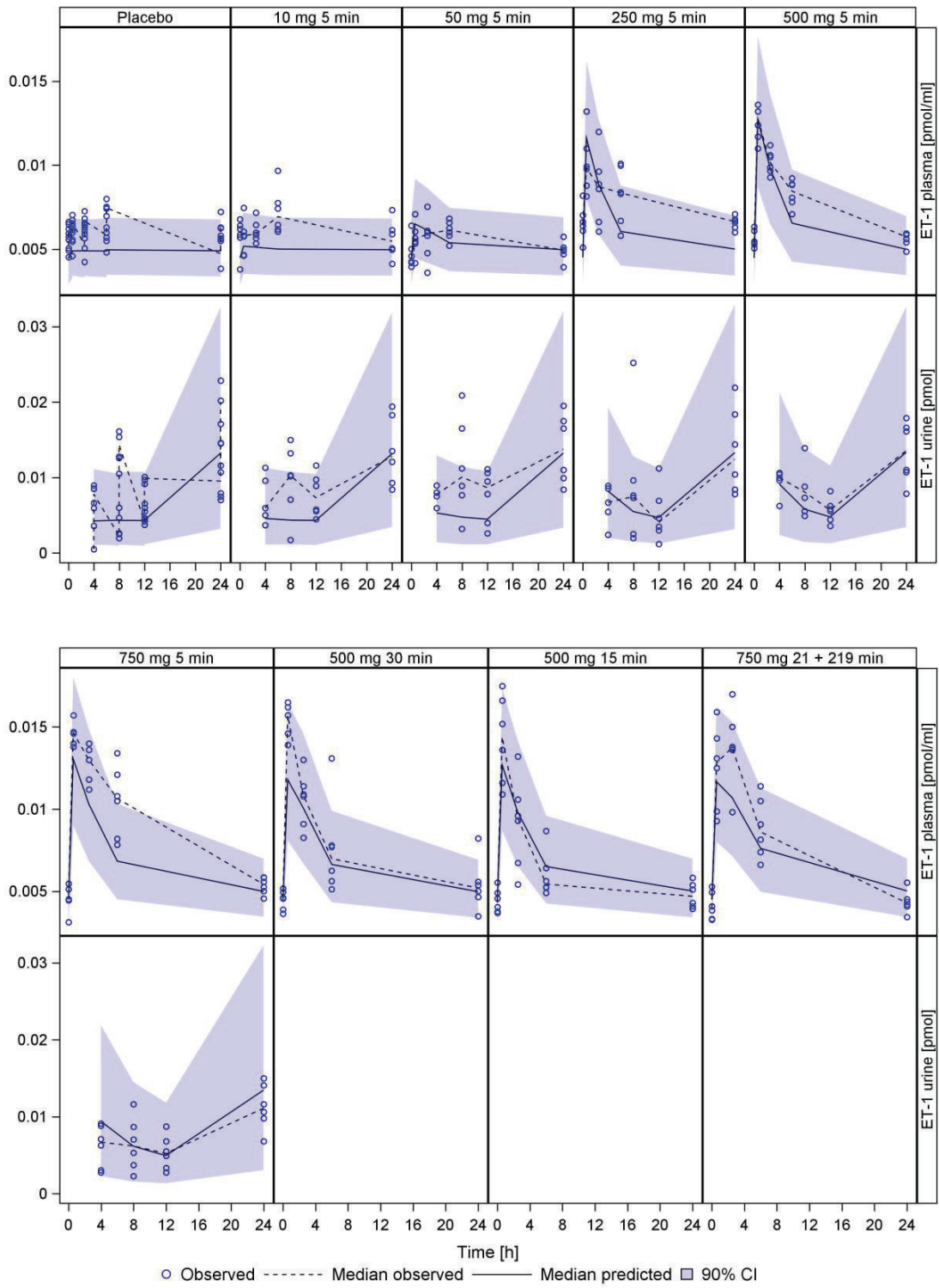
Supplementary Figure S1b Goodness-of-fit plots (**logarithmic scale, base 10**) of pharmacodynamics with observed vs. population predicted (upper panels) or individual predicted (lower panels): systolic blood pressure (BP) [mmHg] (a, d), diastolic BP [mmHg] (b, e), heart rate [bpm] (c, f)



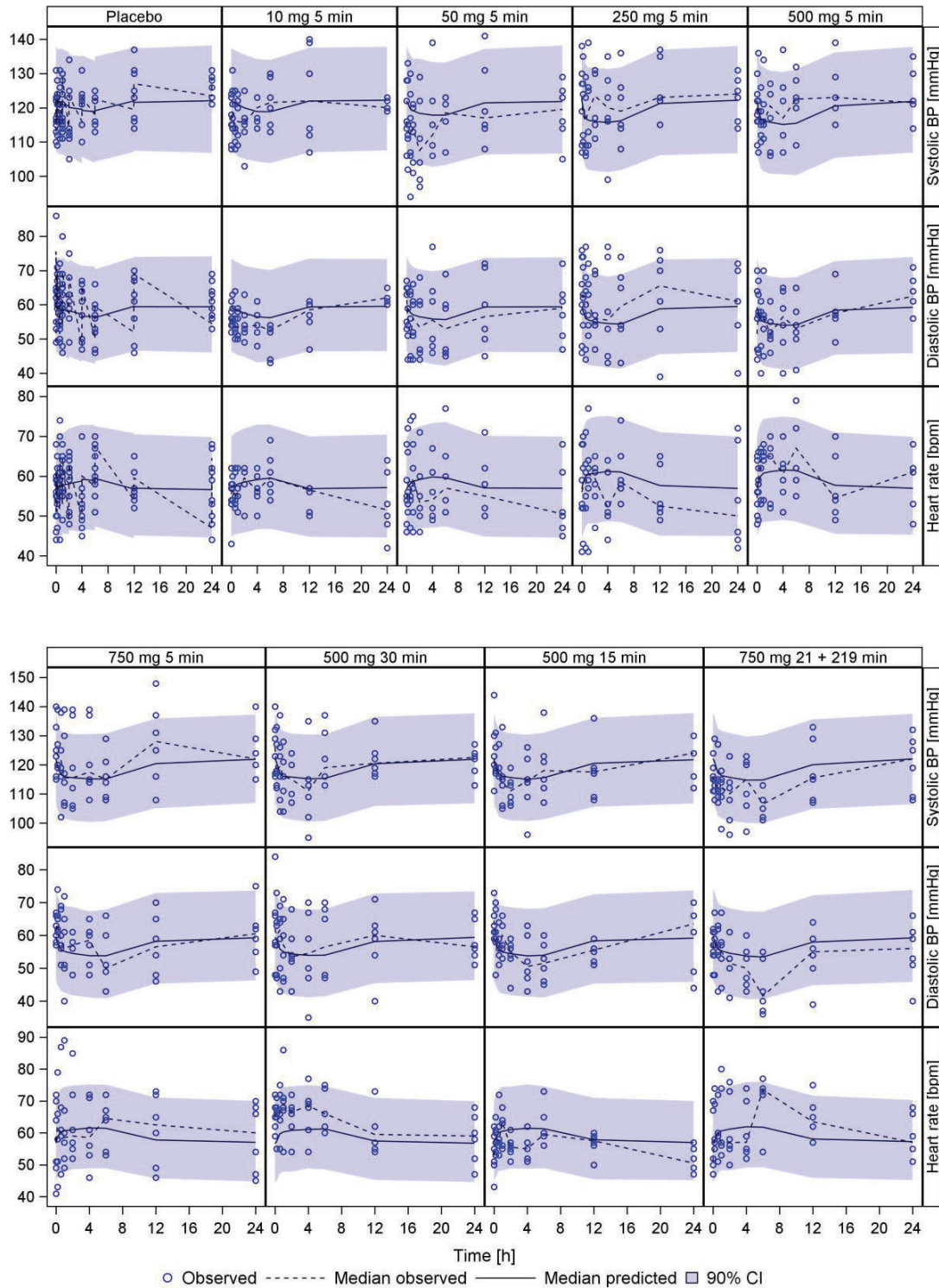
Supplementary Figure S2 Goodness-of-fit plot (logarithmic scale - base 10) of the final competitive PK/PD model: observed versus model population predicted (upper panels) or individual predicted (lower panels) data of the final competitive TMDD model: bosentan plasma concentration [nmol/ml] (a, d), ET-1 concentration [pmol/ml] in plasma (b, e), ET-1 amount in urine [pmol] at the end of each collection interval of 0-4 h, 4-8 h, 8-12 h and 12-24 h (c, f). Colors / symbols denote dosing groups. Black solid line: line of identity



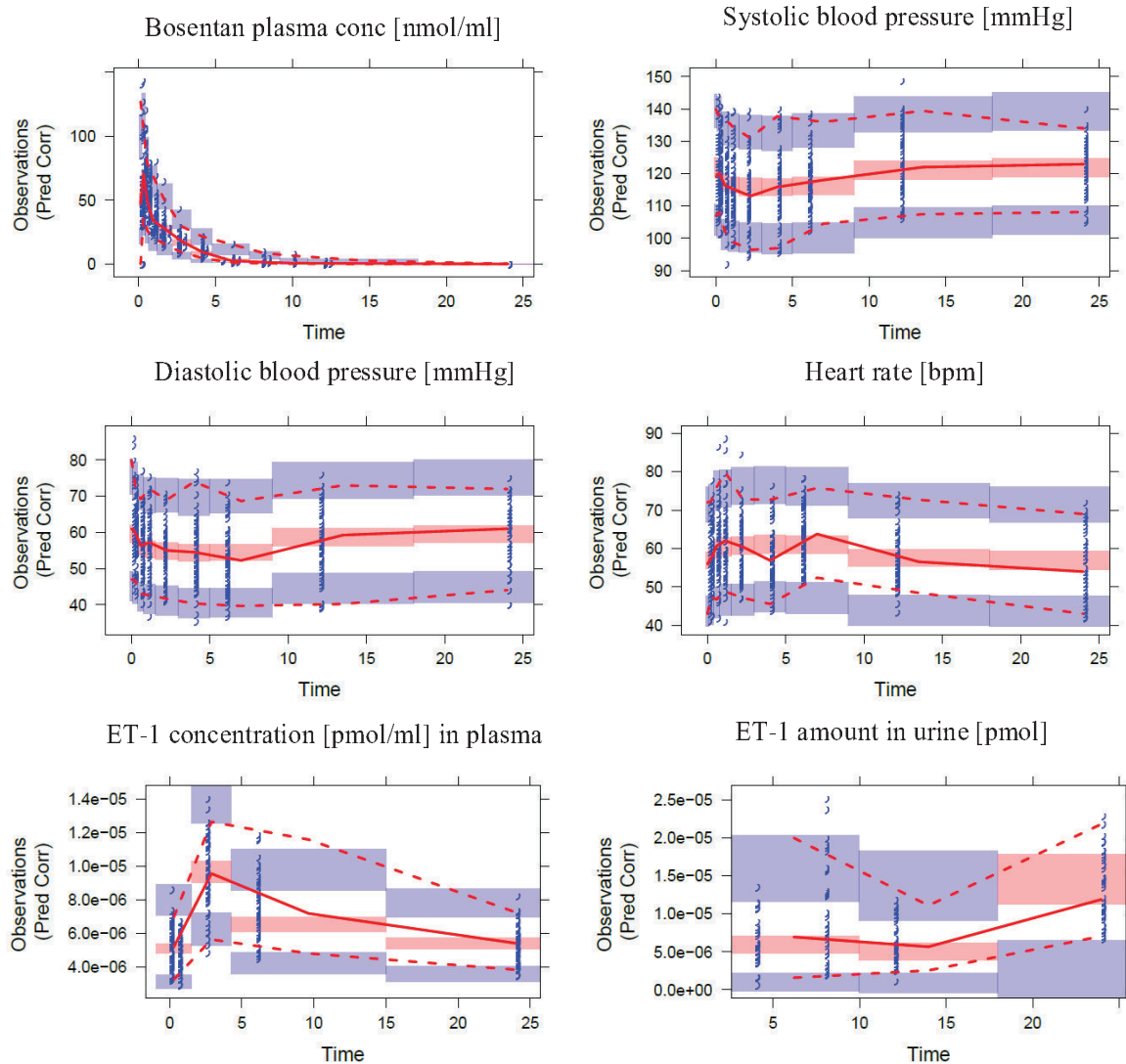
Supplementary Figure S3 Visual predictive check endothelin-1 (ET-1) concentration in plasma [pmol/ml] and amount in urine [pmol] at the end of each collection interval of 0-4 h, 4-8 h, 8-12 h, and 12-24. Open circles – observed concentrations, solid line – median predicted concentration, dashed line – median observed concentration, shaded area indicate 5th to 95th percentile of simulated concentrations in 1000 simulated subjects



Supplementary Figure S4 Visual predictive check of systolic and diastolic blood pressure (BP) [mmHg] and heart rate [bpm]. Open circles – observed concentrations, solid lines – median predicted concentrations, dashed line – median observed concentration, shaded areas indicate 5th to 95th percentile of simulated concentrations in 1000 simulated subjects



Supplementary Figure S5 Prediction corrected goodness-of-fit plot (linear scale) of the final competitive PK/PD model. Solid /dashed red line denote prediction corrected observed 5th percentile, median, 95th percentile. Shaded blue and red areas indicate respective confidence interval of the prediction corrected predicted 5th percentile, median, 95th percentile. Open circles represent prediction corrected observed data.



Clinical Pharmacokinetics

A target-mediated drug disposition pharmacokinetic-pharmacodynamic model of bosentan and endothelin-1

Anke-Katrin Volz, Andreas Krause, Walter Emil Haefeli, Jasper Dingemanse, Thorsten Lehr

Author for correspondence:

Thorsten Lehr, Clinical Pharmacy, Saarland University, 66123 Saarbrücken, Germany

E-mail: thorsten.lehr@mx.uni-saarland.de

Electronic supplementary material – NONMEM Code

\$PROBLEM Competitive bosentan-ET-1 PKPD

\$INPUT

\$DATA ../.csv IGNORE=@

\$SUBROUTINES ADVAN6 TOL=9

\$MODEL

COMP(Cent) ;1 central compartment bosentan
COMP(R) ;2 unoccupied receptor
COMP(RCB) ;3 receptor complex bosentan
COMP(P) ;4 peripheral compartment bosentan
COMP(ET1) ;5 endothelin-1 unbound (free)
COMP(RCE) ;6 receptor complex endothelin-1
COMP(ET1U) ;7 endothelin-1 in urine
COMP(Effect) ;8 pharmacodynamics: effect compartment
COMP(FCosBP) ;9 pharmacodynamics: cosine function blood pressure/heart rate

\$PK

Vc = THETA(1)*EXP(ETA(1)) ;volume central compartment
Vp = THETA(2)*EXP(ETA(2)) ;volume peripheral compartment
Q = THETA(3) ;intercompartmental clearance
kCP = Q/Vc
kPC = Q/Vp
RBase = THETA(4) ;receptor baseline at time point zero
A_0(2) = RBase
kDegR = THETA(5) ;rate constant degradation free receptor
kOnB = THETA(6) ;rate constant complex building bosentan
KdB = THETA(7) ;dissociation rate constant bosentan
kOffB = kOnB * KdB
kIntRCB = THETA(8)*EXP(ETA(3)) ;rate constant internalisation receptor complex bosentan
CL = THETA(9)*EXP(ETA(4)) ;total body clearance
kEB = CL/Vc ;elimination rate constant

BST0 = 0 ;concentration bosentan at time point zero
A_0(1) = ((kIntRCB*kOnB*RBase*BST0)/(kIntRCB+kOffB))+kEB*BST0
RCB0 = kOnB*RBase*BST0/(kIntRCB+kOffB)
A_0(3) = RCB0 ;RCB0 amount receptor complex bosentan at time point zero

EBase = THETA(10)*EXP(ETA(5)) ;endothelin-1 baseline level at time point zero
kEu = THETA(11)*EXP(ETA(6)) ;rate constant elimination endothelin-1 into urine
kEc = THETA(12)*EXP(ETA(7)) ;rate constant second elimination/degradation endothelin-1
kOnE = THETA(13) ;rate constant complex building endothelin-1
KdE = THETA(14) ;dissociation rate constant endothelin-1
kOffE = kOnE * KdE
kIntRCE = kIntRCB ;rate constant internalisation receptor complex endothelin-1

A_0(5) = ((kIntRCE*kOnE*RBase*EBase)/(kIntRCE+kOffE))+kEu*EBase+kEc*EBase
;endothelin-1 at time point zero
RCE0 = kOnE*EBase*RBase/(kIntRCE+kOffE)

A_0(6) = RCE0 ;amount receptor complex endothelin-1 at time point zero

PI = 3.1415927

alphaPD = THETA(15) ;amplitude cosine function blood pressure/heart rate

omegaPD = THETA(16) ;period cosine function blood pressure/heart rate

shiftPD = THETA(17) ;phase shift cosine function blood pressure/heart rate

SBase = THETA(18)*EXP(ETA(8)) ;baseline systolic blood pressure

DBase = THETA(19)*EXP(ETA(9)) ;baseline diastolic blood pressure

HBase = THETA(20)*EXP(ETA(10)) ;baseline diastolic blood pressure

kEffect = THETA(21) ;rate constant effect compartment

SMax = THETA(22) ;maximum effect systolic blood pressure

DMax = THETA(23) ;maximum effect diastolic blood pressure

EC50 = THETA(24) ;concentration at which effect is half maximum

+++++

;calculations compartment initialisation A(1),(3),(5) and (6) adapted from

;Yan X, Chen Y, Krzyzanski W.

;Methods of solving rapid binding target-mediated drug disposition model

;for two drugs competing for the same receptor.

;J. Pharmacokinet. Pharmacodyn. 2012;39:543–60.:

;bosentan at time point zero was set to 0: BST0 = 0

;Equation (16) page 545: $A_0(1) = ((k_{IntRCB} * k_{OnB} * R_{Base} * BST0) / (k_{IntRCB} + k_{OffB})) + k_{EB} * BST0$

;Equation (10) page 545: $RCB0 = k_{OnB} * R_{Base} * BST0 / (k_{IntRCB} + k_{OffB})$ then $A_0(3) = RCB0$

;Equation (17) page 545:

$A_0(5) = ((k_{IntRCE} * k_{OnE} * R_{Base} * E_{Base}) / (k_{IntRCE} + k_{OffE})) + k_{Eu} * E_{Base} + k_{Ec} * E_{Base}$

;Equation (13) page 545: $RCE0 = k_{OnE} * E_{Base} * R_{Base} / (k_{IntRCE} + k_{OffE})$ then $A_0(6) = RCE0$

+++++

S1 = Vc/1000 ;scaling central compartment for liter with DV [ng/ml] and AMT (DOSE) [mg]

```

;-----
$DES
;-----
;just information:
;Rtot = R + RCB + RCE total amount receptor
;BSTtot = BST + RCB total bosentan
;ET1tot = ET1 + RCE total endothelin-1

FB = kOnB*BST0*RBase-(kOffB*BST0*RBase/(kIntRCB+kOffB))
FE = kOnE*EBase*RBase-(kOffE*EBase*RBase/(kIntRCE+kOffE))
kSynR = kDegR * RBase + FB + FE ;rate constant synthesis free receptor
kSynE = kEu*EBase + kEc*EBase + kIntRCE*RCE0 ;rate constant synthesis endothelin-1

;+++++
;FB, FE, kSynR, kSynE calculations adapted from:
;Yan X, Chen Y, Krzyzanski W.
;Methods of solving rapid binding target-mediated drug disposition model
;for two drugs competing for the same receptor.
;J. Pharmacokinet. Pharmacodyn. 2012;39:543–60.

;Equation (15) page 545:
;kSynR=kDegR*RBase + kOnB*BST0*RBase-(kOffB*BST0*RBase/(kIntRCB+kOffB)) +
kOnE*EBase*RBase-(kOffE*EBase*RBase/(kIntRCE+kOffE))
;which is kSynR=kDegR*RBase+FB+FE

;Equation (102) page 553:
;kSynE = kEu*EBase + kEc*EBase + kIntRCE*RCE0
;+++++

DADT(1)= -kEB*A(1) -kOnB*A(1)*A(2)+kOffB*A(3) -kCP*A(1)+kPC*A(4)
;1 central compartment bosentan
DADT(2)= -kOnB*A(1)*A(2)+kOffB*A(3) -kOnE*A(2)*A(5)+kOffE*A(6) + kSynR-kDegR*A(2)
;2 unoccupied receptor
DADT(3)= kOnB*A(1)*A(2)-kOffB*A(3) -kIntRCB*A(3)
;3 receptor complex bosentan
DADT(4)= kCP*A(1)-kPC*A(4)
;4 peripheral compartment bosentan
DADT(5)= -kOnE*A(2)*A(5)+kOffE*A(6) +kSynE-kEu*A(5)-kEc*A(5)
;5 endothelin-1 free (measurement plasma)
DADT(6)= kOnE*A(2)*A(5)-kOffE*A(6) -kIntRCE*A(6)
;6 receptor complex endothelin-1
DADT(7)= kEu*A(5)
;7 endothelin-1 in urine (measurement urine)
DADT(8)= kEffect * (A(3)-A(8))
;8 pharmacodynamics: effect compartment
DADT(9)=1+ alphaPD*cos((2*PI/omegaPD)*(T-shiftPD)) -1
;9 pharmacodynamics: cosine function blood pressure/heart rate which is
FCosBP=(alphaPD*sin((2*PI/omegaPD)*(TIME-shiftPD)))

```

;------
\$ERROR

;------
AEffct = A(8) ;rename(theoretical) amount of receptor complex bosentan in effect
compartment
FCosBP = A(9) ;rename cosine function blood pressure/heart rate

EffectSBP = (SMax*AEffct/(AEffct+EC50)) ;Emax function effect systolic blood pressure
SBP = (SBase+FCosBP)*(1-EffectSBP) ;pharmacodynamic effect systolic blood pressure
EffectDBP = (DMax*AEffct/(AEffct+EC50)) ;Emax function effect diastolic blood pressure
DBP = (DBase+FCosBP)*(1-EffectDBP) ;pharmacodynamic effect diastolic blood pressure
MAPbase = DBase + 1/3*(SBase-DBase) ;baseline mean arterial blood pressure
MAP = DBP + 1/3*(SBP-DBP) ;mean arterial blood pressure
HR = HBase*(MAPbase/MAP) ;compensatory increase in heart rate

IPRED = A(1)/S1 ;prediction central compartment bosentan
IF (CMT.EQ.5) IPRED = A(5) ;prediction endothelin-1 plasma
IF (CMT.EQ.7) IPRED = A(7) ;prediction endothelin-1 urine
IF (FLAG.EQ.2) IPRED = SBP ;prediction systolic blood pressure
IF (FLAG.EQ.3) IPRED = DBP ;prediction diastolic blood pressure
IF (FLAG.EQ.4) IPRED = HR ;prediction heart rate

DEL=0
IF (IPRED.EQ.0) DEL=0.0001
W=IPRED
IRES = DV - IPRED
IWRES = IRES/(W+DEL)

Y = IPRED + W * EPS(1) ;residual variability bosentan
IF (CMT.EQ.5) Y = IPRED + IPRED * EPS(2) ;residual variability endothelin-1 plasma
IF (CMT.EQ.7) Y = IPRED + IPRED * EPS(3) ;residual variability endothelin-1 urine
IF (FLAG.EQ.2) Y = IPRED + EPS(4) ;residual variability systolic blood pressure
IF (FLAG.EQ.3) Y = IPRED + EPS(5) ;residual variability diastolic blood pressure
IF (FLAG.EQ.4) Y = IPRED + EPS(6) ;residual variability heart rate

\$THETA

(0,4.14) ;1 Vc
(0,5.72) ;2 Vp
(0,11.3) ;3 Q
(0,0.111) ;4 RBase
(0,0.101) ;5 kDegR
(0,48.4) ;6 kOnB
(0,0.00762) ;7 KdB
(0,0.133) ;8 kIntRCB/RCE
(0,5.18) ;9 CL
(0,0.000005) ;10 EBase
(0,0.23) ;11 kEu
(0,0.298) ;12 kEc
(0,62.3) ;13 kOnE
(0,0.0389,2) ;14 KdE
(0,0.811,1) ;15 alphaPD
(24) FIX ;16 omegaPD
(0,11.8,24) ;17 shiftPD
(0,121) ;18 SBPbase
(0,58.9) ;19 DBPbase
(0,56.9) ;20 HRbase
(0,1.85) ;21 kEffect
(0,0.199,1) ;22 SBPmax
(0.726) FIX ;23 DBPmax
(0,0.485) ;24 EC50

\$OMEGA

0.01 ;1 IIV Vc
0.01 ;2 IIV Vp
0.01 ;3 IIV kInt
0.01 ;4 IIV CL
0.01 ;5 IIV EBase
0.01 ;6 IIV kEu
0.01 ;7 IIV kEc
0.01 ;8 IIV SBPbase
0.01 ;9 IIV DBPbase
0.01 ;10 IIV HRbase

\$SIGMA

0.0579 ;prop. error plasma bosentan
0.0307 ;prop. error endothelin-1 plasma
0.193 ;prop. error endothelin-1 urine
0.01 ;add. error systolic blood pressure
0.01 ;add. error diastolic blood pressure
0.01 ;add. error heart rate

\$ESTIMATION METHOD=1 INTER MAXEVAL=9999 POSTHOC NOABORT PRINT=1 SIGL=9
SIGDIG=3
\$COV
\$TABLE FILE=



Target-Mediated Population Pharmacokinetic Modeling of Endothelin Receptor Antagonists

Anke-Katrin Volz¹ · Jasper Dingemanse² · Andreas Krause² · Thorsten Lehr¹

Received: 10 July 2019 / Accepted: 16 October 2019

© Springer Science+Business Media, LLC, part of Springer Nature 2019

ABSTRACT

Purpose Bosentan, clazosentan, and tezosentan are three small-molecule endothelin receptor antagonists (ERAs), displacing endothelin-1 (ET-1) from its binding site. A target-mediated drug disposition (TMDD) pharmacokinetic (PK) model described the non-linearity in the PK of bosentan caused by its high receptor binding affinity with time-dependent varying receptor expression or re-appearance. The aim of this analysis was to investigate the presence of TMDD for clazosentan and tezosentan and to corroborate the hypothesis of a diurnal receptor synthesis.

Methods PK data from healthy subjects after intravenous (i.v.) administration of single ascending doses of bosentan, clazosentan, and tezosentan were analyzed. Frequent blood samples for PK measurements were collected. Population analyses, simulations, and evaluations were performed using a non-linear mixed-effects modeling approach.

Results Two-compartment TMDD models were successfully developed describing the PK of all three ERAs with different receptor-complex internalization properties. The observed multiple peaks in the concentration-time profiles were captured with cosine functions on the receptor synthesis rate mimicking a diurnal receptor expression or re-appearance. The results strongly suggest that TMDD is a class effect of ERAs.

Conclusion The developed TMDD PK models are a next step towards understanding the complex PK of ERAs and further support the hypothesis that TMDD is a class effect of ERAs.

KEY WORDS bosentan · clazosentan · pharmacokinetic modeling · target-mediated drug disposition · tezosentan

ABBREVIATIONS

ACE	Angiotensin-converting enzyme
AUC	Area under the plasma concentration-time curve
CL	Total body clearance
C _{max}	Maximum plasma concentration
CV	Capital coefficient of variation
CWRes	Conditional weighted residuals
CYP	Cytochrome P450
DDP-4	Dipeptidyl peptidase-4
EHC	Enterohepatic recirculation
ERA	Endothelin receptor antagonist
ET	Endothelin
ET-1	Endothelin-1
ET _A	Endothelin receptor subtype A
ET _B	Endothelin receptor subtype B
F _{Cos}	Cosine function
GOF	Goodness-of-fit
i.v.	Intravenous
IIV	Interindividual variability
K _d	Dissociation rate constants
k _{DegR}	Rate constant degradation free / unoccupied receptor
k _E	Elimination rate constant
k _{IntRC}	Internalization rate constant
k _{Off}	Rate constant complex dissociating drug
k _{On}	Rate constant complex building drug
k _{SynR}	Rate constant receptor synthesis
l	Litre

Electronic supplementary material The online version of this article (<https://doi.org/10.1007/s11095-019-2723-3>) contains supplementary material, which is available to authorized users.

✉ Thorsten Lehr
thorsten.lehr@mx.uni-saarland.de

¹ Clinical Pharmacy, Saarland University, 66123 Saarbrücken, Germany

² Department of Clinical Pharmacology, Idorsia Pharmaceuticals Ltd, 4123 Allschwil, Switzerland

LC-MS/MS	Liquid chromatography with tandem mass spectrometry
LLOQ	Lower limits of quantification
OFV	Objective function value
PBPK	Physiologically-based pharmacokinetic
PD	Pharmacodynamic
PK	Pharmacokinetic
Q	Intercompartmental clearance
R_{base}	Receptor baseline
TMDD	Target-mediated drug disposition
V	Volume of distribution
V_{Central}	Volume of distribution central compartment
VPC	Visual predictive check
$V_{\text{Peripheral}}$	Volume of distribution peripheral compartment
α	Amplitude cosine function
Ω	Period cosine function

INTRODUCTION

Target-mediated drug disposition (TMDD) is a special form of pharmacokinetic (PK) non-linearity in which the strong binding of the drug to its target influences the PK. TMDD (and the resulting non-linearity in PK) is often recognized by a dose-dependent disproportional change in (apparent) volume of distribution (V), total body clearance (CL), maximum plasma concentration (C_{max}), or area under the plasma concentration-time curve (AUC). Monoclonal antibodies are the most prominent class of molecules undergoing TMDD (1). However, TMDD has been described also for some small molecules such as selegiline (2), warfarin (3), the angiotensin-converting enzyme (ACE) inhibitors enalaprilat, perindoprilat, and cilazaprilat (4), and the dipeptidyl peptidase-4 (DDP-4) inhibitor linagliptin (5). Although TMDD might be regarded as an undesirable drug feature, it also offers opportunities. Based on concentration-time profiles it can provide important information on target engagement and exposure can be used as a pharmacodynamic (PD) biomarker (6–8), e.g., plasma endothelin-1 (ET-1) could serve as a potential biomarker to determine the receptor occupancy of bosentan (9). As small and large molecules become more potent, analytical methods more sensitive and with the application of micro-dosing, it is very likely that further reports on TMDD will be emerging (10).

Endothelin (ET) receptors with the subtypes A and B (ET_A and ET_B) are a class of G protein coupled receptors predominantly expressed in vascular smooth muscle cells (ET_A), endothelia cells and renal tubulus (ET_B) (11). They follow different signaling as well as internalization pathways after the natural ligand ET-1 has been bound; the ET_A receptor enters a recycling pathway and is represented at the cell surface again, while ET_B serves as a ‘clearance receptor’ removing ET-1

from the systemic circulation through internalization and degradation (11–17). One reason for a long-lasting vasoconstrictive effect of ET-1 bound to ET_A is binding to the receptor for up to approximately 2 h after internalization (11,16,17).

Endothelin receptor antagonists (ERAs) build a class of small-molecule compounds such as bosentan, macitentan, clazosentan, tezosentan, or ambrisentan, which bind to ET receptors and thereby displace the endogenous binding partner ET-1 from its binding site. Consequently, they cause vasodilatation, reduced blood pressure, as well as other compound-specific PD effects. It was observed that receptor complex internalization is not only induced by the natural ligand ET-1 but that it can also occur after receptor binding of ERAs (18). A TMDD model was previously introduced for bosentan (19) and a mechanistic two-compartment TMDD PK model described the competitive relationship between bosentan and ET-1 (9). The model suggested that strong binding of bosentan to the receptors is responsible for its non-linear PK (9). Observing TMDD for bosentan and considering the properties of ERAs, it is hypothesized that TMDD is a class effect, although so far it has been suggested only for bosentan.

The primary aim of this analysis was to investigate the presence of TMDD for clazosentan and tezosentan in comparison to bosentan (9), using a population PK modeling approach. Additionally, multiple peaks in the plasma concentration-time profiles of bosentan after intravenous (i.v.) administration were observed and explained by a diurnal expression or reoccurrence of the target. Thus, a second aim of the analysis was to further investigate the hypothesis on clock-dependent target fluctuation as a class effect of ERAs investigating three representatives of this class, i.e., bosentan, clazosentan, and tezosentan.

MATERIAL AND METHODS

Compounds and Study Data

Bosentan was the first approved ERA. It is a competitive antagonist on ET_A and ET_B and frequently used in the therapy of pulmonary arterial hypertension. After i.v. administration of single ascending doses in healthy male subjects, it showed non-linear PK (9,20). It is highly bound to albumin (21) and mainly eliminated with feces (22) after metabolism by cytochrome P450 (CYP) enzymes (21). Bosentan affects its own metabolism by inducing CYP3A4, CYP2C9, and possibly CYP2C19 (21). The main metabolite hydroxybosentan contributes to the overall efficacy with 10–20% (21). Uptake into hepatocytes occurs via organic anion transporting polypeptides. Bosentan is also an inhibitor of the bile salt export pump, as well as a substrate and possibly inducer of P-glycoprotein (23). Data used for this population PK analysis were generated in a placebo-controlled first-in-humans study in healthy male

subjects (20). In this study bosentan was administered as single i.v. injection or infusion over a wide dose range from 10 to 750 mg. Blood samples for plasma concentrations were taken pre-dose, and 14 times up to 24 h after dosing of bosentan or placebo, leading to 706 bosentan plasma concentrations from 54 of 70 subjects. Depending on the plasma concentration, HPLC-UV or narrow-bore liquid chromatography with tandem mass spectrometry (LC-MS/MS) detection using ion spray was used. The lower limits of quantification (LLOQ) were 50 ng/ml (0.088 nmol/ml) and 500 pg/ml (8.8×10^{-4} nmol/ml), respectively.

Clazosentan is an ERA which binds with high selectivity to ET_A (24,25) and with lower affinity to ET_B . It was developed for parenteral use for the acute treatment of emergency indications; clazosentan prevented and reversed cerebral vasospasm in a canine model of subarachnoid hemorrhage (24,26). It is highly bound to plasma proteins (> 98%) and primarily eliminated unchanged via bile into feces (26). PK analysis of clazosentan indicated dose-proportionality in C_{max} and AUC (24,26). However, CL and V decreased with higher doses (24,26). One minor metabolite formed by CYP2C9 (26) was identified. For population PK modeling, the first-in-humans study of clazosentan was used in which the compound was administered as single i.v. infusions of 3, 10, 30, or 60 mg/h with varying infusion durations, resulting in six dosing groups. The study population consisted of 48 healthy, male subjects. In each dosing group, six subjects were treated with clazosentan and two received a placebo infusion. The infusions started between 9 and 10 a.m. after an overnight fast. Blood samples for clazosentan plasma concentrations were taken pre-dose, and at 1, 2, 2.5, 3 h during the 3-h infusion, at 1, 3, 5, 6 h during the 6-h infusion, and at 1, 3, 6, 11, 12 h during the 12-h infusion. Blood samples were also taken 0.25, 0.5, 0.75, 1, 1.5, 2, 3, 4, 5, 6, 9, and 12 h after end of the infusions. Plasma levels of clazosentan were determined by LC-MS/MS. The LLOQ was 2 ng/ml (3.2×10^{-3} nmol/ml). Overall, 472 clazosentan plasma concentrations were available for analysis.

Tezosentan is an ERA with high affinity to both receptors, ET_A and ET_B (27,28). It was also developed for parenteral use and found to be effective in animal models of hypertension, acute renal failure, and heart failure (29). It increases cardiac output and renal blood flow, decreases pulmonary pressure and the occurrence of pulmonary edema, and induces coronary vasodilatation (29). Tezosentan showed dose-proportionality in C_{max} and AUC (27,29) while CL and V decreased with higher doses (27,29). It is highly bound to albumin (30) and predominantly eliminated unchanged via liver and bile into the feces (29). Several minor metabolites were detected (30). One metabolite shows an activity towards ET receptors, but its potency is 10–20-fold lower than that of tezosentan (27,30). Overall, 539 tezosentan plasma concentrations from 42 of 56 healthy, male subjects were used for

the analysis (27). The compound was administered as i.v. infusion of 5, 20, 50, 100, 200, 400, and 600 mg over 1 h in seven different dosing groups. In each dosing group, six subjects were treated with tezosentan and two received a placebo infusion. Infusions started between 8 and 10 a.m. after an overnight fasting. Blood samples were taken pre-dose, 0.25, 0.5, 0.75, 1, 1.25, 1.5, 1.75, 2, 2.5, 3, 4, 5, 7, 12, and 15 h after start of infusion. Plasma levels of tezosentan were analyzed by LC-MS/MS. The LLOQ was 2.5 ng/ml (3.5×10^{-3} nmol/ml).

For all three ERAs, all post-dose bioanalytical measurements were above the LLOQ. A summary of dose groups and population characteristics is presented in supplementary Tables S1 and S2, respectively.

Model Development and Evaluation

The non-linear mixed effects modeling approach was used (31); population analyses, simulations, and model evaluation were performed with NONMEM version 7.3 (ICON Development Solutions, Ellicott City, MD, USA). Model selection was based on visual inspection of goodness-of-fit (GOF) plots, precision of parameter estimates, and the objective function value (OFV) provided by NONMEM. A model was considered superior to a nested (reduced) model if the OFV was reduced by 10.83 units (χ^2 test statistic, $p \leq 0.001$, 1 degree of freedom). All pre-dose sampling times were set to zero. SAS version 9.4 (SAS Institute Inc., Cary, NC, USA) was used for statistical analyses and generation of graphics.

Model development was performed sequentially for each compound evaluating the model structure without incorporation of random effects but including residual variability. The model development process started with linear one-, two-, and three-compartment models with different distribution and elimination processes (e.g., Michaelis-Menten kinetics or incorporation of a liver compartment). Afterwards, TMDD models were investigated stepwise and optimized for distribution and elimination characteristics until a good fit for the structural model was obtained. Dissociation rate constants (K_d) were fixed to values that were obtained from *in vitro* assays for clazosentan and tezosentan (25,32) and in case of bosentan to the previously estimated value (9). It was evaluated if the receptor complex could be degraded by incorporating an internalization rate constant (k_{intRC}) in each model. If structural model misspecifications were observed and empirical Bayesian estimates indicated a bimodal distribution, mixture models (two sub-populations) were evaluated for selected parameters such as CL, V, receptor baseline (R_{Base}), or k_{intRC} using the \$Mixture procedure in NONMEM. Important key structural models and their OFV as provided by NONMEM are presented in supplementary Tables S3, S4, and S5 respectively. To evaluate the hypothesized diurnal or circadian fluctuation in target expression or

recurrence, a cosine function (9) was integrated into each model. Interindividual variability (IIV) was tested on the final structural (base) model in a stepwise procedure one by one for statistical significance ($p \leq 0.001$, 1 degree of freedom). Numerical model stabilities were assessed by changing the initial parameter $\pm 10\%$, which did not result in markedly different estimates. Visual predictive checks (VPCs) based on 1000 simulations using the final PK models were performed stratified by dose group. Medians and corresponding 5th and 95th percentiles of data simulated from the models were plotted against time and the observed data superimposed to assess if data simulations from the model were in line with observed data.

RESULTS

For bosentan, clazosentan, and tezosentan, a two-compartment TMDD model described the available plasma concentration-time profiles best and was superior to one-, two- or three-compartment models without TMDD component. The final PK models are illustrated in Fig. 1 and NONMEM codes are provided in the supplementary material. GOF plots of all final PK models are depicted in Fig. S1 in the supplementary materials. Parameter values were estimated with good accuracy (Table I) and the VPC stratified by dose showed a satisfactory descriptive performance for each model (supplementary Fig. S2). The ERAs were administered directly into the central compartment (i.v. administration) from where they were distributed with rate Q to the peripheral compartment (volume of distribution $V_{\text{Peripheral}}$). Elimination occurred from the central compartment (volume of distribution V_{Central}) with first-order rate constant ($k_E = \text{CL} / V_{\text{Central}}$) or the ERAs were bound to the receptor with a second-order rate constant (k_{On}). ET_A and ET_B receptors were considered as one receptor. A turnover model was used to describe the receptor with a zero-order synthesis rate constant (k_{SynR}) and a first-order degradation rate constant (k_{DegR}). The drug-receptor complex was either dissociated

with rate constant k_{Off} ($k_{\text{Off}} = k_{\text{On}} \times R_{\text{Base}}$) or, depending on the compound, also degraded by k_{IntRC} . Compound-specific details are described in the following.

Bosentan PK model: After binding to the receptor, bosentan was internalized or dissociated again. Free bosentan was eliminated from the central compartment with a k_E of approximately 1.2 h^{-1} . The estimated apparent volumes of distribution, V_{Central} and $V_{\text{Peripheral}}$, were 4.26 l and 6.38 l, respectively. A low to moderate IIV was observed for k_{IntRC} (17 %CV), V_{Central} and $V_{\text{Peripheral}}$ (20 to 41 %CV), and CL (34 %CV).

Clazosentan PK model: Clazosentan receptor binding occurred fast with high receptor binding affinity ($K_d = 0.2 \text{ nM}$). No internalization process of the drug-receptor complex could be identified. The clazosentan-receptor complex dissociated again and the free compound in plasma was exclusively eliminated from the central compartment with a k_E of approximately 6.66 h^{-1} . Total CL was approximately eight times as high compared to bosentan (38.1 l/h vs. 4.97 l/h), while the volumes of distribution were as small as for bosentan ($V_{\text{Central}} = 5.76 \text{ l}$ and $V_{\text{Peripheral}} = 3.16 \text{ l}$). Low IIVs were observed on V_{Central} (20 %CV), R_{Base} (20 %CV) and CL (14 %CV).

Tezosentan PK model: Tezosentan (as clazosentan) was bound to the receptor with high affinity ($K_d = 0.26 \text{ nM}$). The tezosentan-receptor complex either dissociated or internalized. From the stepwise model development, it was observed that internalization of the complex was necessary to adequately describe the data ($p < 0.001$). However, some remaining misspecifications in the lower concentration range were still present in the observed vs. predicted GOF plot so that the structural model was not fully satisfactory. Therefore, mixture models were evaluated, finally identifying two subpopulations with different typical values for k_{IntRC} , improving the descriptive performance of the model statistically significantly ($p < 0.001$). For approximately 77% of subjects

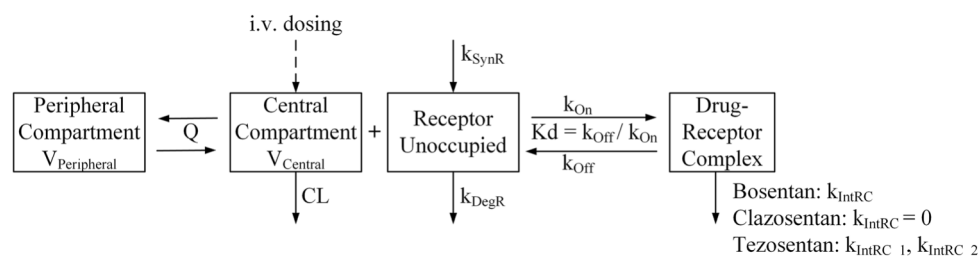


Fig. 1 Two-compartment TMDD PK model for bosentan, clazosentan, and tezosentan. CL total body clearance, K_d dissociation rate constant, k_{DegR} degradation rate constant of unoccupied receptor, k_{IntRC} internalization rate constant of the bosentan, k_{IntRC_1} and k_{IntRC_2} internalization rate constants of tezosentan complex, k_{Off} rate constant for complex dissociation, k_{On} rate constant for complex building, k_{SynR} synthesis rate constant of unoccupied receptor, Q intercompartmental clearance, V_{Central} volume of distribution central compartment, $V_{\text{Peripheral}}$ volume of distribution peripheral compartment.

Table 1 Parameter Estimates of the Final PK Model with Cosine Function on Receptor Production Rate for Bosentan, Clazosentan, and Tezosentan

Parameter	Bosentan		Clazosentan		Tezosentan		
	Value	RSE*[%]	Value	RSE*[%]	Value	RSE*[%]	
Fixed effects							
V _{Central} (l)	4.26	7	5.76	5	5.38	5	Volume of distribution of central compartment
V _{Peripheral} (l)	6.38	7	3.16	10	1.85	10	Volume of distribution of peripheral compartment
Q (l/h)	11.4	13	6.05	9	2.71	10	Intercompartmental clearance
R _{Base} (μmol)	0.106	9	0.0022	8	0.111	50	Receptor baseline
k _{DegR} (h ⁻¹)	0.143	13	4.5	29	1.2	13	Rate constant degradation free receptor
Kd (nM)	(1.5)	N/A	(0.2)	N/A	(0.26)	N/A	Dissociation rate constant drug
k _{On} (μmol ⁻¹ * h ⁻¹)	48.5	11	402	9	22.8	29	Rate constant complex building drug
k _{IntRC} (h ⁻¹)	0.144	5	0	N/A	0.204 ^a / 0.03 ^b	5 ^a / 40 ^b	Rate constant internalization of the drug – receptor complex
CL (l/h)	4.97	6	38.1	3	26.4	14	Total body clearance
α	(1)	N/A	(0.872)	N/A	(0.404)	N/A	Amplitude cosine function
Ω (h)	(8)	N/A	(8)	N/A	(8)	N/A	Period cosine function
Shift (h)	(4.28)	N/A	(7.28)	N/A	(7.53)	N/A	Phase shift cosine function
Random effects: Interindividual variability (IIV)							
IIV V _c (%CV)	41	13	20	15	N/A	N/A	IIV in volume of distribution, central compartment
IIV V _p (%CV)	20	16	N/A	N/A	54	12	IIV in volume of distribution, peripheral compartment
IIV R _{Base} (%CV)	N/A	N/A	20	27	N/A	N/A	IIV in receptor baseline
IIV k _{IntRC} (%CV)	17	14	N/A	N/A	N/A	N/A	IIV in internalization of the (two) complexes
IIV CL (%CV)	34	16	14	10	31	10	IIV in total body clearance
Residual variability							
proportional plasma drug (%)	22	7	15	11	29	5	Proportional residual error plasma
additive plasma drug (nmol/ml)	N/A	N/A	(1*10 ⁻⁶)	N/A	N/A	N/A	Additive residual error plasma

*RSE relative standard error; N/A: not applicable, fixed parameter value or parameter not estimated, Parameter values in parentheses were not estimated but fixed

^a k_{IntRC} population 1, ^b k_{IntRC} population 2,

(population 1), k_{IntRC} (for this population k_{IntRC_1}) was 0.204 h⁻¹, and for 23% of the population (population 2) an internalization rate constant of k_{IntRC_2} = 0.03 h⁻¹ was estimated, i.e., about 15% of the corresponding parameter in population 1. V_{Central} was within the range of bosentan and clazosentan with 5.38 l, whereas V_{Peripheral} was estimated very small with approximately 2 l. Low to moderate IIVs were identified on tezosentan CL and V_{Peripheral} (31 and 54 %CV). The relative contribution of the TMDD on total clearance of bosentan and tezosentan is visualized in Fig. 2.

Multiple peaks in individual plasma concentration-time profiles were observed for all three ERAs, leading to wave-like patterns in conditional weighted residuals (CWRs) over time (Fig. 3). Such patterns might, for example, be a consequence of enterohepatic recirculation (EHC) of a drug (33). As far as known, EHC could not be shown for the investigated ERAs, and implementation of an established EHC model (34)

did not improve model fits (data not shown). Therefore, the formerly developed cosine function (F_{Cos}) (9) for k_{SynR} was implemented in each PK model mimicking a time-dependent receptor synthesis or reappearance:

$$F_{Cos} = 1 + \alpha \times \cos((2\pi/\Omega) \times (time - shift)),$$

$$k_{SynR} = k_{DegR} \times R_{Base} \times F_{Cos}$$

The period Ω was tested in a stepwise manner and fixed to 24, 12, 8, and 6 h allowing to estimate the time of occurrence of the maximum (shift) relative to time after start of treatment. k_{DegR} denotes the degradation rate of the unoccupied receptor with a baseline R_{Base} at time zero. The period to best fit the data was found to be 8 h with an estimated shift of 4.3, 7.3, and 7.5 h for bosentan, clazosentan, and tezosentan, respectively. The amplitude α was estimated to 0.87 for clazosentan and 0.40 for tezosentan. Since α was estimated close to the upper boundary of 1 for bosentan, it was fixed to 1.

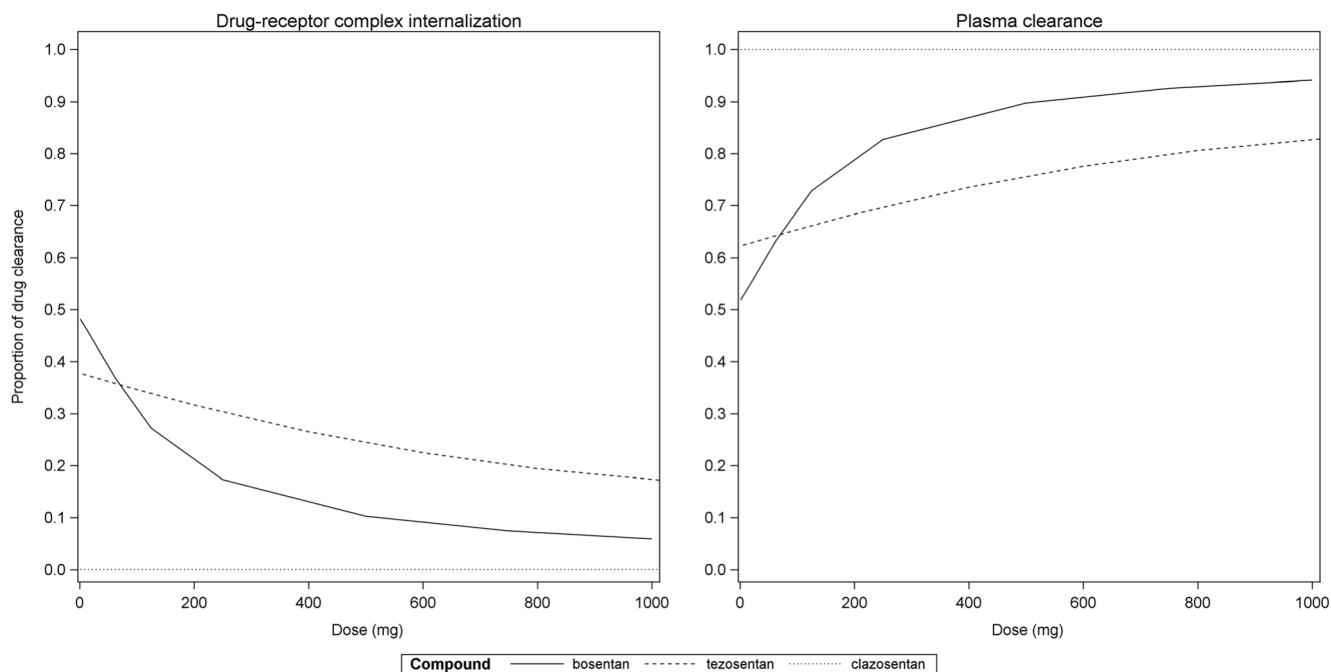


Fig. 2 Proportion of different clearance processes for bosentan (solid lines), clazosentan (dotted lines) and tezosentan (dashed lines). *Left panel:* Drug-receptor complex internalization. *Right panel:* Plasma clearance (elimination from central compartment).

Subsequently the parameters of the cosine function (α , Ω , and shift) were fixed to avoid numerical instabilities. Overall the trends in the CWRes were reduced (Fig. 4) and the model fits

improved statistically significantly ($p < 0.001$). Illustrative individual plasma concentration-time profiles are shown in Fig. 4. Parameter estimates remained precise with low relative

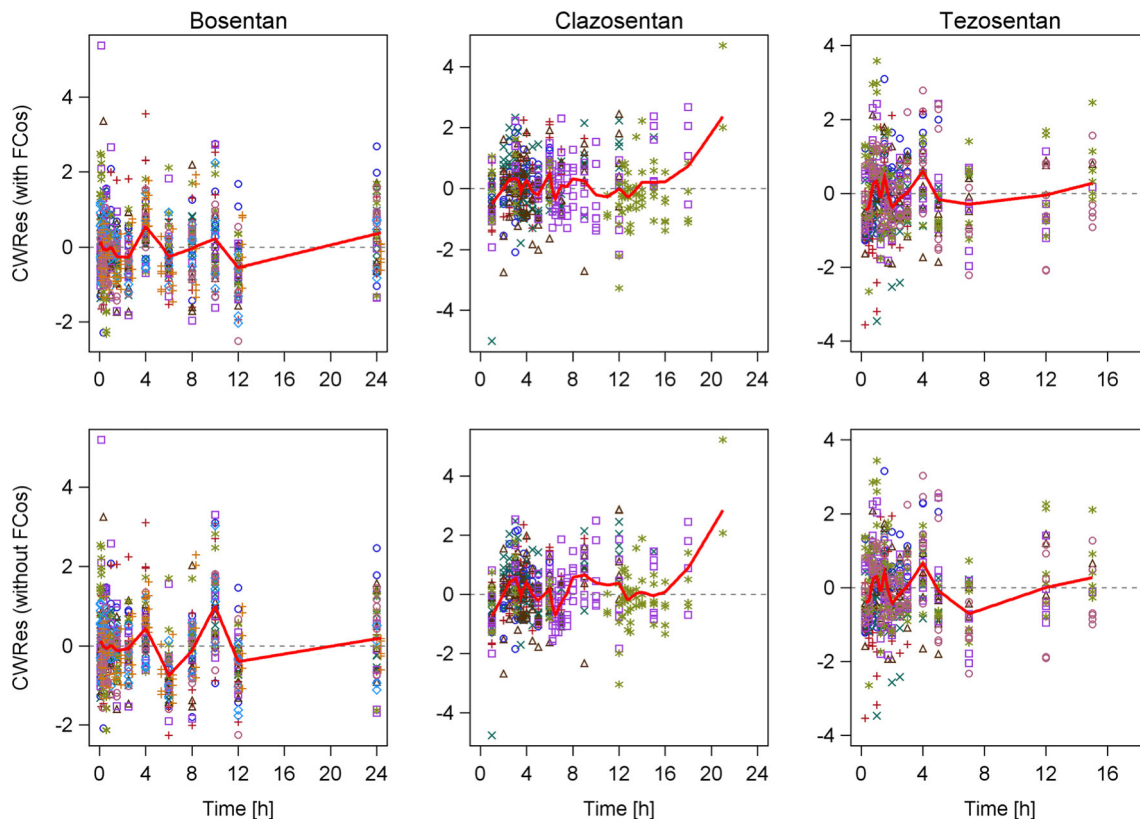


Fig. 3 Conditional weighted residuals versus time of the final two-compartment TMDD models with (upper panels) and without (lower panels) diurnal receptor synthesis for bosentan, clazosentan, and tezosentan. Solid thick red lines indicates polynomial regression fits (loess). Colors and symbols indicate dose groups.

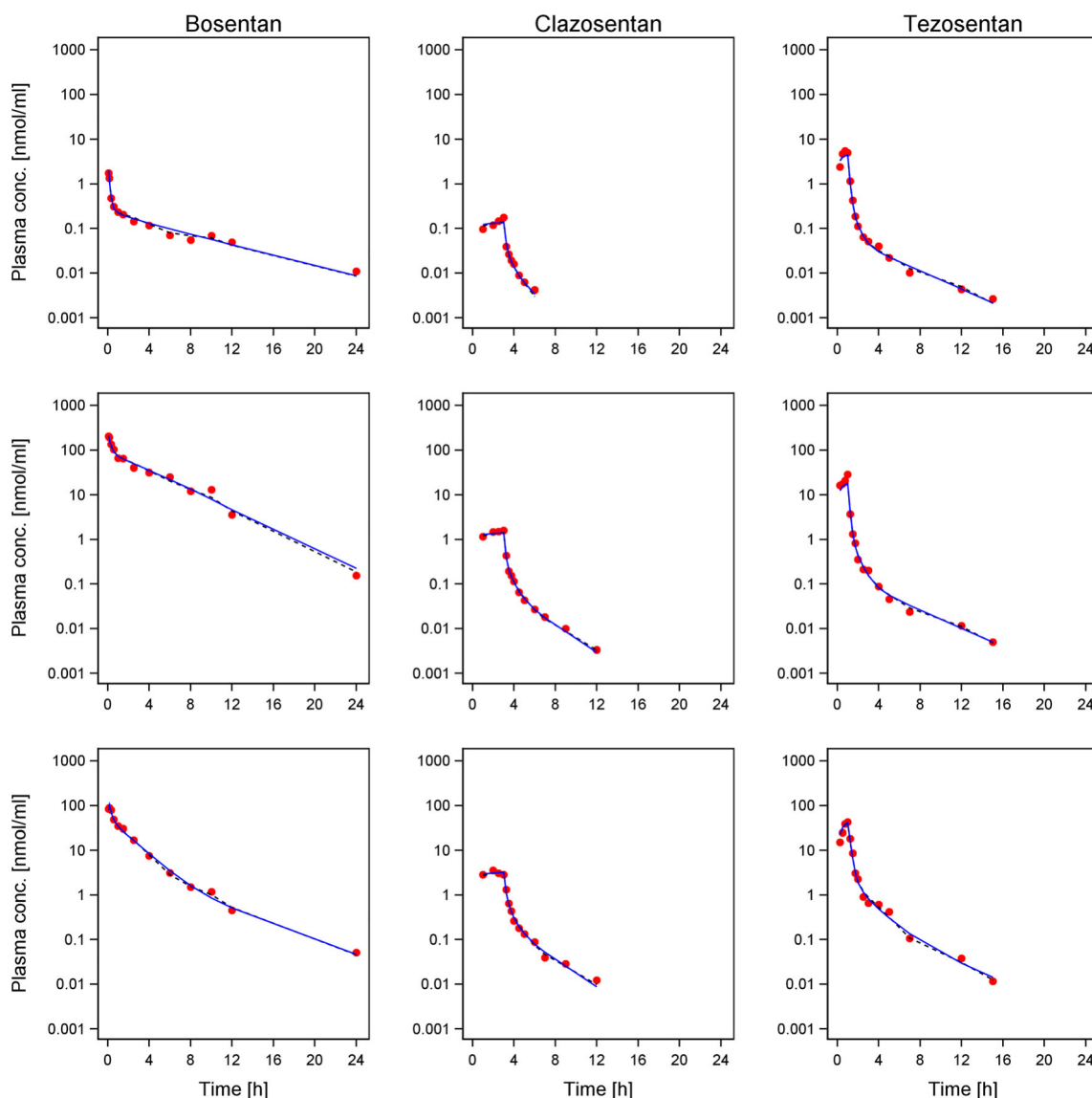


Fig. 4 Representative individual plasma concentration-time profiles (nmol/ml) for bosentan (left column), clazosentan (middle column), and tezosentan (right column). Circles indicate observed concentrations, blue solid lines indicate the model-predicted individual profile without diurnal receptor synthesis, black dashed lines indicate the model-predicted individual with diurnal receptor synthesis.

standard errors ($\leq 29\%$, except for R_{Base} of tezosentan with 50%) and did not change markedly for all three models after the inclusion of the diurnal rhythm (Table I).

Simulations over 48 h for each PK model without incorporation of receptor fluctuation were performed over a broad dose range in order to visualize the non-linear PK triggered by the underlying TMDD process (Fig. 5). Bosentan administration was simulated for doses from 1 to 1000 mg over 5 min. Binding to the receptor occurred fast ($K_d = 1.5$ nM) and almost completely. Receptor baseline values were reached again after 48 h. Clazosentan 3-h infusions were simulated for doses from 1 to 1920 mg/h. Elimination from the systemic circulation was fast, and receptor binding was

almost complete. There was no evidence of receptor complex internalization for clazosentan, so that unoccupied receptor was degraded with k_{DegR} of approximately 4.5 h^{-1} , and receptor baseline was reached again after 18 h. Tezosentan administration was simulated for 1-h infusions for doses from 5 to 1600 mg. The highest doses of tezosentan were eliminated approximately twice as fast as bosentan, and receptor baseline was reached within 8 h after start of the infusion. After administration of low doses, bosentan and tezosentan were almost completely cleared by internalization. As receptor binding is saturable, the amount of drug eliminated from systemic circulation (i.e., the central compartment) via liver and bile increased with increasing doses.

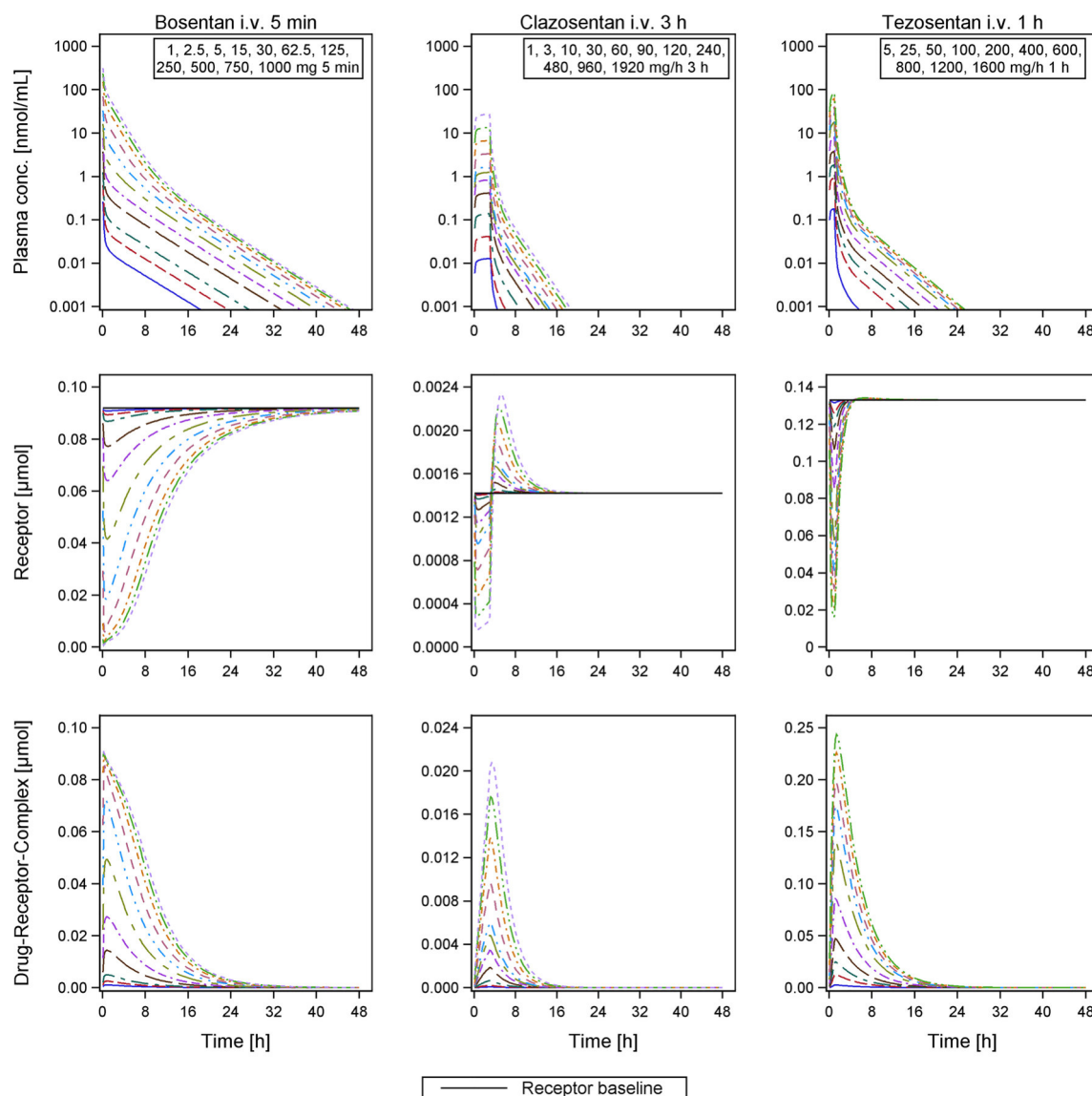


Fig. 5 Simulations over 48 h of the final PK models of bosentan (left), clazosentan (middle), and tezosentan (right) after single i.v. administration of different doses. Upper panels: plasma concentration-time profiles (nmol/ml), middle panels: unoccupied receptor (μmol), lower panels: drug-receptor complex (μmol). Solid black line: unoccupied receptor at baseline.

DISCUSSION

TMDD models are valuable tools to better understand, describe, and predict the PK primarily of large biologicals (1,6). However, also for small chemical molecules with distinct target affinity, this concept is increasingly becoming a focus in PK modeling and simulation to study non-linearity caused by target-binding (10). Although TMDD has become a more commonly investigated feature, few investigations have been performed on TMDD as class effects of therapeutics. Nevertheless, the extent of drug-target-complex building for compounds of the same class can serve as a surrogate marker to understand and predict compound-specific pharmacology.

In the work presented, it was investigated whether TMDD might be a class effect of ERAs, studying bosentan, clazosentan, and tezosentan. For all three drugs, data after i.v. administration over a broad dose range were available and a TMDD model could be fit that could explain the dose-dependent non-linear PK behavior. This is in contrast to previous population PK analyses for clazosentan and tezosentan, in which linear two-compartment models were used characterizing the PK after administration to humans (24,27). However, these previous analyses also indicated a non-linear PK for clazosentan and tezosentan after single-dose administration over broad dose ranges. Since the non-linear PK may also be a consequence of saturable elimination processes (35), different types of models were investigated using saturable

processes such as Michaelis-Menten kinetics. For instance, the introduction of a liver compartment and subsequent saturable uptake from the liver to the central compartment were tested in particular for bosentan, which interacts with various transporters and metabolic enzymes (e.g., organic anion transporting polypeptides, bile salt export pump, or CYP enzymes), but such models were inferior regarding statistical significance, GOF or predictive performance, compared to the TMDD model (data not shown). Nonetheless, these findings do not necessarily exclude that in particular for bosentan, additional saturable processes due to transporter-mediated liver uptake and hepatic metabolism exist and may influence the PK behavior to a certain extent. Since metabolism of clazosentan and tezosentan differs from that of bosentan (both are predominantly eliminated unchanged via liver and bile into the feces) and for both compounds liver uptake appears not to occur via saturable transporters, it was assumed that a saturable elimination is not the leading cause for the non-linear PK. The selection of the drugs was based on accessibility of individual data, broad dose ranges applied, and the existence of i.v. administrations, as overlaying absorption processes and first-pass effects after oral administration would have hampered identifying the receptor binding processes (10). Other ERAs such as macitentan, ambrisentan, atrasentan, zibotentan, or sitaxentan were not investigated in this analysis due to non-existence of i.v. data and the inaccessibility of individual data. Nonetheless, published mean data of these oral ERAs indicate a dose-disproportional trend in PK (e.g., (36–38)). However, it can be hypothesized that for all ERAs TMDD is applicable, as many prerequisites for TMDD apply such as a target that is plasma-based and a high affinity binding of ERAs to the target to replace its endogenous ligand ET-1. As far as known, this is the first attempt to generalize TMDD as a class effect for ERAs. So far, TMDD has been suggested for many ACE inhibitors and a class effect can be hypothesized for DPP-4 inhibitors and vitamin-k-antagonists as for some representatives of these therapeutic classes TMDD has been demonstrated based on similar pharmacological features.

The endogenous ligand ET-1 binds tightly to ET_A and ET_B receptors and is internalized via two different pathways, as described above. For simplification and due to lack of data to separate these processes, ET_A and ET_B receptors were combined into a single model component and represented as one binding partner in the model. This combination of binding partners leads also to the phenomenon that the parameters k_{DegR} , R_{Base} , and k_{SynR} turn from systems parameters, which are independent of the compound, into compound-specific parameters. For example, the estimated receptor baselines were similar for bosentan and tezosentan, while it was estimated considerably lower for clazosentan (0.106, 0.111, and 0.0022 μmol , respectively). In our model,

R_{Base} is a mixture of ET_A and ET_B and in the case of clazosentan it may only represent one receptor subtype (i.e., ET_A), potentially explaining the lower R_{Base} value for clazosentan.

Ideally, these binding processes could be included in a mechanistic approach such as a whole body physiologically-based PK (PBPK) model. Additionally, for bosentan, such a model could account for transporter-mediated liver uptake and inhibition of the bile salt export pump. A published PBPK model incorporated various PK properties and predicted liver exposure after administration of bosentan (39,40). However, although this model also accounted for the binding process of bosentan to ET receptors, for the receptors were not differentiated, the competitive antagonism with the natural ligand ET-1 was not included, and no internalization process was incorporated.

Even so the model was simplified regarding the ET_A and ET_B receptors, it was able to discriminate the different binding affinities to ET_A and ET_B and is appropriate for the objectives of this work. For example, clazosentan binding occurs with 55 times as high affinity to ET_A ($K_d = 0.2$ nM) than to ET_B ($K_d = 11$ nM). Therefore, binding to ET_B may be less relevant and clearance from the systemic circulation as drug-receptor complex via endocytosis may play a minor role. Consequently, clazosentan is exclusively eliminated from plasma, for example, via liver and bile, as reflected in the model, in which the degradation of the receptor-ligand complex was estimated to be close to zero and thus removed from the model. However, for bosentan and tezosentan receptor recycling via ET_A and internalization followed by degradation (ET_B), are indiscernible as binding to both receptors has a similar magnitude (32). Accordingly, a second elimination process, reflecting the degradation of the drug-receptor complex (k_{IntRC}) was incorporated for both compounds. Simulations show that the amount of free receptor decreases after single-dose administration of bosentan and tezosentan and returns to baseline. For clazosentan also a decrease in free receptor is visible. However, after 3 h an increase above baseline becomes visible which disappears after 16 h. This behavior is caused by the fact that clazosentan has a large k_{On} value which is responsible for a quick formation of the receptor-ligand complex. Compared to bosentan and tezosentan, this complex is not cleared and accumulates. Simultaneously, free receptor is synthesized or presented and after the 3-h infusion stop, free clazosentan is massively cleared from the system and the equilibrium is shifted from the bound receptor-ligand complex towards free clazosentan and receptor, causing a short-term and transient rebound of free receptor. As the free receptor is not measured *in vivo*, it is unclear whether this represents a true effect or a model-derived artefact. Since a subsequent intracellular degradation process is currently not described, experimental work is necessary to better understand the processes of agonist- and antagonist-mediated internalization and degradation of the ET receptors and their binding partners.

Nonetheless, the described compound-specific internalization processes are supported by the extent of plasma ET-1 elevation as consequence of its replacement from the target binding sites after administration of different ERAs. With the competitive antagonism of bosentan and ET-1 using a complex TMDD model, ET-1 plasma levels increased dose-dependently (9). While clearance via ET_B receptors was reduced, ET-1 was increasingly cleared into urine with higher doses of bosentan. The same phenomenon was observed for tezosentan (27). In contrast, since clazosentan mainly binds to ET_A , ET-1 binding to ET_B is still possible and therefore it may partly be cleared from the systemic circulation via ET_B , finally leading to a less pronounced increase of free ET-1 concentrations in plasma after administration of clazosentan (24).

In the tezosentan model, two sub-populations with different internalization rates of the receptor-ligand complex were identified using a mixture model, which improved the model statistically significantly ($p < 0.001$) and identified about 77% of the population with an estimated internalization rate in the same order of magnitude as for bosentan (k_{IntRC} bosentan: 0.144 h^{-1} , tezosentan: 0.204 h^{-1}). In 23% of the population, an eight times lower internalization rate was identified ($k_{IntRC} = 0.03 \text{ h}^{-1}$). None of the available covariates explained the sub-population and no sub-population with different internalization rates of the receptor-ligand complex was identified for the two other ERAs. However, a genetic polymorphism in ET_A or ET_B may lead to functional consequences of, e.g., agonist-mediated down regulation (41) and thus it may be possible that antagonist-mediated internalization is altered, too. In addition, several diseases and conditions such as Parkinson's disease and Foot-and-mouth disease are described for which an altered lysosomal activity is reported (42–44). On the other hand, there were some indications during the model development process that a subpopulation with a different clearance from the central compartment (plasma) may also be possible for tezosentan and possibly also for bosentan. Nonetheless, these models (Table S3 and Table S5) were not superior in the current analysis. Furthermore, it might also be possible that the identified subpopulations are mere artefacts. Overall, further research is required to investigate the existence of this subpopulation and the possible reasons.

Multiple peaks in the plasma concentration-time profiles of bosentan, clazosentan, and tezosentan were observed after i.v. administration. As potential explanation, EHC was investigated but neither confirmed by literature nor by the application of an EHC model (34). Recently, a circadian variation in the ET system was discussed (9) where ET-1, ET_A , and ET_B showed a clock time-dependent mRNA expression regulated by Per1 in liver, heart, kidney, and lung (45).

Therefore, it was tested whether mimicking the circadian fluctuation by a cosine function on the synthesis of the ET

receptors improved the descriptive performance. For all three ERAs investigated, a circadian variation of the time-dependent synthesis of the ET receptor described the data best by modulating the receptor production or reappearance every 8 h (diurnal rhythm), which is encoded by the Ω parameter in our model. The shift parameter in the cosine model indicates the shift from the origin. For our compounds a shift of 4.28 h was estimated for bosentan, 7.28 h for clazosentan, and 7.53 h for tezosentan. As all studies started at around 8 to 10 am, the shift and Ω parameters result in a maximum appearance of the receptor in the morning, afternoon, and around midnight for bosentan and around 3 h later for clazosentan and tezosentan. The reason for the differences in shift parameter is unclear. One reason might be the different sampling schedule for the compounds as bosentan was sampled for the longest duration. In addition and as mentioned before, the two receptors ET_A and ET_B were combined in our model but both receptors are expressed to a different extent in different tissues, and it is very likely that the circadian (or diurnal) variation is also different between organs and tissues (45).

Our model showed that a period of 8 h described the data best for all three compounds investigated. However, as PK data were only generated over a maximum of 24 h, the 8 h period is an approximation and further investigations over a longer time period are required to confirm this high frequency as typically physiological processes fluctuate less frequently in a 24-h (circadian) rhythm as for instance blood pressure (46), vasoactive intestinal peptide, or cortisol (47). Nonetheless, *in vitro* findings also suggested a period of 8 h fluctuation for the ET production in humans (48) and other peptides (substance P, neuropeptide Y (47)), such that these findings corroborate the results presented here and thereby support the hypothesis of a diurnal ET receptor production or reappearance.

CONCLUSION

Mechanistic TMDD PK models were successfully developed describing the PK of the small chemical molecules bosentan, clazosentan, and tezosentan. These suggest TMDD as a class effect of ERAs. The model enabled to differentiate between a selective ET_A antagonist and dual ET_A and ET_B antagonists as reflected by their target binding affinity as well as the target-complex internalization behavior. These models contribute to corroboration of the hypotheses of diurnal ET receptor production or reappearance, which leads to multiple peak plasma concentrations. The results presented here are a next step towards understanding the complex PK of ERAs and further support the hypothesis that TMDD is a class effect of ERAs.

ACKNOWLEDGMENTS AND DISCLOSURES

All procedures performed in studies involving human participants were in accordance with the ethical standards of the institutional and/or national research committee and with the 1964 Helsinki declaration and its later amendments or comparable ethical standards. Informed consent was obtained from all individual participants included. Anke-Katrin Volz performed this work at the Saarland University and is currently an employee at the Federal Institute for Drugs and Medical Devices (BfArM) in Bonn, Germany. She declares no potential conflicts of interest with respect to the research, authorship, and/or publication of this article. She did not receive financial support for the research, authorship, and/or publication of this article. Thorsten Lehr performed this work at the Saarland University and reports no potential conflicts of interest. Jasper Dingemans and Andreas Krause are employees of Idorsia Pharmaceuticals Ltd.

Publisher's Note Springer Nature remains neutral with regard to jurisdictional claims in published maps and institutional affiliations.

REFERENCES

- Tang L, Persky AM, Hochhaus G, Meibohm B. Pharmacokinetic aspects of biotechnology products. *J Pharm Sci*. 2004;93(9):2184–204.
- An G. Small-molecule compounds exhibiting target-mediated drug disposition (TMDD): a Minireview. *J Clin Pharmacol*. 2017;57(2):137–50.
- Cheung WK, Levy G. Comparative pharmacokinetics of coumarin anticoagulants. XLIX: nonlinear tissue distribution of S-warfarin in rats. *J Pharm Sci*. 1989;78(7):541–6.
- Levy G. Pharmacologic target-mediated drug disposition. *Clin Pharmacol Ther*. 1994;56(3):248–52.
- Retlich S, Withopf B, Greischel A, Staab A, Jaehde U, Fuchs H. Binding to dipeptidyl peptidase-4 determines the disposition of linagliptin (BI 1356) – investigations in DPP-4 deficient and wildtype rats. *Biopharm Drug Dispos*. 2009;30:422–36.
- Blank A, Markert C, Hohmann N, Carls A, Mikus G, Lehr T, et al. First-in-human application of the novel hepatitis B and hepatitis D virus entry inhibitor myrcludex B. *J Hepatol*. 2016;65(3):483–9.
- Bogomolov P, Alexandrov A, Voronkova N, Macievich M, Kokina K, Petrachenkova M, et al. Treatment of chronic hepatitis D with the entry inhibitor myrcludex B: first results of a phase Ib/IIa study. *J Hepatol*. 2016;65(3):490–8.
- Retlich S, Duval V, Graefe-Mody U, Jaehde U, Staab A. Impact of target-mediated drug disposition on linagliptin pharmacokinetics and DPP-4 inhibition in type 2 diabetic patients. *J Clin Pharmacol*. 2010;50(8):873–85.
- Volz A-K, Krause A, Haefeli WE, Dingemans J, Lehr T. Target-mediated drug disposition pharmacokinetic-Pharmacodynamic model of Bosentan and Endothelin-1. *Clin Pharmacokinet*. 2017;56(12):1499–511.
- van Waterschoot RAB, Parrott NJ, Olivares-Morales A, Lavé T, Rowland M, Smith DA. Impact of target interactions on small-molecule drug disposition: an overlooked area. *Nature Reviews Drug Discovery*. 2018. p. <https://doi.org/10.1038/nrd.2018.26>.
- Kohan DE, Rossi NF, Inscho EW, Pollock DM. Regulation of blood pressure and salt homeostasis by endothelin. *Physiol Rev*. 2011;91(1):1–77.
- Bremnes T, Paasche JD, Mehlum A, Sandberg C, Bremnes B, Attramadal H. Regulation and intracellular trafficking pathways of the endothelin receptors. *J Biol Chem*. 2000;275(23):17596–604.
- Boesen E. Endothelin receptors, renal effects and blood pressure. *Curr Opin Pharmacol*. 2015;21:25–34.
- Fukuroda T, Fujikawa T, Ozaki S, Ishikawa K, Yano M, Nishikibe M. Clearance of circulating endothelin-1 by ETB receptors in rats. *Biochem Biophys Res Commun*. 1994;199(3):1461–5.
- de Nucci G, Thomas R, D'Orleans-Juste P, Antunes E, Walder C, Warner TD, et al. Pressor effects of circulating endothelin are limited by its removal in the pulmonary circulation and by the release of prostacyclin and endothelium-derived relaxing factor. *Proc Natl Acad Sci U S A*. 1988;85(24):9797–800.
- Paasche JD, Attramadal T, Sandberg C, Johansen HK, Attramadal H. Mechanisms of Endothelin receptor subtype-specific targeting to distinct intracellular trafficking pathways. *J Biol Chem*. 2001;276(36):34041–50.
- Chun M, Lin HY, Henis YI, Lodish HF. Endothelin-induced endocytosis of cell surface ETA receptors: Endothelin remains intact and bound to the ETA receptor. *J Biol Chem*. 1995;270(18):10855–60.
- Bhowmick N, Narayan P, Puett D. The endothelin subtype a receptor undergoes agonist- and antagonist- mediated internalization in the absence of signaling. *Endocrinology*. 1998;139(7):3185–92.
- Mager DE, Jusko WJ. General pharmacokinetic model for drugs exhibiting target-mediated drug disposition. *J Pharmacokin Pharmacodyn*. 2001;28(6):507–32.
- Weber C, Schmitt R, Birnboeck H, Hopfgartner G, Van Marle SP, Peeters PAM, et al. Pharmacokinetics and pharmacodynamics of the endothelin-receptor antagonist bosentan in healthy human subjects. *Clin Pharmacol Ther*. 1996;60(2):124–37.
- Dingemans J, van Giersbergen PLM. Clinical pharmacology of bosentan, a dual endothelin receptor antagonist. *Clin Pharmacokinet*. 2004;43(15):1089–115.
- Weber C, Gasser R, Hopfgartner G. Absorption, excretion, and metabolism of the endothelin receptor antagonist bosentan in healthy male subjects. *Drug Metab Dispos*. 1999;27(7):810–5.
- Venitz J, Zack J, Gillies H, Allard M, Regnault J, Dufton C. Clinical pharmacokinetics and drug-drug interactions of endothelin receptor antagonists in pulmonary arterial hypertension. *J Clin Pharmacol*. 2012;52(12):1784–805.
- van Giersbergen PLM, Dingemans J. Tolerability, pharmacokinetics, and pharmacodynamics of clazosentan, a parenteral endothelin receptor antagonist. *Eur J Clin Pharmacol*. 2007;63(2):151–8.
- Roux S, Breu V, Giller T, Neidhart W, Ramuz H, Coassolo P, et al. Ro 61-1790, a new hydrosoluble endothelin antagonist: general pharmacology and effects on experimental cerebral vasospasm. *J Pharmacol Exp Ther*. 1997;283(3):1110–8.
- van Giersbergen PLM, Dingemans J. Effect of gender on the tolerability, safety and pharmacokinetics of clazosentan following long-term infusion. *Clin Drug Investig*. 2007;27(11):797–802.
- Dingemans J, Clozel M, van Giersbergen PLM. Entry-into-humans study with tezosentan, an intravenous dual endothelin receptor antagonist. *J Cardiovasc Pharmacol*. 2002;39(6):795–802.
- Clozel M, Ramuz H, Clozel JP, Breu V, Hess P, Löffler BM, et al. Pharmacology of tezosentan, new endothelin receptor antagonist designed for parenteral use. *J Pharmacol Exp Ther*. 1999;290(2):840–6.
- Dingemans J, Clozel M, van Giersbergen PLM. Pharmacokinetics and pharmacodynamics of tezosentan, an intravenous dual endothelin receptor antagonist, following chronic infusion in healthy subjects. *Br J Clin Pharmacol*. 2002;53(4):355–62.

30. Treiber A, van Giersbergen PLM, Dingemanse J. In vivo and in vitro disposition profile of tezosentan, an intravenous dual endothelin receptor antagonist, in humans. *Xenobiotica*. 2003;33:399–414.
31. Mould DR, Upton RN. Basic concepts in population modeling, simulation, and model-based drug development-part 2: introduction to pharmacokinetic modeling methods. *CPT Pharmacometrics Syst Pharmacol*. 2013;2: <https://doi.org/10.1038/psp.2013.14>.
32. Gatfield J, Mueller Grandjean C, Sasse T, Clozel M, Nayler O. Slow receptor dissociation kinetics differentiate macitentan from other endothelin receptor antagonists in pulmonary arterial smooth muscle cells. *PLoS One*. 2012;7(10):e47662.
33. Davies NM, Takemoto JK, Brocks DR, Yáñez AJ. Multiple peaking phenomena in pharmacokinetic disposition. *Clin Pharmacokinet*. 2010;49(6):351–77.
34. Lehr T, Staab A, Tillmann C, Trommeshauser D, Schaefer H-G, Kloft C. A quantitative enterohepatic circulation model: development and evaluation with tesofensine and meloxicam. *Clin Pharmacokinet*. 2009 Jan;48(8):529–42.
35. Sato M, Toshimoto K, Tomaru A, Yoshikado T, Tanaka Y. Physiologically based pharmacokinetic modeling of bosentan identifies the saturable hepatic uptake as a major contributor to its nonlinear pharmacokinetics. *Drug Metab Dispos*. 2018;46:740–8.
36. Zonnenberg BA, Groenewegen G, Janus TJ, Leahy TW, Humerickhouse RA, Isaacson JD, et al. Phase I dose-escalation study of the safety and pharmacokinetics of atrasentan: an endothelin receptor antagonist for refractory prostate cancer 1. *Clin Cancer Res*. 2003;9:2965–72.
37. Dutta S, Samara E, Lam W, Granneman GR, Leese PT, Laboratories A, et al. Multiple-Dose Pharmacokinetics of Atrasentan, an Endothelin-A Receptor Antagonist. *Clin Pharmacokinet* 2001;21(2):129–136.
38. FDA. Ambrisentan Clinical Pharmacology Biopharmaceutics Review P3 [Internet]. 2007. Available from: https://www.accessdata.fda.gov/drugsatfda_docs/nda/2007/022081s000_ClinPharmR_P3.pdf
39. Li R, Niosi M, Johnson N, Tess DA, Kimoto E, Lin J, et al. A study on pharmacokinetics of bosentan with systems modeling, Part 1: translating systemic plasma concentration to liver exposure in healthy subjects. *Drug Metab Dispos*. 2018;46:346–56.
40. Li R, Kimoto E, Niosi M, Tess DA, Lin J, Tremaine LM, et al. A Study on Pharmacokinetics of Bosentan with Systems Modeling, Part 2: Prospectively Predicting Systemic and Liver Exposure in Healthy Subjects. *Drug Metab Dispos*. 2018;46:357–66.
41. Rana BK, Shiina T, Insel PA. Genetic variations and polymorphism of G protein-coupled receptors: functional and therapeutic implications. *Annu Rev Pharmacol Toxicol*. 2001;41:593–624.
42. Dehay B, Martínez-Vicente M, Caldwell AG, Caldwell AK, Yue Z, Cookson MR, et al. Lysosomal impairment in Parkinson's disease. *Mov Disord*. 2013;28(6):725–32.
43. Feng H-H, Zhu Z-X, Cao W-J, Yang F, Zhang X-L, Du X-L, et al. Foot-and-mouth disease virus induces lysosomal degradation of NME1 to impair p53-regulated interferon-inducible antiviral genes expression. *Cell Death Dis*. 2018;9(9):885.
44. Fredericksen BL, Wei BL, Yao J, Luo T, Garcia JV. Inhibition of Endosomal/Lysosomal degradation increases the infectivity of human immunodeficiency virus. *J Virol*. 2002;76(22):11440–6.
45. Richards J, Welch AK, Barilovits SJ, All S, Cheng KY, Wingo CS, et al. Tissue-specific and time-dependent regulation of the endothelin axis by the circadian clock protein Per1. *Life Sci*. 2014;118(2): 255–62.
46. Middeke M. Chronopathologie und Chronotherapie. *Kompend Herz-Kreislauf*. 2007;3(1):17–21.
47. Löckinger A, Köberle D, St. König P, Saria A, Herold M, Cornélissen G, et al. neuropeptide chronomics in clinically healthy young adults: Circaoctohoran and circadian patterns. *Peptides*. 2004;25(4):533–542.
48. Herold M, Cornélissen G, Loockinger A, Koeberle D, Koenig P, Halberg F. About 8-hour variation of circulating human Endothelin-1. *Peptides*. 1998;19(5):821–5.

Publisher's Note Springer Nature remains neutral with regard to jurisdictional claims in published maps and institutional affiliations.

Supplementary material

Target-mediated Population Pharmacokinetic Modeling of Endothelin Receptor Antagonists

Anke-Katrin Volz¹, Jasper Dingemans², Andreas Krause², Thorsten Lehr^{1,3}

Running head: Target-mediated drug disposition of ERAs

¹ Saarland University, Clinical Pharmacy, Saarbrücken, Germany

² Idorsia Pharmaceuticals Ltd, Department of Clinical Pharmacology, 4123 Allschwil, Switzerland

³ Author for correspondence. (Saarland University, Clinical Pharmacy, 66123 Saarbrücken, Germany, phone: +49/681/302-70255, fax: +49/681/302-70258, E-mail: thorsten.lehr@mx.uni-saarland.de)

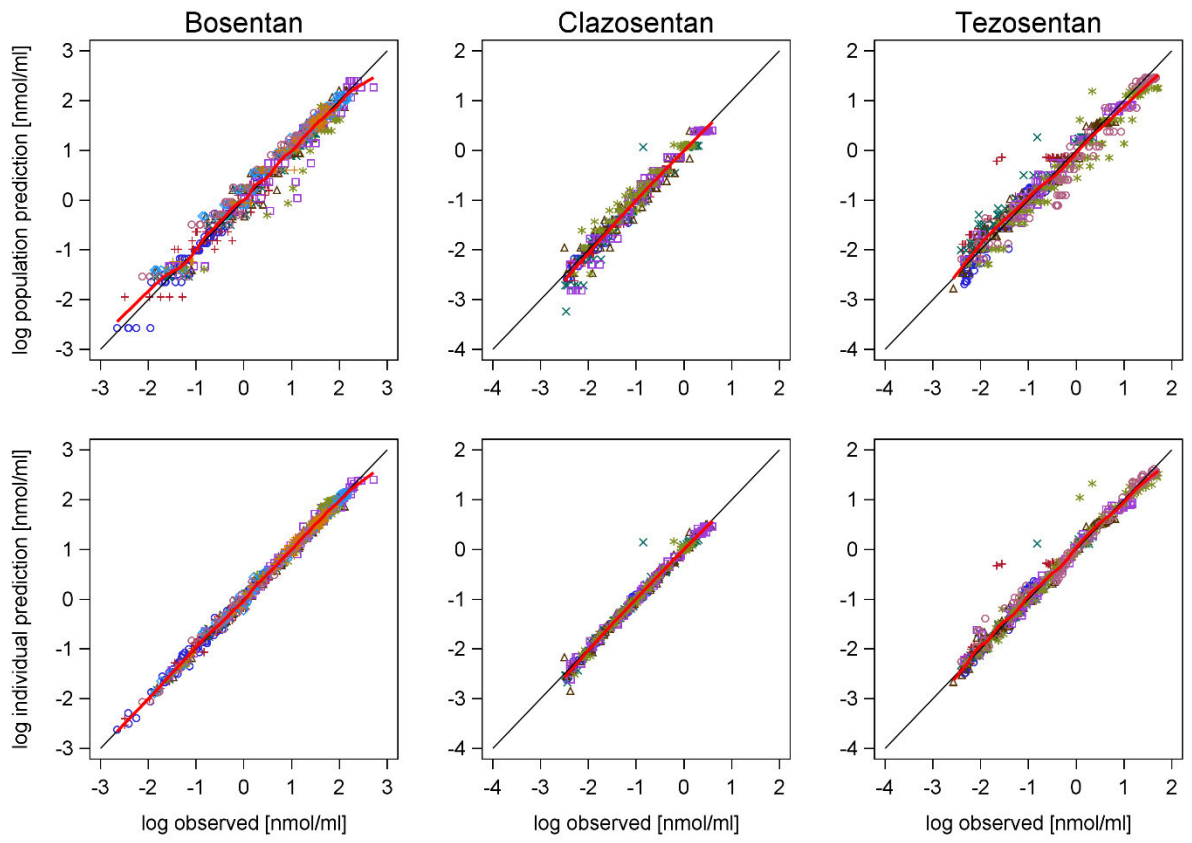
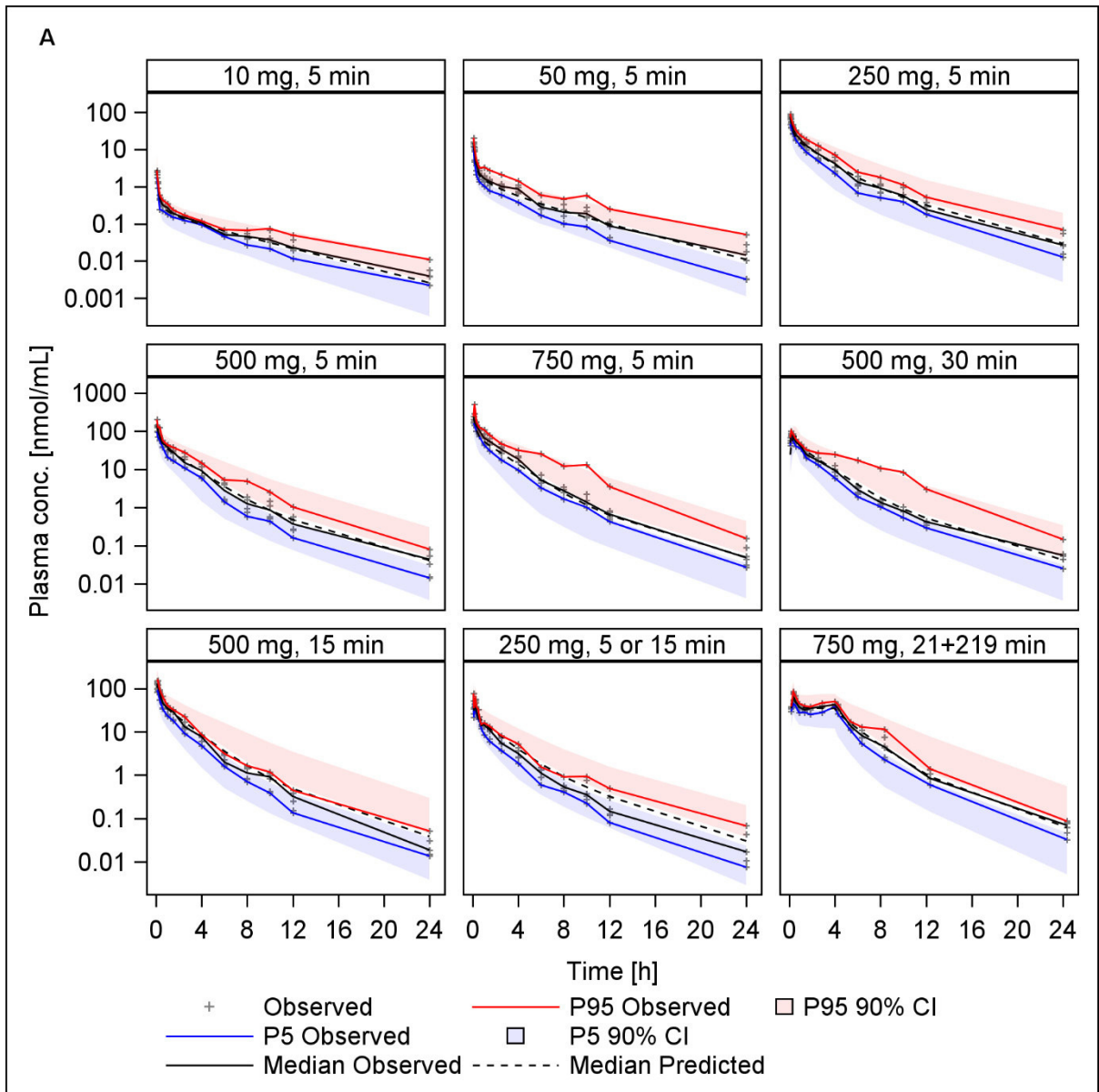
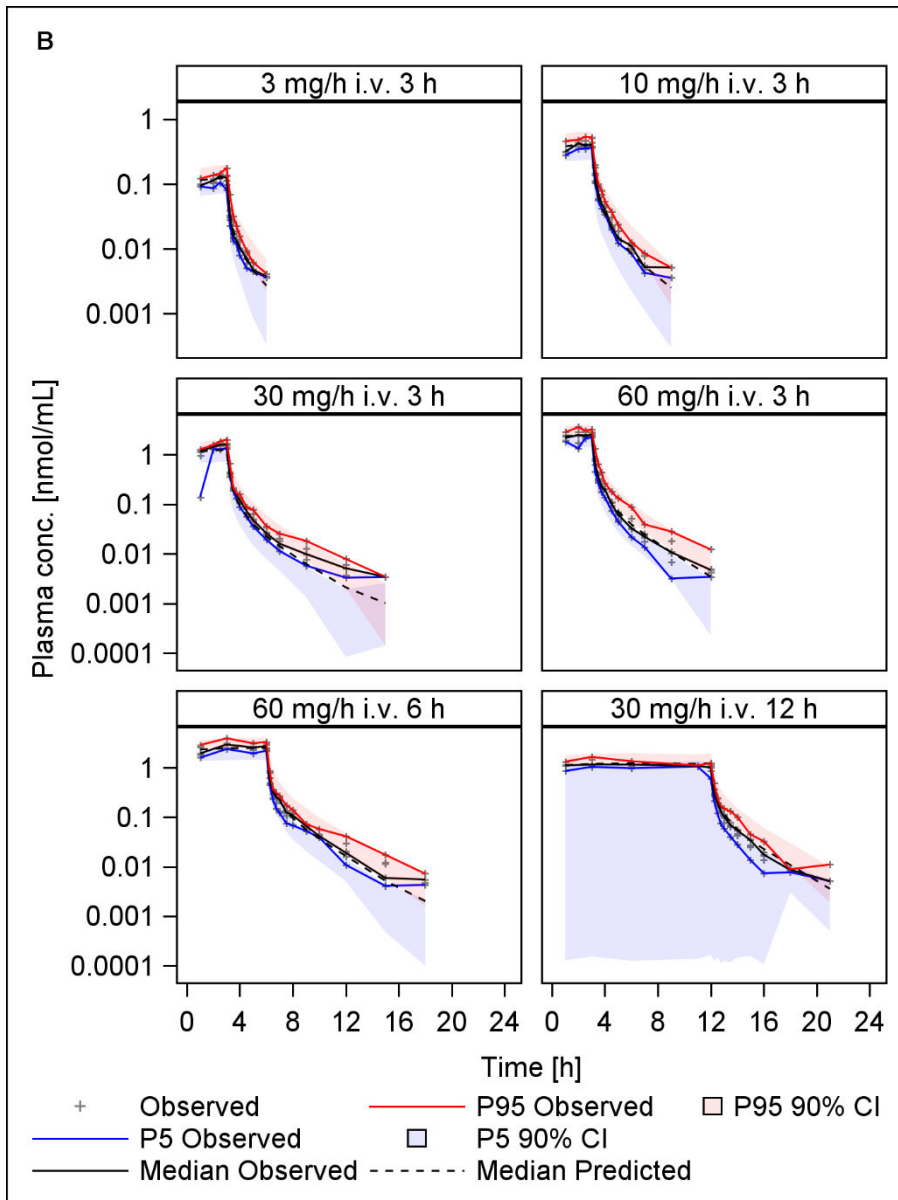


Figure S1 Goodness-of-fit plots of observed versus population prediction (upper panels) and individual prediction (lower panels) of the final two-compartment TMDD models for bosentan, clazosentan, and tezosentan by dose groups. Colors and symbols indicate the different dose groups. The black line indicates the line of identity, and the thick red lines indicate polynomial regression fits (loess).





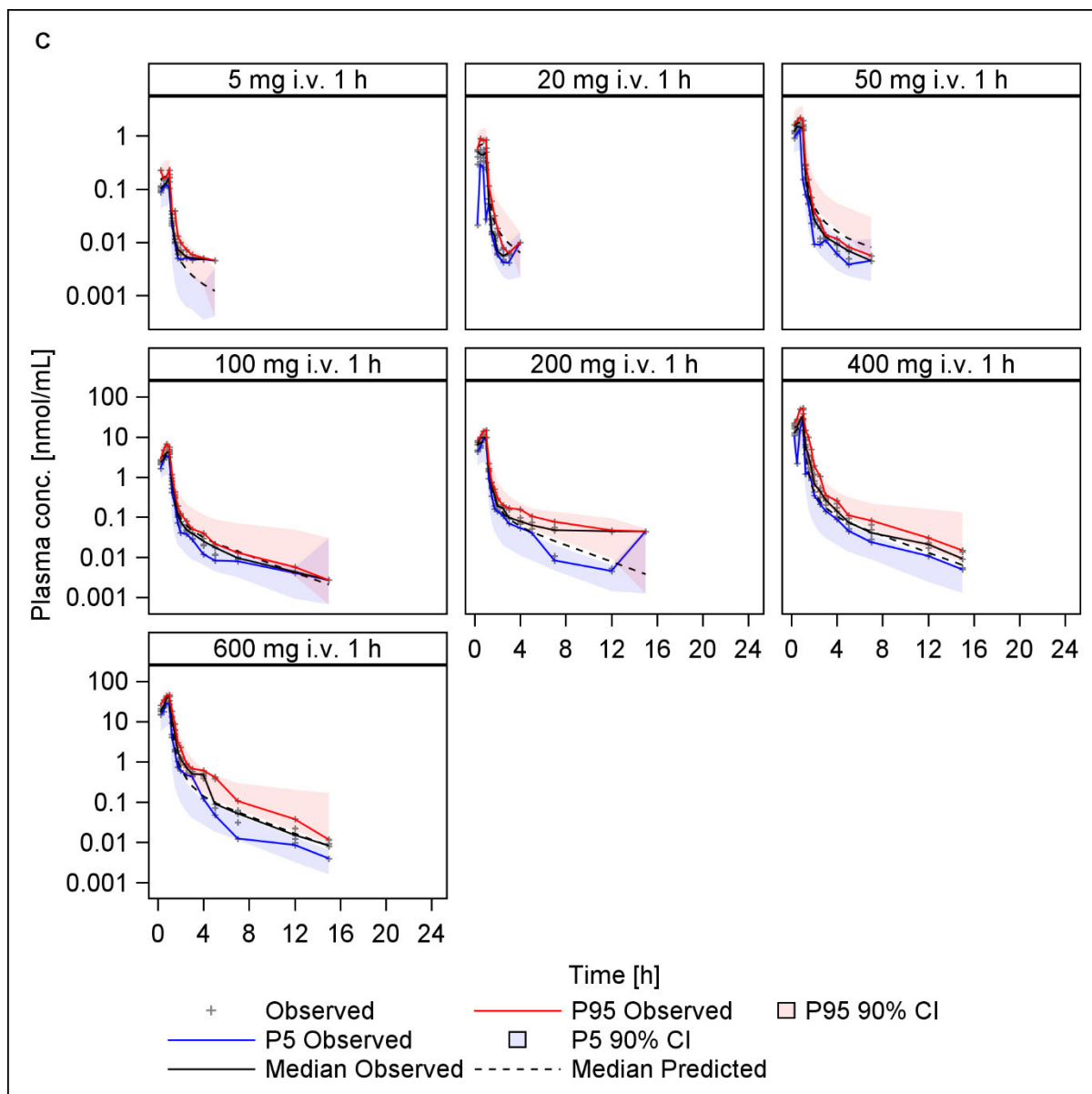


Figure S2 Visual predictive checks of the final TMDD PK model of bosentan (A), clazosentan (B), and tezosentan (C) stratified by dose group. *Open circles* indicate observed concentrations, *dashed lines* indicate median observed concentrations, *solid lines* indicate median model-predicted concentrations, *shaded areas* indicate the 5th and the 95th percentile of simulated concentrations in 1000 simulated subjects.

Table S1 Dose groups studied

Dose group	Single dose	Duration of i.v. administration
Bosentan		
1	10 mg	5 min
2	50 mg	5 min
3	250 mg	5 min
4	500 mg	5 min
5	750 mg	5 min
6	500 mg	30 min
7	500 mg	15 min
8	250 mg	5 or 15 min
9	750 mg	350 mg over 21 min followed by 400 mg over 219 min
Clazosentan		
1	3 mg/h	3 h
2	10 mg/h	3 h
3	30 mg/h	3 h
4	60 mg/h	3 h
5	60 mg/h	6 h
6	30 mg/h	12 h
Tezosentan		
1	5 mg/h	1 h
2	20 mg/h	1 h
3	50 mg/h	1 h
4	100 mg/h	1 h
5	200 mg/h	1 h
6	400 mg/h	1 h
7	600 mg/h	1 h

Table S2 Summary statistics of subject characteristics at baseline

	Bosentan	Clazosentan	Tezosentan
Total subjects	70	48	56
Race			
Caucasian	70	42	46
Black	0	4	9
Others	0	2	1
Treatment			
Active	54	36	42
Placebo	16	12	14
Age [years]			
Min	19	19	20
5 th percentile	19	21	21
Mean	22	25	25
Standard deviation	2.33	3.93	3.64
Median	22	24	24
95 th percentile	26	33	33
Max	31	36	37
Body weight [kg]			
Min	57	54	55
5 th percentile	65	59	59
Mean	78	71	70
Standard deviation	8.43	8.74	6.25
Median	77	69	70
95 th percentile	90	87	78
Max	101	91	88
Height [cm]			
Min	167	163	170
5 th percentile	176	165	170
Mean	184	176	180
Standard deviation	6.27	5.86	5.57
Median	184	177	180
95 th percentile	195	185	191
Max	201	188	193
Body mass index [kg/m²]			
Min	20	18	18
5 th percentile	20	20	19
Mean	23	23	22
Standard deviation	1.91	2.16	1.73
Median	23	23	22
95 th percentile	27	27	25
Max	27	27	26

Table S3 Bosentan model development: objective function values (OFV) as provided by NONMEM for key models

Bosentan				
Model #	Model structure	OFV	Δ OFV	Comment
Models with linear elimination: $k_E = CL/V_{Central}$				
1	One-compartment	3239.631	N/A	
2	Two-compartment	2284.568	-955.063	Compared to #1.
3	Three-compartment	2185.351	-99.217	Compared to #2.
Models with Michaelis-Menten elimination: $k_E = (VM*A)/(KM+A)$				
4	One-compartment	3361.606	+121.975	Compared to #1.
5	Two-compartment	2257.287	-27.281	Compared to #2.
6	Three-compartment	2132.292	-53.059	Compared to #3.
TMDD models				
7	One-compartment without k_{IntRC}	2454.992	+322.7	Compared to #6.
8	Two-compartment without k_{IntRC}	2149.883	+17.59	Compared to #6.
9	One-compartment with one k_{IntRC}	2115.008	-17.284	Compared to #6.
10	Two-compartment with one k_{IntRC}	2030.39	-84.618	Compared to #9.
11	Two-compartment with one k_{IntRC} <i>with IIV on CL</i>	1079.619	-950.771	Compared to #10.
12	Two-compartment with one k_{IntRC} with IIV on CL, $V_{Central}$, $V_{Peripheral}$, k_{IntRC}	921.483	-1108.907	Compared to #10. Final full model after investigation of IIVs.
13	Two-compartment with mixture model on k_{IntRC}	N/A	N/A	No second population identified.
14	Two-compartment with mixture model on CL	1509.72	+430.101	Compared to #11.
15	Two-compartment with mixture model on CL <i>with IIV on $V_{Central}$, $V_{Peripheral}$, k_{IntRC}</i>	1058.355	+136.872	Compared to #12.
16	Two-compartment with mixture model on R_{Base}	N/A	N/A	No second population identified.
<p><i>Model structure</i> is the basic model structure without incorporation of random effects (interindividual variabilities, IIVs) but including residual variability. In addition, selected key models after inclusion of IIVs are listed for comparison. <i>A</i> amount of unbound drug in the central compartment, <i>CL</i> total body clearance, <i>IIV</i> interindividual variability, k_E elimination rate constant, <i>KM</i> concentration at which elimination is half maximum, <i>OFV</i> objective function value, $V_{Central}$ volume of distribution central compartment, <i>VM</i> rate of elimination which approaches maximum.</p>				

Table S4 Clazosentan model development: objective function values (OFV) as provided by NONMEM for key models

Clazosentan				
Model #	Model structure	OFV	Δ OFV	Comment
Models with linear elimination: $k_E = CL/V_{Central}$				
1	One-compartment	-1951.36	N/A	
2	Two-compartment	-3184.565	-1233.205	Compared to #1.
3	Three-compartment	-3249.516	-64.951	Compared to #2.
Models with Michaelis-Menten elimination: $k_E = (VM \cdot A)/(KM + A)$				
4	One-compartment	-1938.099	+13.27	Compared to #1.
5	Two-compartment	-3167.852	+16.713	Compared to #2.
6	Three-compartment	-3234.94	+14.576	Compared to #3.
TMDD models				
7	One-compartment without k_{IntRC}	-3307.168	-57.652	Compared to #3.
8	Two-compartment without k_{IntRC}	-3395.047	-87.879	Compared to #7.
9	Two-compartment without k_{IntRC} with <i>IIV</i> on R_{Base}	-3648.017	-252.97	Compared to #8.
10	Two-compartment without k_{IntRC} with <i>IIV</i> on CL, $V_{Central}$, R_{Base}	-3885.47	-490.423	Compared to #8. Final full model after investigation of IIVs.
11	One-compartment with one k_{IntRC}	-3310.451	+84.596	Compared to #8
12	Two-compartment with one k_{IntRC}	-3396.645	-1.598	Compared to #8. k_{IntRC} estimated zero during investigation of IIVs (models not listed here).
13	Two-compartment with mixture model on k_{IntRC}	N/A	N/A	Not tested, no k_{IntRC} estimated for clazosentan.
14	Two-compartment with mixture model on CL	N/A	N/A	No second population identified.
15	Two-compartment with mixture model on R_{Base}	-3589.988	+58.029	Compared to #9.
16	Two-compartment with mixture model on R_{Base} with <i>IIV</i> on CL , $V_{Central}$	-3878.006	+7.464	Compared to #10. Second population could not be estimated but need to be fixed.
<p><i>Model structure</i> is the basic model structure without incorporation of random effects (interindividual variabilities, IIVs) but including residual variability. In addition, selected key models after inclusion of IIVs are listed for comparison. <i>A</i> amount of unbound drug in the central compartment, <i>CL</i> total body clearance, <i>IIV</i> interindividual variability, k_E elimination rate constant, <i>KM</i> concentration at which elimination is half maximum, <i>OFV</i> objective function value, $V_{Central}$ volume of distribution central compartment, <i>VM</i> rate of elimination which approaches maximum.</p>				

Table S5 Tezosentan model development: objective function values (OFV) as provided by NONMEM for key models

Tezosentan				
Model #	Model structure	OFV	Δ OFV	Comment
Models with linear elimination: $k_E = CL/V_{Central}$				
1	One-compartment	693.543	N/A	
2	Two-compartment	-1138.885	-1832.428	Compared to #1.
3	Three-compartment	-1161.902	-23.017	Compared to #2, but $Q_{Peripheral_2}$ and $V_{Peripheral_2}$ not plausible with very high RSE.
Models with Michaelis-Menten elimination: $k_E = (VM \cdot A)/(KM + A)$				
4	One-compartment	747.263	+53.72	Compared to #1.
5	Two-compartment	-1318.727	-179.842	Compared to #2.
6	Three-compartment	-1366.028	-204.126	Compared to #3, but $V_{Peripheral}$ not plausible with very high RSE.
TMDD models				
7	One-compartment without k_{IntRC}	-1237,929	+128,099	Compared to #6.
8	Two-compartment without k_{IntRC}	-1294,996	+71,032	Compared to #6.
9	One-compartment with one k_{IntRC}	-1396.249	-30.221	Compared to #6.
10	Two-compartment with one k_{IntRC}	-1440.002	-43.753	Compared to #9.
11	Two-compartment with one k_{IntRC} with IIV on k_{IntRC}	-1761.626	-321.624	Compared to #10.
12	Two-compartment with one k_{IntRC} with IIV on k_{IntRC} , CL , $V_{Peripheral}$	-2046.672	-606.669	Compared to #10.
13	Two-compartment with mixture model on k_{IntRC}	-1579.561	-139.559	Compared to #10.
14	Two-compartment with mixture model on k_{IntRC} and IIV on CL and $V_{Peripheral}$	-2095.545	-48.875	Compared to #12. Final full model after investigation of IIVs.
15	Two-compartment with mixture model on CL	-1636.535	-56.974	Compared to #13.
16	Two-compartment with mixture model on CL and IIV on k_{IntRC} and $V_{Peripheral}$	-1924.59	+170.955	Compared to #14.
17	Two-compartment with mixture model on R_{Base}	-1628.333	-48.772	Compared to #13.
18	Two-compartment with mixture model on R_{Base} and IIV on CL and $V_{Peripheral}$	-2070.521	+25.024	Compared to #14. High RSE.
<p><i>Model structure</i> is the basic model structure without incorporation of random effects (interindividual variabilities, IIVs) but including residual variability. In addition, selected key models after inclusion of IIVs are listed for comparison. <i>A</i> amount of unbound drug in the central compartment, <i>CL</i> total body clearance, <i>IIV</i> interindividual variability, <i>k_E</i> elimination rate constant, <i>KM</i> concentration at which elimination is half maximum, <i>OFV</i> objective function value, <i>RSE</i> relative standard error, <i>V_{Central}</i> volume of distribution central compartment, <i>V_{Peripheral}</i> volume of distribution peripheral compartment, <i>VM</i> rate of elimination which approaches maximum.</p>				

NONMEM model codes

Bosentan

```
;; 1. Based on: run011
;; 2. Description: 2 CMT TMDD, IIV Vc Vp kIntRCB CL KdB not fixed
;; x1. Author: AKV

$PROBLEM Bosentan PK i.v. SRD 10, 50, 250, 500, 750 mg day 1 in healthy human subjects
$INPUT ID TIME DV _2=DROP DV AMT2=DROP AMT CMT=DROP EVID BLQ DOSE RATE
CONC DAY ADM STUD DGR SUBJ=DROP SAMP=DROP PTNO=DROP SEX AGE WT HT
BMI BILI SGPT AP SGOT GGT ALB PROT CHOL HGB HCT SCR CRCL

$DATA ../DATASET/BOSENTAN_PK_V01.csv
IGNORE=@

$SUBROUTINES ADVAN9 TOL=9

$MODEL
COMP(C) ;1 Central compartment
COMP(R) ;2 Unoccupied target
COMP(RCB) ;3 Drug-target complex
COMP(P) ;4 Peripheral compartment

$PK
Vc = THETA(1)*EXP(ETA(1)) ; Volume of distribution of central compartment
Vp = THETA(2)*EXP(ETA(2)) ; Volume of distribution of peripheral compartment
Q = THETA(3) ; Intercompartmental clearance
kOnB = THETA(4) ; Rate constant complex building drug
KdB = Vc*THETA(5) ; Dissociation rate constant drug (0.00966 µmol/l)
kIntRCB = THETA(6)*EXP(ETA(3)) ; Rate constant internalization of the drug – receptor
complex
RBase = THETA(7) ; Receptor baseline
A_0(2) = RBase
kDegR = THETA(8) ; Rate constant degradation free receptor
CL = THETA(9)*EXP(ETA(4)) ; Clearance

S1 = Vc/1000 ; scaling for litre with DV [ng/ml] and AMT (DOSE) [mg]

$DES
kCP = Q/Vc
kPC = Q/Vp
kOffB = kOnB * KdB
kSynR = kDegR*RBase ; rate constant synthesis unoccupied target
kEB = CL/Vc ; Elimination rate constant

DADT(1)= -kEB*A(1)-kOnB*A(1)*A(2)+kOffB*A(3)-kCP*A(1)+kPC*A(4)
DADT(2)= -kOnB*A(1)*A(2)+kOffB*A(3)+kSynR-kDegR*A(2)
DADT(3)= kOnB*A(1)*A(2)-kOffB*A(3)-kIntRCB*A(3)
DADT(4)= kCP*A(1)-kPC*A(4)

$ERROR
IPRED = A(1) / S1 ; Central compartment bosentan PK
DEL=0
```

```

IF (IPRED.EQ.0) DEL=0.0001
W   = IPRED
IRES = DV - IPRED
IWRES = IRES / (W + DEL)
Y = IPRED + IPRED * EPS(1) ; Bosentan PK

$THETA
(0, 4.26) ;1 VCentral
(0, 5.93) ;2 VPeripheral
(0, 6.59) ;3 Q
(0, 19.4) ;4 kOnB
(0, 0.0077) ;5 KdB
(0, 0.142) ;6 kIntRCB
(0, 0.327) ;7 RBase
(0, 0.0847) ;8 kDegR
(0, 4.49) ;9 CL

$OMEGA
0.01 ;1 IIV VCentral
0.01 ;2 IIV VPeripheral
0.01 ;3 IIV kIntRCB
0.01 ;4 IIV CL

$$SIGMA
0.339 ;proportional error plasma bosentan

$ESTIMATION METHOD=1 INTER MAXEVAL=9999 POSTHOC NOABORT PRINT=1
$COV UNCONDITIONAL
$TABLE ID TIME DOSE DGR DV PRED IPRED IWRES CWRES ONEHEADER NOPRINT
FILE=sdtab012

```

Clazosentan

```
;; 1. Based on: run115
;; 2. Description: 2 CMT TMDD, IIV CL Vc RBase
;; x1. Author: AKV

$PROBLEM Clazosentan PK Study 1161

$INPUT ID TIME DV DV2=DROP AMT AMT2=DROP CMT=DROP EVID DOSE DGR RATE
INFT FLAG BLQ
$DATA .././DATASET/
IGNORE=@

$SUBROUTINES ADVAN13 TOL=9

$MODEL
COMP(C) ;1 Central compartment
COMP(R) ;2 Unoccupied target
COMP(RCC) ;3 Drug-target complex
COMP(P) ;4 Peripheral compartment

$PK
Vc = THETA(1)*EXP(ETA(2)) ; Volume of distribution of central compartment
Vp = THETA(2) ; Volume of distribution of peripheral compartment
Q = THETA(3) ; Intercompartmental clearance
RBase = THETA(4)*EXP(ETA(3)) ; Receptor baseline
A_0(2) = RBase
kDegR = THETA(5) ; Rate constant degradation free receptor
KdC = (Vc*0.0002) ; Dissociation rate constant drug (0.0002 µmol/l)
kOnC = THETA(6) ; Rate constant complex building drug
CL = THETA(7)*EXP(ETA(1)) ; Clearance

S1 = Vc/1000 ;scaling for litre with DV [ng/ml] and AMT (DOSE) [mg]

$DES
kCP= Q/Vc
kPC= Q/Vp
kOffC = kOnC * KdC
kSynR = kDegR * RBase ; Rate constant degradation unoccupied target
kEc = CL/Vc ; Elimination rate constant

DADT(1) = -kOnC*A(1)*A(2) +kOffC*A(3) -kEc*A(1) -kCP*A(1)+kPC*A(4)
DADT(2) = -kOnC*A(1)*A(2) +kOffC*A(3) +kSynR-kDegR*A(2)
DADT(3) = kOnC*A(1)*A(2) -kOffC*A(3)
DADT(4) = kCP*A(1)-kPC*A(4)

$ERROR
IPRED = A(1)/S1 ; Central compartment clazosentan PK

DEL=0
IF (IPRED.EQ.0) DEL=0.0001
W = IPRED
IRES = DV - IPRED
IWRES = IRES / (W + DEL)
```

```
Y = IPRED + IPRED * EPS(1) + EPS(2) ; Clazosentan PK
$THETA
(0,10.6) ;1 VCentral
(0,9.96) ;2 VPeripheral
(0,11.3) ;3 Q
(0,0.0015) ;4 RBase
(0,2.42) ;5 kDegR
(0,308) ;6 kOnC
(0,44.8) ;7 CL

$OMEGA
0.01 ;1 IIV CL
0.01 ;2 IIV VCentral
0.01 ;3 IIV RBase

$SIGMA
0.01 ;proportional.error plasma clazosentan
0.000001 FIX ; additive error plasma clazosentan

$ESTIMATION METHOD=1 INTER MAXEVAL=9999 POSTHOC NOABORT PRINT=1
$COV
$TABLE ID TIME DOSE DGR DV FLAG IPRED IWRES CWRES ONEHEADER NOPRINT
FILE=sdtab116
```

Tezosentan

```
:: 1. Based on: run023
:: 2. Description: 2 CMT TMDD, mixture kIntRC, IIV Vp CL
:: x1. Author: AKV

$PROBLEM Tezosentan PK

$INPUT ID TIME DV DV2=DROP AMT AMT2=DROP CMT EVID DOSE DUR RATE CONC
DGR FLAG BLQ CLOC=DROP SEX AGE WT HT BMI RACE STUD MDV

$DATA .././DATASET/
IGNORE=@

$SUBROUTINES ADVAN13 TOL=9

$MODEL
COMP(C)      ; 1 Central compartment
COMP(R)      ; 2 Unoccupied target
COMP(RCB)    ; 3 Drug-target-complex
COMP(P)      ; 4 Peripheral compartment

$PK
Vc = THETA(1)                ; Volume of distribution of central compartment
Vp = THETA(2)*EXP(ETA(1))    ; Volume of distribution of peripheral compartment
Q = THETA(3)                 ; Intercompartmental clearance
RBase = THETA(4)             ; Receptor baseline
kDegR = THETA(5)             ; Rate constant degradation free receptor
KDT = Vc*0.00026             ; Dissociation rate constant drug (0.00026 µmol/l)
kOnT = THETA(6)              ; Rate constant complex building drug
EST=MIXEST
IF(MIXNUM.EQ.1)THEN
kIntRCT = THETA(7)           ; Rate constant internalization of the drug – receptor
population 1
POP=1
ELSE
kIntRCT = THETA(8)*THETA(7) ;Rate constant internalization of the drug – receptor population
2
POP=2
ENDIF
CL = THETA(10)*EXP(ETA(2))   ; Clearance

S1 = Vc/1000 ; scaling for liter with DV [nmol/ml] and AMT tezosentan (DOSE) [mmol]

$DES
kCP = Q/Vc
kPC = Q/Vp
kOffT = kOnT * KDT
kSynR=kDegR*RBase           ; Rate constant degradation unoccupied target
kET = Cl / Vc                ; Elimination rate constant

DADT(1)= -kET*A(1) - kOnT*A(1)*A(2) + kOffT*A(3) -kCP*A(1) +kPC*A(4)
DADT(2)= -kOnT*A(1)*A(2) + kOffT*A(3) + kSynR - kDegR*A(2)
DADT(3)= kOnT*A(1)*A(2) - kOffT*A(3) -kIntRCT*A(3)
```

DADT(4)= kCP*A(1) -kPC*A(4)

\$ERROR

IPRED = F

DEL=0

IF (IPRED.EQ.0) DEL=0.0001

W = F

IRES = DV - IPRED

IWRES = IRES / (W + DEL)

Y = IPRED + IPRED * EPS(1) ;Tezosentan PK

\$MIX

NSPOP=2

P(1)=THETA(9) ;proportion population 1

P(2)=1-THETA(9) ; proportion population 2

\$THETA

(0,5.58) ;1 VCentral

(0,2.66) ;2 VPeriheral

(0,3.65) ;3 Q4

(0,0.044) ;4 RBase

(0,4.8) ;5 kDegR

(0,115) ;6 kONT

(0,0.203) ;7 kIntRCT_1

(0,0.125) ;8 fraction kIntRCT_2

(0,0.778) ;9 proportion population 1

(0,20.7) ;10 CL

\$OMEGA

0.01 ;1 IIV VPeripheral

0.01 ;2 IIV CL

\$SIGMA

0.268 ;proportional.error plasma tezosentan

\$ESTIMATION METHOD=1 INTER MAXEVAL=9999 POSTHOC NOABORT PRINT=1

\$COV UNCONDITIONAL

\$TABLE ID TIME DV DOSE DGR FLAG CMT STUD PRED IPRED CWRES NOPRINT

FILE=sdtab026

ARTICLE

Physiologically-Based Pharmacokinetic Models for CYP1A2 Drug–Drug Interaction Prediction: A Modeling Network of Fluvoxamine, Theophylline, Caffeine, Rifampicin, and Midazolam

Hannah Britz¹, Nina Hanke¹, Anke-Katrin Volz¹, Olav Spigset^{2,3}, Matthias Schwab^{4,5,6}, Thomas Eissing⁷, Thomas Wendl⁷, Sebastian Frechen⁷ and Thorsten Lehr^{1,*}

This study provides whole-body physiologically-based pharmacokinetic models of the strong index cytochrome P450 (CYP)1A2 inhibitor and moderate CYP3A4 inhibitor fluvoxamine and of the sensitive CYP1A2 substrate theophylline. Both models were built and thoroughly evaluated for their application in drug–drug interaction (DDI) prediction in a network of perpetrator and victim drugs, combining them with previously developed models of caffeine (sensitive index CYP1A2 substrate), rifampicin (moderate CYP1A2 inducer), and midazolam (sensitive index CYP3A4 substrate). Simulation of all reported clinical DDI studies for combinations of these five drugs shows that the presented models reliably predict the observed drug concentrations, resulting in seven of eight of the predicted DDI area under the plasma curve (AUC) ratios (AUC during DDI/AUC control) and seven of seven of the predicted DDI peak plasma concentration (C_{max}) ratios (C_{max} during DDI/ C_{max} control) within twofold of the observed values. Therefore, the models are considered qualified for DDI prediction. All models are comprehensively documented and publicly available, as tools to support the drug development and clinical research community.

Study Highlights

WHAT IS THE CURRENT KNOWLEDGE ON THE TOPIC?

☑ Physiologically-based pharmacokinetic (PBPK) models are a valuable tool to investigate and predict the drug–drug interaction (DDI) potential of investigational drugs. A publicly available library of thoroughly and transparently evaluated models of relevant perpetrator and victim drugs used in clinical studies is needed to accelerate the drug development process.

WHAT QUESTION DID THIS STUDY ADDRESS?

☑ The aim of this study was to provide whole-body PBPK models of the most important cytochrome (CYP)1A2 perpetrator and victim drugs and to evaluate them for their application in PBPK DDI modeling.

WHAT DOES THIS STUDY ADD TO OUR KNOWLEDGE?

☑ This study provides publicly available and transparently built and evaluated PBPK models of fluvoxamine and theophylline. Both models integrate the current knowledge on relevant pharmacokinetic (PK) mechanisms, including the impact of different genotypes and smoking on the PK of fluvoxamine.

HOW MIGHT THIS CHANGE DRUG DISCOVERY, DEVELOPMENT, AND/OR THERAPEUTICS?

☑ The developed PBPK models are ready to use for their application in DDI modeling and might help to support the drug development process.

Cytochrome P450 (CYP)1A2 is an important enzyme for the metabolism of several endogenous substances (e.g., melatonin), and it is involved in the elimination of 15% of all therapeutic drugs.¹ CYP1A2 is exclusively expressed in the liver, where it accounts for about 13% of total CYP content in liver microsomes.² The expression of CYP1A2 can be markedly induced by smoking, whereas rifampicin, a strong

CYP3A4 inducer, shows only a moderate potential to induce CYP1A2.^{1,3} Well-known substrates of CYP1A2 include caffeine and theophylline, which are mainly metabolized via CYP1A2 (fractions metabolized of 0.95⁴ and 0.7,^{5,6} respectively) and can, therefore, be used as sensitive CYP1A2 substrates to evaluate the activity of CYP1A2 *in vivo*.⁷ The most important inhibitor of CYP1A2 is fluvoxamine.

¹Clinical Pharmacy, Saarland University, Saarbrücken, Germany; ²Department of Clinical and Molecular Medicine, Norwegian University of Science and Technology, Trondheim, Norway; ³Department of Clinical Pharmacology, St. Olav University Hospital, Trondheim, Norway; ⁴Dr. Margarete Fischer-Bosch-Institute of Clinical Pharmacology, Stuttgart, Germany; ⁵Department of Clinical Pharmacology, University Hospital Tübingen, Tübingen, Germany; ⁶Department of Pharmacy and Biochemistry, University Tübingen, Tübingen, Germany; ⁷Clinical Pharmacometrics, Bayer AG, Leverkusen, Germany. *Correspondence: Thorsten Lehr (thorsten.lehr@mx.uni-saarland.de)

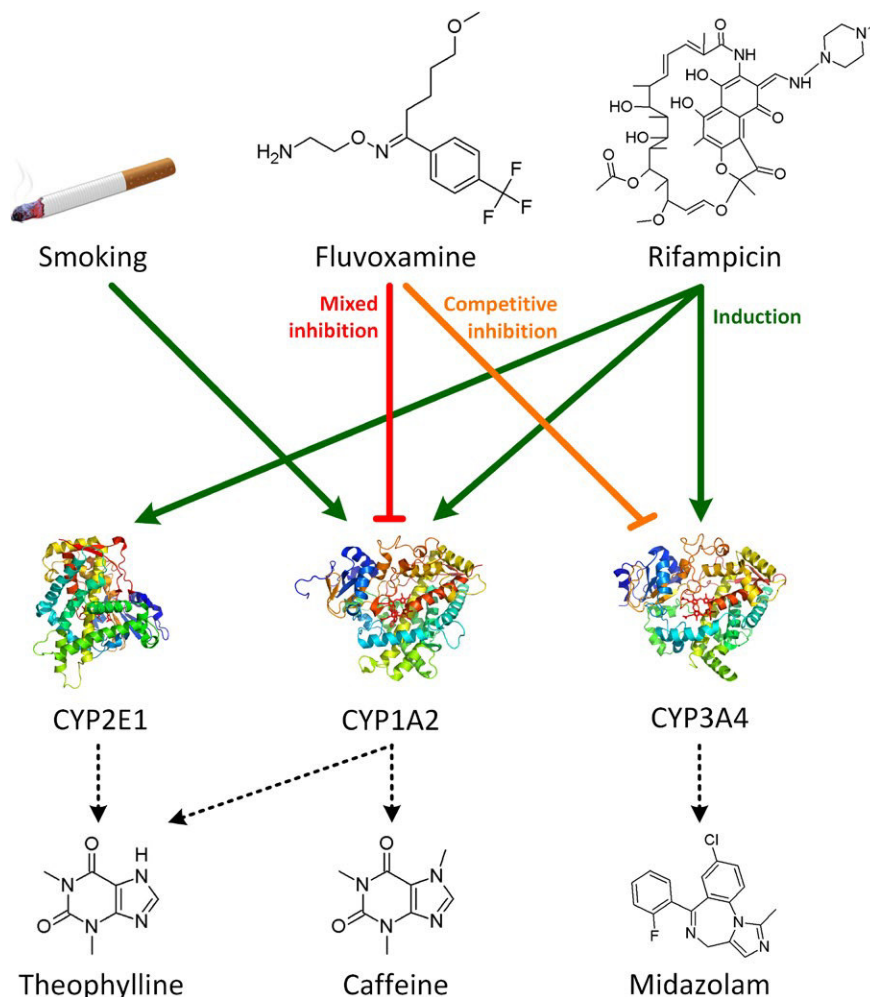


Figure 1 Cytochrome P450 (CYP) 1A2 drug–drug interaction (DDI) network. Schematic illustration of the developed CYP1A2 DDI network with fluvoxamine and rifampicin as CYP1A2 perpetrator drugs and theophylline and caffeine as CYP1A2 victim drugs. Midazolam was used as CYP3A4 victim drug for fluvoxamine. Dark green lines indicate induction by rifampicin or smoking, and the red and orange lines indicate inhibition by fluvoxamine.

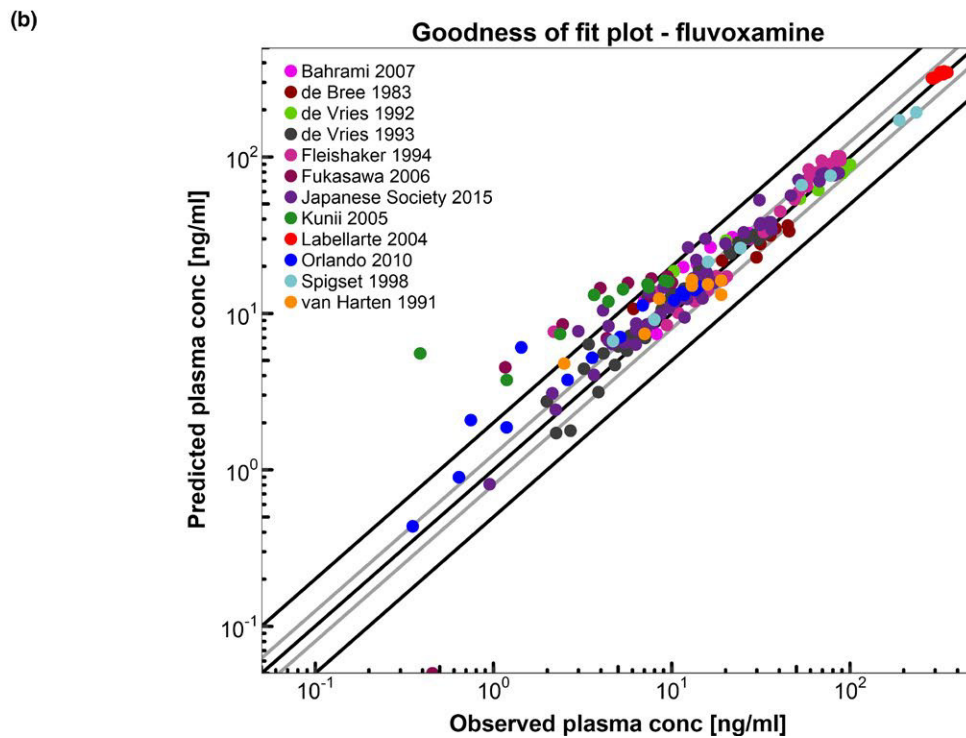
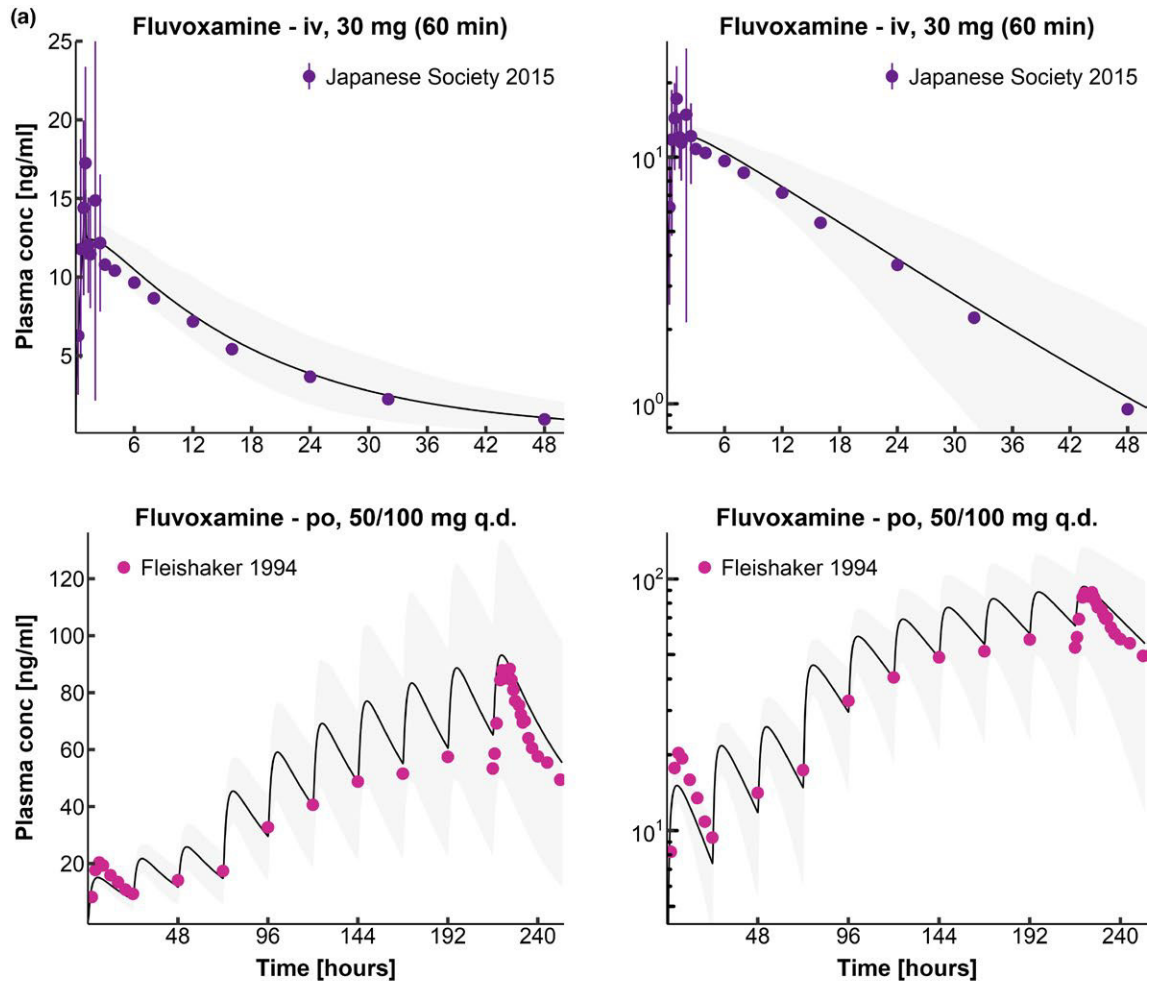
The US Food and Drug Administration (FDA) specifies caffeine as a sensitive clinical index substrate and fluvoxamine as a strong clinical index inhibitor for CYP1A2. Furthermore, they recommend considering a clinical study in smokers for investigational drugs that are CYP1A2 substrates.⁸ Theophylline is classified as a sensitive clinical substrate and rifampicin as moderate clinical inducer of CYP1A2.⁹

Physiologically-based pharmacokinetic (PBPK) modeling is a valuable method, recognized by the FDA and the European Medicines Agency, to explore and quantitatively predict the pharmacokinetics (PK) of drugs, to evaluate

drug–drug interactions (DDIs), and to support clinical study design, dose selection, and labeling.^{8,10–12} The FDA furthermore supports the prediction of DDI studies with weak and moderate index inhibitors and inducers as an alternative to prospective clinical studies, if the sponsors can demonstrate adequate model performance using clinical data from DDI studies with strong index perpetrators.⁸

The aim of this study was to develop a PBPK DDI network for CYP1A2 and thereby to extend the library of publicly available PBPK models for DDI prediction.^{13,14} For this purpose, whole-body PBPK models of fluvoxamine and theophylline have been developed and existing models of

Figure 2 Fluvoxamine plasma concentrations. (a) Population predictions of selected fluvoxamine plasma concentration–time profiles compared with observed data in linear (left panel) and semilogarithmic plots (right panel). The upper panel shows i.v. application, the lower panel p.o. administration of fluvoxamine. Observed data are shown as dots \pm SD.^{34,35} Population simulation arithmetic means are shown as lines; the shaded areas illustrate the 68% population prediction intervals. (b) Predicted compared with observed fluvoxamine plasma concentration values of all clinical studies. Line of identity and 0.5-fold to 2.0-fold acceptance limits are shown as black lines. The 0.8-fold to 1.25-fold limits are shown as grey lines. Details on dosing regimens and study populations are listed in **Table S1a of Supplement S1**. Predicted and observed pharmacokinetic parameters are summarized in **Table S1d of Supplement S1**.



caffeine,¹⁵ rifampicin,¹³ and midazolam¹³ have been expanded and coupled for mutual validation of the DDI performance of these five models. The evaluation of the single models and of the network was accomplished by prediction of multiple clinical DDI studies, demonstrating their performance with different victim or perpetrator drugs. **Figure 1** shows the successfully developed CYP1A2 PBPK DDI network, with caffeine and theophylline as sensitive substrates, fluvoxamine as a strong inhibitor, and rifampicin and smoking as moderate inducers (owing to the lack of strong CYP1A2 inducers). The evaluation of the final fluvoxamine PBPK model, including the fluvoxamine fraction metabolized via CYP2D6, was supported by a *post hoc* population pharmacokinetic (PopPK) analysis to confirm the PBPK results concerning the impact of CYP2D6 poor metabolism and smoking on the metabolism of fluvoxamine. The supplementary document (**Supplement S1**) to this paper was devised as comprehensive documentation and reference guide and provides detailed information on the single models and modeled DDI studies, including all model parameters, plots, and quantitative assessments of model performance.

METHODS

Software

PBPK modeling was performed with PK-Sim and MoBi modeling software version 7.3.0 (part of the Open Systems Pharmacology Suite,¹⁶ www.open-systems-pharmacology.org). Parameter optimization was accomplished using the Monte Carlo algorithm implemented in PK-Sim. Sensitivity analysis was performed within PK-Sim. PopPK analysis was performed with NONMEM version 7.3 (ICON Development Solutions, Ellicott City, MD). Digitization of published plasma concentration-time profiles was accomplished using GetData Graph Digitizer version 2.26.0.20 (S. Fedorov). PK parameter analysis was performed with MATLAB version R2013b (The MathWorks, Natick, MA). Graphics were compiled with R version 3.5.1 (The R Foundation for Statistical Computing, Vienna, Austria) and RStudio version 1.1.453 (RStudio, Boston, MA). SAS version 9.4 (SAS Institute, Cary, NC) was used for statistical analysis and graphics of the PopPK analysis.

PBPK model building

Fluvoxamine and theophylline PBPK model building was started with an extensive literature search to collect physicochemical parameters, information on absorption, distribution, metabolism, and excretion processes and clinical studies of i.v. and p.o. administration of fluvoxamine and theophylline in single-dose and multiple-dose regimens.

The PBPK models were built based on healthy individuals, using the reported mean values for age, weight, height,

and genetic background for each study protocol. If no information on these parameters could be found, a healthy male European individual, 30 years of age, with a body weight of 73 kg and a height of 176 cm was used.

To model the specific metabolic clearance, relevant CYP enzymes were implemented in accordance with literature, using the PK-Sim expression database reverse transcription-polymerase chain reaction profiles¹⁷ to define their relative expression in the different organs of the body. For more details see **Table S6 in Supplement S1**. Glomerular filtration and enterohepatic cycling were enabled, as they are active under physiological conditions.

To build the data sets for PBPK modeling, the reported observed plasma concentration-time profiles were digitized and divided into “training data set” and “test data set.” Model parameters that could not be informed from experimental reports were optimized by simultaneously fitting the model to all measured plasma concentration-time profiles assigned to the training data set. To limit the parameters to be optimized during model building, the minimal number of processes necessary was implemented into the model. Model evaluation was carried out based on the clinical data of the test data set. Descriptive (training data set) and predictive (test data set) performance of the model for all published clinical studies is transparently presented in **Supplement S1**.

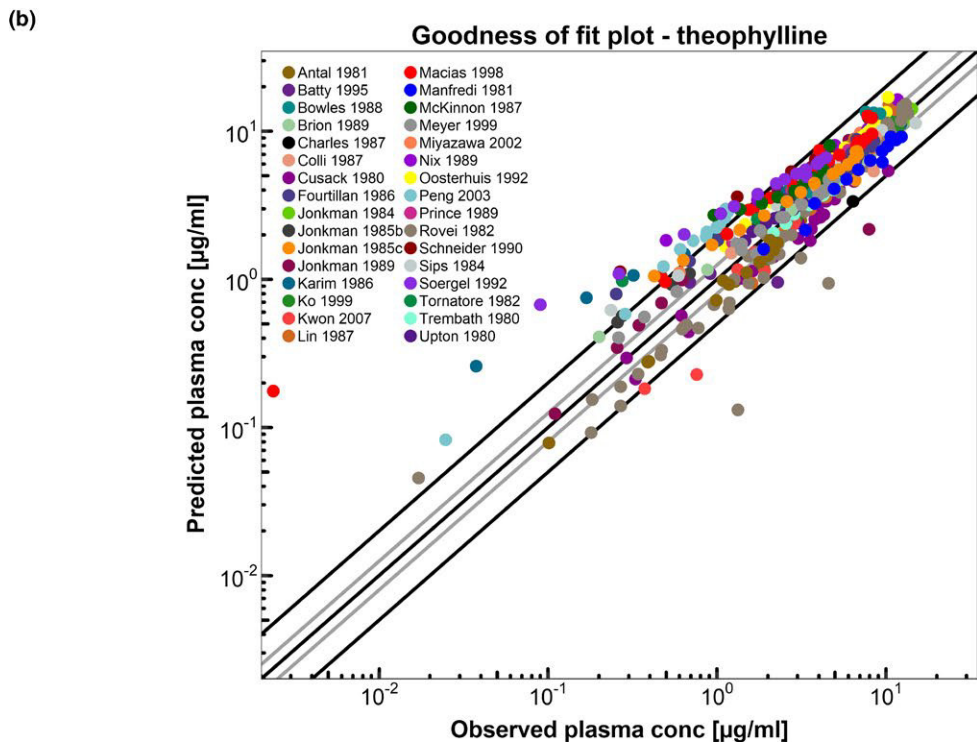
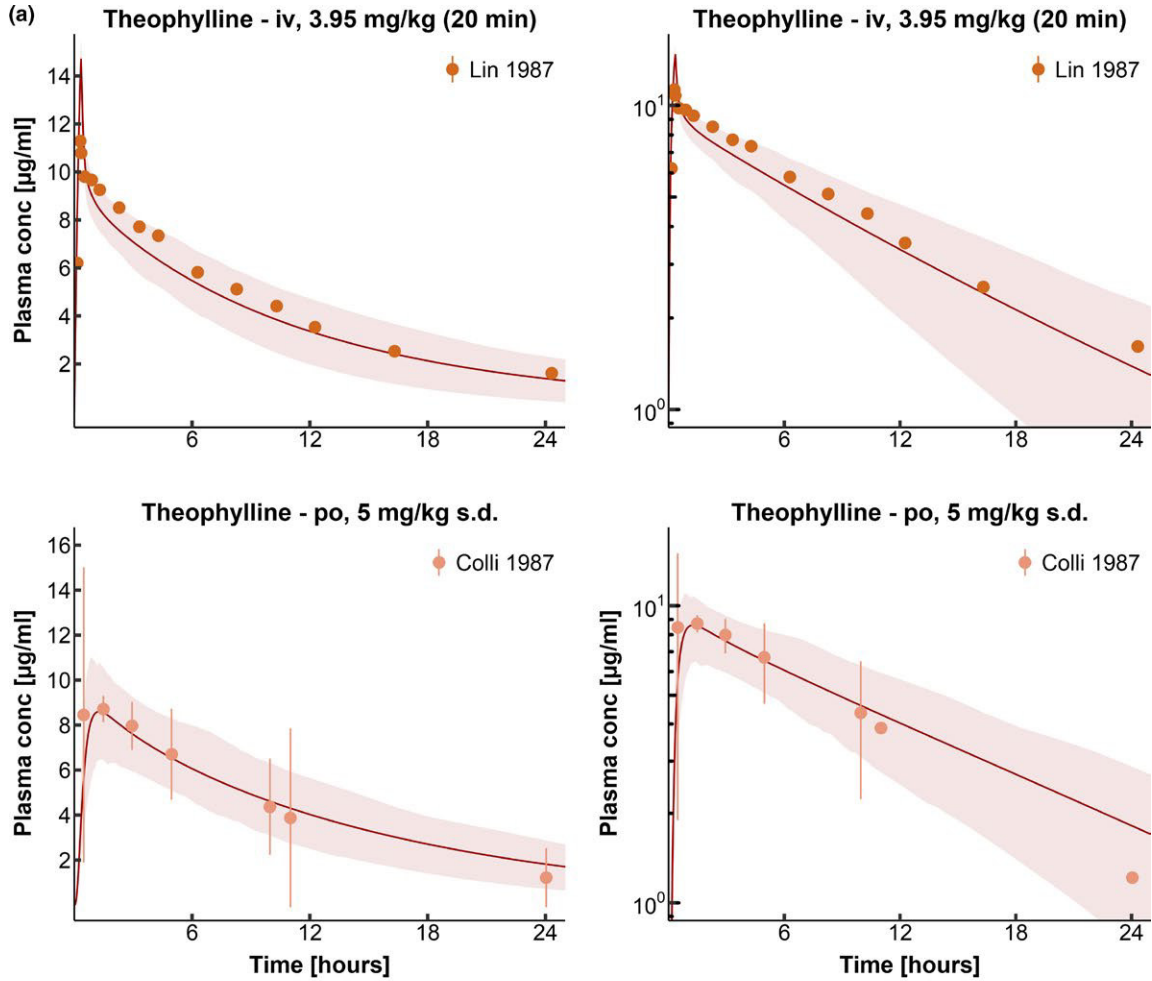
PBPK model evaluation

Model performance was evaluated with different methods. The predicted population plasma concentration-time profiles were compared with the plasma concentration-time profiles observed in the clinical studies. Furthermore, predicted plasma concentration values of all studies were compared with the observed plasma concentrations in goodness-of-fit plots. In addition, the performance was evaluated by comparison of predicted to observed area under the plasma curve (AUC) and peak plasma concentration (C_{max}) values. As quantitative measures of the descriptive and predictive performance of the models, the mean relative deviation (MRD) according to Edginton *et al.*¹⁸ and the geometric mean fold error (GMFE) were calculated. MRD was calculated for all observed plasma concentrations according to Eq. 1.

$$MRD = 10^x; x = \sqrt{\frac{\sum_{i=1}^N (\log_{10} c_{obs} - \log_{10} c_{pred})^2}{N}} \quad (1)$$

with $\log_{10} c_{obs}$ = logarithm of the observed plasma concentration, $\log_{10} c_{pred}$ = logarithm of the predicted plasma concentration, and N = number of observed values. An MRD value ≤ 2 characterizes an adequate prediction.

Figure 3 Theophylline plasma concentrations. (a) Population predictions of selected theophylline plasma concentration-time profiles compared with observed data in linear (left panel) and semilogarithmic plots (right panel). The upper panel shows i.v. application, the lower panel p.o. administration of theophylline. Observed data are shown as dots \pm SD.^{36,37} Population simulation arithmetic means are shown as lines, and the shaded areas illustrate the 68% population prediction intervals. (b) Predicted compared with observed theophylline plasma concentration values of all clinical studies. Line of identity and 0.5-fold to 2.0-fold acceptance limits are shown as black lines. The 0.8-fold to 1.25-fold limits are shown as grey lines. Details on dosing regimens and study populations are listed in **Table S2a of Supplement S1**. Predicted and observed pharmacokinetic parameters are summarized in **Table S2d of Supplement S1**.



The GMFE was calculated for all observed AUC and C_{\max} values according to Eq. 2.

$$\text{GMFE} = 10 \left(\sum \left| \log_{10} \left(\frac{\text{pred PK parameter}}{\text{obs PK parameter}} \right) \right| \right) / n \quad (2)$$

with pred PK parameter = predicted AUC or C_{\max} value, obs PK parameter = observed AUC or C_{\max} value, and n = number of studies. A GMFE value below two characterizes an adequate prediction.

PopPK model building and evaluation

Fluvoxamine PBPK model evaluation was supported by a *post hoc* PopPK analysis to quantify the effect of CYP2D6 poor metabolism and the impact of smoking on fluvoxamine clearance and to compare the results to the effect sizes predicted by the PBPK model.

PopPK analysis, model evaluation, and simulation were performed using nonlinear mixed-effects modeling techniques implemented in NONMEM. A full description of the PopPK methodology is available in **Supplement S1**.

DDI network building

In addition to the evaluation methods described above, a CYP1A2 DDI network was built to evaluate the DDI performance of the developed models (**Figure 1**). Fluvoxamine was used as a CYP1A2 and CYP3A4 inhibitor theophylline and caffeine as CYP1A2 victim drugs, rifampicin as CYP1A2 and CYP2E1 inducer, and midazolam as a CYP3A4 victim drug. Mathematical implementation of the drug interaction processes in general is specified in **Supplement S1**. All induction and inhibition processes were modeled using interaction parameter values from *in vitro* experimental reports without further adjustment or fitting.

DDI network evaluation

All predicted DDI simulations were evaluated by comparison of predicted vs. observed victim drug plasma concentration-time profiles alone and during coadministration, DDI AUC ratios (Eq. 3), and DDI C_{\max} ratios (Eq. 4).

$$\text{DDI AUC ratio} = \frac{\text{AUC}_{\text{victim drug during coadministration}}}{\text{AUC}_{\text{victim drug alone}}} \quad (3)$$

$$\text{DDI } C_{\max} \text{ ratio} = \frac{C_{\max, \text{victim drug during coadministration}}}{C_{\max, \text{victim drug alone}}} \quad (4)$$

As a quantitative measure of the prediction accuracy for each DDI interaction, GMFEs of the predicted DDI AUC ratios and DDI C_{\max} ratios were calculated according to Eq. 2.

Sensitivity analysis

Sensitivity of the final PBPK models to single parameters (local sensitivity analysis) was calculated, measured as relative changes of the AUC of one dosing interval in steady-state conditions for simulations of the highest recommended doses for fluvoxamine (300 mg once daily) and theophylline (500 mg once daily), respectively.

Parameters were included into the analysis if they have been optimized (**Table S1b or S2b in Supplement S1**), if they might have a strong influence due to calculation methods used in the model (fraction unbound) or if they had significant impact in former models (solubility, blood/plasma ratio, and glomerular filtration rate fraction).

Sensitivity to a parameter is calculated as the ratio of the relative change of the simulated AUC to the relative variation of the parameter around the value used in the final model according to Eq. 5.

$$S = \frac{\Delta \text{AUC}}{\text{AUC}} * \frac{p}{\Delta p} \quad (5)$$

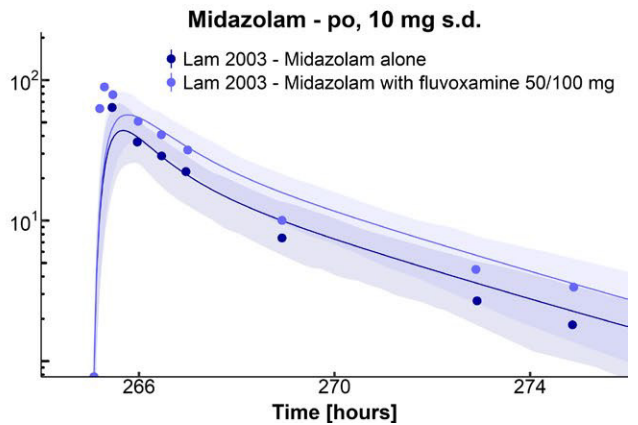
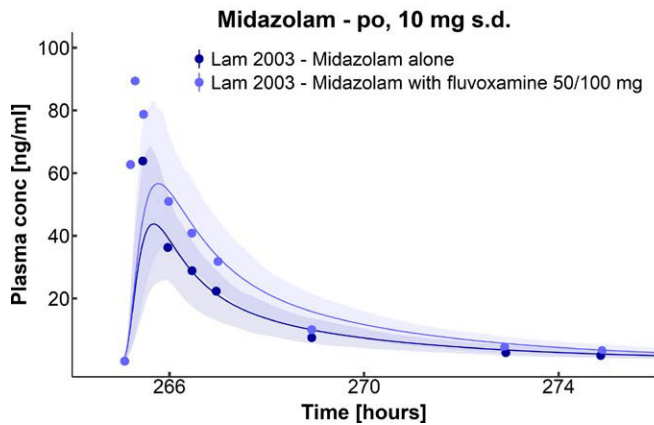
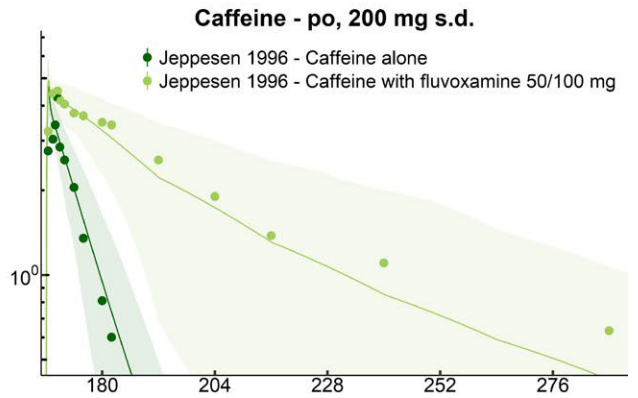
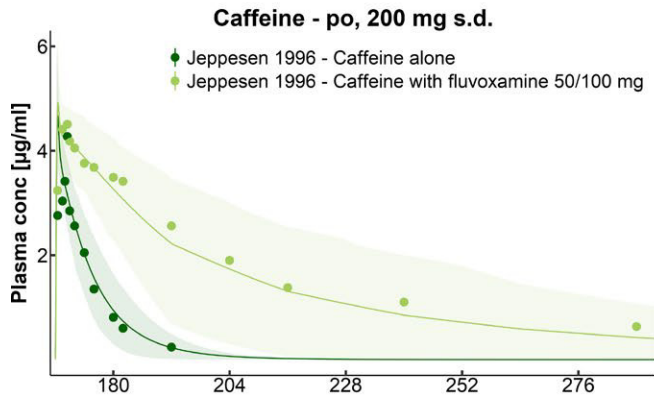
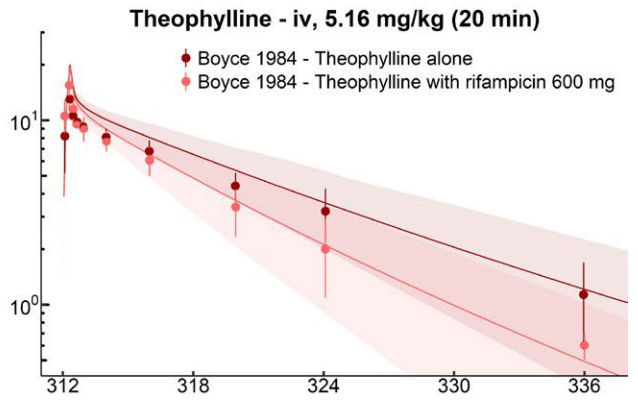
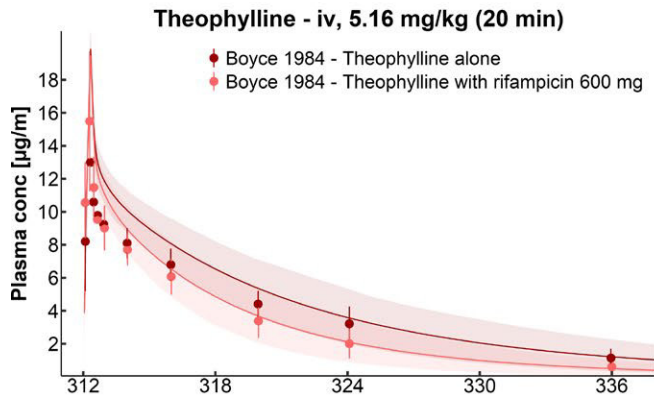
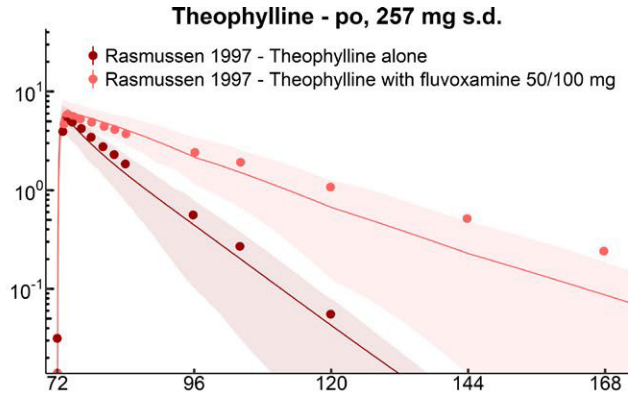
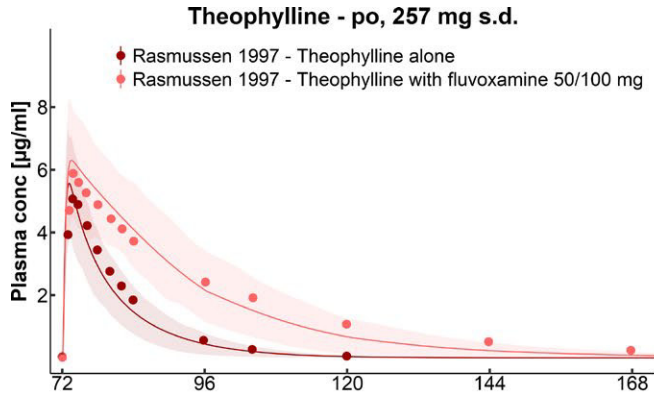
with S = sensitivity of the AUC to the examined model parameter, ΔAUC = change of the AUC, AUC = simulated AUC with the original parameter value, Δp = change of the examined model parameter value, and p = original model parameter value. A sensitivity value of + 1.0 signifies that a 10% increase of the examined parameter causes a 10% increase of the simulated AUC.

Virtual population characteristics

To predict the variability of the simulated plasma concentration-time profiles, virtual populations of 100 individuals were generated, containing European, Asian, or Japanese individuals. The percentage of male and female individuals and the age and weight ranges were set corresponding with the reported demographics. If not specified, virtual populations containing 50 male and 50 female individuals 20–50 years of age were used, without specific body weight or height restriction as implemented in the software. For details on study populations see **Tables S1a, S2a, S7a, S8a, S9a, and S10a in Supplement S1**. In the generated virtual populations, corresponding organ volumes, tissue compositions, blood flow rates, etc. were varied by an implemented algorithm within the limits of the International Commission on Radiological Protection,^{19,20} Tanaka and Kawamura,²¹ or Japanese²² databases. In addition, the reference concentrations of the implemented CYP enzymes were set to be distributed with the default variabilities for their expression available in PK-Sim. **Table S6 in Supplement S1** summarized the implemented enzymes with their reference concentrations and variabilities.

With these populations, simulations were generated and compared with observed data. As the observed data were

Figure 4 Plasma concentration-time profiles of the drug–drug interaction (DDI) network. Population predictions of selected plasma concentration-time profiles compared with observed data for the fluvoxamine-theophylline, rifampicin-theophylline, fluvoxamine-caffeine, and fluvoxamine-midazolam DDIs in linear (left panel) and semilogarithmic plots (right panel). Observed data are shown as dots \pm SD.^{38–41} Population simulation arithmetic means are shown as lines, and the shaded areas illustrate the 68% population prediction intervals. Details on dosing regimens and study populations are listed in **Tables S7a, S8a, S9a, and S10a of Supplement S1**. Predicted and observed pharmacokinetic parameters are summarized in **Tables S7b, S8b, S9b, and S10b of Supplement S1**.



reported in terms of arithmetic means and SDs, simulated 68% population prediction intervals were plotted that correspond to the range span of ± 1 SD around the mean assuming normal distribution.

RESULTS

PBPK model building and evaluation

The final PBPK models of fluvoxamine and theophylline precisely describe and predict the plasma concentration-time profiles following i.v. and p.o. administration for a large range of administered doses.

Plots of population predicted compared with observed plasma concentration-time profiles of all studies obtained from literature are shown in linear as well as in semilogarithmic plots in **Figure 2a** (selected fluvoxamine studies), **Figure 3a** (selected theophylline studies), and **Figures S1a, S1b, S2a, and S2b of Supplement S1** (all studies). Goodness-of-fit plots are presented in **Figure 2b** (fluvoxamine), **Figure 3b** (theophylline), and **Figures S1c and S2c of Supplement S1**. MRD values of all studies are listed in **Tables S1c and S2c of Supplement S1**.

Predicted compared with observed AUC and C_{max} values of all studies with calculated GMFEs are listed in **Tables S1d and S2d of Supplement S1**. Plots showing the correlation of predicted to observed AUC and C_{max} values of all studies are presented in **Figures S1f and S2d of Supplement S1**.

For fluvoxamine PBPK model development, 26 different clinical studies with PK blood sampling were used, with 9 studies assigned to the training data set (**Table S1a in**

Supplement S1). The fluvoxamine PBPK model applies metabolism by CYP1A2, CYP2D6, and glomerular filtration.

To distinguish between fluvoxamine metabolism in CYP2D6 extensive metabolizers (EMs) and poor metabolizers (PMs), the CYP2D6 catalytic rate constant (k_{cat}) of PMs was set to zero. This assumption was made because CYP2D6 PMs were characterized by absent CYP2D6 enzymatic activity,²³ which results in a predicted 1.5-fold increase of the fluvoxamine AUC in CYP2D6 PMs compared with CYP2D6 EMs (observed: 1.3-fold increase²⁴). Population predictions of fluvoxamine plasma concentration-time profiles compared with observed data for CYP2D6 EMs and PMs are shown in **Figure S1d of Supplement S1**.

Furthermore, the final model is able to describe the influence of smoking on the PK of fluvoxamine. Smoking is the strongest known inducer of CYP1A2 and results in higher metabolism of CYP1A2 substrates.¹ As no detailed information on the frequency, duration, and amount of smoking was available from literature, the induction of CYP1A2 was implemented as a static 1.38-fold increase in enzyme activity. This factor was optimized based on the study of Spigset *et al.*,²⁵ resulting in a 39% reduction of the fluvoxamine AUC in smokers (observed: 31% reduction). Population predictions of fluvoxamine plasma concentration-time profiles compared with observed data for nonsmokers and smokers are shown in **Figure S1e of Supplement S1**. Drug-dependent parameters of the final fluvoxamine model are listed in **Table S1b of Supplement S1**. System-dependent parameters are given in **Table S6 of Supplement S1**.

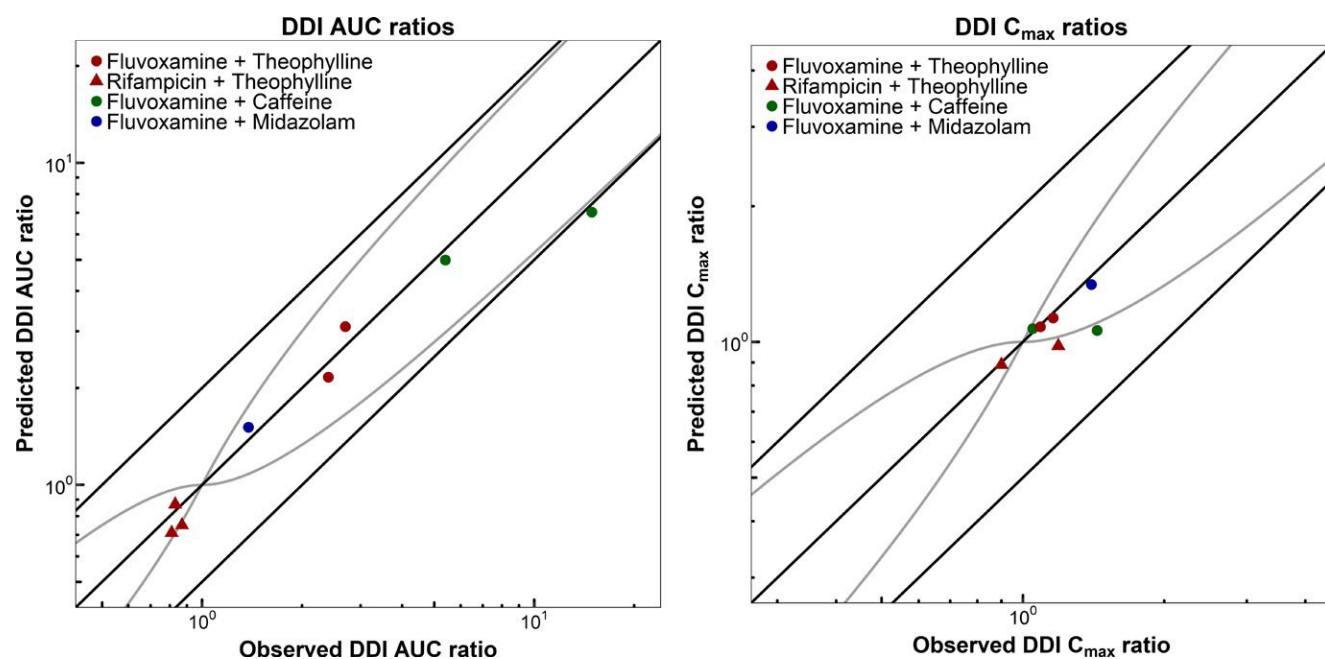


Figure 5 Correlation of predicted to observed drug–drug interaction (DDI) area under the curve (AUC) ratios, and DDI peak plasma concentration (C_{max}) ratios. The left panel illustrates the predicted compared with observed DDI AUC ratios, the right panel illustrates the predicted compared with observed DDI C_{max} ratios of the fluvoxamine-theophylline, rifampicin-theophylline, fluvoxamine-caffeine, and fluvoxamine-midazolam DDIs. Fluvoxamine interaction studies are shown as dots and rifampicin interaction studies are shown as triangles. The colors represent the different victim drugs. The line of identity and the 0.5-fold to 2.0-fold acceptance limits are shown as straight black lines. The curved grey lines are the prediction acceptance limits proposed by Guest *et al.*⁴² Study references, dosing regimens, and values of predicted and observed DDI AUC ratios and DDI C_{max} ratios are listed in **Table 1**.

Sensitivity analysis of a simulation of 300 mg fluvoxamine p.o. once daily with a sensitivity threshold of 0.5 reveals that the fluvoxamine model is sensitive to the values of lipophilicity (optimized), CYP2D6 catalytic rate constant (optimized), CYP2D6 Michaelis-Menten constant (literature value), and fraction unbound (literature value; see **Figure S1g of Supplement S1**).

For theophylline PBPK model development, 40 different clinical studies with PK blood sampling and additional fraction excreted unchanged to urine measurements and CYP1A2 fraction metabolized information were used, with 13 clinical studies assigned to the training data set (**Table S2a in Supplement S1**). The theophylline PBPK model applies metabolism by CYP1A2, CYP2E1, and glomerular filtration with reabsorption in the renal tubulus.

In the model, CYP1A2 metabolizes theophylline with high affinity but low capacity, whereas CYP2E1 metabolizes theophylline with low affinity and high capacity, as described in the literature,²⁶ resulting in a good prediction of the observed concentration dependency of theophylline metabolism. About 95% of an administered theophylline dose are

excreted with the urine but only 14–17% as unchanged drug.^{27,28} Due to the lack of valid *in vitro* data on renal tubular reabsorption transporters for theophylline, the glomerular filtration rate fraction was optimized to a value of 0.22 to describe the fraction of theophylline excreted unchanged to urine. Drug-dependent parameters of the final theophylline model are listed in **Table S2b of Supplement S1**. System-dependent parameters are given in **Table S6 of Supplement S1**.

Sensitivity analysis of a simulation of 500 mg theophylline p.o. once daily with a sensitivity threshold of 0.5 reveals that the theophylline model is sensitive to the values of fraction unbound (literature value), CYP1A2 catalytic rate constant (optimized), and CYP1A2 Michaelis-Menten constant (literature value; see **Figure S2e of Supplement S1**).

DDI network modeling

For the CYP1A2 DDI network modeling, eight different clinical DDI studies were available, consisting of two studies of fluvoxamine with theophylline, three studies

Table 1 DDI AUC ratios, DDI C_{max} ratios, and GMFE values of DDI studies

Perpetrator drug	Victim drug	Observed DDI AUC ratio	Predicted DDI AUC ratio	Pred/Obs DDI AUC ratio	Observed DDI C _{max} ratio	Predicted DDI C _{max} ratio	Pred/Obs DD C _{max} ratio	Reference		
<i>Fluvoxamine</i>	<i>Theophylline</i>	50 mg p.o., q.d./b.i.d.	3.21 mg/kg p.o., s.d.	2.40	2.16	0.90	1.09	1.08	0.99	Orlando 2006 ⁴³
		50/100 mg p.o., q.d.	257 mg p.o., s.d.	2.70	3.10	1.15	1.16	1.13	0.97	Rasmussen 1997 ³⁸
		GMFE (range)		1.13 (1.11–1.15)		1.02 (1.01–1.03)		2/2		
		Pred/Obs within twofold		2/2		2/2				
<i>Rifampicin</i>	<i>Theophylline</i>	600 mg p.o., q.d.	3.95 mg/kg i.v. (30 minutes)	0.83	0.87	1.05	0.98	0.98	0.82	Powell-Jackson 1985 ⁴⁴
		600 mg p.o., q.d.	5.19 mg/kg i.v. (20 minutes)	0.81	0.71	0.89	1.19	0.98	0.82	Boyce 1984 ³⁹
		600 mg p.o., q.d.	355.5 mg p.o., s.d.	0.87	0.75	0.87	0.90	0.89	0.99	Powell-Jackson 1985 ⁴⁴
		GMFE (range)		1.12 (1.05–1.16)		1.11 (1.01–1.21)		2/2		
Pred/Obs within twofold		3/3		2/2						
<i>Fluvoxamine</i>	<i>Caffeine</i>	50/100 mg p.o., q.d.	200 mg p.o., s.d.	5.40	4.99	0.92	1.06	1.07	1.01	Jeppesen 1996 ⁴⁰
		100 mg p.o., b.i.d.	250 mg p.o., s.d.	14.90	7.03	0.47	1.44	1.06	0.74	Culm-Merdek 2005 ⁴⁵
		GMFE (range)		1.51 (1.08–2.12)		1.17 (1.01–1.36)		2/2		
		Pred/Obs within twofold		1/2		2/2				
<i>Fluvoxamine</i>	<i>Midazolam</i>	50 mg p.o., b.i.d.	10 mg p.o., s.d.	1.38	1.51	1.09	1.40	1.34	0.95	Lam 2003 ⁴¹
		GMFE		1.09		1.04				
		Pred/Obs within twofold		1/1		1/1				

AUC, area under the plasma concentration-time curve; C_{max}, peak plasma concentration; DDI, drug-drug interaction; GMFE, geometric mean fold error; Pred/Obs, predicted/observed; -, no data available.

of rifampicin with theophylline, two studies of fluvoxamine with caffeine, and one study of fluvoxamine with midazolam. The victim drug plasma concentration-time profiles of these studies, before and during perpetrator treatment, were predicted and compared with observed data. **Tables S7a, S8a, S9a, and S10a of Supplement S1** list the administration protocols and study population details of the clinical DDI studies. The parameters to model the CYP1A2, CYP2E1, and CYP3A4 induction and inhibition processes are described in **Supplement S1**. Population predictions of plasma concentration-time profiles of the different victim drugs before and during coadministration are presented in linear as well as semi-logarithmic plots in **Figure 4** (selected studies) and **Figures S7a, S8a, S9a, and S10a of Supplement S1** (all studies). All victim drug plasma concentration-time profiles before and during coadministration with fluvoxamine or rifampicin are well-predicted over the full range of reported administration protocols.

Figure 5 shows the correlation of predicted to observed DDI AUC ratios and DDI C_{\max} ratios of the modeled DDI studies as a visualization of the performance of the entire network. **Table 1** lists the corresponding DDI AUC ratio and DDI C_{\max} ratio values shown in **Figure 5**, with calculated GMFE values for each perpetrator-victim drug combination, demonstrating the good performance of the developed models when applied for DDI prediction.

PopPK modeling of fluvoxamine

The PK of fluvoxamine were best described by a one-compartment model with zero-order absorption with a lag time and linear elimination from the central compartment. As shown in **Table S11 of Supplement S1**, parameter estimates were precise. Goodness-of-fit plots (**Figure S11a in Supplement S1**) and visual predictive checks (**Figure S11b in Supplement S1**) demonstrate the good descriptive performance of the model.

The impact of CYP2D6 phenotype on total clearance of fluvoxamine was best described as a categorical covariate. Volunteers who are CYP2D6 PMs show a 22% lower total clearance of fluvoxamine compared with EMs. Furthermore, fluvoxamine clearance was found to be 28% higher in smokers compared with nonsmokers.

DISCUSSION

The developed PBPK models of fluvoxamine and theophylline reliably describe and predict plasma concentration-time profiles over the full range of published doses and administration protocols. Their good descriptive and predictive performance has been demonstrated by comparison of predicted to observed plasma concentration-time profiles, AUC and C_{\max} values, calculation of MRDs and GMFEs, as well as with the prediction of different DDIs. Although the populations used for model predictions were carefully generated according to the reported study demographics, CYP1A2 and CYP2D6 show high interindividual variability, and information on smoking status and CYP2D6 phenotype were lacking in most of the study reports. This could explain why a small percentage of the fluvoxamine and theophylline

studies cannot be accurately predicted using the same k_{cat} values for all studies.

There are two previously published PBPK models of fluvoxamine: a minimal PBPK model (three compartments)²⁹ and a model built on the basis of few clinical studies (four studies).³⁰ For theophylline, one PBPK model has been previously reported, developed to predict the disposition of theophylline during pregnancy.³¹ All three models have not been challenged by prediction of DDIs. The whole-body PBPK models presented in this study have been built using a multitude of clinical studies, are transparently documented, and they have been evaluated in a DDI network.

To describe the metabolism of fluvoxamine, CYP1A2 and CYP2D6 were implemented into the PBPK model. Model building was started with the working hypothesis that CYP2D6 accounts for up to 60% of fluvoxamine metabolism.³² However, our PBPK analysis suggested a higher fraction of fluvoxamine metabolized by CYP1A2 than by CYP2D6. This result was supported by the finding that fluvoxamine total apparent clearance (CL/F) in CYP2D6 PMs (no CYP2D6 activity) was only 25% lower than in CYP2D6 EMs.³² (Taking into account that CYP2D6 is also expressed in the intestine, CYP2D6 PMs might show a higher bioavailability of fluvoxamine, reducing CL/F, and thereby further reducing the impact of CYP2D6 poor metabolism on fluvoxamine clearance.)

To confirm this relatively small impact of CYP2D6 poor metabolism on fluvoxamine PK, a PopPK analysis of fluvoxamine was conducted. The reduction of fluvoxamine CL/F in CYP2D6 PMs compared with EMs was quantified at 22%. This is the first reported compartmental analysis of fluvoxamine, which is in very good agreement with the noncompartmental result for reduction of CL/F in CYP2D6 PMs of 25%.³²

Simulation of fluvoxamine fraction metabolized using the final PBPK model and a single dose of 50 mg predicts fractions metabolized of 20% by CYP2D6 and of 71% by CYP1A2, which is very close to the PopPK analysis result. Neither fraction metabolized information nor the CYP2D6 PM fluvoxamine plasma profiles were used during the final PBPK model parameter optimization. Fitting the catalytic rate constants of CYP2D6 and CYP1A2 and, therefore, the contribution of both enzymes to fluvoxamine metabolism to get a good description of the nonlinear PK of fluvoxamine for the different doses administered already resulted in a model that accurately describes the fractions metabolized.

The inducing effect of smoking on the metabolism of fluvoxamine is also well-described by the PBPK model, with AUC ratios smoking/nonsmoking of 0.61 predicted and 0.69 observed. The fluvoxamine PopPK analysis gives a 28% higher CL/F of fluvoxamine in smokers compared with nonsmokers. The small overprediction of the fluvoxamine C_{\max} in smokers could be attributed to gastrointestinal effects of smoking that reduce the absorption of fluvoxamine but were not accounted for in the model. However, due to a lack of more detailed information on the frequency, duration, and amount of smoking, the induction of CYP1A2 could only be implemented as a static increase of the enzyme activity. To model this CYP induction in a mechanistic and dynamic

way, for example, to predict the return of CYP1A2 activity to baseline when smoking is stopped before a surgical intervention, as well as to validate the estimated factor on CYP1A2 enzyme activity for the smoking population, more data are needed.

The developed theophylline model can be used for prediction of plasma concentration-time profiles following i.v. administration or p.o. administration of syrup, solution, or immediate-release formulations. As the reported plasma concentration profiles of the different sustained release dosage forms strongly vary with the mechanism used for prolongation of drug release, sustained release or enteric coated theophylline formulations were not considered in the current investigation. If needed, the model can be easily extended by implementation of sustained release drug dissolution profiles.³³

The DDIs presented in this study have been modeled using reported experimental values to inform all necessary interaction parameters. This approach is followed as an additional means of model evaluation, predicting all available reported clinical DDI studies, and comparing the observed data to model predictions. The caffeine,¹⁵ rifampicin,¹³ and midazolam¹³ PBPK models applied have been evaluated and described elsewhere. The existing rifampicin model has been extended to predict the induction of CYP1A2 and CYP2E1 by rifampicin. The DDI performance of the enhanced rifampicin model has been successfully evaluated with the data of three different clinical rifampicin-theophylline DDI studies.

The presented CYP1A2 DDI network demonstrates the good performance of all models for DDI prediction over the full range of reported DDI study protocols. This has been shown by victim drug concentration-time profiles, DDI AUC ratios, DDI C_{max} ratios, and corresponding GMFE values. All DDIs of fluvoxamine with the sensitive CYP1A2 victim drugs theophylline and caffeine are well predicted. The moderate inhibition of CYP3A4 by fluvoxamine was successfully implemented and evaluated by prediction of the fluvoxamine-midazolam DDI. Due to the present lack of models for CYP2C19 victim drugs, the strong inhibition of CYP2C19 by fluvoxamine could not be tested. However, fluvoxamine CYP2C19 interaction parameters are reported and can be easily implemented into the presented fluvoxamine PBPK model.

In summary, a PBPK CYP1A2 DDI network has been successfully developed. Whole-body PBPK models of fluvoxamine and theophylline have been carefully built and evaluated by DDI prediction using different kinds of perpetrator (induction, competitive inhibition, and mixed inhibition) and victim drugs (CYP1A2 and CYP3A4). Furthermore, a previously developed model of rifampicin has been expanded with parameters for CYP1A2 and CYP2E1 interaction and tested. The resulting PBPK network of fluvoxamine, theophylline, caffeine, rifampicin, and midazolam adequately predicts the observed data of all clinical DDI studies reported for combinations of these drugs and, therefore, all models are considered ready to use for DDI prediction. The newly developed models of fluvoxamine and theophylline are transparently documented and the model files, also including DDI model files, are provided as **Supplementary Material** to this paper (**Data S1-S6**) as well as in the Open Systems Pharmacology

repository (www.open-systems-pharmacology.org), to extend the library of publicly available PBPK models for DDI prediction. They can be applied to help understand and characterize the DDI potential of investigational drugs, to inform the design of clinical trials, or to generate dose recommendations for comedication.

Supporting Information. Supplementary information accompanies this paper on the *CPT: Pharmacometrics & Systems Pharmacology* website (www.psp-journal.com).

Supplement S1. Model information and evaluation.

Data S1. Fluvoxamine model file.

Data S2. Theophylline model file.

Data S3. Fluvoxamine-theophylline DDI model file.

Data S4. Rifampicin-theophylline DDI model file.

Data S5. Fluvoxamine-caffeine DDI model file.

Data S6. Fluvoxamine-midazolam DDI model file.

Funding. This project has received funding from the European Union's Horizon 2020 Research and Innovation Programme under grant agreement No. 668353. M.S. was supported by the Robert Bosch Stiftung, Stuttgart, Germany.

Conflict of Interest. T.E., T.W., and S.F. are employees of Bayer AG. A.K.V. performed this work at the Saarland University. Since January 2018, she is an employee of the Federal Institute for Drugs and Medical Devices (BfArM) and declares no potential conflicts of interest with respect to the research, authorship, and/or publication of this article. No potential conflicts of interest were disclosed by the other authors.

Author Contributions. H.B., N.H., A.K.V., and T.L. wrote the manuscript. N.H., O.S., M.S., T.E., T.W., S.F., and T.L. designed the research. H.B., N.H., A.K.V., S.F., and T.L. performed the research.

Disclaimer. The views expressed in this article are the views of A.K.V. and do not necessarily reflect the views and opinions of the BfArM.

1. Zhou, S.F., Yang, L.P., Zhou, Z.W., Liu, Y.H. & Chan, E. Insights into the substrate specificity, inhibitors, regulation, and polymorphisms and the clinical impact of human cytochrome P450 1A2. *AAPS J.* **11**, 481–494 (2009).
2. Shimada, T., Yamazaki, H., Mimura, M., Inui, Y. & Guengerich, F.P. Interindividual variations in human liver cytochrome P-450 enzymes involved in the oxidation of drugs, carcinogens and toxic chemicals: studies with liver microsomes of 30 Japanese and 30 caucasians. *J. Pharmacol. Exp. Ther.* **270**, 414–423 (1994).
3. Chen, Y., Liu, L., Laille, E., Kumar, G. & Surapaneni, S. In vitro assessment of cytochrome P450 inhibition and induction potential of azacitidine. *Cancer Chemother. Pharmacol.* **65**, 995–1000 (2010).
4. Kalow, W. & Tang, B. The use of caffeine for enzyme assays: a critical appraisal. *Clin. Pharmacol. Ther.* **53**, 503–514 (1993).
5. Karjalainen, M.J., Neuvonen, P.J. & Backman, J.T. Rofecoxib is a potent, metabolism-dependent inhibitor of CYP1A2: implications for in vitro prediction of drug interactions. *Drug Metab. Dispos.* **34**, 2091–2096 (2006).
6. Lu, P. et al. Mechanism-based inhibition of human liver microsomal cytochrome P450 1A2 by zileuton, a 5-lipoxygenase inhibitor. *Drug Metab. Dispos.* **31**, 1352–1360 (2003).
7. Faber, M.S., Jetter, A. & Fuhr, U. Assessment of CYP1A2 activity in clinical practice: why, how, and when? *Basic Clin. Pharmacol. Toxicol.* **97**, 125–134 (2005).
8. US Food and Drug Administration. Clinical drug interaction studies - study design, data analysis, implications for dosing, and labeling recommendations. Draft Guidance for Industry <<https://www.fda.gov/downloads/drugs/guidancecomplianceregulatoryinformation/guidances/ucm292362.pdf>> (2017).
9. US Food and Drug Administration. Drug development and drug interactions: table of substrates, inhibitors and inducers. <<https://www.fda.gov/Drugs/DevelopmentApprovalProcess/DevelopmentResources/DrugInteractionsLabeling/ucm093664.htm>> (2017). Accessed October 2, 2018.

10. European Medicines Agency. Guideline on the investigation of drug interactions. <https://www.ema.europa.eu/documents/scientific-guideline/guideline-investigation-drug-interactions_en.pdf> (2015).
11. European Medicines Agency. Draft guideline on the qualification and reporting of physiologically based pharmacokinetic (PBPK) modelling and simulation. <https://www.ema.europa.eu/documents/scientific-guideline/draft-guideline-qualification-reporting-physiologically-based-pharmacokinetic-pbpbk-modelling_en.pdf> (2016).
12. US Food and Drug Administration. Physiologically based pharmacokinetic analyses - format and content. Guidance for Industry. <<https://www.fda.gov/downloads/Drugs/GuidanceComplianceRegulatoryInformation/Guidances/UCM531207.pdf>> (2018).
13. Hanke, N. et al. PBPK models for CYP3A4 and P-gp DDI prediction: a modeling network of rifampicin, itraconazole, clarithromycin, midazolam, alfentanil, and digoxin. *CPT Pharmacometrics Syst. Pharmacol.* **7**, 647–659 (2018).
14. Open Systems Pharmacology (OSP). OSP repository. <<https://github.com/Open-Systems-Pharmacology>> (2018). Accessed October 2, 2018.
15. Open Systems Pharmacology (OSP). OSP repository: caffeine template model. <https://github.com/Open-Systems-Pharmacology/Example_Caffeine/blob/master/Caffeine.pksim5> (2018). Accessed October 2, 2018.
16. Eissing, T. et al. A computational systems biology software platform for multiscale modeling and simulation: integrating whole-body physiology, disease biology, and molecular reaction networks. *Front. Physiol.* **2**, 1–10 (2011).
17. Meyer, M., Schneckener, S., Ludewig, B., Kuepfer, L. & Lippert, J. Using expression data for quantification of active processes in physiologically-based pharmacokinetic modeling. *Drug Metab. Dispos.* **40**, 892–901 (2012).
18. Edginton, A.N., Schmitt, W. & Willmann, S. Development and evaluation of a generic physiologically based pharmacokinetic model for children. *Clin. Pharmacokinet.* **45**, 1013–1034 (2006).
19. Valentin, J. Basic anatomical and physiological data for use in radiological protection: reference values. A report of age- and gender-related differences in the anatomical and physiological characteristics of reference individuals. ICRP Publication 89. *Ann. ICRP* **32**, 5–265 (2002).
20. Willmann, S. et al. Development of a physiology-based whole-body population model for assessing the influence of individual variability on the pharmacokinetics of drugs. *J. Pharmacokinet. Pharmacodyn.* **34**, 401–431 (2007).
21. Tanaka, G. & Kawamura, H. Anatomical and physiological characteristics for Asian reference man: male and female of different ages: Tanaka model. Division of Radioecology, National Institute of Radiological Sciences. Hitachinaka 311-12 Japan. NIRS-M-115 (1996).
22. Open Systems Pharmacology Suite. Open Systems Pharmacology Suite Manual, Version 7.0.0. (2017).
23. Crews, K.R. et al. Clinical Pharmacogenetics Implementation Consortium guidelines for cytochrome P450 2D6 genotype and codeine therapy: 2014 update. *Clin. Pharmacol. Ther.* **95**, 376–382 (2014).
24. Spigset, O., Granberg, K., Hägg, S., Norström, A. & Dahlqvist, R. Relationship between fluvoxamine pharmacokinetics and CYP2D6/CYP2C19 phenotype polymorphisms. *Eur. J. Clin. Pharmacol.* **52**, 129–133 (1997).
25. Spigset, O., Carleborg, L., Hedenmalm, K. & Dahlqvist, R. Effect of cigarette smoking on fluvoxamine pharmacokinetics in humans. *Clin. Pharmacol. Ther.* **58**, 399–403 (1995).
26. Zhang, Z. & Kaminsky, L.S. Characterization of human cytochromes P450 involved in theophylline 8-hydroxylation. *Biochem. Pharmacol.* **50**, 205–211 (1995).
27. Macias, W.L. et al. Lack of effect of olanzapine on the pharmacokinetics of a single aminophylline dose in healthy men. *Pharmacotherapy* **18**, 1237–1248 (1998).
28. Rovei, V., Chanoine, F. & Strolin Benedetti, M. Pharmacokinetics of theophylline: a dose-range study. *Br. J. Clin. Pharmacol.* **14**, 769–778 (1982).
29. Iga, K. Use of three-compartment physiologically based pharmacokinetic modeling to predict hepatic blood levels of fluvoxamine relevant for drug-drug interactions. *J. Pharm. Sci.* **104**, 1478–1491 (2015).
30. Alqahtani, S. & Kaddoumi, A. Development of a physiologically based pharmacokinetic/pharmacodynamic model to predict the impact of genetic polymorphisms on the pharmacokinetics and pharmacodynamics represented by receptor/transporter occupancy of central nervous system drugs. *Clin. Pharmacokinet.* **55**, 957–969 (2016).
31. Ke, A.B. et al. A physiologically based pharmacokinetic model to predict disposition of CYP2D6 and CYP1A2 metabolized drugs in pregnant women. *Drug Metab. Dispos.* **41**, 801–813 (2013).
32. Spigset, O., Axelsson, S., Norström, A., Hägg, S. & Dahlqvist, R. The major fluvoxamine metabolite in urine is formed by CYP2D6. *Eur. J. Clin. Pharmacol.* **57**, 653–658 (2001).
33. Thelen, K., Coboecken, K., Willmann, S., Dressman, J.B. & Lippert, J. Evolution of a detailed physiological model to simulate the gastrointestinal transit and absorption process in humans, part II: extension to describe performance of solid dosage forms. *J. Pharm. Sci.* **101**, 1267–1280 (2012).
34. Japanese Society of Hospital Pharmacists. Pharmaceutical interview form (Article in Japanese). <https://www.abbvie.co.jp/content/dam/abbviecorp/japan/docs/if_luvox_201412.pdf> (2015). Accessed October 2, 2018.
35. Fleishaker, J. & Hulst, L. A pharmacokinetic and pharmacodynamic evaluation of the combined administration of alprazolam and fluvoxamine. *Eur. J. Clin. Pharmacol.* **46**, 35–39 (1994).
36. Lin, J.H., Chremos, A.N., Chiou, R., Yeh, K.C. & Williams, R. Comparative effect of famotidine and cimetidine on the pharmacokinetics of theophylline in normal volunteers. *Br. J. Clin. Pharmacol.* **24**, 669–672 (1987).
37. Colli, A. et al. Ticlopidine-theophylline interaction. *Clin. Pharmacol. Ther.* **41**, 358–362 (1987).
38. Rasmussen, B.B., Jeppesen, U., Gaist, D. & Brøsen, K. Griseofulvin and fluvoxamine interactions with the metabolism of theophylline. *Ther. Drug Monit.* **19**, 56–62 (1997).
39. Boyce, E.G. The effect of rifampin on theophylline pharmacokinetic parameters (following intravenous aminophylline) in normal volunteers. (1984).
40. Jeppesen, U., Loft, S., Poulsen, H.E. & Brøsen, K. A fluvoxamine-caffeine interaction study. *Pharmacogenetics* **6**, 213–222 (1996).
41. Lam, Y.W.F., Alfaro, C.L., Ereshefsky, L. & Miller, M. Pharmacokinetic and pharmacodynamic interactions of oral midazolam with ketoconazole, fluoxetine, fluvoxamine, and nefazodone. *J. Clin. Pharmacol.* **43**, 1274–1282 (2003).
42. Guest, E.J., Aarons, L., Houston, J.B., Rostami-Hodjegan, A. & Galetin, A. Critique of the two-fold measure of prediction success for ratios: application for the assessment of drug-drug interactions. *Drug Metab. Dispos.* **39**, 170–173 (2011).
43. Orlando, R., et al. Liver dysfunction markedly decreases the inhibition of cytochrome P450 1A2-mediated theophylline metabolism by fluvoxamine. *Clin. Pharmacol. Ther.* **79**, 489–499 (2006).
44. Powell-Jackson, P.R., Jamieson, A.P., Gray, B.J., Moxham, J. & Williams, R. Effect of rifampicin administration on theophylline pharmacokinetics in humans. *Am. Rev. Respir. Dis.* **131**, 939–940 (1985).
45. Culm-Merdek, K.E., von Moltke, L.L., Hartz, J.S. & Greenblatt, D.J. Fluvoxamine impairs single-dose caffeine clearance without altering caffeine pharmacodynamics. *Br. J. Clin. Pharmacol.* **60**, 486–493 (2005).

© 2019 The Authors *CPT: Pharmacometrics & Systems Pharmacology* published by Wiley Periodicals, Inc. on behalf of the American Society for Clinical Pharmacology and Therapeutics. This is an open access article under the terms of the Creative Commons Attribution-NonCommercial License, which permits use, distribution and reproduction in any medium, provided the original work is properly cited and is not used for commercial purposes.

PBPK models for CYP1A2 DDI prediction: a modelling network of fluvoxamine, theophylline, caffeine, rifampicin and midazolam

Supplement S1

Hannah Britz¹, Nina Hanke¹, Anke-Katrin Volz¹, Olav Spigset^{2,3}, Matthias Schwab^{4,5,6}, Thomas Eissing⁷, Thomas Wendl⁷, Sebastian Frechen⁷ and Thorsten Lehr¹

¹ Clinical Pharmacy, Saarland University, Saarbrücken, Germany

² Department of Clinical and Molecular Medicine, Norwegian University of Science and Technology, Trondheim, Norway

³ Department of Clinical Pharmacology, St. Olav University Hospital, Trondheim, Norway

⁴ Dr. Margarete Fischer-Bosch-Institute of Clinical Pharmacology, Stuttgart, Germany

⁵ Department of Clinical Pharmacology, University Hospital Tübingen, Tübingen, Germany

⁶ Department of Pharmacy and Biochemistry, University Tübingen, Tübingen, Germany

⁷ Clinical Pharmacometrics, Bayer AG, Leverkusen, Germany

Corresponding Author:

Thorsten Lehr, thorsten.lehr@mx.uni-saarland.de

Clinical Pharmacy, Saarland University, Campus C2 2, 66123 Saarbrücken

Phone: +49 681 302 70255; Fax: +49 681 302 70258

Table of contents

1	Mathematical implementation of drug-drug interactions	1-3
1.1	DDI modelling: Mixed inhibition.....	1-3
1.2	DDI modelling: Competitive inhibition	1-3
1.3	DDI modelling: Induction.....	1-3
2	PBPK model development	2-5
2.1	PBPK model development - general.....	2-5
2.2	Fluvoxamine model development.....	2-6
2.3	Theophylline model development	2-20
2.4	Caffeine model development.....	2-38
2.5	Rifampicin model development	2-40
2.6	Midazolam model development	2-42
2.7	System-dependent parameters.....	2-44
3	DDI prediction	3-45
3.1	DDI modelling - general	3-45
3.2	Fluvoxamine-theophylline DDI	3-46
3.3	Rifampicin-theophylline DDI.....	3-50
3.4	Fluvoxamine-caffeine DDI	3-54
3.5	Fluvoxamine-midazolam DDI.....	3-58
4	Population pharmacokinetic modelling of fluvoxamine.....	4-62
4.1	Objectives	4-62
4.2	Methods.....	4-62
4.3	Results.....	4-63
5	References	5-68

1 Mathematical implementation of drug-drug interactions

1.1 DDI modelling: Mixed inhibition

In the case of mixed inhibition, the inhibitor can bind reversibly to the enzyme in a competitive manner or to the enzyme-substrate complex in an uncompetitive manner. Substrate and inhibitor have different binding sites on the enzyme. Equations (1) and (2) describe the changes in Michaelis-Menten constant (K_M) and maximal reaction velocity (V_{max}) in the presence of a mixed inhibitor:

$$K_{M,app} = K_M * \frac{1 + \frac{[I]}{K_{Ic}}}{1 + \frac{[I]}{K_{Iu}}} \quad (1)$$

$$V_{max,app} = \frac{V_{max}}{1 + \frac{[I]}{K_{Iu}}} \quad (2)$$

with $K_{M,app}$ = apparent Michaelis-Menten constant in the presence of a mixed inhibitor, K_M = Michaelis-Menten constant, $[I]$ = inhibitor concentration, K_{Ic} = dissociation constant of the competitive inhibitor-enzyme complex, K_{Iu} = dissociation constant of the uncompetitive inhibitor-(enzyme-substrate) complex, $V_{max,app}$ = apparent maximum reaction velocity in the presence of a mixed inhibitor, V_{max} = maximum reaction velocity.

1.2 DDI modelling: Competitive inhibition

In the case of competitive inhibition, the inhibitor binds reversibly to the enzyme. Substrate and inhibitor compete for free enzyme and the inhibitor can be replaced by high substrate concentrations. The apparent maximum reaction velocity remains constant and Equation (3) describes the increase in K_M for the substrate in the presence of a competitive inhibitor:

$$K_{M,app} = K_M * \left(1 + \frac{[I]}{K_i}\right) \quad (3)$$

with $K_{M,app}$ = Michaelis-Menten constant in the presence of inhibitor, K_M = Michaelis-Menten constant in the absence of inhibitor, $[I]$ = free inhibitor concentration, K_i = dissociation constant of the inhibitor-enzyme complex.

1.3 DDI modelling: Induction

In the case of enzymes or transporters induction, the protein synthesis rate (R_{syn}) in enzyme turnover equation is replaced by the apparent protein synthesis rate in the presence of an inducer ($R_{syn,app}$), described by Equations (4) and (5):

$$\frac{d[E]}{dt} = R_{syn,app} - k_{deg} * [E] \quad (4)$$

$$R_{\text{syn,app}} = R_{\text{syn}} * \left(1 + \frac{E_{\text{max}} * [I]}{EC_{50} + [I]} \right) \quad (5)$$

with $d[E]/dt$ = enzyme or transporter turnover, $R_{\text{syn,app}}$ = rate of enzyme or transporter synthesis in the presence of an inducer, k_{deg} = degradation rate constant, $[E]$ = enzyme or transporter concentration, R_{syn} = rate of enzyme or transporter synthesis in the absence of inducer, E_{max} = maximal induction effect in vivo, $[I]$ = free inducer concentration, EC_{50} = concentration for half-maximal induction in vivo.

2 PBPK model development

2.1 PBPK model development - general

Physiologically-based pharmacokinetic (PBPK) models of the cytochrome P450 (CYP) 1A2 perpetrator drug **fluvoxamine** and of the CYP1A2 substrate **theophylline** were developed with clinical data of healthy subjects, covering the full dosing range of reported studies for intravenous as well as oral administration. Previously developed models of the CYP1A2 substrate **caffeine**, the CYP1A2 inducer **rifampicin** and the CYP3A4 substrate **midazolam** (a fluvoxamine victim drug) were used to build a CYP1A2 DDI network.

The following sections on fluvoxamine (Section 2.2) and theophylline (Section 2.3) model development present figures showing plasma concentration-time profiles of population predictions compared to observed data for all available studies in linear and semilogarithmic plots (Figures S1a, S1b, S1d, S1e, S2a and S2b), goodness of fit plots to compare predicted to observed plasma concentration values (Figures S1c and S2c), figures showing predicted compared to observed area under the plasma concentration-time curve (AUC) and peak plasma concentration (C_{max}) values (Figures S1f and S2d), and bar graphs illustrating sensitivity analysis results (Figures S1g and S2e). They also contain study tables with details on the clinical studies used for model development (Tables S1a and S2a), PBPK model parameter tables with drug-dependent parameters of the final models (Tables S1b and S2b), tables of mean relative deviation (MRD) values for all observed plasma concentrations obtained from clinical studies (Tables S1c and S2c) and tables listing predicted and observed AUC and C_{max} values together with calculated geometric mean fold error (GMFE) (Tables S1d and S2d).

Sections 2.4, 2.5 and 2.6 summarize the drug-dependent parameters of previously developed caffeine, rifampicin and midazolam PBPK models that were applied for DDI prediction in this study (Tables S3, S4 and S5) ^{1,2}.

System-dependent parameters, such as reference concentrations (concentration in the tissue with the highest expression) and tissue expression profiles of metabolizing enzymes and transporters, are listed in Table S6.

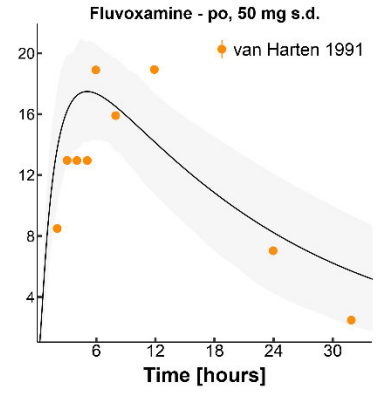
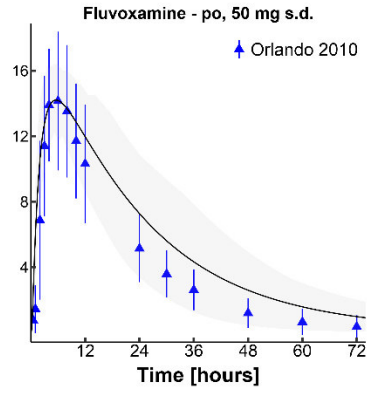
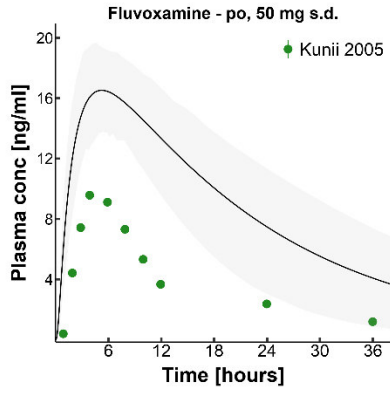
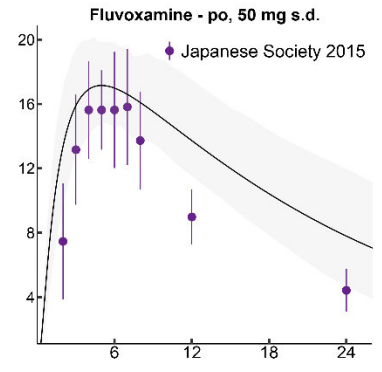
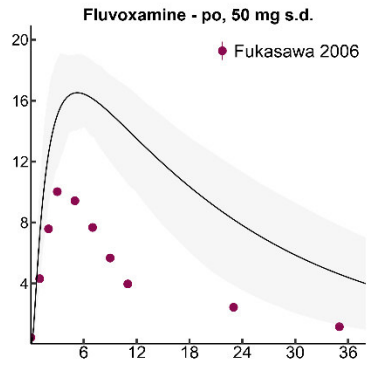
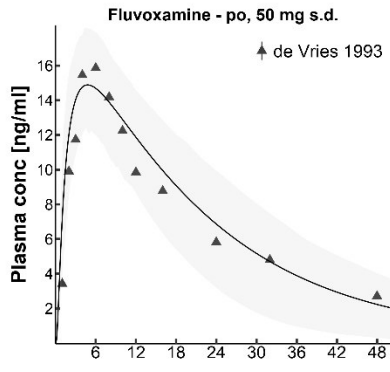
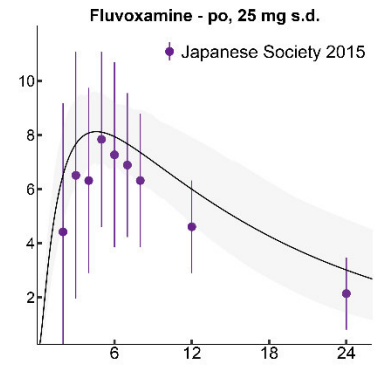
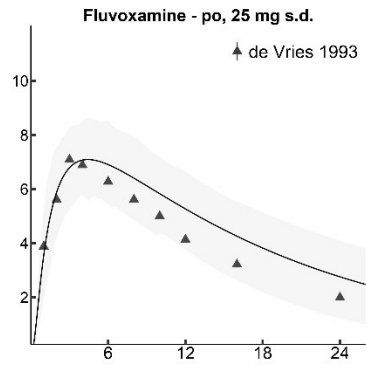
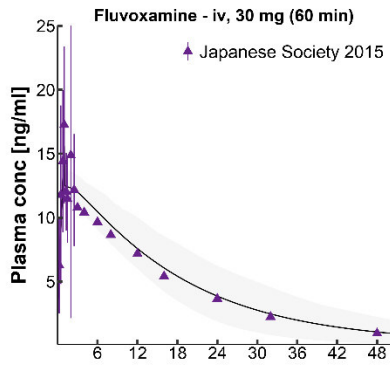
2.2 Fluvoxamine model development

Fluvoxamine is a selective serotonin reuptake inhibitor used to treat major depression and obsessive compulsive disorder^{3,4}. Recommended doses are 50 to 300 mg once daily. The pharmacokinetics of orally administered single doses are linear. Following multiple oral administration, the pharmacokinetics at steady-state become non-linear, due to saturable Michaelis-Menten kinetics of the metabolic pathways⁵. Metabolism of fluvoxamine includes hydroxylation via CYP1A2 and O-demethylation via the very polymorphic CYP2D6^{6,7}. Following oral administration fluvoxamine is excreted via the urine as metabolites⁸. The U.S. Food and Drug Administration (FDA) recommends fluvoxamine as strong clinical CYP1A2 and CYP2C19 inhibitor to evaluate the impact of CYP1A2/CYP2C19 inhibition on CYP1A2/CYP2C19 substrates⁹. Furthermore, the FDA lists fluvoxamine as moderate CYP3A4 inhibitor.

The fluvoxamine PBPK model was developed using 26 different clinical studies with pharmacokinetic (PK) blood sampling. These studies include 1 study of 30 mg fluvoxamine administered intravenously (iv) as a single-dose, and 25 studies of fluvoxamine administered orally (po) in single- or multiple-doses. In the single-dose (s.d.) po studies fluvoxamine was administered in doses of 25 - 200 mg. In the multiple-dose po studies fluvoxamine was administered once (q.d.) or twice daily (b.i.d.), in doses of 10 - 150 mg per administration. Details on dosing regimens, patient demographics and literature references of these studies are listed in Table S1a. The final fluvoxamine PBPK model applies metabolism by CYP1A2, CYP2D6 and glomerular filtration. Drug-dependent parameters are summarized in Table S1b. System-dependent parameters are given in Table S6.

The good descriptive and predictive performance of the final fluvoxamine PBPK model is demonstrated in linear (Figure S1a) as well as semilogarithmic plots (Figure S1b) of population predicted compared to observed plasma concentration-time profiles of all clinical studies. Figure S1c shows predicted versus observed plasma concentration values in a goodness of fit plot. Linear and semilogarithmic plots of population predicted compared to observed plasma concentration-time profiles of CYP2D6 extensive (EMs) and poor metabolizers (PMs) are presented in Figure S1d. Population predicted compared to observed plasma concentration-time profiles of non-smokers and smokers are illustrated in Figure S1e. Calculated MRD values are presented in Table S1c. Furthermore, predicted and observed AUC and C_{max} values of fluvoxamine with calculated GMFEs are presented in Table S1d and Figure S1f.

Sensitivity analysis results of a simulation of 300 mg fluvoxamine po q.d. are illustrated in Figure S1g. The fluvoxamine model is sensitive to the values of lipophilicity (optimized), CYP2D6 catalytic rate constant (optimized), CYP2D6 Michaelis-Menten constant (literature value) and fraction unbound (literature value).



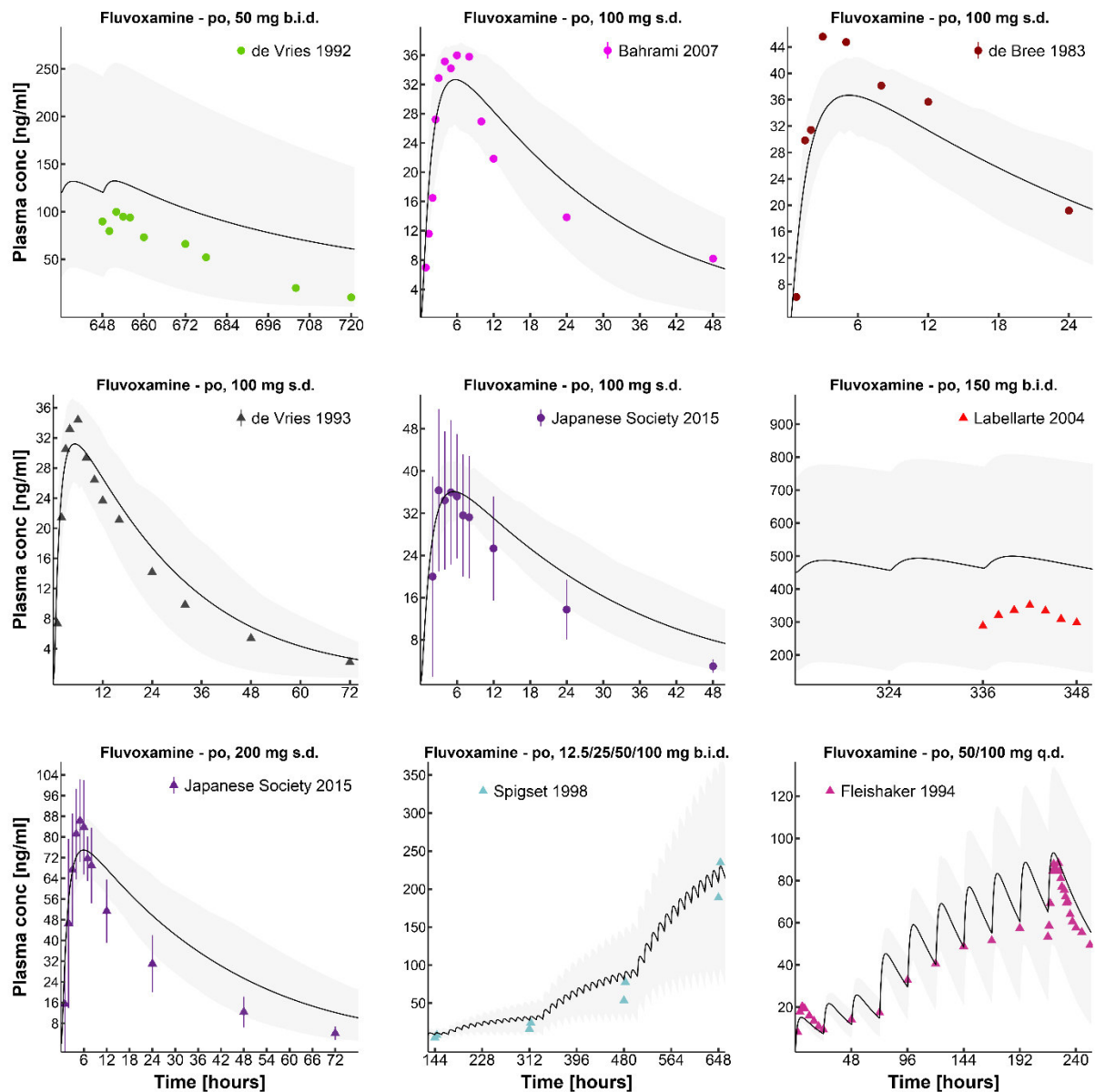
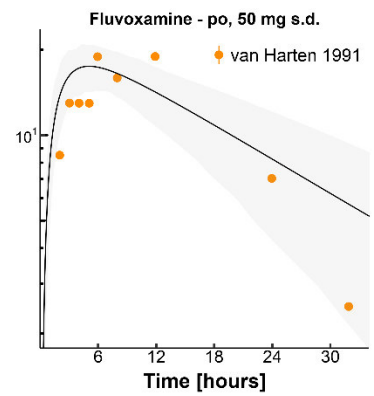
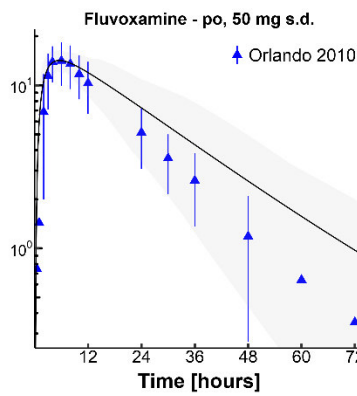
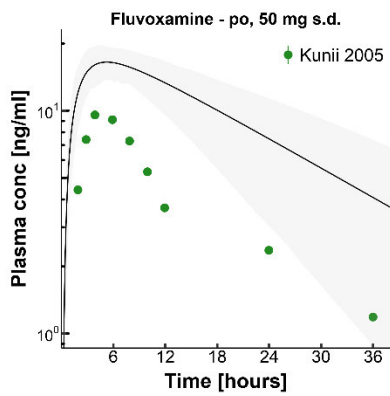
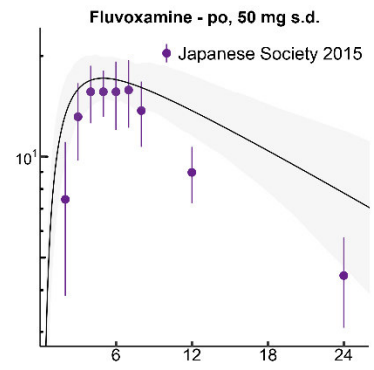
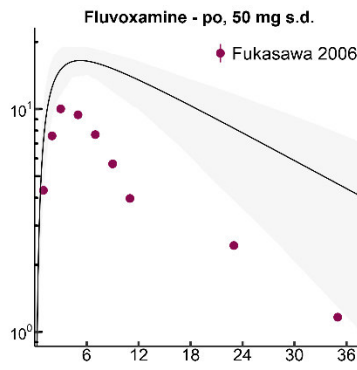
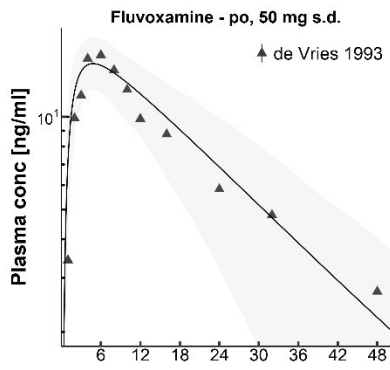
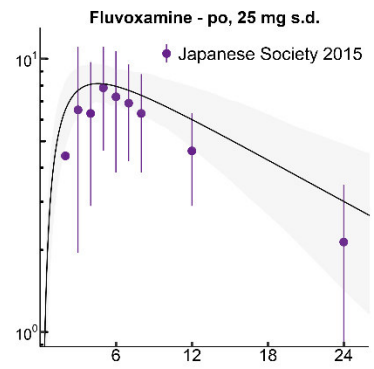
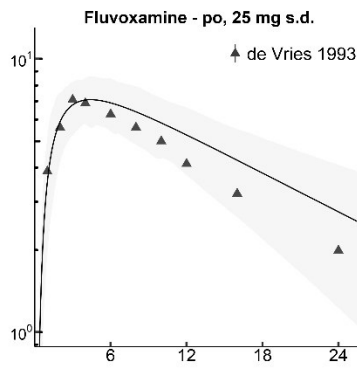
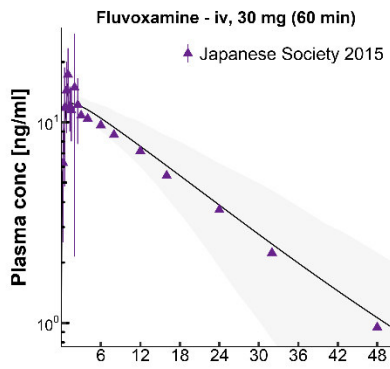


Figure S1a. Fluvoxamine (iv, po) linear. Population predictions of fluvoxamine plasma concentration-time profiles compared to observed data. Observed data are shown as triangles (training dataset) or dots (test dataset) \pm SD. Population simulation arithmetic means are shown as lines; the shaded areas illustrate the 68% population prediction intervals. Details on dosing regimens, study populations and literature references are listed in Table S1a. Predicted and observed PK parameters are summarized in Table S1d.



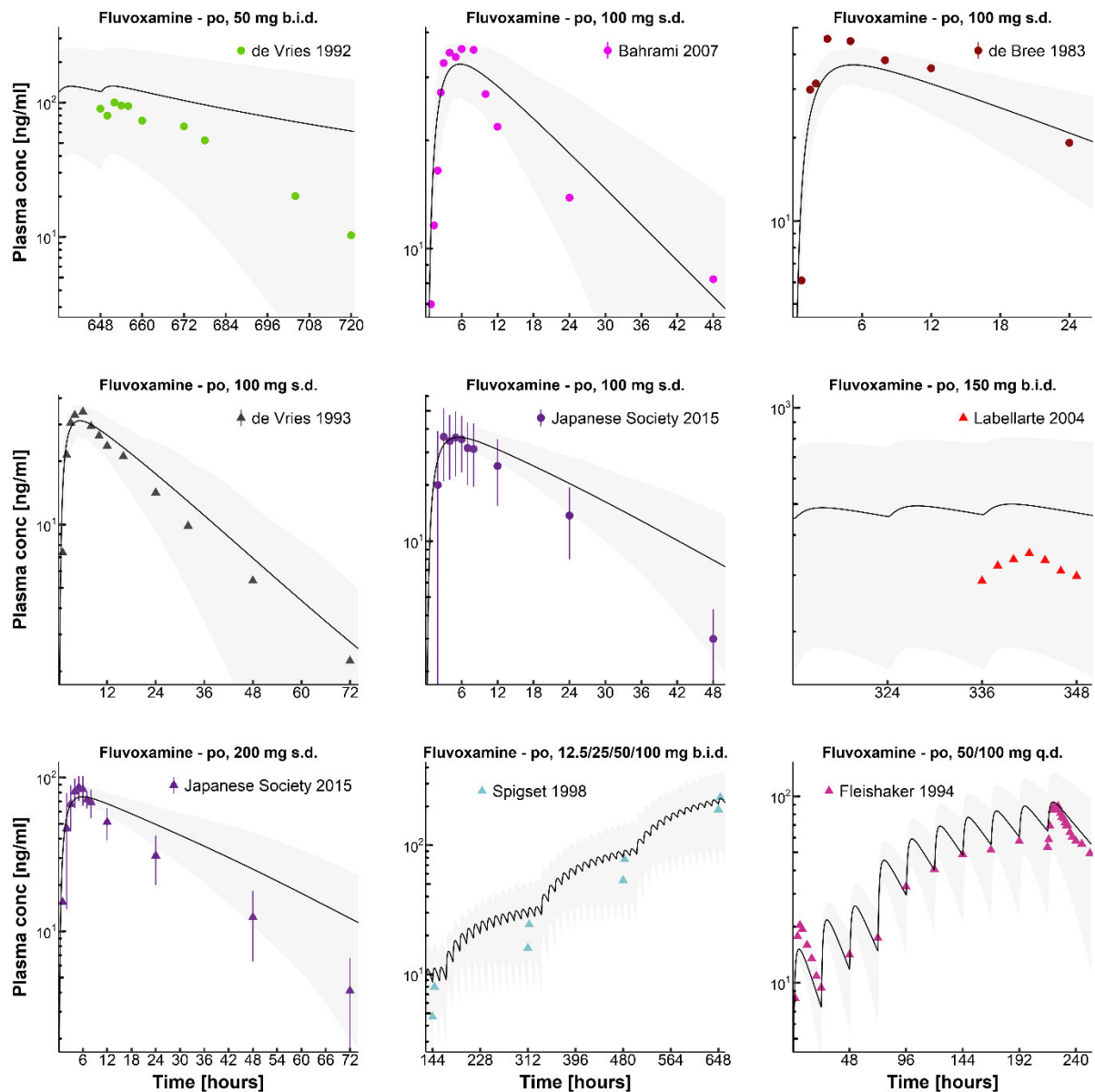


Figure S1b. Fluvoxamine (iv, po) semilogarithmic. Population predictions of fluvoxamine plasma concentration-time profiles compared to observed data. Observed data are shown as triangles (training dataset) or dots (test dataset) \pm SD. Population simulation arithmetic means are shown as lines; the shaded areas illustrate the 68% population prediction intervals. Details on dosing regimens, study populations and literature references are listed in Table S1a. Predicted and observed PK parameters are summarized in Table S1d.

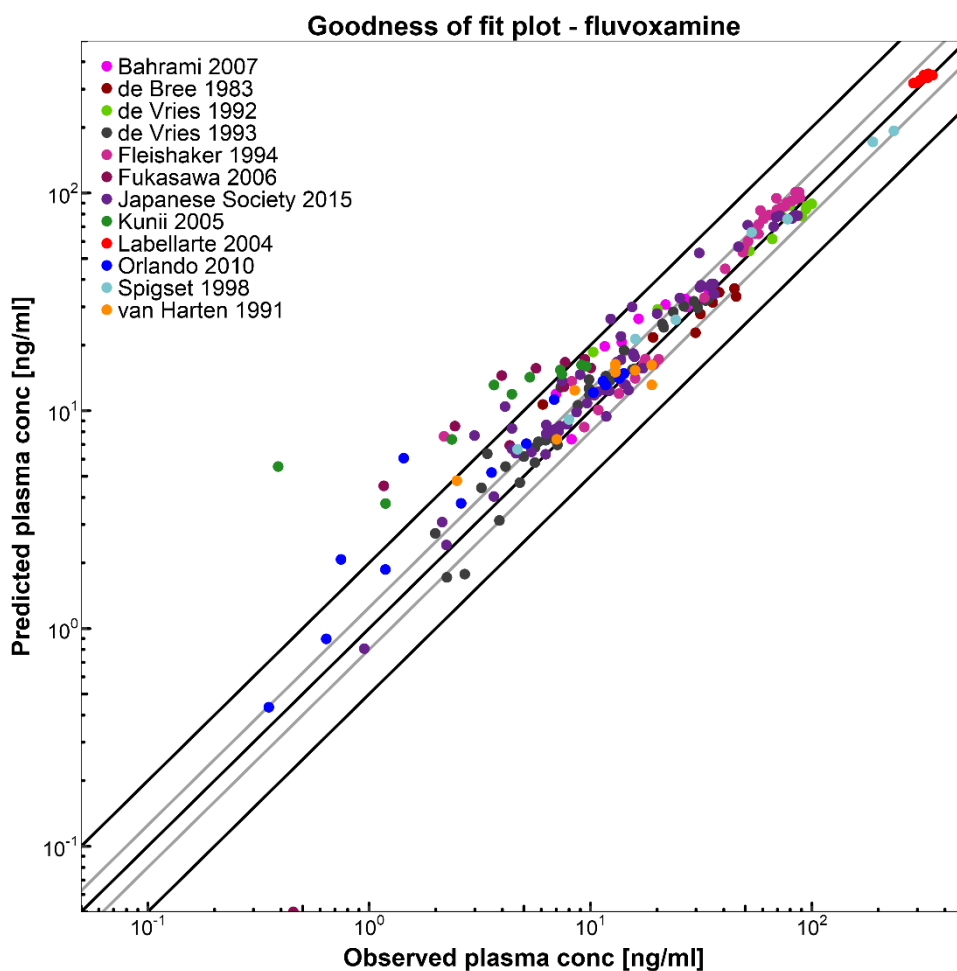


Figure S1c. Goodness of fit plot. Predicted compared to observed fluvoxamine plasma concentration values of all clinical studies. Line of identity and 0.5- to 2.0-fold acceptance limits are shown as black lines. The 0.8- to 1.25-fold limits are shown as grey lines. Details on dosing regimens, study populations and literature references are listed in Table S1a. Predicted and observed PK parameters are summarized in Table S1d.

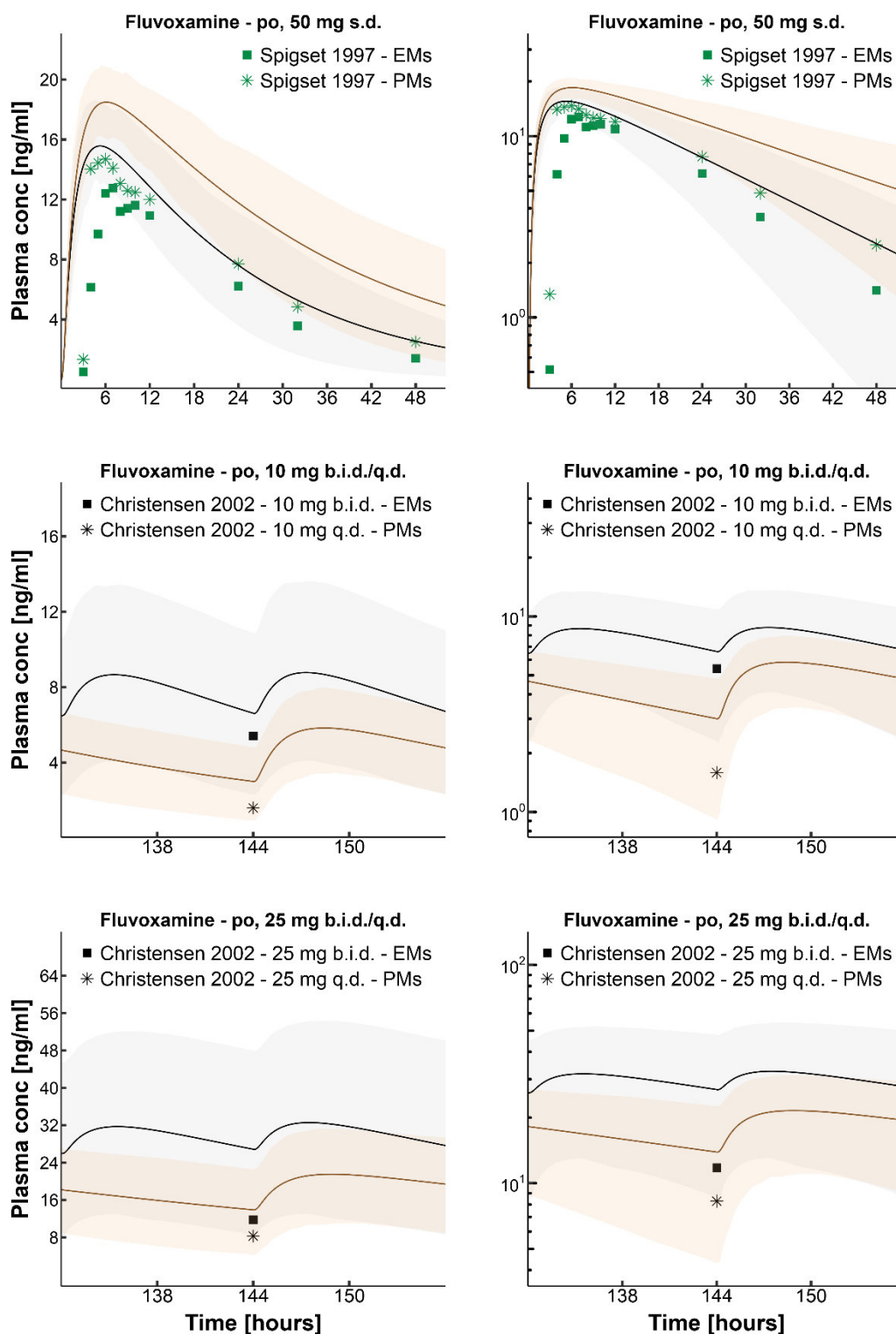


Figure S1d. Fluvoxamine (po) in CYP2D6 extensive and poor metabolizers. Population predictions of fluvoxamine plasma concentration-time profiles in CYP2D6 extensive (EMs) and poor metabolizers (PMs) compared to observed data in linear (left panel) and semilogarithmic (right panel) plots. Observed data are shown as squares (EMs) or asterisks (PMs). Population simulation arithmetic means are shown as black (EMs) or brown (PMs) lines; the shaded areas illustrate the respective 68% population prediction intervals. Details on dosing regimens, study populations and literature references are listed in Table S1a. Predicted and observed PK parameters are summarized in Table S1d.

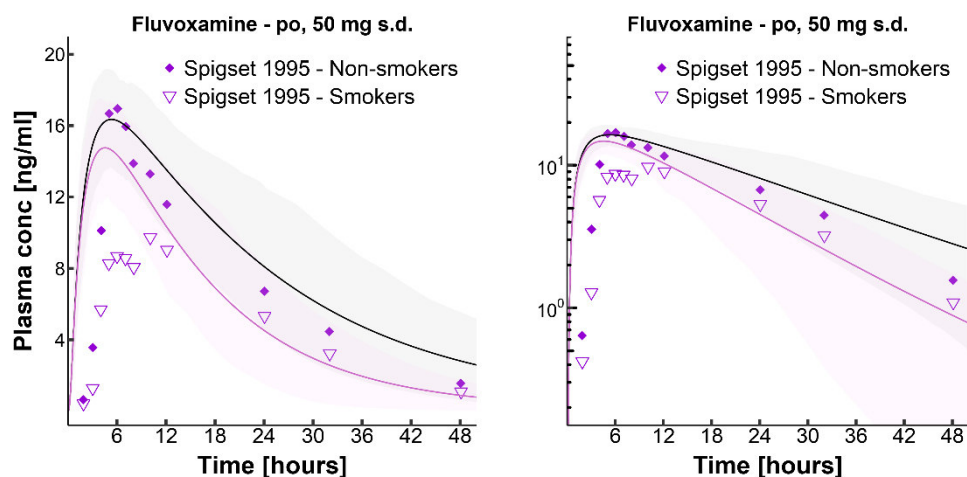


Figure S1e. Fluvoxamine (po) in non-smokers and smokers. Population predictions of fluvoxamine plasma concentration-time profiles in non-smokers and smokers compared to observed data in linear (left panel) and semilogarithmic (right panel) plots. Observed data are shown as diamonds (non-smokers) or open triangles (smokers). Population simulation arithmetic means are shown as dark grey (non-smokers) or violet (smokers) lines; the shaded areas illustrate the 68% population prediction intervals. Details on dosing regimens, study populations and literature references are listed in Table S1a. Predicted and observed PK parameters are summarized in Table S1d.

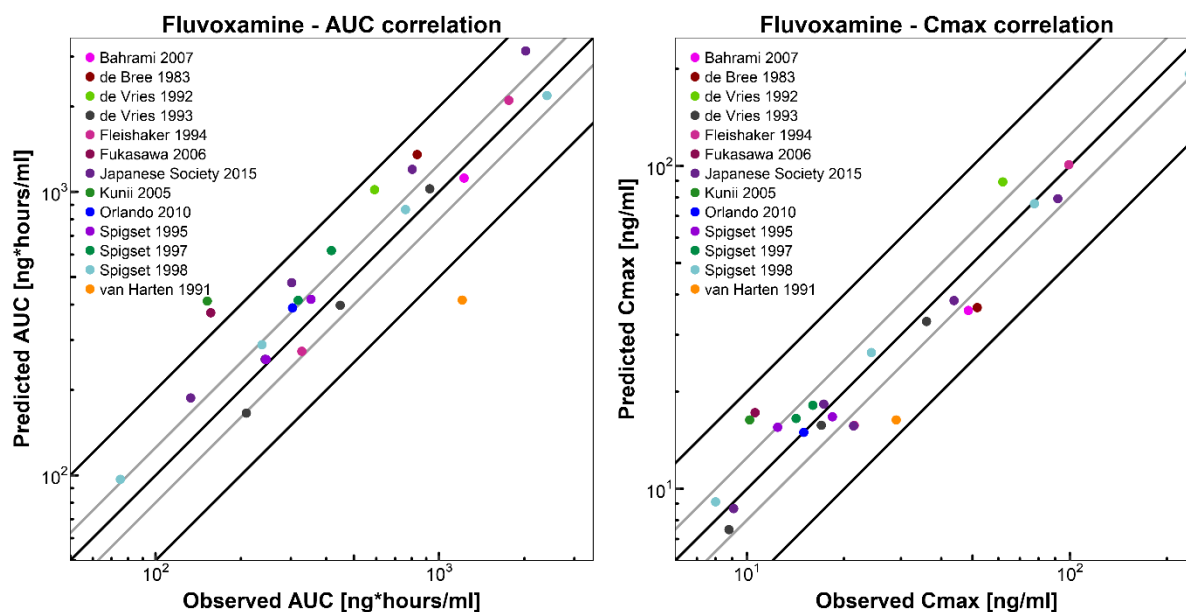


Figure S1f. Predicted compared to observed AUC and C_{max} values. Predicted compared to observed fluvoxamine AUC values (left) and C_{max} values (right) of all clinical studies. Line of identity and 0.5- to 2.0-fold acceptance limits are shown as black lines. The 0.8- to 1.25-fold limits are shown as grey lines. Details on dosing regimens, study populations and literature references are listed in Table S1a. Predicted and observed PK parameters are summarized in Table S1d.

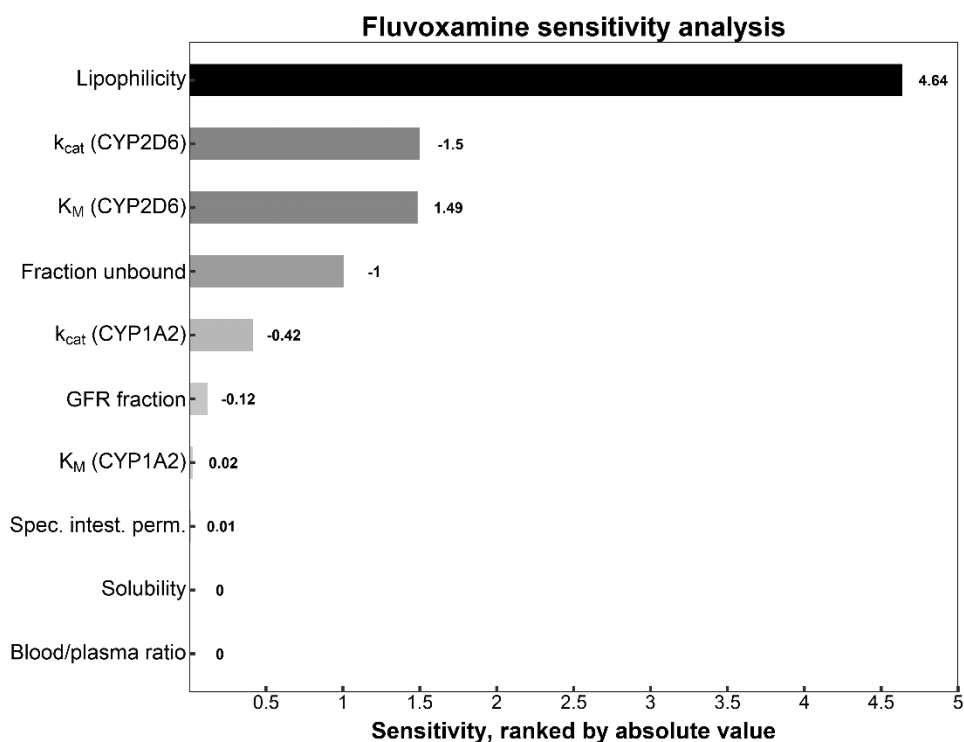


Figure S1g. Fluvoxamine model sensitivity analysis. Sensitivity of the model to single parameters, measured as change of the simulated AUC under steady-state conditions of a 300 mg po q.d. fluvoxamine regimen. A sensitivity value of + 1.0 signifies that a 10% increase of the examined parameter causes a 10% increase of the simulated AUC. CYP1A2, cytochrome P450 1A2; CYP2D6, cytochrome P450 2D6; GFR, glomerular filtration rate; k_{cat} , catalytic rate constant; K_M , Michaelis-Menten constant; Spec. intest. perm., specific intestinal permeability.

Table S1a. Clinical studies used for fluvoxamine model development

Dose [mg]	Route	n	Age [years]	Weight [kg]	Females [%]	CYP2D6 phenotype [%]	Smokers [%]	Dataset	Reference
30	iv (60 min), s.d.	17	-	-	-	-	-	training	Japanese Society 2015 ¹⁰
10	po (caps), b.i.d.	7	30 (22-45)	56-94	-	EM	0	test	Christensen 2002 ¹¹
10	po (caps), q.d.	5	30 (22-45)	56-94	-	PM	0	test	Christensen 2002 ¹¹
25	po (sol), s.d.	12	30 (22-41)	73 (54-86)	0	-	-	training	de Vries 1993 ¹²
25	po (tab), s.d.	6	-	-	-	-	-	test	Japanese Society 2015 ¹⁰
25	po (caps), b.i.d.	7	30 (22-45)	56-94	-	EM	0	test	Christensen 2002 ¹¹
25	po (caps), q.d.	5	30 (22-45)	56-94	-	PM	0	test	Christensen 2002 ¹¹
50	po (sol), s.d.	12	30 (22-41)	73 (54-86)	0	-	-	training	de Vries 1993 ¹²
50	po (tab), s.d.	12	30 ± 5	68 ± 8	0	EM	50	test	Fukasawa 2006 ¹³
50	po (tab), s.d.	6	-	-	-	-	-	test	Japanese Society 2015 ¹⁰
50	po (tab), s.d.	10	30 (25-36)	69 (56-83)	0	EM	50	test	Kunii 2005 ¹⁴
50	po (tab), s.d.	10	35 ± 7	79 ± 10	0	-	-	training	Orlando 2010 ¹⁵
50	po (tab), s.d.	12	35 (21-49)	67 (51-86)	42	EM	0	test	Spigset 1995 ¹⁶
50	po (tab), s.d.	12	39 (24-51)	66 (55-95)	42	EM	100	test	Spigset 1995 ¹⁶
50	po (tab), s.d.	10	29 (22-45)	69 (61-85)	30	EM	0	test	Spigset 1997 ¹⁷
50	po (tab), s.d.	5	24 (22-26)	73 (55-86)	0	PM	0	test	Spigset 1997 ¹⁷
50	po (tab), s.d.	12	18-30	55-91	34	-	-	test	van Harten 1991 ¹⁸
50	po (tab), b.i.d.	6	25-31	53-80	50	-	-	test	de Vries 1992 ¹²
100	po (tab), s.d.	24	27 ± 3	68 ± 8	0	-	-	test	Bahrami 2007 ¹⁹
100	po (caps), s.d.	10	22 (20-25)	71 (56-81)	10	-	-	test	de Bree 1983 ⁸
100	po (sol), s.d.	12	30 (22-41)	73 (54-86)	0	-	-	training	de Vries 1993 ¹²
100	po (tab), s.d.	6	-	-	-	-	-	test	Japanese Society 2015 ¹⁰
150	po (-), b.i.d.	16	-	-	-	EM	-	training	Labellarte 2004 ²⁰
200	po (tab), s.d.	6	-	-	-	-	-	training	Japanese Society 2015 ¹⁰
12.5/25/50/100	po (tab), b.i.d.	10	29 ± 5	86 ± 8	-	EM: 80, PM: 20	0	training	Spigset 1998 ⁵
50/100	po (tab), q.d.	60	20-44	59-100	0	-	50	training	Fleishaker 1994 ²¹

caps, capsule; CYP2D6, cytochrome P450 2D6; EM, extensive metabolizers; iv, intravenous; n, number of individuals studied; PM, poor metabolizers; po, oral; Route, route of administration; sol, solution; tab, tablet; test, test dataset (model evaluation); training, training dataset (parameter optimization); -, no data available. Values are means ± standard deviation or ranges.

Table S1b. Drug-dependent parameters of the final fluvoxamine PBPK model

Parameter	Unit	Fluvoxamine model	Literature values	Source	Reference	Description
MW	g/mol	318.34	318.34	lit.	^a	Molecular weight
pKa		9.40 (base)	9.40 (base)	lit.	²²	Acid dissociation constant
Solubility (pH)	mg/ml	14.66 (7.0)	14.66 (7.0)	lit.	MSDS	Solubility
logP		3.57	2.80, 2.89, 3.20	opt.	^a	Lipophilicity
fu	%	23.00	23.00	lit.	²³	Fraction unbound
CYP1A2 K_M	nmol/l	7.35	-	opt.	-	Michaelis-Menten constant
CYP1A2 k_{cat} non-smokers	1/min	0.016	-	opt.	-	CYP1A2 catalytic rate constant for non-smokers
CYP1A2 k_{cat} smokers	1/min	0.022	-	opt.	-	CYP1A2 catalytic rate constant for smokers
CYP2D6 K_M	μ mol/l	76.30	76.30	lit.	⁶	Michaelis-Menten constant
CYP2D6 k_{cat} EMs	1/min	110.56	-	opt.	-	CYP2D6 catalytic rate constant for EMs
CYP2D6 k_{cat} PMs	1/min	0	0	lit.	²⁴	CYP2D6 catalytic rate constant for PMs
GFR fraction		1	-	asm.	-	Fraction of filtered drug reaching the urine
EHC continuous fraction		1	-	asm.	-	Fraction of bile continually released from the gallbladder
Competitive inhibition K_{ic} CYP1A2	nmol/l	10.00	10.00	lit.	^{25,26}	Concentration for half-maximal competitive inhibition
Uncompetitive inhibition K_{iu} CYP1A2	nmol/l	10.00	10.00	lit.	^{25,26}	Concentration for half-maximal uncompetitive inhibition
K_i CYP3A4	μ mol/l	1.60	1.60	lit.	^{26,27}	Concentration for half-maximal competitive inhibition
Formulation		solution	-	asm.	-	Formulation used in predictions
Cellular permeabilities		PK-Sim	-	calc.	²⁸	Permeation across cell membranes
Partition coefficients		Schmitt	-	calc.	²⁹	Organ-plasma partition coefficients
Specific intest. perm.	dm/min	2.74E-06	-	opt.	-	Normalized to surface area
Specific organ perm.	dm/min	2.90E-02	-	calc.	³⁰	Normalized to surface area

^a, <https://www.drugbank.ca/drugs/DB00176>, last view: 22 October 2018; asm., assumed; calc., calculated; CYP1A2, cytochrome P 450 1A2; CYP2D6, cytochrome P 450 2D6; EHC, enterohepatic circulation; EMs, extensive metabolizers; GFR, glomerular filtration rate; intest., intestinal; lit., literature; MSDS, material safety data sheet of fluvoxamine; opt., optimized; perm., permeability; PK-Sim, PK-Sim Standard calculation method; PMs, poor metabolizers; Schmitt, Schmitt calculation method; -, not available.

Table S1c. Mean relative deviation values of fluvoxamine plasma concentration predictions

Dose [mg]	Route	n	CYP2D6 phenotype [%]	Smokers [%]	MRD	Reference
30	iv (60 min), s.d.	17	-	-	1.13	Japanese Society 2015 ¹⁰
25	po (sol), s.d.	10	-	-	1.23	de Vries 1993 ¹²
25	po (tab), s.d.	6	-	-	1.31	Japanese Society 2015 ¹⁰
50	po (sol), s.d.	10	-	-	1.29	de Vries 1993 ¹²
50	po (tab), s.d.	5	EM	50	2.53	Fukasawa 2006 ¹³
50	po (tab), s.d.	12	-	-	1.44	Japanese Society 2015 ¹⁰
50	po (tab), s.d.	12	EM	50	3.39	Kunii 2005 ¹⁴
50	po (tab), s.d.	6	-	-	1.70	Orlando 2010 ¹⁵
50	po (tab), s.d.	10	-	-	1.36	van Harten 1991 ¹⁸
50	po (tab), b.i.d.	5	-	-	1.27	de Vries 1992 ¹²
100	po (tab), s.d.	12	-	-	1.34	Bahrami 2007 ¹⁹
100	po (caps), s.d.	6	-	-	1.31	de Bree 1983 ⁸
100	po (sol), s.d.	10	-	-	1.27	de Vries 1993 ¹²
100	po (tab), s.d.	60	-	-	1.45	Japanese Society 2015 ¹⁰
150	po (-), b.i.d.	24	EM	-	1.07	Labellarte 2004 ²⁰
200	po (tab), s.d.	10	-	-	1.56	Japanese Society 2015 ¹⁰
12.5/25/50/100	po (tab), b.i.d.	12	EM: 80, PM: 20	0	1.22	Spigset 1998 ⁵
50/100	po (tab), q.d.	6	-	50	1.32	Fleishaker 1994 ²¹
				MRD (range)	1.51 (1.07-3.39)	
				MRD < 2	16/18 studies	

caps, capsule; CYP2D6, cytochrome P450 2D6; EM, extensive metabolizers; iv, intravenous; MRD, mean relative deviation; n, number of individuals studied; PM, poor metabolizers; po, oral; Route, route of administration; sol, solution; tab, tablet; -, no data available.

Table S1d. Observed and predicted AUC and C_{max} values of fluvoxamine

Dose [mg]	Route	n	CYP2D6 phenotype [%]	Smokers [%]	AUC obs [ng*hours/ml]	AUC pred [ng*hours/ml]	Pred/Obs AUC	C _{max} obs [ng/ml]	C _{max} pred [ng/ml]	Pred/Obs C _{max}	Reference	
30	iv (60 min), s.d.	17	-	-	243.40	256.42	1.05	21.40	15.67	0.73	Japanese Society 2015 ¹⁰	
10	po (caps), b.i.d.	7	EM	0	-	-	-	-	-	-	Christensen 2002 ¹¹	
10	po (caps), q.d.	5	PM	0	-	-	-	-	-	-	Christensen 2002 ¹¹	
12.5	po (tab), b.i.d.	10	EM: 80, PM: 20	0	75.10 ^a	96.72 ^a	1.29	8.00	9.12	1.14	Spigset 1998 ⁵	
25	po (tab), s.d.	6	-	-	209.00	165.59	0.79	8.80	7.48	0.85	de Vries 1993 ¹²	
25	po (sol), s.d.	12	-	-	133.00	187.37	1.41	9.10	8.69	0.95	Japanese Society 2015 ¹⁰	
25	po (caps), b.i.d.	7	EM	0	-	-	-	-	-	-	Christensen 2002 ¹¹	
25	po (tab), b.i.d.	10	EM: 80, PM: 20	0	237.20 ^a	288.80 ^a	1.22	24.30	26.45	1.09	Spigset 1998 ⁵	
25	po (caps), q.d.	5	PM	0	-	-	-	-	-	-	Christensen 2002 ¹¹	
50	po (sol), s.d.	12	-	-	448.00	397.64	0.89	17.00	15.74	0.93	de Vries 1993 ¹²	
50	po (tab), s.d.	12	EM	50	156.50 ^b	374.40 ^b	2.39	10.60	17.23	1.63	Fukasawa 2006 ¹³	
50	po (tab), s.d.	6	-	-	302.00	477.88	1.58	17.30	18.30	1.06	Japanese Society 2015 ¹⁰	
50	po (tab), s.d.	10	EM	50	152.20	411.69	2.70	10.20	16.36	1.60	Kunii 2005 ¹⁴	
50	po (tab), s.d.	10	-	-	304.00	389.57	1.28	15.00	14.97	1.00	Orlando 2010 ¹⁵	
50	po (tab), s.d.	12	EM	0	353.36	417.62	1.18	18.40	16.73	0.91	Spigset 1995 ¹⁶	
50	po (tab), s.d.	12	EM	100	245.44	256.12	1.04	12.45	15.52	1.25	Spigset 1995 ¹⁶	
50	po (tab), s.d.	10	EM	0	318.30	414.24	1.30	14.20	16.53	1.16	Spigset 1997 ¹⁷	
50	po (tab), s.d.	5	PM	0	417.00	620.57	1.49	16.00	18.16	1.13	Spigset 1997 ¹⁷	
50	po (tab), s.d.	12	-	-	1207.00	415.01	0.34	29.00	16.36	0.56	van Harten 1991 ¹⁸	
50	po (tab), b.i.d.	6	-	-	592.00 ^a	1017.65 ^a	1.72	62.00	89.35	1.44	de Vries 1992 ¹²	
50	po (tab), b.i.d.	10	EM: 80, PM: 20	0	761.10 ^a	865.89 ^a	1.14	77.70	76.47	0.98	Spigset 1998 ⁵	
50	po (tab), q.d.	60	-	50	328.00 ^c	273.68 ^c	0.83	21.50	15.73	0.73	Fleishaker 1994 ²¹	
100	po (tab), s.d.	24	-	-	1224.90	1118.22	0.91	48.50	35.72	0.74	Bahrami 2007 ¹⁹	
100	po (caps), s.d.	10	-	-	837.00	1353.63	1.62	51.67	36.46	0.71	de Bree 1983 ⁸	
100	po (sol), s.d.	12	-	-	927.00	1024.87	1.11	36.00	33.02	0.92	de Vries 1993 ¹²	
100	po (tab), s.d.	6	-	-	804.00	1200.39	1.49	43.80	38.33	0.88	Japanese Society 2015 ¹⁰	
100	po (tab), b.i.d.	10	EM: 80, PM: 20	0	2401.80 ^a	2186.49 ^a	0.91	234.90	192.89	0.82	Spigset 1998 ⁵	
100	po (tab), q.d.	60	-	50	1762.00 ^c	2103.05 ^c	1.19	99.30	100.99	1.02	Fleishaker 1994 ²¹	
200	po (tab), s.d.	6	-	-	2020.00	3141.64	1.56	91.80	79.27	0.86	Japanese Society 2015 ¹⁰	
GMFE (range)							1.40 (1.04-2.91)	1.22 (1.00-1.77)		25/25 studies		
Pred/Obs within twofold							22/25 studies					

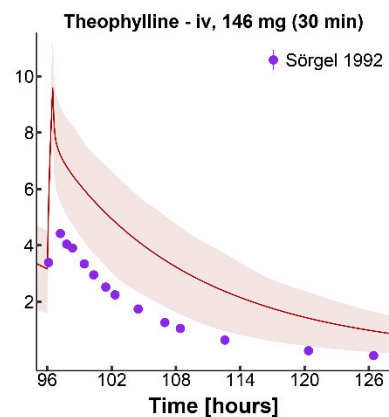
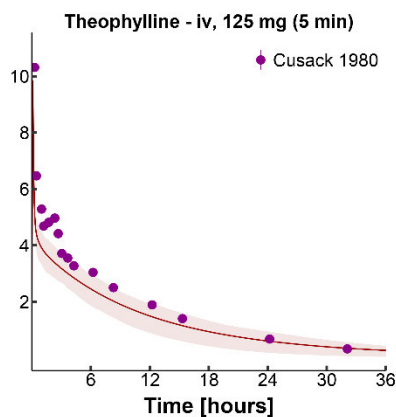
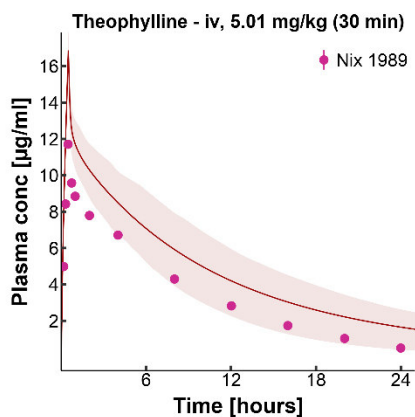
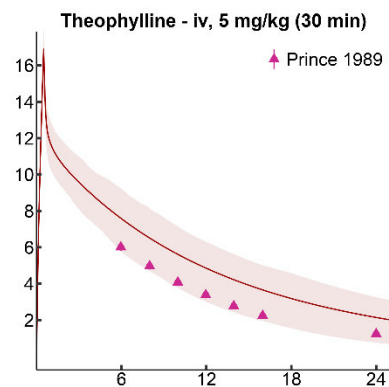
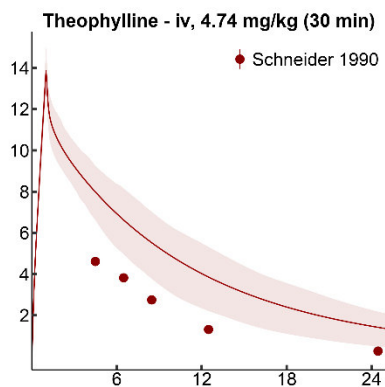
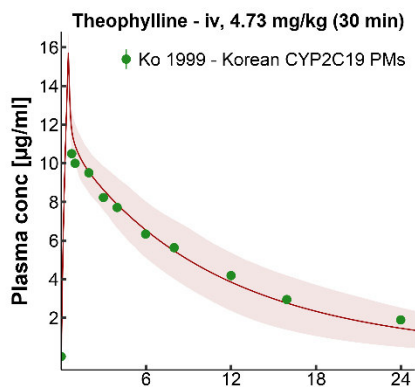
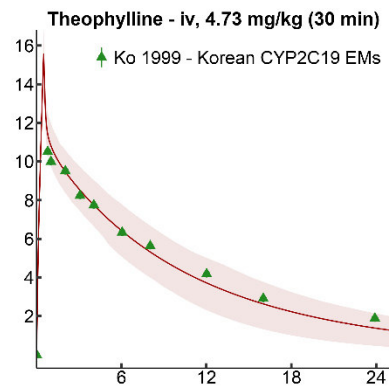
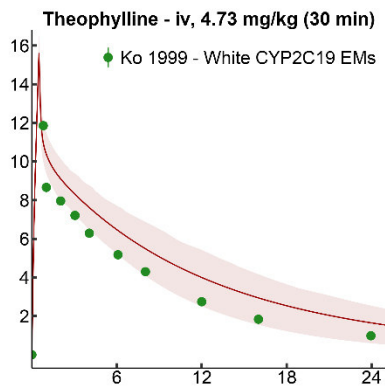
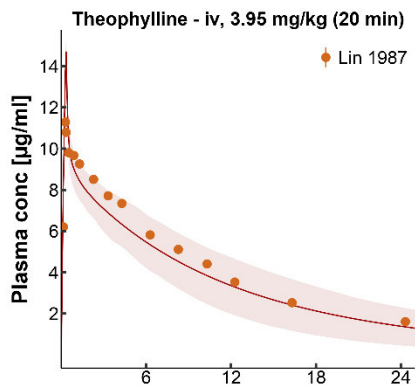
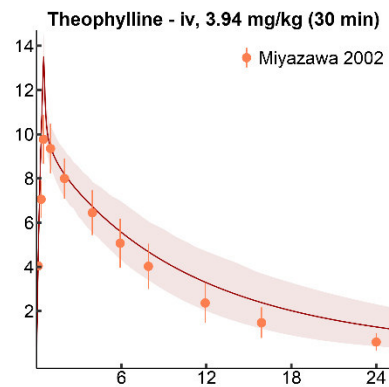
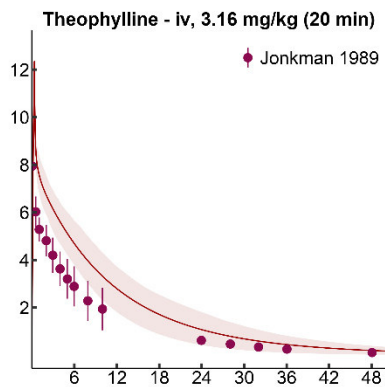
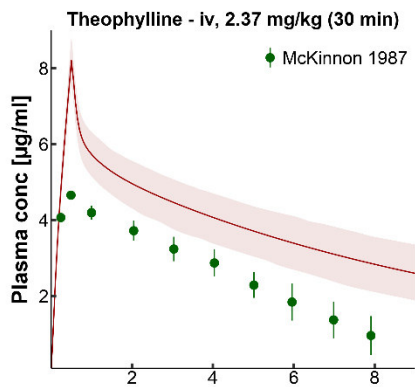
^a, AUC₀₋₁₂; ^b, AUC₀₋₃₆; ^c, AUC₀₋₂₄; AUC values are 0-∞ if not specified differently; AUC, area under the plasma concentration-time curve; caps, capsule; C_{max}, peak plasma concentration; CYP2D6, cytochrome P450 2D6; EM, extensive metabolizers; GMFE, geometric mean fold error; iv, intravenous; n, number of individuals studied; obs, observed; PM, poor metabolizers; po, oral; pred, predicted; Route, route of administration; sol, solution; tab, tablet; -, no data available.

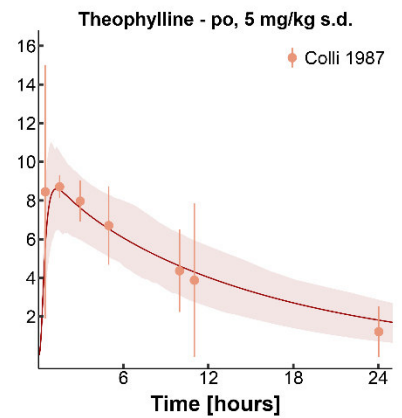
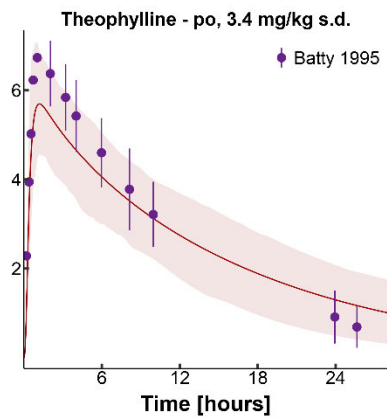
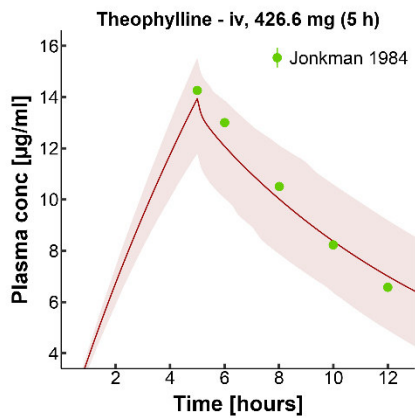
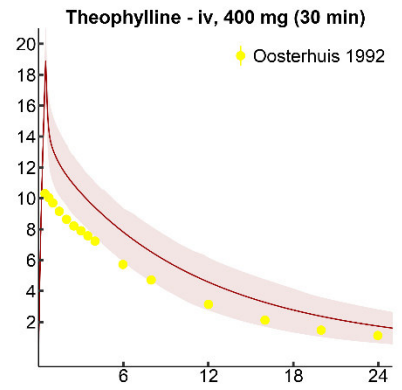
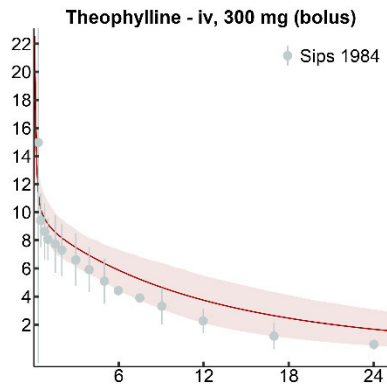
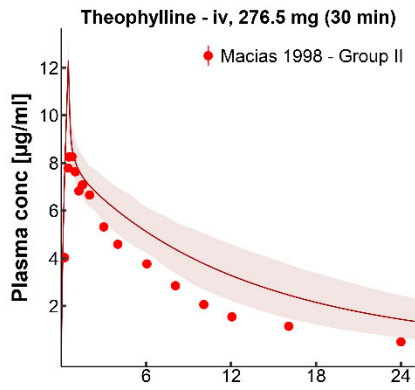
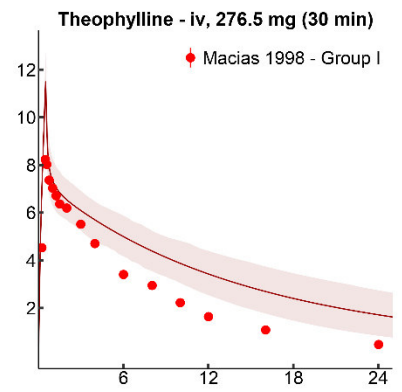
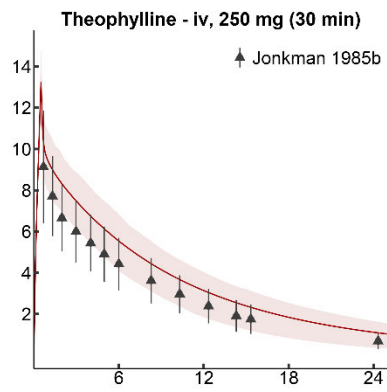
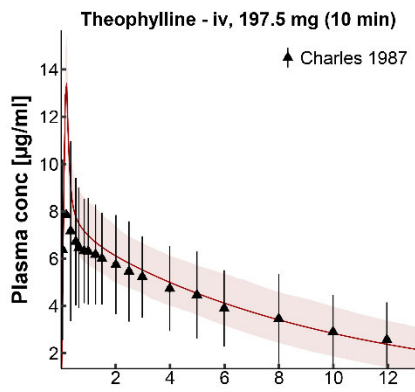
2.3 Theophylline model development

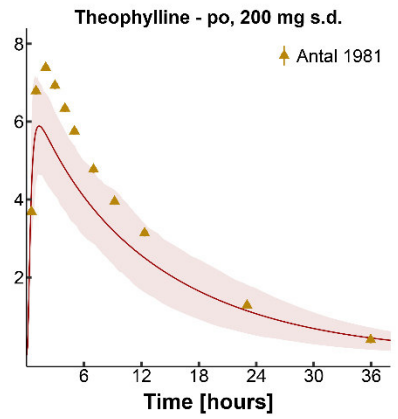
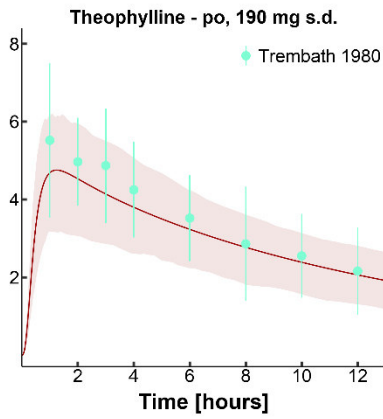
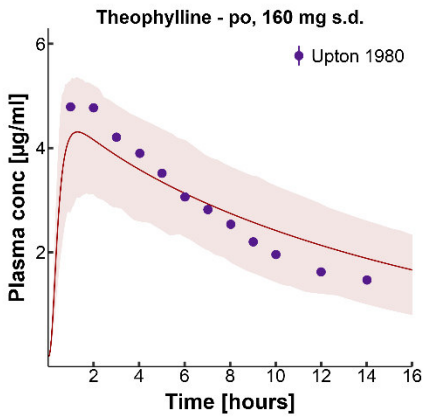
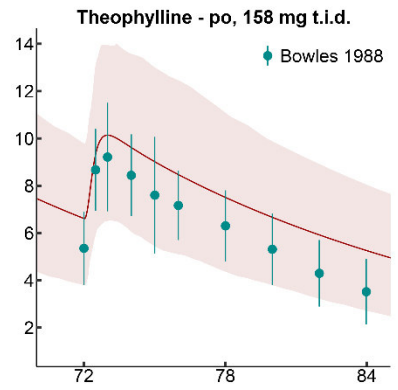
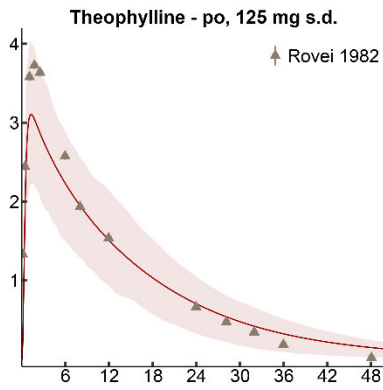
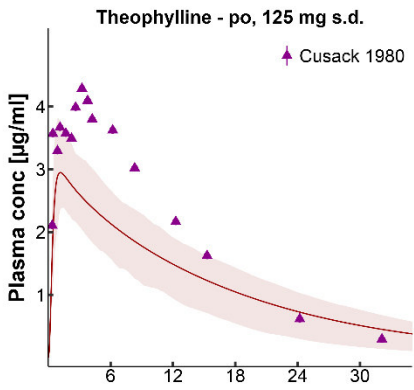
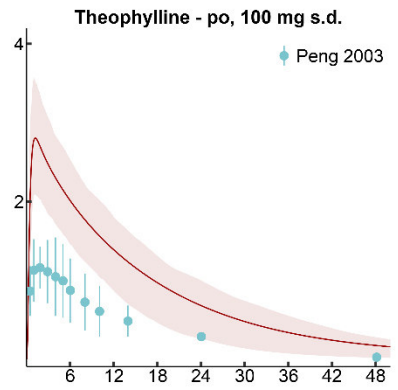
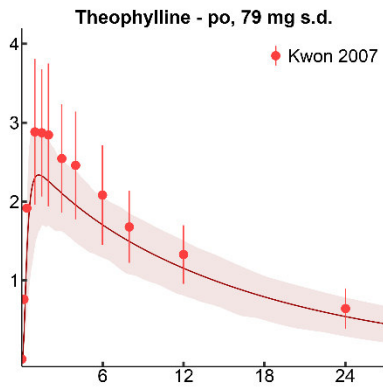
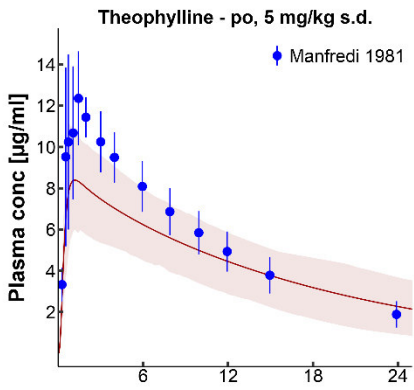
Theophylline is a methylxanthine and a therapeutic for the treatment of asthma and obstructive pulmonary disease³¹. Recommended doses are between 11 and 13 mg/kg body weight, to achieve theophylline plasma concentrations of 8 to 20 µg/ml³². Metabolism of theophylline includes 8-hydroxylation by CYP1A2 or CYP2E1 as well as demethylation by CYP1A2³³, resulting in a fraction metabolized via CYP1A2 of 0.7^{34,35}. About 95% of an administered theophylline dose are excreted with the urine, but only 14 - 17% as unchanged drug^{36,37}. The FDA lists theophylline as a sensitive clinical CYP1A2 substrate³⁸.

The theophylline PBPK model was developed using 40 different clinical studies with PK blood sampling. These studies include 19 studies of theophylline administered iv as a single-dose, and 21 studies of theophylline administered po in single- or multiple-doses. In the single-dose iv studies theophylline was administered in doses of 2.37 mg/kg - 426.6 mg. In the single-dose po studies theophylline was administered in doses of 3.1 mg/kg - 500 mg. In the multiple-dose po studies theophylline was administered three times daily (t.i.d.) in doses of 158 - 200 mg per administration. Analyzing all 40 studies used for PBPK model development, the pharmacokinetics of theophylline were found to be linear. In addition to plasma concentration-time profiles, the training dataset of the theophylline model included fraction excreted unchanged to urine measurements and CYP1A2 fraction metabolized information. Details on dosing regimens, patient demographics and literature references of these studies are listed in Table S2a. The final theophylline PBPK model applies metabolism by CYP1A2, CYP2E1 and glomerular filtration with reabsorption in the renal tubules. Due to the lack of valid in vitro data on renal reabsorption transporters for theophylline, the glomerular filtration rate fraction was optimized to describe the fraction of theophylline excreted unchanged to urine. Drug-dependent parameters are summarized in Table S2b. System-dependent parameters are given in Table S6.

The good descriptive and predictive performance of the final theophylline PBPK model is demonstrated in linear (Figure S2a) as well as semilogarithmic plots (Figure S2b) of population predicted compared to observed plasma concentration-time profiles of all clinical studies. Figure S2c shows predicted versus observed plasma concentration values in a goodness of fit plot. Calculated MRD values are presented in Table S2c. Furthermore, predicted and observed AUC and C_{max} values of theophylline with calculated GMFEs are presented in Table S2d and Figure S2d. Sensitivity analysis results of a simulation of 500 mg theophylline po q.d. are illustrated in Figure S2e. The theophylline model is sensitive to the values of fraction unbound (literature value), CYP1A2 catalytic rate constant (optimized) and CYP1A2 Michaelis-Menten constant (literature value).







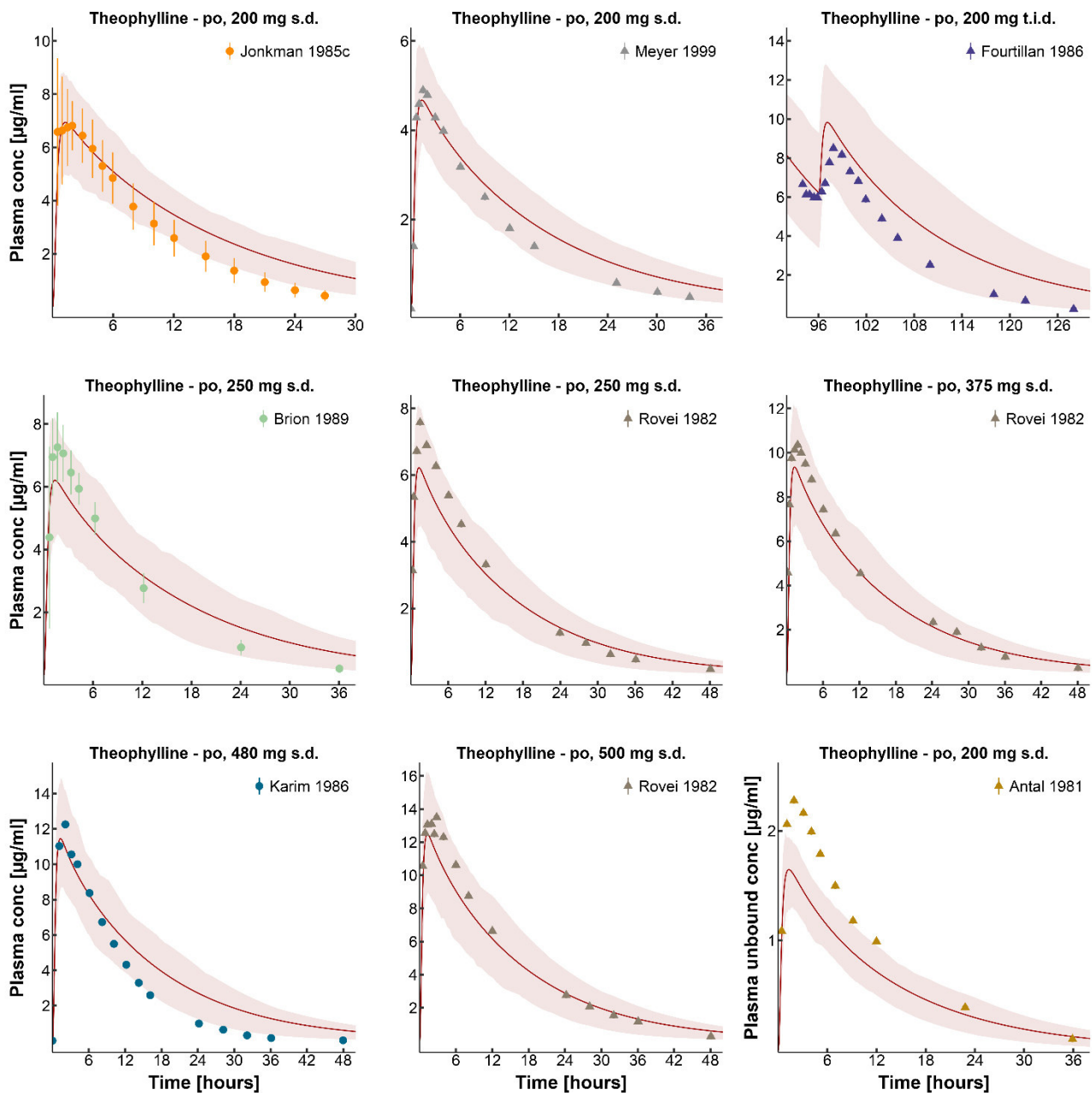
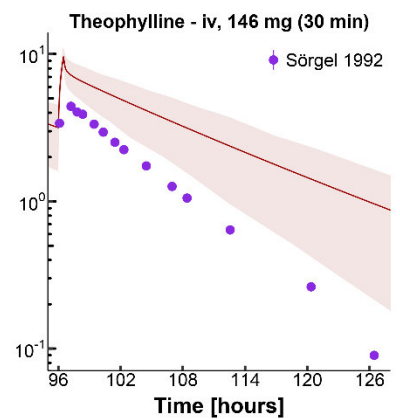
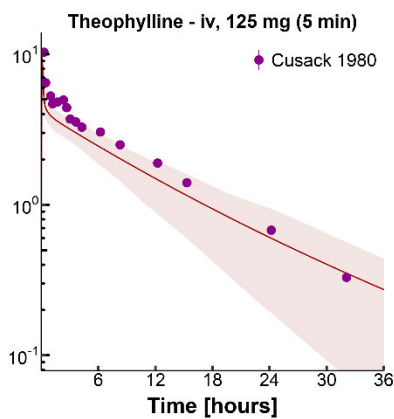
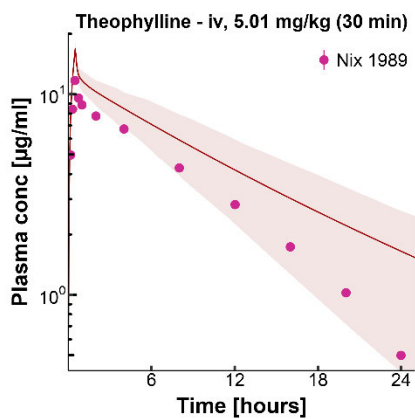
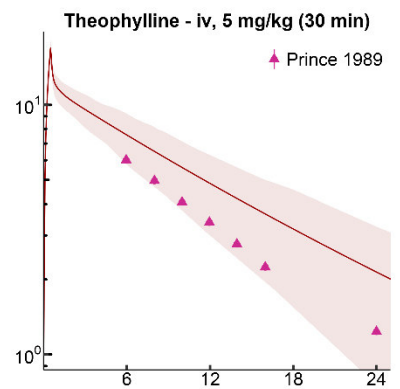
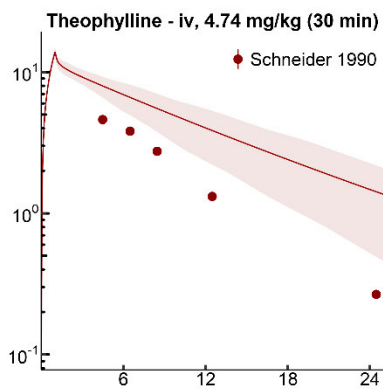
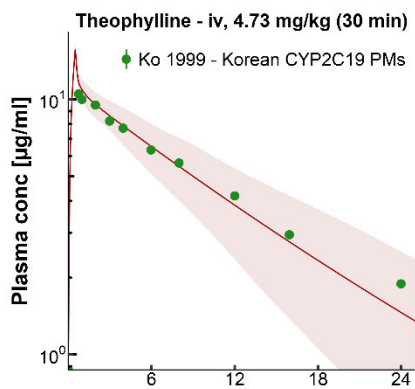
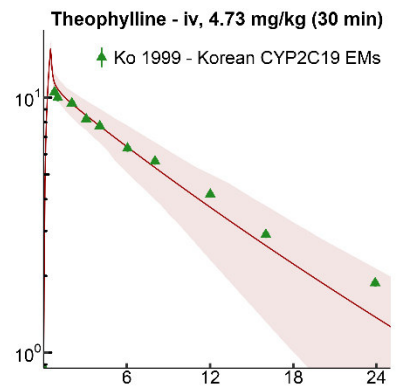
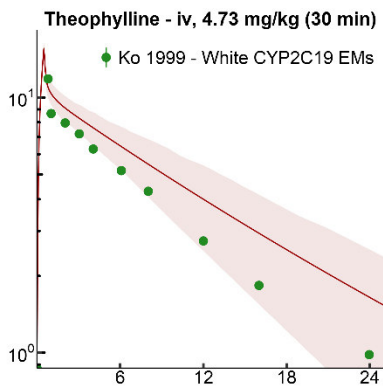
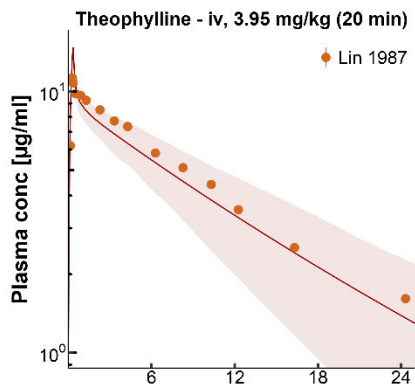
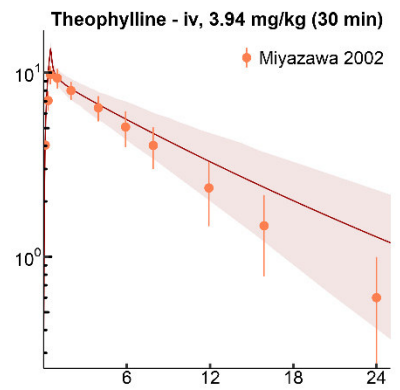
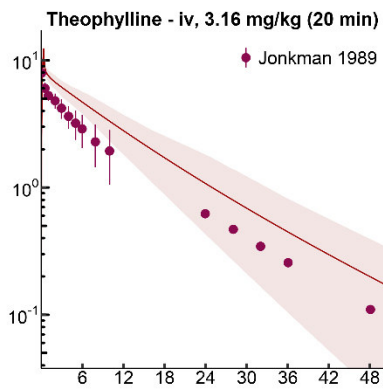
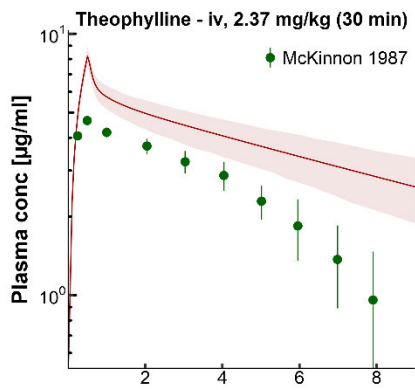
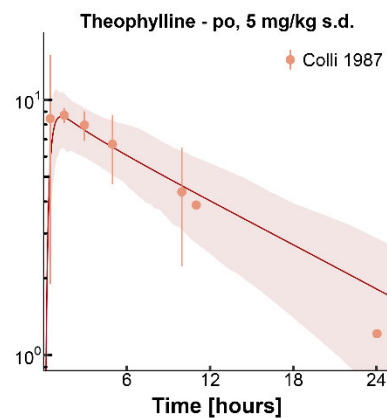
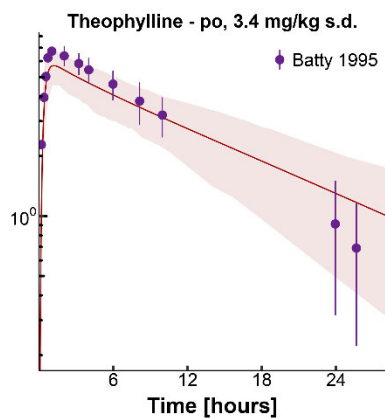
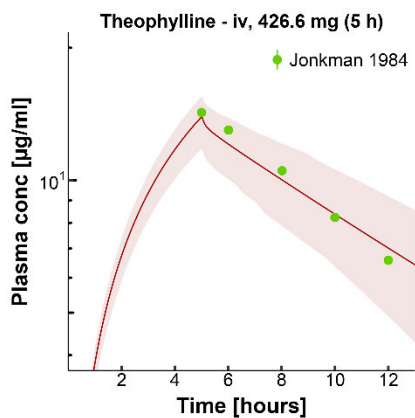
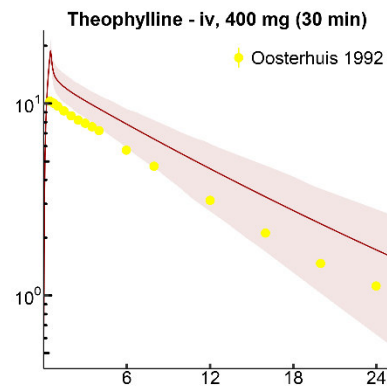
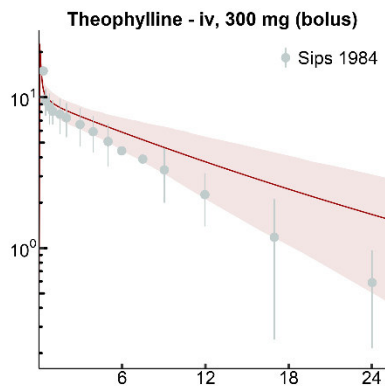
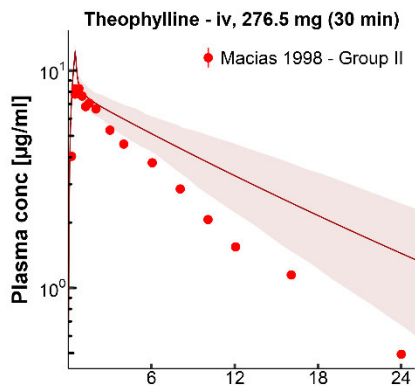
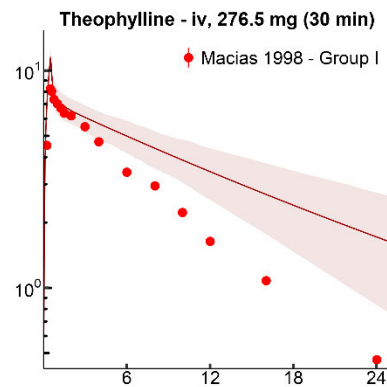
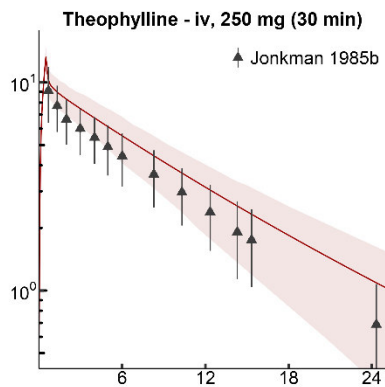
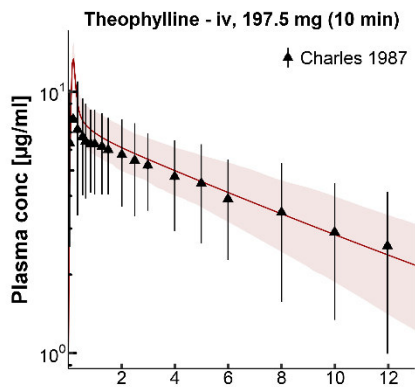
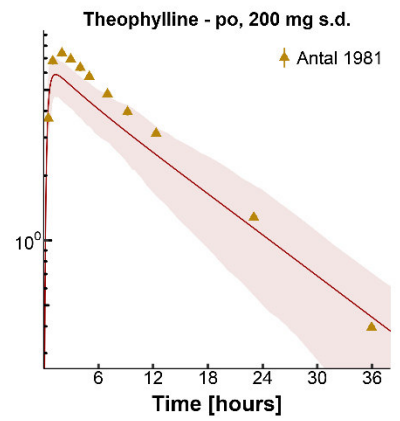
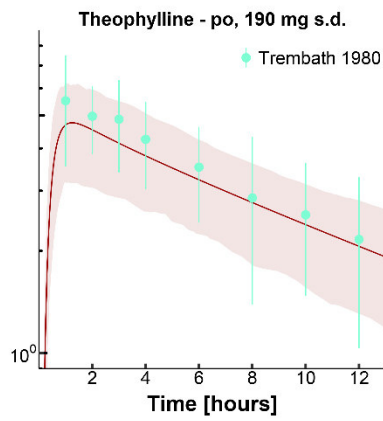
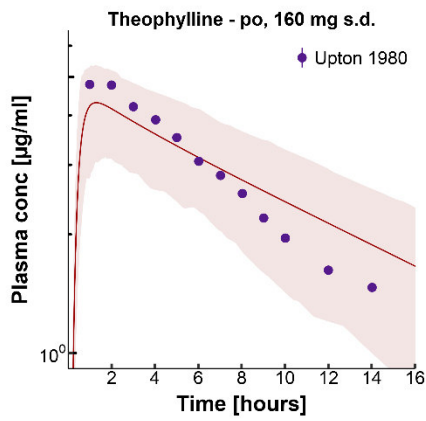
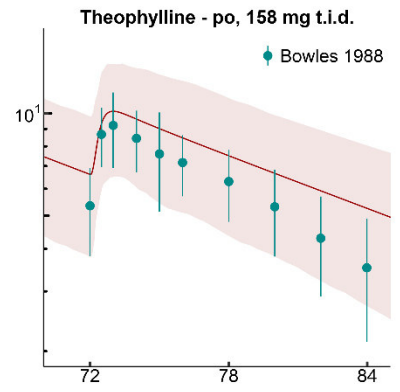
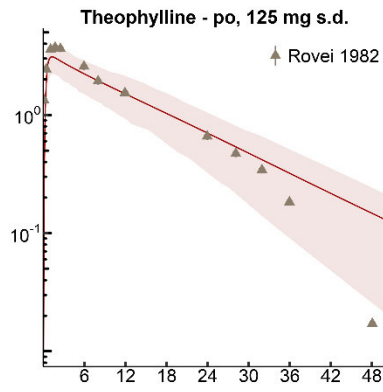
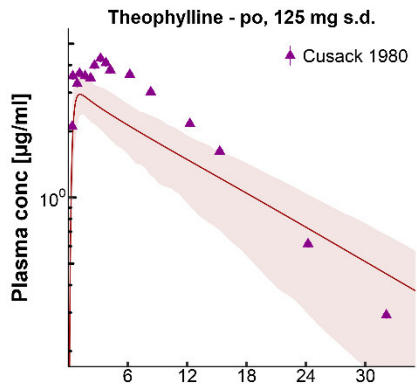
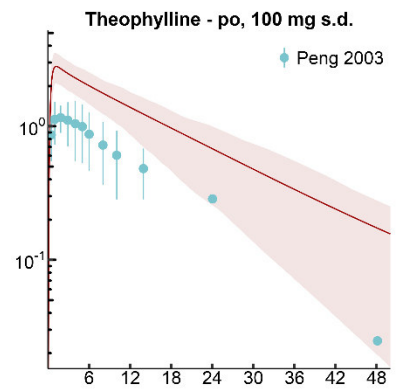
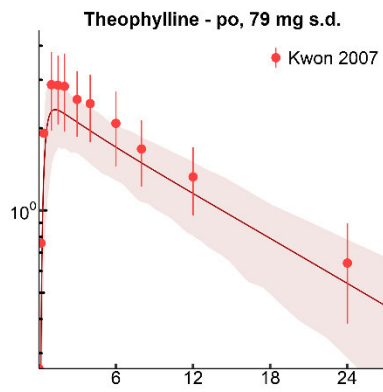
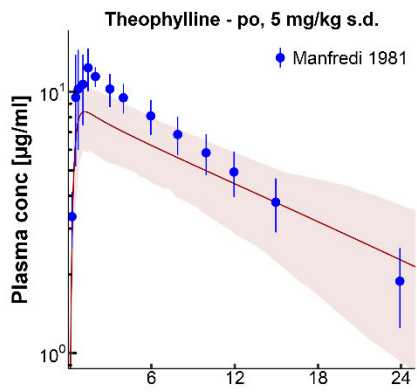


Figure S2a. Theophylline (iv, po) linear. Population predictions of theophylline plasma concentration-time profiles compared to observed data. Observed data are shown as triangles (training dataset) or dots (test dataset) \pm SD. Population simulation arithmetic means are shown as lines; the shaded areas illustrate the 68% population prediction intervals. Details on dosing regimens, study populations and literature references are listed in Table S2a. Predicted and observed PK parameters are summarized in Table S2d.







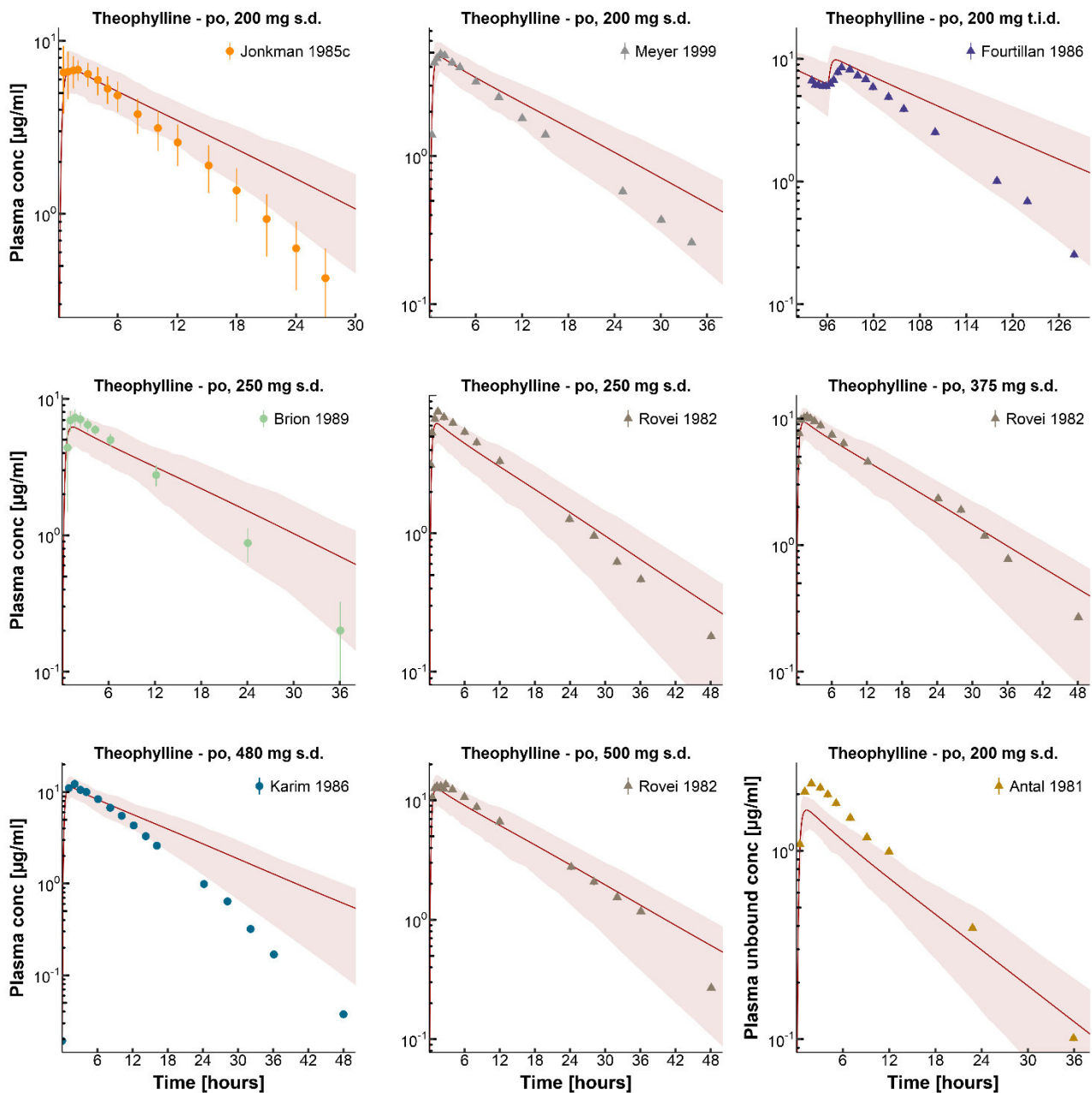


Figure S2b. Theophylline (iv, po) semilogarithmic. Population predictions of theophylline plasma concentration-time profiles compared to observed data. Observed data are shown as triangles (training dataset) or dots (test dataset) \pm SD. Population simulation arithmetic means are shown as lines; the shaded areas illustrate the 68% population prediction intervals. Details on dosing regimens, study populations and literature references are listed in Table S2a. Predicted and observed PK parameters are summarized in Table S2d.

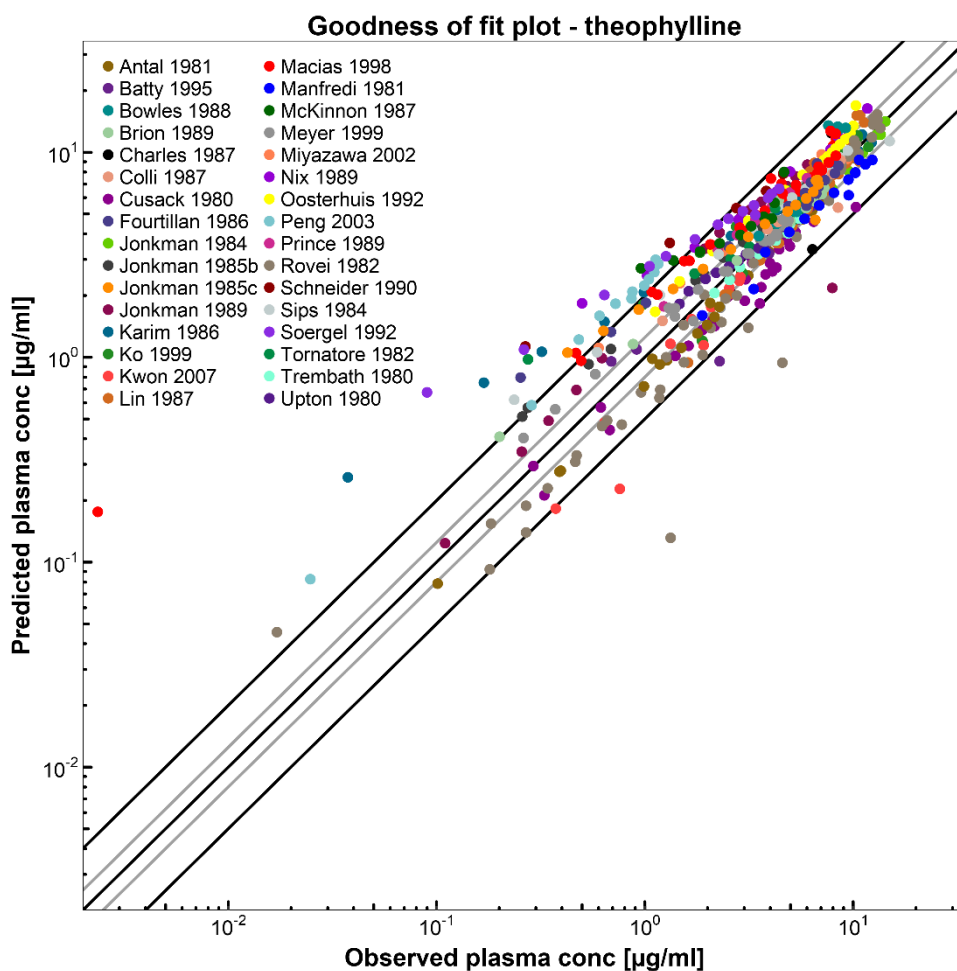


Figure S2c. Goodness of fit plot. Predicted compared to observed theophylline plasma concentration values of all clinical studies. Line of identity and 0.5- to 2.0-fold acceptance limits are shown as black lines. The 0.8- to 1.25-fold limits are shown as grey lines. Details on dosing regimens, study populations and literature references are listed in Table S2a. Predicted and observed PK parameters are summarized in Table S2d.

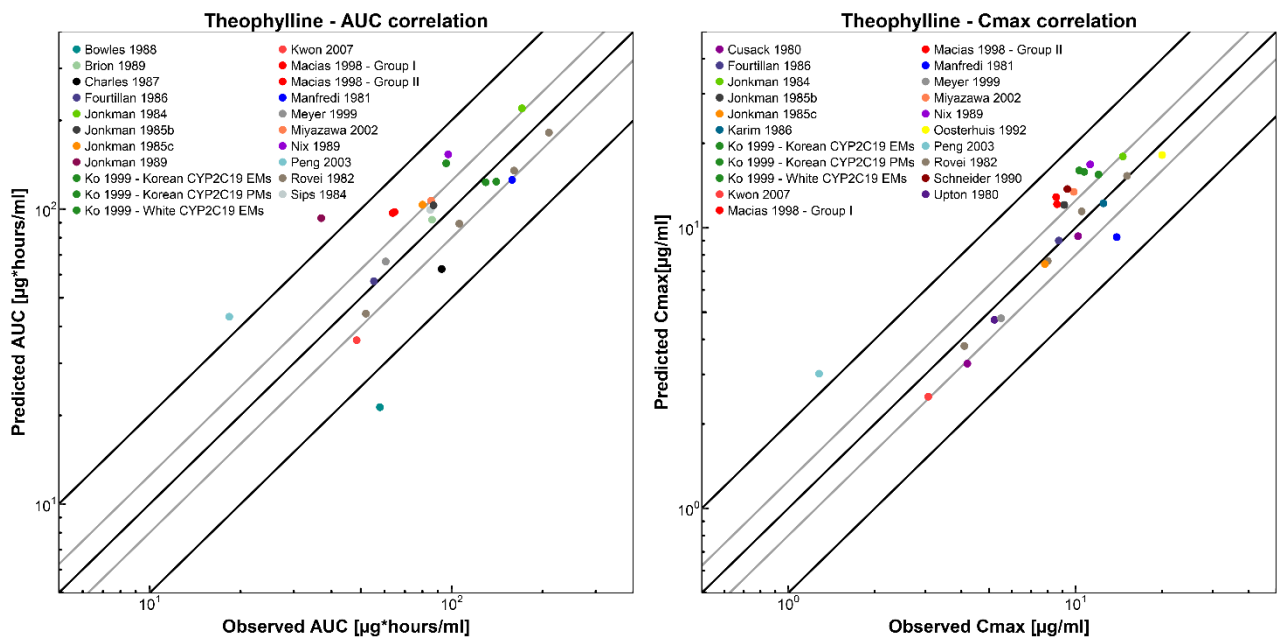


Figure S2d. Predicted compared to observed AUC and C_{\max} values. Predicted compared to observed theophylline AUC values (left panel) and C_{\max} values (right panel) of all clinical studies. Line of identity and 0.5- to 2.0-fold acceptance limits are shown as black lines. The 0.8- to 1.25-fold limits are shown as grey lines. Details on dosing regimens, study populations and literature references are listed in Table S2a. Predicted and observed PK parameters are summarized in Table S2d.

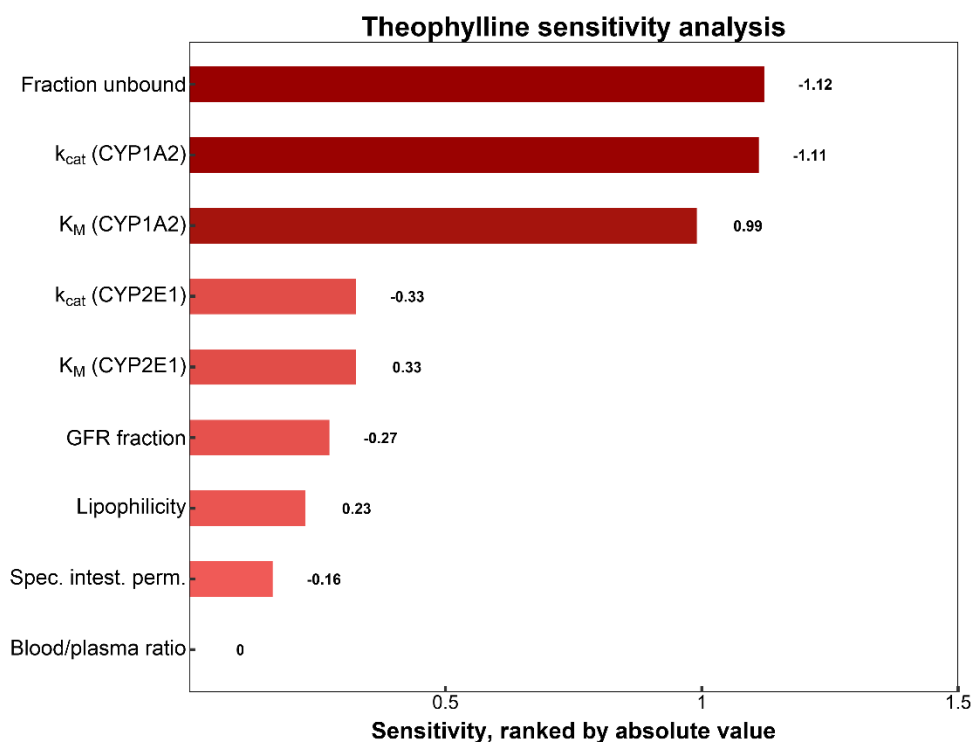


Figure S2e. Theophylline model sensitivity analysis. Sensitivity of the model to single parameters, measured as change of the simulated AUC under steady-state conditions of a 500 mg po q.d. theophylline regimen. A sensitivity value of + 1.0 signifies that a 10% increase of the examined parameter causes a 10% increase of the simulated AUC. CYP1A2, cytochrome P450 1A2; CYP2E1, cytochrome P450 2E1; GFR, glomerular filtration rate; k_{cat} , catalytic rate constant; K_M , Michaelis-Menten constant; Spec. intest. perm., specific intestinal permeability.

Table S2a. Clinical studies used for theophylline model development

Dose [mg]	Dose [mg/kg]	Route	n	Age [years]	Weight [kg]	Females [%]	Smokers [%]	Dataset	Reference
	2.37	iv (30 min), s.d.	6	-	-	0	0	test	McKinnon 1987 ³⁹
	3.16	iv (20 min), s.d.	11	22 (21-26)	69 (63-79)	9	0	test	Jonkman 1989 ⁴⁰
	3.94	iv (30 min), s.d.	10	27 (19-39)	73	0	0	test	Miyazawa 2002 ⁴¹
	3.95	iv (20 min), s.d.	10	-	-	-	-	test	Lin 1987 ⁴²
	4.73	iv (30 min), s.d.	5	27 ± 1	74 ± 5	60	-	test	Ko 1999 ⁴³ - White CYP2C19 EMs
	4.73	iv (30 min), s.d.	6	23 ± 1	55 ± 3	50	-	training	Ko 1999 ⁴³ - Korean CYP2C19 EMs
	4.73	iv (30 min), s.d.	7	26 ± 3	56 ± 4	43	-	test	Ko 1999 ⁴³ - Korean CYP2C19 PMs
	4.74	iv (30 min), s.d.	6	28 (24-34)	70 (66-74)	0	0	test	Schneider 1990 ⁴⁴
	5	iv (30 min), s.d.	8	23 ± 2	77 ± 8	0	0	training	Prince 1989 ⁴⁵
	5.01	iv (30 min), s.d.	25	22 ± 3	77 (64-91)	0	0	test	Nix 1989 ⁴⁶
125		iv (5 min), s.d.	5	26 (21-30)	70 (61-80)	-	0	test	Cusack 1980 ⁴⁷
146		iv (30 min), s.d.*	12	26 (22-32)	82 (70-100)	0	0	test	Sörgel 1992 ⁴⁸
197.5		iv (10 min), s.d.	10	22-35	49-85	40	-	training	Charles 1987 ⁴⁹
250		iv (30 min), s.d.	6	21 (19-22)	69 (53-80)	50	0	training	Jonkman 1985b ⁵⁰
276.5		iv (30 min), s.d.	12	35 (29-42)	79 (72-100)	-	92	test	Macias 1998 ³⁶ - Group I
276.5		iv (30 min), s.d.	7	34 (25-44)	74 (70-81)	-	71	test	Macias 1998 ³⁶ - Group II
300		iv (bolus), s.d.	10	22-76	75 ± 14	20	30	test	Sips 1984 ⁵¹
400		iv (30 min), s.d.	8	26 (21-36)	75 (61-86)	0	-	test	Oosterhuis 1992 ⁵²
426.6		iv (5 h), s.d.	8	23 (20-25)	63 (51-69)	25	0	test	Jonkman 1984 ⁵³
	3.1	po (sol), s.d.	8	24 (22-28)	54 ± 5	100	0	test	Tornatore 1982 ⁵⁴
	3.4	po (syr), s.d.	9	18-36	-	56	0	test	Batty 1995 ⁵⁵
	5	po (sol), s.d.	10	32 (25-39)	71 (58-85)	0	20	test	Colli 1987 ⁵⁶
	5	po (sol), s.d.	12	21-30	69-96	0	0	test	Manfredi 1981 ⁵⁷
79		po (tab), s.d.	8	21 (20-25)	58 ± 15	50	0	test	Kwon 2007 ⁵⁸
100		po (-), s.d.	20	25 (22-28)	61 (52-75)	50	0	test	Peng 2003 ⁵⁹
125		po (tab), s.d.	5	26 (21-30)	70 (61-80)	-	0	training	Cusack 1980 ⁴⁷
125		po (tab), s.d.	8	29 (22-35)	62 (52-77)	50	0	training	Rovei 1982 ³⁷
158		po (-), t.i.d.	10	24-34	-	0	0	test	Bowles 1988 ⁶⁰
160		po (tab), s.d.	12	22-37	43-76	58	-	test	Upton 1980 ⁶¹
190		po (syr), s.d.	10	21-36	-	-	10	test	Trembath 1980 ⁶²
200		po (tab), s.d.	14	23 ± 3	57 ± 9	-	0	training	Antal 1981 ⁶³

continued ...

continued ...

Dose [mg]	Dose [mg/kg]	Route	n	Age [years]	Weight [kg]	Females [%]	Smokers [%]	Dataset	Reference
200		po (tab), s.d.	14	23 ± 3	57 ± 9	-	0	training	Antal 1981 ⁶³
200		po (-), t.i.d.	12	18-30	61-88	0	-	training	Fourtillan 1986 ⁶⁴
200		po (caps), s.d.	18	20-33	77 (66-93)	0	0	training	Meyer 1999 ⁶⁵
250		po (tab), s.d.	10	23-27	54-80	10	0	test	Brion 1989 ⁶⁶
250		po (tab), s.d.	8	29 (22-35)	62 (52-77)	50	0	training	Rovei 1982 ³⁷
270		po (sol), s.d.	8	23 ± 2	67 ± 8	25	0	test	Jonkman 1985c ⁶⁷
375		po (tab), s.d.	8	29 (22-35)	62 (52-77)	50	0	training	Rovei 1982 ³⁷
480		po (tab), s.d.	20	-	-	0	0	test	Karim 1986 ⁶⁸
500		po (tab), s.d.	8	29 (22-35)	62 (52-77)	50	0	training	Rovei 1982 ³⁷

* , from day 1 to day 4 po administration of 146 mg theophylline b.i.d. and on day 5 iv administration; caps, capsule; CYP2C19, cytochrome P450 2C19; EMs, extensive metabolizers; iv, intravenous; n, number of individuals studied; PMs, poor metabolizers; po, oral; Route, route of administration; sol, solution; syr, syrup; tab, tablet; test, test dataset (model evaluation); training, training dataset (parameter optimization); -, no data available. Values are means ± standard deviation or ranges.

Table S2b. Drug-dependent parameters of the final theophylline PBPK model

Parameter	Unit	Theophylline model	Literature values	Source	Reference	Description
MW	g/mol	180.17	180.17	lit.	^a	Molecular weight
pKa		8.77 (acid)	8.77 (acid)	lit.	⁶⁹	Acid dissociation constant
		11.50 (base)	11.50 (base)	lit.	⁶⁹	
		13.50 (base)	13.50 (base)	lit.	⁶⁹	
Solubility (pH)	mg/ml	8.33 (7.0)	8.33 (7.0)	lit.	⁶⁹	Solubility
logP		0.41	- 0.77, - 0.26, - 0.02	opt.	^a	Lipophilicity
fu	%	28.00	28.00, 51.00, 54.00, 60.00	lit.	⁷⁰⁻⁷³	Fraction unbound
CYP1A2 K _M	mmol/l	0.23	0.23, 0.60	lit.	^{33,74,75}	Michaelis-Menten constant
CYP1A2 k _{cat}	1/min	6.48	-	opt.	-	CYP1A2 catalytic rate constant
CYP2E1 K _M	mmol/l	15.30	15.30, 19.90	lit.	^{33,74}	Michaelis-Menten constant
CYP2E1 k _{cat}	1/min	103.40	-	opt.	-	CYP2E1 catalytic rate constant
GFR fraction		0.22	-	opt.	-	Fraction of filtered drug reaching the urine
EHC continuous fraction		1	-	asm.	-	Fraction of bile continually released from the gallbladder
Formulation		solution	-	asm.	-	Formulation used in predictions
Cellular permeabilities		PK-Sim	-	calc.	²⁸	Permeation across cell membranes
Partition coefficients		PK-Sim	-	calc.	²⁸	Organ-plasma partition coefficients
Specific intest. perm.	dm/min	5.45E-07	-	opt.	-	Normalized to surface area
Specific organ perm.	dm/min	2.18E-04	-	calc.	³⁰	Normalized to surface area

^a, <https://www.drugbank.ca/drugs/DB00277>, last view: 22 October 2018; asm., assumed; calc., calculated; CYP1A2, cytochrome P 450 1A2; CYP2E1, cytochrome P 450 2E1; EHC, enterohepatic circulation; GFR, glomerular filtration rate; intest., intestinal; lit., literature; opt., optimized; perm., permeability; PK-Sim, PK-Sim Standard calculation method; -, not available.

Table S2c. Mean relative deviation values of theophylline plasma concentration predictions

Dose [mg]	Dose [mg/kg]	Route	n	Smokers [%]	MRD	Reference
	2.37	iv (30 min), s.d.	6	0	1.71	McKinnon 1987 ³⁹
	3.16	iv (20 min), s.d.	11	0	1.70	Jonkman 1989 ⁴⁰
	3.94	iv (30 min), s.d.	10	0	1.34	Miyazawa 2002 ⁴¹
	3.95	iv (20 min), s.d.	10	-	1.25	Lin 1987 ⁴²
	4.73	iv (30 min), s.d.	5	-	1.41	Ko 1999 ⁴³ - White CYP2C19 EMs
	4.73	iv (30 min), s.d.	6	-	1.17	Ko 1999 ⁴³ - Korean CYP2C19 EMs
	4.73	iv (30 min), s.d.	7	-	1.18	Ko 1999 ⁴³ - Korean CYP2C19 PMs
	4.74	iv (30 min), s.d.	6	0	2.47	Schneider 1990 ⁴⁴
	5.00	iv (30 min), s.d.	8	0	1.38	Prince 1989 ⁴⁵
	5.01	iv (30 min),s.d.	25	0	1.80	Nix 1989 ⁴⁶
125		iv (5 min), s.d.	5	0	1.38	Cusack 1980 ⁴⁷
146		iv (30 min), s.d.*	12	-	2.51	Sörgel 1992 ⁴⁸
197.5		iv (10 min), s.d.	10	-	1.23	Charles 1987 ⁴⁹
250		iv (30 min), s.d.	6	0	1.42	Jonkman 1985b ⁵⁰
276.5		iv (30 min), s.d.	12	0	3.05	Macias 1998 ³⁶ - Group I
276.5		iv (30 min), s.d.	7	0	1.52	Macias 1998 ³⁶ - Group II
300		iv (bolus), s.d.	10	30	1.42	Sips 1984 ⁵¹
400		iv (30 min), s.d.	8	-	1.39	Oosterhuis 1992 ⁵²
426.6		iv (5 h), s.d.	8	0	1.04	Jonkman 1984 ⁵³
	3.10	po (sol), s.d.	8	0	1.62	Tornatore 1982 ⁵⁴
	3.40	po (syr), s.d.	9	0	1.33	Batty 1995 ⁵⁵
	5.00	po (sol), s.d.	10	20	1.21	Colli 1987 ⁵⁶
	5.00	po (sol), s.d.	12	0	1.31	Manfredi 1981 ⁵⁷
79		po (tab), s.d.	8	0	1.58	Kwon 2007 ⁵⁸
100		po (-), s.d.	20	0	2.48	Peng 2003 ⁵⁹
125		po (tab), s.d.	5	0	1.43	Cusack 1980 ⁴⁷
125		po (tab), s.d.	8	0	2.06	Rovei 1982 ³⁷
158		po (-), t.i.d.	10	0	1.34	Bowles 1988 ⁶⁰
160		po (tab), s.d.	12	-	1.14	Upton 1980 ⁶¹
190		po (syr), s.d.	10	10	1.12	Trembath 1980 ⁶²
200		po (tab), s.d.	14	0	1.23	Antal 1981 ⁶³
200		po (tab), s.d.	14	0	1.31	Antal 1981 ⁶³
200		po (-), t.i.d.	12	-	1.43	Fourtillan 1986 ⁶⁴
200		po (caps), s.d.	18	0	1.23	Meyer 1999 ⁶⁵
250		po (tab), s.d.	10	0	1.31	Brion 1989 ⁶⁶
250		po (tab), s.d.	8	0	1.42	Rovei 1982 ³⁷
270		po (sol), s.d.	8	0	1.47	Jonkman 1985c ⁶⁷
375		po (tab), s.d.	8	0	1.66	Rovei 1982 ³⁷
480		po (tab), s.d.	20	0	2.17	Karim 1986 ⁶⁸
500		po (tab), s.d.	8	0	1.31	Rovei 1982 ³⁷
Mean MRD (range)					1.54 (1.04-3.05)	
MRD < 2					34/40 studies	

*, from day 1 to day 4 po administration of 146 mg theophylline b.i.d. and on day 5 iv administration; caps, capsule; CYP2C19, cytochrome P450 2C19; EMs, extensive metabolizers; iv, intravenous; MRD, mean relative deviation; n, number of individuals studied; PMs, poor metabolizers; po, oral; Route, route of administration; sol, solution; syr, syrup; tab, tablet; -, no data available.

Table S2d. Observed and predicted AUC and C_{max} values of theophylline

Dose [mg]	Dose [mg/kg]	Route	n	Smokers [%]	AUC obs [µg*hours/ml]	AUC pred [µg*hours/ml]	Pred/Obs AUC	C _{max} obs [µg/ml]	C _{max} pred [µg/ml]	Pred/Obs C _{max}	Reference
	2.37	iv (30 min), s.d.	6	0	-	-	-	-	-	-	McKinnon 1987 ³⁹
	3.16	iv (20 min), s.d.	11	0	37.00	93.21	2.52	-	-	-	Jonkman 1989 ⁴⁰
	3.94	iv (30 min), s.d.	10	0	85.50	106.87	1.25	9.85	13.43	1.36	Miyazawa 2002 ⁴¹
	3.95	iv (20 min), s.d.	10	-	-	-	-	-	-	-	Lin 1987 ⁴²
	4.73	iv (30 min), s.d.	5	-	95.90	143.03	1.49	12.02	15.47	1.29	Ko 1999 ⁴³ - White CYP2C19 EMs
	4.73	iv (30 min), s.d.	6	-	140.50	123.99	0.88	10.71	15.82	1.48	Ko 1999 ⁴³ - Korean CYP2C19 EMs
	4.73	iv (30 min), s.d.	7	-	129.60	123.38	0.95	10.30	16.00	1.55	Ko 1999 ⁴³ - Korean CYP2C19 PMs
	4.74	iv (30 min), s.d.	6	0	-	-	-	9.36	13.74	1.47	Schneider 1990 ⁴⁴
	5.00	iv (30 min), s.d.	8	0	-	-	-	-	-	-	Prince 1989 ⁴⁵
	5.01	iv (30 min),s.d.	25	0	97.42	153.37	1.57	11.24	16.81	1.50	Nix 1989 ⁴⁶
125		iv (5 min), s.d.	5	0	-	-	-	10.20	9.33	0.91	Cusack 1980 ⁴⁷
146		iv (30 min), s.d.*	12	-	-	-	-	-	-	-	Sörgel 1992 ⁴⁸
197.5		iv (10 min), s.d.	10	-	92.70 ^a	62.64 ^a	0.68	-	-	-	Charles 1987 ⁴⁹
250		iv (30 min), s.d.	6	0	87.10	103.03	1.18	9.13	12.06	1.32	Jonkman 1985b ⁵⁰
276.5		iv (30 min), s.d.	12	0	63.80	97.06	1.52	8.62	12.13	1.41	Macias 1998 ³⁶ - Group I
276.5		iv (30 min), s.d.	7	0	64.70	97.79	1.51	8.56	12.86	1.50	Macias 1998 ³⁶ - Group II
300		iv (bolus), s.d.	10	30	85.00 ^b	99.50 ^b	1.17	-	-	-	Sips 1984 ⁵¹
400		iv (30 min), s.d.	8	-	-	-	-	20.00	18.16	0.91	Oosterhuis 1992 ⁵²
426.6		iv (5 h), s.d.	8	0	171.00	219.76	1.29	14.60	17.94	1.23	Jonkman 1984 ⁵³
	3.10	po (sol), s.d.	8	0	-	-	-	-	-	-	Tornatore 1982 ⁵⁴
	3.40	po (syr), s.d.	9	0	-	-	-	-	-	-	Batty 1995 ⁵⁵
	5.00	po (sol), s.d.	10	20	-	-	-	-	-	-	Colli 1987 ⁵⁶
	5.00	po (sol), s.d.	12	0	158.60	125.65	0.79	13.90	9.26	0.67	Manfredi 1981 ⁵⁷
79		po (tab), s.d.	8	0	48.47	35.95	0.74	3.07	2.50	0.81	Kwon 2007 ⁵⁸
100		po (-), s.d.	20	0	18.35	43.18	2.35	1.28	3.02	2.36	Peng 2003 ⁵⁹
125		po (tab), s.d.	5	0	-	-	-	4.20	3.28	0.78	Cusack 1980 ⁴⁷
125		po (tab), s.d.	8	0	52.00	44.23	0.85	4.10	3.79	0.92	Rovei 1982 ³⁷
158		po (-), t.i.d.	10	0	57.89 ^c	21.31 ^c	0.37	-	-	-	Bowles 1988 ⁶⁰
160		po (tab), s.d.	12	-	-	-	-	5.22	4.70	0.90	Upton 1980 ⁶¹
190		po (syr), s.d.	10	10	-	-	-	-	-	-	Trembath 1980 ⁶²

continued ...

continued ...

Dose [mg]	Dose [mg/kg]	Route	n	Smokers [%]	AUC obs [µg*hours/ml]	AUC pred [µg*hours/ml]	Pred/Obs AUC	C _{max} Obs [µg/ml]	C _{max} pred [µg/ml]	Pred/Obs C _{max}	Reference
200		po (tab), s.d.	14	0	-	-	-	-	-	-	Antal 1981 ⁶³
200		po (tab), s.d.	14	0	-	-	-	-	-	-	Antal 1981 ⁶³
200		po (-), t.i.d.	12	-	55.30 ^c	56.99 ^c	1.03	8.74	9.00	1.03	Fourtillan 1986 ⁶⁴
200		po (caps), s.d.	18	0	60.50	66.44	1.10	5.50	4.76	0.87	Meyer 1999 ⁶⁵
250		po (tab), s.d.	10	0	86.10	92.08	1.07	-	-	-	Brion 1989 ⁶⁶
250		po (tab), s.d.	8	0	106.00	89.28	0.84	8.00	7.61	0.95	Rovei 1982 ³⁷
270		po (sol), s.d.	8	0	80.10	103.55	1.29	7.82	7.42	0.95	Jonkman 1985c ⁶⁷
375		po (tab), s.d.	8	0	161.00	135.14	0.84	10.50	11.44	1.09	Rovei 1982 ³⁷
480		po (tab), s.d.	20	0	-	-	-	12.50	12.22	0.98	Karim 1986 ⁶⁸
500		po (tab), s.d.	8	0	210.00	181.79	0.87	15.10	15.30	1.01	Rovei 1982 ³⁷
					GMFE (range)	1.36 (1.03-2.72)				1.27 (1.01-2.36)	
					Pred/Obs within twofold		21/24			24/25	

^a, AUC₀₋₂₄; ^b, AUC₀₋₃₀; ^c, AUC₀₋₈; AUC values are 0-∞ if not specified differently; *, from day 1 to day 4 po administration of 146 mg theophylline b.i.d. and on day 5 iv administration; AUC, area under the plasma concentration-time curve; caps, capsule; C_{max}, peak plasma concentration; CYP2C19, cytochrome P450 2C19; EMs, extensive metabolizers; GMFE, geometric mean fold error; iv, intravenous; n, number of individuals studied; obs, observed; PMs, poor metabolizers; po, oral; pred, predicted; Route, route of administration; sol, solution; syr, syrup; tab, tablet; -, no data available.

2.4 Caffeine model development

Caffeine is a methylxanthine and stimulant of the central nervous system. For the investigation of DDIs, caffeine is recommended by the FDA as sensitive clinical CYP1A2 index substrate ⁹. The caffeine PBPK model applied for DDI prediction is a template model integrated in the PK-Sim[®] modelling platform ¹. The model incorporates metabolism via CYP1A2 and a first order renal plasma clearance process. Drug-dependent parameters of the caffeine template model are summarized in Table S3 ¹.

Table S3. Drug-dependent parameters of the caffeine PBPK model

Parameter	Unit	Caffeine model	Literature values	Source	Reference	Description
MW	g/mol	194.20	194.20	lit.	^a	Molecular weight
pKa		0.80 (base)	0.80 (base)	lit.	1	Acid dissociation constant
Solubility (pH)	mg/ml	2.1.60 (water)	21.60 (water)	lit.	1	Solubility
logP		- 0.07	- 0.07	lit.	1	Lipophilicity
fu	%	70.00	70.00	lit.	⁷⁶	Fraction unbound
CYP1A2 K_M	$\mu\text{mol/l}$	14.70	-	opt.	-	Michaelis-Menten constant
CYP1A2 k_{cat}	1/min	1.01	-	opt.	-	CYP1A2 catalytic rate constant
CL_{ren}	1/min	2.46E-03	2.46E-03	lit.	⁷⁷	Renal plasma clearance (first order)
EHC continuous fraction		1	-	asm.	-	Fraction of bile continually released from the gallbladder
Formulation		solution	-	asm.	-	Formulation used in predictions
Cellular permeabilities		PK-Sim	-	calc.	²⁸	Permeation across cell membranes
Partition coefficients		PK-Sim	-	calc.	²⁸	Organ-plasma partition coefficients
Specific intest. perm.	dm/min	6.85E-06	-	opt.	-	Normalized to surface area
Specific organ perm.	dm/min	4.57E-03	-	calc.	³⁰	Normalized to surface area

^a, <https://www.drugbank.ca/drugs/DB00201>, last view: 22 October 2018; asm., assumed; calc., calculated; CL_{ren} , renal plasma clearance; CYP1A2, cytochrome P 450 1A2; EHC, enterohepatic circulation; intest., intestinal; lit., literature; opt., optimized; perm., permeability; PK-Sim, PK-Sim Standard calculation method; -, not available.

2.5 Rifampicin model development

Rifampicin is an antibiotic used for the treatment of mycobacterium infections. It induces multiple metabolizing enzymes and transporters and is classified by the FDA as strong clinical index inducer of CYP2C19 and CYP3A4 and as moderate clinical index inducer of CYP1A2³⁸. The rifampicin PBPK model applied for DDI prediction has been developed previously², but was extended in this study by inclusion and evaluation of parameters to model the induction of CYP1A2 and CYP2E1. Drug-dependent parameters of the extended rifampicin model are summarized in Table S4².

Table S4. Drug-dependent parameters of the rifampicin PBPK model

Parameter	Unit	Rifampicin model	Literature values	Source	Reference	Description
MW	g/mol	822.94	822.94	lit.	^a	Molecular weight
pKa		1.70 (acid)	1.70 (acid)	lit.	69	Acid dissociation constant
		7.90 (base)	7.90 (base)	lit.	69	
Solubility (pH)	mg/l	2800 (7.5)	1100 (6.5), 1400 (6.8), 2540 (6.8), 2800 (7.5), 3350 (7.4)	lit.	78-81	Solubility
logP		2.50	1.30, 2.70	opt.	78,82	Lipophilicity
fu	%	17.00	11.00, 16.00, 17.00, 17.50	lit.	78,81,83,84	Fraction unbound
B/P ratio		0.89	0.90 ^b	calc.	85	Blood/plasma ratio
OATP1B1 K_M	$\mu\text{mol/l}$	1.50	1.50	lit.	86	Michaelis-Menten constant
OATP1B1 k_{cat}	1/min	7.80	-	opt.	-	OATP1B1 catalytic rate constant
AADAC K_M	$\mu\text{mol/l}$	195.10	195.10	lit.	87	Michaelis-Menten constant
AADAC k_{cat}	1/min	9.87	-	opt.	-	AADAC catalytic rate constant
P-gp K_M	$\mu\text{mol/l}$	55.00	55.00	lit.	88	Michaelis-Menten constant
P-gp k_{cat}	1/min	0.61	-	opt.	-	P-gp catalytic rate constant
GFR fraction		1	-	asm.	-	Fraction of filtered drug reaching the urine
EHC continuous fraction		1	-	asm.	-	Fraction of bile continually released from the gallbladder
Induction EC_{50}	$\mu\text{mol/l}$	0.34	0.34	lit.	83,84	Concentration for half-maximal induction
E_{max} OATP1B1		0.38	-	opt.	-	Maximum in vivo induction effect
E_{max} AADAC		0.99	-	opt.	-	Maximum in vivo induction effect
E_{max} P-gp		2.50	2.50	lit.	89	Maximum in vivo induction effect
E_{max} CYP1A2		0.65	0.65	lit.	90	Maximum in vivo induction effect
E_{max} CYP2E1		0.80	0.80	lit.	91	Maximum in vivo induction effect
E_{max} CYP3A4		9.00	9.00	lit.	83	Maximum in vivo induction effect
Inhibition K_i P-gp	$\mu\text{mol/l}$	169.00	169.00	lit.	92	Concentration for half-maximal competitive inhibition
Inhibition K_i CYP3A4	$\mu\text{mol/l}$	18.50	18.50	lit.	93	Concentration for half-maximal competitive inhibition
Formulation		solution	-	asm.	-	Formulation used in predictions
Cell permeabilities		PK-Sim	-	calc.	94	Permeation across cell membranes
Partition coefficients		R+R	-	calc.	95,96	Organ-plasma partition coefficients
Specific intest. perm.	dm/min	1.24E-06	-	calc.	-	Normalized to surface area
Specific organ perm.	dm/min	2.93E-06	-	calc.	30	Normalized to surface area

^a, <https://www.drugbank.ca/drugs/DB01045>, last view: 22 October 2018; ^b, blood/serum concentration ratio; AADAC, arylacetamide deacetylase; asm., assumed; calc., calculated; CYP1A2, cytochrome P 450 1A2; CYP2E1, cytochrome P 450 2E1; CYP3A4, cytochrome P 450 3A4; EHC, enterohepatic circulation; GFR, glomerular filtration rate; intest., intestinal; lit., literature; OATP1B1, organic anion transporting polypeptide 1B1; opt., optimized; perm., permeability; P-gp, P-glycoprotein; PK-Sim, PK-Sim Standard calculation method; R+R, Rodgers and Rowland calculation method; -, not available.

2.6 Midazolam model development

Midazolam is a sedative and is exclusively metabolized via CYP3A4. The FDA lists midazolam as a sensitive clinical CYP3A4 index substrate for the investigation of DDIs⁹. The midazolam PBPK model applied for DDI prediction has been described previously². Drug-dependent parameters of the midazolam model are summarized in Table S5².

Table S5. Drug-dependent parameters of the midazolam PBPK model

Parameter	Unit	Midazolam model	Literature values	Source	Reference	Description
MW	g/mol	325.77	325.77	lit.	^a	Molecular weight
pKa		6.15 (base)	6.15 (base)	lit.	97	Acid dissociation constant
Solubility (pH)	mg/l	49.00 (6.5)	49.00 (6.5)	lit.	98	Solubility
logP		3.13	2.90, 3.90	opt.	99,100	Lipophilicity
fu	%	1.60	1.60, 2.40	lit.	99,101	Fraction unbound
CYP3A4 K_M	$\mu\text{mol/l}$	2.73	2.73	lit.	102	Michaelis-Menten constant
CYP3A4 k_{cat}	1/min	13.00	-	opt.	-	CYP3A4 catalytic rate constant
GFR fraction		1	-	asm.	-	Fraction of filtered drug reaching the urine
EHC continuous fraction		1	-	asm.	-	Fraction of bile continually released from the gallbladder
Formulation		solution	-	asm.	-	Formulation used in predictions
Cell permeabilities		PK-Sim	-	calc.	94	Permeation across cell membranes
Partition coefficients		R+R	-	calc.	95,96	Organ-plasma partition coefficients
Specific intest. perm.	dm/min	2.00E-06	-	opt.	-	Normalized to surface area
Specific organ perm.	dm/min	7.00E-03	-	calc.	30	Normalized to surface area

^a, <https://www.drugbank.ca/drugs/DB00683>, last view: 22 October 2018; asm., assumed; calc., calculated; CYP3A4, cytochrome P 450 3A4; EHC, enterohepatic circulation; GFR, glomerular filtration rate; intest., intestinal; lit., literature; opt., optimized; perm., permeability; PK-Sim, PK-Sim Standard calculation method; R+R, Rodgers and Rowland calculation method; -, not available.

2.7 System-dependent parameters

System-dependent parameters, such as reference concentrations and tissue expression profiles of metabolizing enzymes and transporters, are listed in Table S6.

Within virtual populations, the reference concentrations of the implemented enzymes and transporters were distributed according to the variabilities for enzyme expression provided in PK-Sim. If no information was available in the modelling platform, they were set to be log-normally distributed according to literature reports or otherwise with a moderate geometric standard deviation of 1.4 (35 %CV).

Table S6. System-dependent parameters, expression of ADME relevant proteins

Protein	Mean reference concentration [$\mu\text{mol protein/l}$ in the tissue of highest expression]	Geometric standard deviation of reference concentration	Relative expression in the different organs (PK-Sim expression database profile)	Half-life liver [hours]	Half-life intestine [hours]
AADAC	1.0^{103}	1.40^a	RT-PCR ¹⁰⁴	36	23
CYP1A2	1.80^{105}	1.63^{106}	RT-PCR ¹⁰⁷	39	23
CYP2D6	0.40^{105}	2.49^{106}	RT-PCR ¹⁰⁷	51	23
CYP2E1	1.96^{105}	1.35^{106}	RT-PCR ¹⁰⁷	20	23
CYP3A4	4.32^{105}	1.18 liver, 1.46 intestine ¹⁰⁶	RT-PCR ¹⁰⁷	36^{108}	23^{109}
OATP1B1	1.0^{103}	1.54^{110}	RT-PCR ¹¹¹	36	23
P-gp (efflux)	1.41 optimized	1.60^{110}	RT-PCR ¹¹¹ , with the relative expression in intestinal mucosa increased by factor 3.57 (optimized)	36	23

EHC continuous fraction: Fraction of biliary secreted compound directly entering the duodenum = 1

^a, CV of 35% assumed; AADAC, arylacetamide deacetylase; CYP1A2, cytochrome P450 1A2; CYP2D6, cytochrome P450 2D6; CYP2E1, cytochrome P450 2E1; CYP3A4, cytochrome P450 3A4; EHC, enterohepatic circulation; OATP1B1, organic anion transporting polypeptide 1B1; P-gp, P-glycoprotein; RT-PCR, reverse transcription-polymerase chain reaction profile. If no information on reference concentration was available, it was set to $1.0 \mu\text{mol/l}$ and the catalytic rate constant (k_{cat}) was optimized according to ¹⁰³.

3 DDI prediction

3.1 DDI modelling - general

All induction and inhibition processes were modelled using interaction parameter values from in vitro experimental reports. No co-administration studies were used for parameter optimization during the fluvoxamine and theophylline model building. The aim of this approach was, to evaluate the built models not only by their performance in the prediction of the test dataset studies, but also by the prediction of DDI studies^{9,112-114}.

The expression and the activity of CYP1A2 are highly variable between individuals and populations¹¹⁵. Furthermore, the influence of polymorphisms, such as CYP1A2*1C and CYP1A2*1F, on the metabolism of CYP1A2 substrates has been investigated in different studies, but the clinical relevance of these genotypes has not been conclusively clarified¹¹⁶⁻¹¹⁹. Since theophylline and caffeine are mainly metabolized via CYP1A2, indicated by fractions metabolized of 0.7^{34,35} and 0.95¹²⁰, respectively, a strong influence of the interindividual variability of CYP1A2 expression on the pharmacokinetics of the two drugs can be assumed. This effect is most likely more pronounced on caffeine due to its higher fraction metabolized via CYP1A2. For CYP3A4 and the sensitive clinical CYP3A4 index substrate midazolam, the same effects has been observed^{121,122}.

The developed theophylline victim drug PBPK model shows a good descriptive and predictive performance for 34 of the 40 modelled theophylline studies (see Table S2c). Furthermore, the PBPK models of caffeine¹ and midazolam² have been thoroughly evaluated and showed a good performance. However, to model some of the reported DDI studies, the CYP1A2 or CYP3A4 k_{cat} of the victim drugs was adjusted to describe the plasma concentration-time profiles of the control groups (no co-medication) and the adjusted k_{cat} was then also used for the co-administration group (one of two fluvoxamine-theophylline studies, one of three rifampicin-theophylline studies, both fluvoxamine-caffeine studies and the fluvoxamine-midazolam study). After adaptation of either CYP1A2 or CYP3A4 k_{cat} , the predicted DDI AUC ratios showed no relevant difference in comparison to the predicted DDI AUC ratios without adaptation of CYP1A2 or CYP3A4 k_{cat} (documented in 3.2 to 3.5). When applying the presented PBPK models for DDI prediction, adaptation of k_{cat} values for variable CYP enzymes that account for a high fraction metabolized of a modeled drug ($f_m \geq 0.7$) to the control group of the analyzed study should be considered.

Plots of population predicted compared to observed plasma concentration-time profiles and plots of predicted compared to observed DDI AUC ratios and DDI C_{max} ratios of all **fluvoxamine-theophylline, rifampicin-theophylline, fluvoxamine-caffeine and fluvoxamine-midazolam** DDIs that could be obtained from literature are shown in this supplementary document. Details on dosing regimens, study population characteristics and literature references of all clinical studies are summarized in Tables S7a, S8a, S9a and S10a. Predicted and observed DDI AUC and C_{max} values and ratios as well as GMFE values are summarized in Tables S7b, S8b, S9b and S10b.

3.2 Fluvoxamine-theophylline DDI

For fluvoxamine DDI modelling, the reported in vitro CYP inhibition constants were corrected for fluvoxamine binding in human liver microsomal preparations according to Yao et al. ²⁶. To calculate the in vivo inhibition constant $K_{i, \text{in vivo}}$, the free fraction of fluvoxamine in the test system used to measure the $K_{i, \text{in vitro}}$ has to be taken into account, see equation (6):

$$K_{i, \text{in vivo}} = f_{u, \text{mic}} * K_{i, \text{in vitro}} \quad (6)$$

with $K_{i, \text{in vivo}}$ = inhibition constant used for DDI prediction, $f_{u, \text{mic}}$ = free fraction of fluvoxamine in the microsomal in vitro assay and $K_{i, \text{in vitro}}$ = inhibition constant measured in vitro.

The free fraction of fluvoxamine in the microsomal assay increases, as the microsomal protein concentration decreases, as described by equation (7):

$$f_{u, \text{mic}} = 0.195 * C_{\text{prot}}^{-0.686} \quad (7)$$

with C_{prot} = microsomal protein concentration in the microsomal assay ²⁶.

To predict the fluvoxamine-theophylline DDI, the $K_{i, \text{in vitro}} = 11 \text{ nmol/l}$ for fluvoxamine inhibition of CYP1A2 reported by Karjalainen et al. ²⁵ was corrected according to equations (6) and (7) and the resulting $K_{i, \text{in vivo}} = 10 \text{ nmol/l}$ was used as K_{ic} and K_{iu} to model the mixed-inhibition of CYP1A2 by fluvoxamine.

To adequately describe the plasma concentration-time profile of the control group in the study of Rasmussen et al. ¹²³, the CYP1A2 k_{cat} of the final theophylline model (6.48 min^{-1}) was adjusted to 16.01 min^{-1} to match the control group of this study. The predicted DDI AUC ratio changed from 2.18 to 3.10. To model the fluvoxamine-theophylline interaction study of Orlando et al. ¹²⁴, the original CYP1A2 k_{cat} of the theophylline PBPK model was used.

The fluvoxamine-theophylline DDI model shows a good performance predicting the theophylline plasma concentrations for the first 48 h after dosing. After 48 h, the theophylline clearance is overpredicted (see Figure S7a, lower panel). This limitation only causes negligible changes in theophylline AUC, but should be considered during the application of the fluvoxamine-theophylline DDI model.

Plots of population predicted compared to observed theophylline plasma concentration-time profiles of all fluvoxamine-theophylline DDI studies obtained from literature are shown in linear and semilogarithmic plots in Figure S7a. A comparison of predicted to observed DDI AUC ratios and DDI C_{max} ratios is shown in Figure S7b. Details on the two clinical studies are summarized in Table S7a. Predicted and observed AUC and C_{max} values, DDI ratios and GMFE values are summarized in Table S7b.

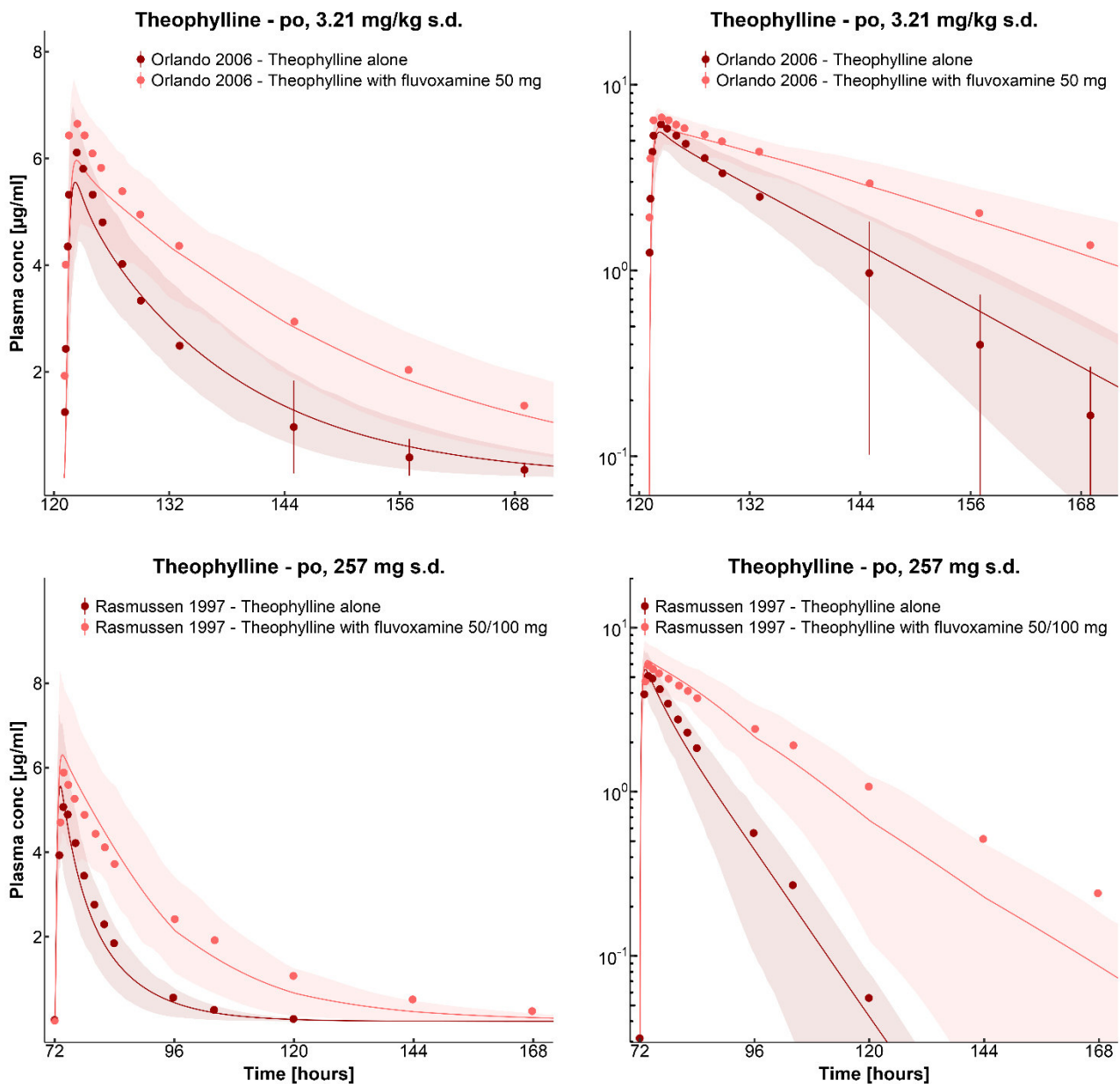


Figure S7a. Fluvoxamine-theophylline DDI. Population predictions of theophylline plasma concentration-time profiles compared to observed data of the fluvoxamine-theophylline interaction in linear (left panel) and semilogarithmic plots (right panel). Observed data are shown as dark red (control) or red dots (DDI) \pm SD. Population simulation arithmetic means are shown as dark red (control) or red lines (DDI); the shaded areas illustrate the respective 68% population prediction intervals. Details on dosing regimens, study populations and literature references are listed in Table S7a. Predicted and observed PK parameters are summarized in Table S7b.

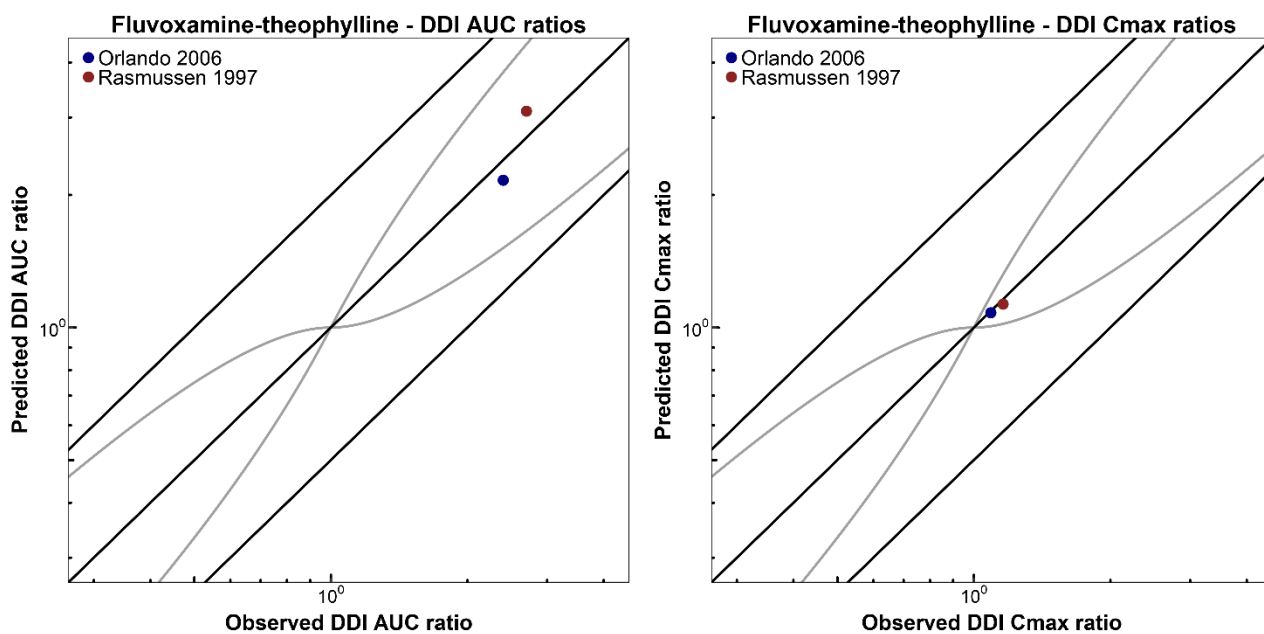


Figure S7b. Correlation of predicted to observed DDI AUC ratios and DDI C_{max} ratios. The left panel illustrates the predicted compared to observed DDI AUC ratios, the right panel illustrates the predicted compared to observed DDI C_{max} ratios of the fluvoxamine-theophylline DDI. The line of identity and the 0.5- to 2.0-fold acceptance limits are shown as straight black lines. The curved grey lines are the prediction acceptance limits proposed by Guest et al.¹²⁵. Details on dosing regimens, study populations and literature references are listed in Table S7a. Predicted and observed PK parameters are summarized in Table S7b.

Table S7a. Clinical studies of the fluvoxamine-theophylline DDI

Fluvoxamine administration	Theophylline administration	Day and time of victim drug administration	n	Age [years]	Weight [kg]	Females [%]	CYP2D6 phenotype [%]	Smokers [%]	Reference
Dose	Route	Dose	Route						
50 mg	po (tab), q.d. (D1-2)	3.21 mg/kg	po (sol), s.d.	D6 (+1 h)	10	42 ± 14	72 ± 8	0	Orlando 2006 ¹²⁴
	po (tab), b.i.d. (D3-8)								
50 mg	po (tab), q.d. (D1)	257 mg	po (tab), s.d.	D4 (-)	12	23 (22-30)	-	0	Rasmussen 1997 ¹²³
100 mg	po (tab), q.d. (D2-6)								

CYP2D6, cytochrome P450 2D6; D, days of administration; n, number of individuals studied; po, oral; Route, route of administration; sol, solution; tab, tablet; -, no data available. Values are means ± standard deviation or ranges.

Table S7b. AUC and C_{max} values, DDI ratios and GMFE values of the fluvoxamine-theophylline DDI

Theophylline	AUC obs [µg*hours/ml]	AUC pred [µg*hours/ml]	Pred/Obs	C _{max} obs [µg/ml]	C _{max} pred [µg/ml]	Pred/Obs	Reference
			DDI AUC ratio			DDI C _{max} ratio	
3.21 mg/kg po, s.d.	83.06	80.00		6.11	5.97		Orlando 2006 ¹²⁴
3.21 mg/kg po, s.d. with fluvoxamine 50 mg po, q.d./b.i.d.	199.76	173.09		6.65	6.43		Orlando 2006 ¹²⁴
Ratio DDI/control	2.40	2.16	0.90	1.09	1.08	0.99	
Theophylline							
257 mg po, s.d.	59.91	49.63		5.07	6.51		Rasmussen 1997 ¹²³
257 mg po, s.d. with fluvoxamine 50/100 mg po, q.d.	161.72	154.10		5.89	7.34		Rasmussen 1997 ¹²³
Ratio DDI/control	2.70	3.10	1.15	1.16	1.13	0.97	
	GMFE (range)		1.13 (1.11-1.15)	1.02 (1.01-1.03)			
	Pred/Obs within twofold		2/2	2/2			

AUC, area under the plasma concentration-time curve; AUC values are 0-∞; observed AUC and C_{max} values were calculated; C_{max} peak plasma concentration; DDI, drug-drug interaction; GMFE, geometric mean fold error; obs, observed; po, oral; pred, predicted.

3.3 Rifampicin-theophylline DDI

To predict the rifampicin-theophylline DDI, a previously developed PBPK model of rifampicin² was expanded with parameters to model the induction of CYP1A2 and CYP2E1. Induction of CYP1A2 and CYP2E1 was implemented using the same in vivo half-maximal induction concentration (EC_{50}) of 0.34 $\mu\text{mol/l}$ as reported for the induction of CYP3A4^{83,84}. The maximal induction effect (E_{max}) for CYP1A2 was set to 0.65⁹⁰ and for CYP2E1 to 0.8⁹¹.

To adequately describe the plasma concentration-time profile of the control group in the study of Boyce et al.¹²⁶, the CYP1A2 k_{cat} of the final theophylline model (6.48 min^{-1}) was adjusted to 9.18 min^{-1} to match the control group of this study. The change in the predicted DDI AUC ratio was negligibly small, from 0.74 to 0.71. To model the rifampicin-theophylline interaction studies of Powell-Jackson et al.¹²⁷, the CYP1A2 k_{cat} of the theophylline PBPK model was used.

In one of the reported DDI studies, theophylline was administered orally as a sustained release formulation (Phyllocontin®)¹²⁷. To model this study, the effect of the sustained release on the plasma concentration-time profile was implemented using a Weibull function to slow down the theophylline dissolution¹²⁸. Fitting of the Weibull parameters to describe the theophylline plasma concentration-time profile of the control group resulted in a dissolution time of 113.49 min (50% dissolved) and a shape of 1.51, which were then implemented to simulate the theophylline PK of the control group and of the rifampicin-theophylline co-administration group of this study¹²⁷.

Plots of population predicted compared to observed theophylline plasma concentration-time profiles of all rifampicin-theophylline DDI studies obtained from literature are shown in linear and semilogarithmic plots in Figure S8a. A comparison of predicted to observed DDI AUC ratios and DDI C_{max} ratios is shown in Figure S8b. Details on the clinical studies are summarized in Table S8a. Predicted and observed AUC and C_{max} values, DDI ratios and GMFE values are summarized in Table S8b.

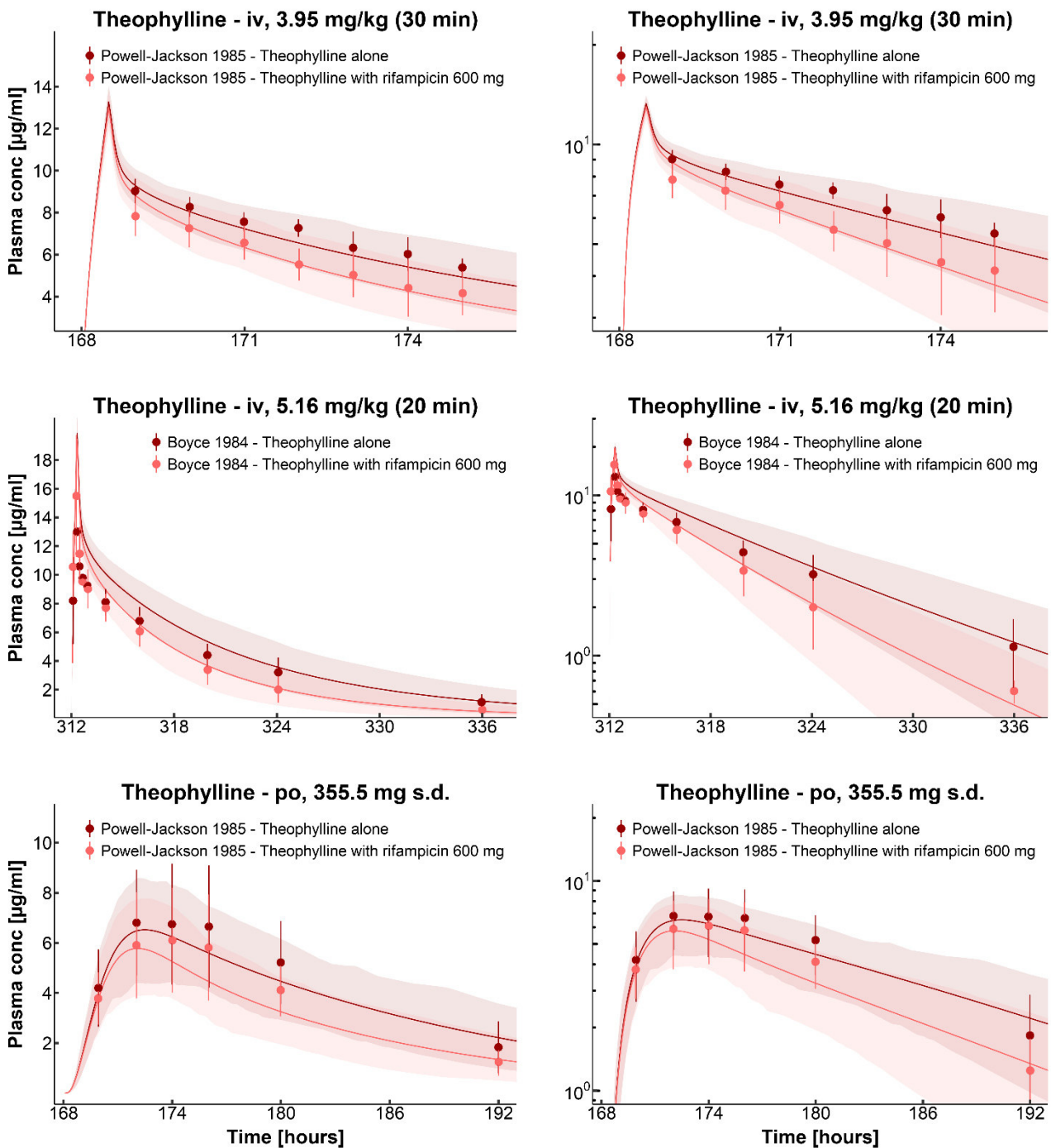


Figure S8a. Rifampicin-theophylline DDI. Population predictions of theophylline plasma concentration-time profiles compared to observed data of the rifampicin-theophylline interaction in linear (left panel) and semilogarithmic plots (right panel). Observed data are shown as dark red (control) or red dots (DDI) \pm SD. Population simulation arithmetic means are shown as dark red (control) or red lines (DDI); the shaded areas illustrate the respective 68% population prediction intervals. Details on dosing regimens, study populations and literature references are listed in Table S8a. Predicted and observed PK parameters are summarized in Table S8b.

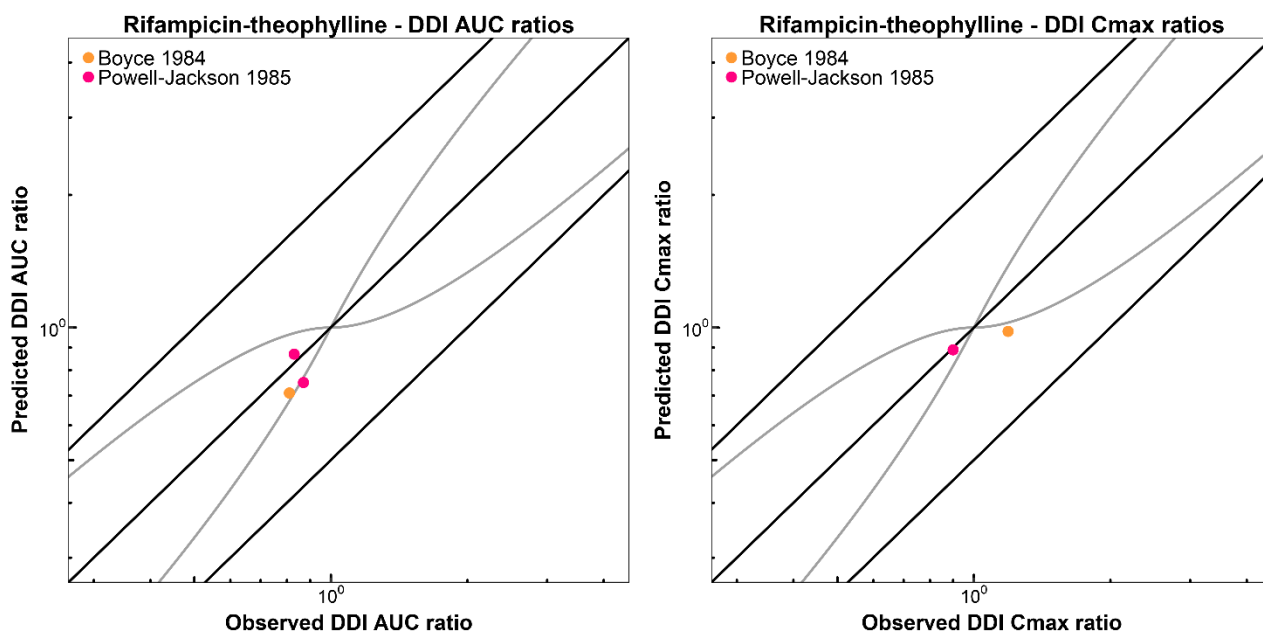


Figure S8b. Correlation of predicted to observed DDI AUC ratios and DDI C_{max} ratios. The left panel illustrates the predicted compared to observed DDI AUC ratios, the right panel illustrates the predicted compared to observed DDI C_{max} ratios of the rifampicin-theophylline DDI. The line of identity and the 0.5- to 2.0-fold acceptance limits are shown as straight black lines. The curved grey lines are the prediction acceptance limits proposed by Guest et al.¹²⁵. Details on dosing regimens, study populations and literature references are listed in Table S8a. Predicted and observed PK parameters are summarized in Table S8b.

Table S8a. Clinical studies of the rifampicin-theophylline DDI

Rifampicin administration	Theophylline administration	Day and time of victim drug administration	<i>n</i>	Age [years]	Weight [kg]	Females [%]	Smokers [%]	Reference
<i>Dose</i>	<i>Route</i>	<i>Dose</i>	<i>Route</i>					
600 mg po (caps), q.d. (D1-D7)	3.95 mg/kg iv (30 min), s.d.	D8 (-)	8	19-36	-	0	0	Powell-Jackson 1985 ¹²⁷
600 mg po (caps), q.d. (D1-D14)	5.19 mg/kg iv (20 min), s.d.	D14 (-)	10	30 (23-42)	80 (69-89)	0	0	Boyce 1984 ¹²⁶
600 mg po (caps), q.d. (D1-D7)	355.5 mg po (-), s.d.	D8 (-)	7	19-36	-	0	0	Powell-Jackson 1985 ¹²⁷

caps, capsule; D, days of administration; iv, intravenous; *n*, number of individuals studied; po, oral; Route, route of administration; -, no data available. Values are means and ranges.

Table S8b. AUC and C_{max} values, DDI ratios and GMFE values of the rifampicin-theophylline DDI

	AUC obs [µg*hours/ml]	AUC pred [µg*hours/ml]	DDI AUC ratio	C _{max} obs [µg/ml]	C _{max} pred [µg/ml]	Pred/Obs DDI C _{max} ratio	Reference
Theophylline							
3.95 mg/kg iv (30 min)	37.06 ^a	49.94 ^a		-	13.57		Powell-Jackson 1985 ¹²⁷
3.95 mg/kg iv (30 min) with rifampicin 600 mg po, q.d.	30.59 ^a	43.69 ^a		-	13.28		Powell-Jackson 1985 ¹²⁷
Ratio DDI/control	0.83	0.87	1.05	-	0.98	-	
Theophylline							
5.19 mg/kg iv (20 min)	96.49 ^b	107.00 ^b		13.00	20.50		Boyce 1984 ¹²⁶
5.19 mg/kg iv (20 min) with rifampicin 600 mg po, q.d.	77.69 ^b	76.28 ^b		15.50	19.64		Boyce 1984 ¹²⁶
Ratio DDI/control	0.81	0.71	0.89	1.19	0.98	0.82	
Theophylline							
355.5 mg po, s.d.	61.99 ^b	94.94 ^b		6.81	6.50		Powell-Jackson 1985 ¹²⁷
355.5 mg po, s.d. with rifampicin 600 mg po, q.d.	53.79 ^b	71.42 ^b		6.11	5.77		Powell-Jackson 1985 ¹²⁷
Ratio DDI/control	0.87	0.75	0.87	0.90	0.89	0.99	
	GMFE (range)		1.12 (1.05-1.16)			1.11 (1.01-1.21)	
	Pred/Obs within twofold		3/3			2/2	

AUC, area under the plasma concentration-time curve; AUC values are ^a AUC₀₋₇ or ^b AUC₀₋₂₄; observed AUC and C_{max} values were calculated; C_{max}, peak plasma concentration; DDI, drug-drug interaction; GMFE, geometric mean fold error; iv, intravenous; obs, observed; po, oral; pred, predicted; -, no data available.

3.4 Fluvoxamine-caffeine DDI

To predict the fluvoxamine-caffeine DDI, mixed-inhibition of CYP1A2 by fluvoxamine was modelled using K_{ic} and K_{iu} values of 10 nmol/l as described for the fluvoxamine-theophylline DDI.

To adequately describe the plasma concentration-time profiles of the control groups in the studies of Jeppesen et al.¹²⁹ and Culm-Merdek et al.¹³⁰, the CYP1A2 k_{cat} of the previously developed caffeine PBPK model (1.01 min^{-1})¹ was adjusted to 0.96 min^{-1} and 0.74 min^{-1} , respectively, to match the control groups of these studies. The predicted DDI AUC ratio for Jeppesen et al.¹²⁹ remained the same, the predicted DDI AUC ratio for the study of Culm-Merdek et al.¹³⁰ changed from 6.91 to 7.03.

Plots of population predicted compared to observed caffeine plasma concentration-time profiles of all fluvoxamine-caffeine DDI studies obtained from literature are shown in linear and semilogarithmic plots in Figure S9a. A comparison of predicted to observed DDI AUC ratios and DDI C_{max} ratios is shown in Figure S9b. Details on the two clinical studies are summarized in Table S9a. Predicted and observed AUC and C_{max} values, DDI ratios and GMFE values are summarized in Table S9b.

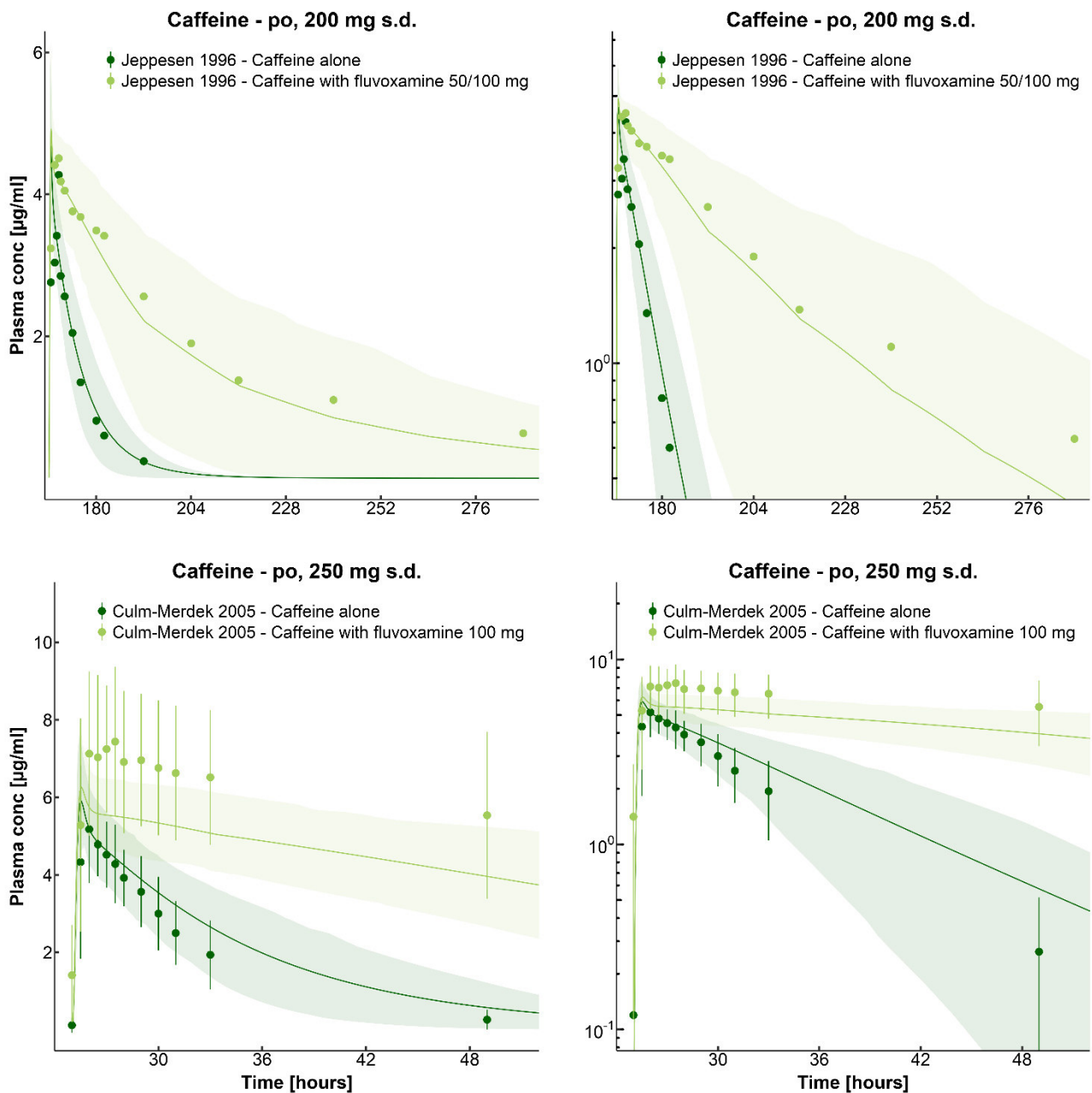


Figure S9a. Fluvoxamine-caffeine DDI. Population predictions of caffeine plasma concentration-time profiles compared to observed data of the fluvoxamine-caffeine interaction in linear (left panel) and semilogarithmic plots (right panel). Observed data are shown as dark green (control) or green dots (DDI) \pm SD. Population simulation arithmetic means are shown as dark green (control) or green lines (DDI); the shaded areas illustrate the respective 68% population prediction intervals. Details on dosing regimens, study populations and literature references are listed in Table S9a. Predicted and observed PK parameters are summarized in Table S9b.

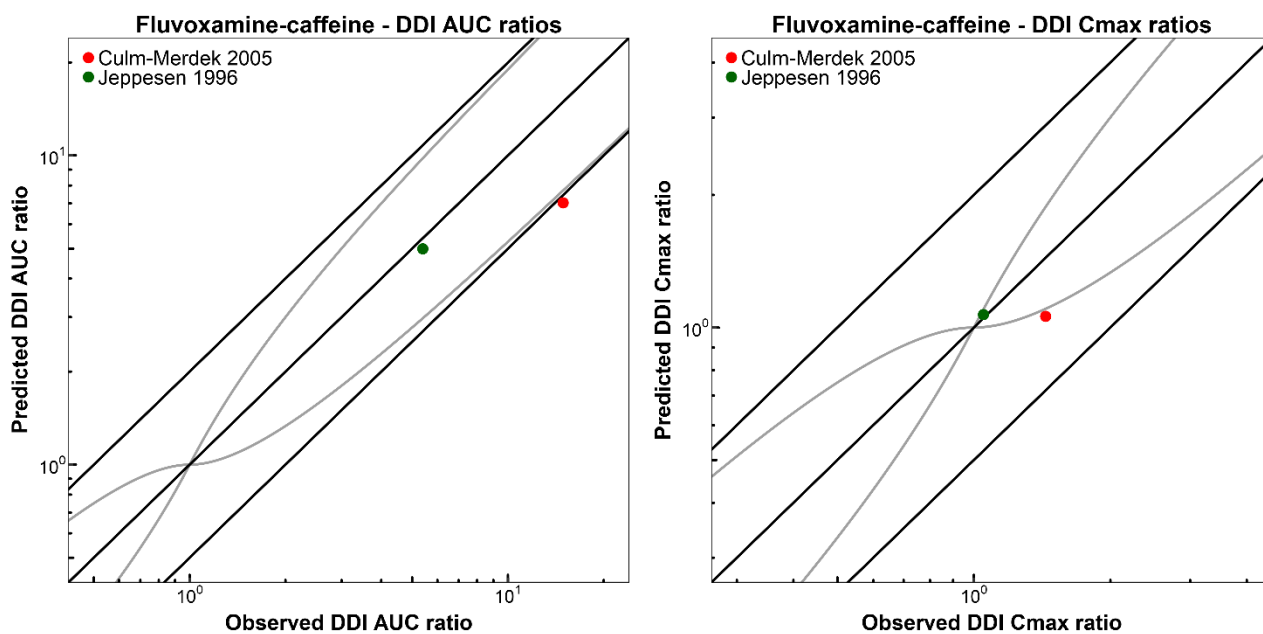


Figure S9b. Correlation of predicted to observed DDI AUC ratios and DDI C_{max} ratios. The left panel illustrates the predicted compared to observed DDI AUC ratios, the right panel illustrates the predicted compared to observed DDI C_{max} ratios of the fluvoxamine-caffeine DDI. The line of identity and the 0.5- to 2.0-fold acceptance limits are shown as straight black lines. The curved grey lines are the prediction acceptance limits proposed by Guest et al. ¹²⁵. Details on dosing regimens, study populations and literature references are listed in Table S9a. Predicted and observed PK parameters are summarized in Table S9b.

Table S9a. Clinical studies of the fluvoxamine-caffeine DDI

Fluvoxamine administration	Caffeine administration	Day and time of victim drug administration	<i>n</i>	Age [years]	Weight [kg]	Females [%]	CYP2D6 phenotype [%]	Smokers [%]	Reference
<i>Dose</i>	<i>Route</i>	<i>Dose</i>	<i>Route</i>						
50 mg po (tab), q.d. (D1-4)	200 mg po (tab), s.d.	D8 (-)	8	27 (21-33)	-	0	EM: 100	0	Jeppesen 1996 ¹²⁹
100 mg po (tab), q.d. (D5-12)									
100 mg po (tab), b.i.d.	250 mg po (tab), s.d.	D2 (+1.5 h)	7	50	82	14	-	-	Culm-Merdek 2005 ¹³⁰

CYP2D6, cytochrome P450 2D6; D, days of administration; EM, extensive metabolizers; *n*, number of individuals studied; po, oral; Route, route of administration; tab, tablet; -, no data available. Values are means and ranges.

Table S9b. AUC and C_{max} values, DDI ratios and GMFE values of the fluvoxamine-caffeine DDI

	AUC obs [µg*hours/ml]	AUC pred [µg*hours/ml]	Pred/Obs	C _{max} obs [µg/ml]	C _{max} pred [µg/ml]	Pred/Obs	DDI C _{max} ratio	Reference
			ratio			ratio		
Caffeine								
200 mg po, s.d.	31.50	29.07		4.27	5.09			Jeppesen 1996 ¹²⁹
200 mg po, s.d. with fluvoxamine 50/100 mg po, q.d.	170.00	145.12		4.51	5.45			Jeppesen 1996 ¹²⁹
Ratio DDI/control	5.40	4.99	0.92	1.06	1.07		1.01	
Caffeine								
250 mg po, s.d.	46.48	46.53		5.18	5.74			Culm-Merdek 2005 ¹³⁰
250 mg po, s.d. with fluvoxamine 100 mg po, b.i.d.	692.51	326.96		7.44	6.07			Culm-Merdek 2005 ¹³⁰
Ratio DDI/control	14.90	7.03	0.47	1.44	1.06		0.74	
		GMFE (range)	1.51 (1.08-2.12)				1.17 (1.01-1.36)	
		Pred/Obs within twofold	1/2				2/2	

AUC, area under the plasma concentration-time curve; AUC values are 0-∞; observed AUC and C_{max} values were calculated; C_{max}, peak plasma concentration; DDI, drug-drug interaction; GMFE, geometric mean fold error; obs, observed; po, oral; pred, predicted.

3.5 Fluvoxamine-midazolam DDI

To predict the fluvoxamine-midazolam DDI, competitive inhibition of CYP3A4 by fluvoxamine was modelled using a K_i of 1.6 $\mu\text{mol/l}$. This value was calculated with equations (6) and (7) using in vitro data from Olesen et al.²⁷ and dividing the calculated value by 10 as described by Yao et al.²⁶.

To adequately describe the plasma concentration-time profile of the control group in the fluvoxamine-midazolam study of Lam et al.¹³¹, the CYP3A4 k_{cat} of the previously developed midazolam PBPK model (13.0 min^{-1})² was adjusted to 15.6 min^{-1} to match the control group of this study. The change in the predicted DDI AUC ratio was negligibly small, from 1.45 to 1.51.

Plots of population predicted compared to observed midazolam plasma concentration-time profiles of the only fluvoxamine-midazolam DDI study available from literature are shown in linear and semilogarithmic plots in Figure S10a. A comparison of predicted to observed DDI AUC ratios and DDI C_{max} ratios is shown in Figure S10b. Details on the clinical study are summarized in Table S10a. Predicted and observed AUC and C_{max} values, DDI ratios and GMFE values are summarized in Table S10b.

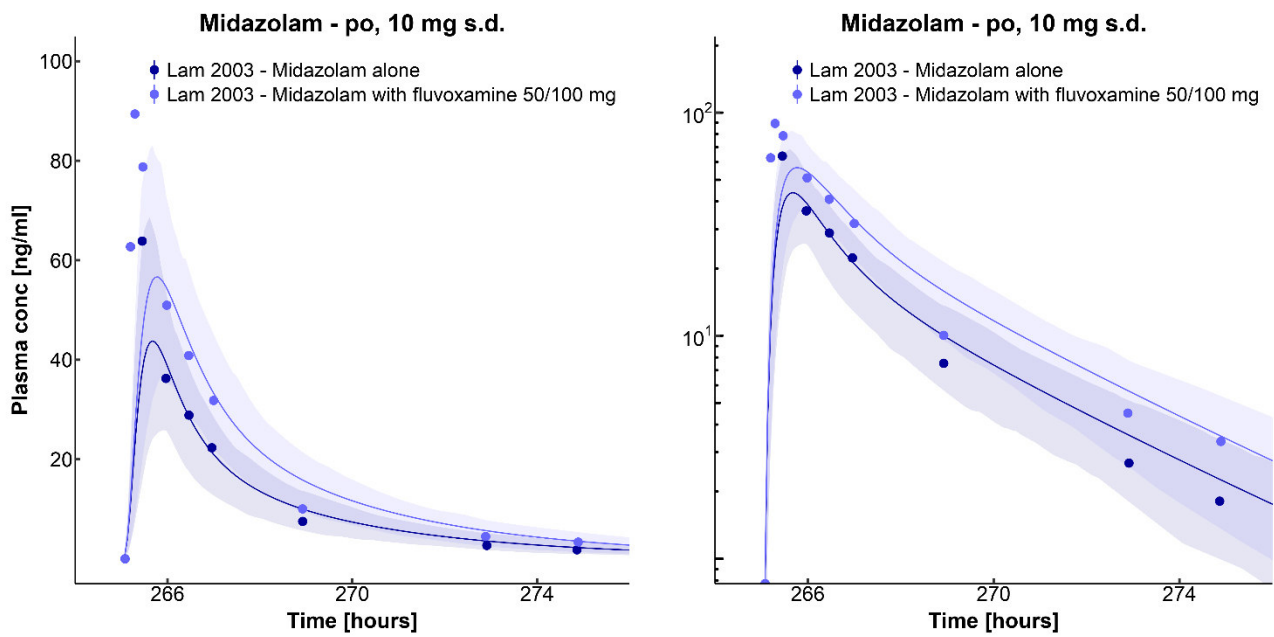


Figure S10a. Fluvoxamine-midazolam DDI. Population predictions of midazolam plasma concentration-time profiles compared to observed data of the fluvoxamine-midazolam interaction in linear (left panel) and semilogarithmic plots (right panel). Observed data are shown as dark blue (control) or blue dots (DDI). Population simulation arithmetic means are shown as dark blue (control) or blue lines (DDI); the shaded areas illustrate the respective 68% population prediction intervals. Details on dosing regimens, study populations and literature references are listed in Table S10a. Predicted and observed PK parameters are summarized in Table S10b.

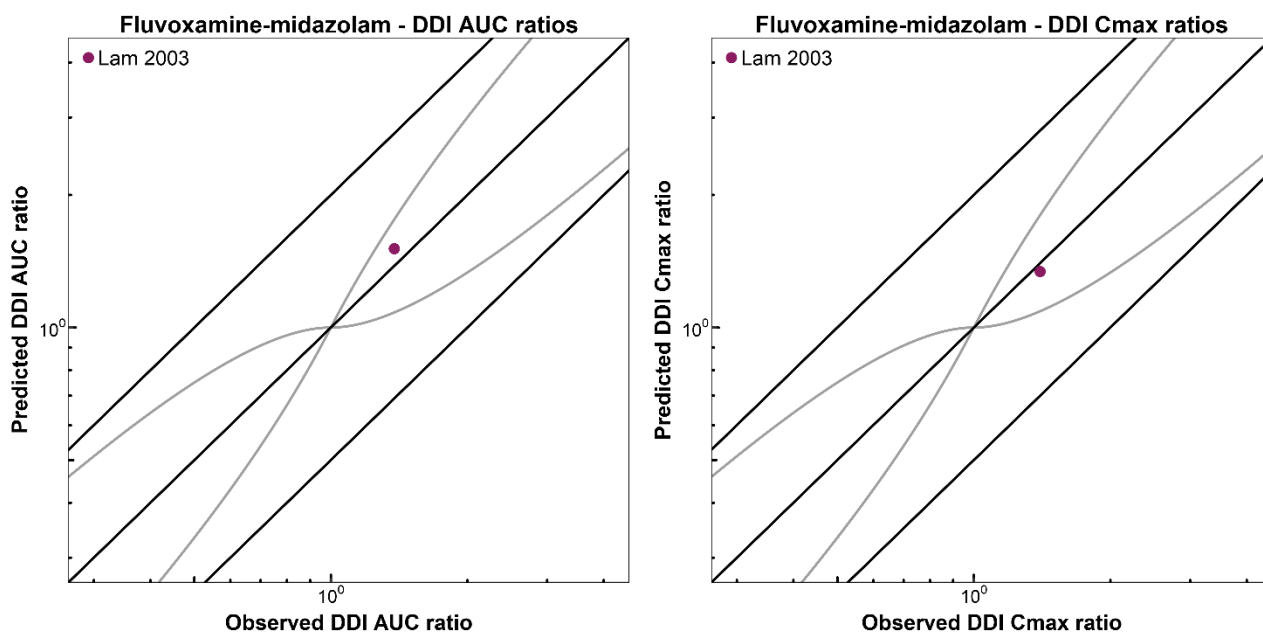


Figure S10b. Correlation of predicted to observed DDI AUC ratios and DDI C_{max} ratios. The left panel illustrates the predicted compared to observed DDI AUC ratios, the right panel illustrates the predicted compared to observed DDI C_{max} ratios of the fluvoxamine-midazolam DDI. The line of identity and the 0.5- to 2.0-fold acceptance limits are shown as straight black lines. The curved grey lines are the prediction acceptance limits proposed by Guest et al.¹²⁵. Details on dosing regimens, study populations and literature references are listed in Table S10a. Predicted and observed PK parameters are summarized in Table S10b.

Table S10a. Clinical studies of the fluvoxamine-midazolam DDI

Fluvoxamine administration		Midazolam administration		Day and time of victim drug administration	<i>n</i>	Age [years]	Weight [kg]	Females [%]	CYP2D6 phenotype [%]	Smokers [%]	Reference
<i>Dose</i>	<i>Route</i>	<i>Dose</i>	<i>Route</i>								
50 mg	po (tab), b.i.d. (D1-6)	10 mg	po (sol), s.d.	D12 (+1 h)	40	34 ± 8	72 ± 14	58	-	-	Lam 2003 ¹³¹
100 mg	po (tab), b.i.d. (D7-12)										

CYP2D6, cytochrome P450 2D6; D, days of administration; *n*, number of individuals studied; po, oral; Route, route of administration; sol, solution; tab, tablet; -, no data available. Values are means ± standard deviation.

Table S10b. AUC and C_{max} values, DDI ratios and GMFE values of the fluvoxamine-midazolam DDI

	AUC [ng*hours/ml]		AUC pred [ng*hours/ml]		Pred/Obs		C _{max}		Pred/Obs		Reference
	obs	pred	obs	pred	DDI AUC ratio	DDI C _{max} ratio	obs [ng/ml]	pred [ng/ml]	DDI C _{max} ratio	DDI C _{max} ratio	
Midazolam											
10 mg po, s.d.	128.43	100.07					63.85	41.87			Lam 2003 ¹³¹
10 mg po, s.d. with fluvoxamine 50 mg po, b.i.d.	177.44	151.32					89.39	55.91			Lam 2003 ¹³¹
Ratio DDI/control	1.38	1.51			1.09		1.40	1.34		0.95	
	GMFE 1.09		GMFE 1.09							1.04	
	Pred/Obs within twofold 1/1		Pred/Obs within twofold 1/1							1/1	

AUC, area under the plasma concentration-time curve; AUC values are AUC₀₋₁₀; observed AUC and C_{max} values were calculated; C_{max}, peak plasma concentration; DDI, drug-drug interaction; GMFE, geometric mean fold error; obs, observed; po, oral; pred, predicted.

4 Population pharmacokinetic modelling of fluvoxamine

4.1 Objectives

The objectives of this analysis were (1) the development of a population pharmacokinetic (PopPK) model of fluvoxamine after single oral administration in healthy volunteers, and (2) to evaluate the influence of CYP2D6 phenotype and cigarette smoking on fluvoxamine pharmacokinetics. Furthermore, it was examined which was the best predictor of the effect of CYP2D6 phenotype on fluvoxamine clearance: dextromethorphan metabolic ratio (MR) (linear or logarithmic values) or CYP2D6 phenotype used as categorical covariate.

4.2 Methods

Dataset

Data from two studies assessing the pharmacokinetics of fluvoxamine in healthy volunteers were used for the population pharmacokinetic analysis. In the study of Spigset et al. 1997¹⁷ the relationship between fluvoxamine pharmacokinetics and CYP2D6 phenotype (extensive or poor metabolizers) was investigated, whereas in the study of Spigset et al. 1995¹⁶ the effect of cigarette smoking on fluvoxamine pharmacokinetics was examined. In both studies fluvoxamine was administered orally as a single dose of 50 mg to healthy female and male volunteers. Blood samples were taken pre-dose and 1, 2, 3, 4, 5, 6, 7, 8, 10, 12, 24, 32, and 48 h after dosing. Plasma levels of fluvoxamine were determined by HPLC; the lower limit of quantification was 0.5 nmol/l.

Model building and evaluation

Population analysis, model evaluation and simulation were performed using non-linear mixed-effects modelling techniques implemented in NONMEM. These allow estimation of population medians for pharmacokinetic model parameters with simultaneous quantification of interindividual variability (IIV) and residual (unexplained) variability. Model selection was based on the objective function value (OFV) provided by NONMEM, visual inspection of goodness of fit plots, precision of parameter estimates and visual predictive checks. A nested model was considered superior to another when the OFV was reduced by 3.84 units (χ^2 test statistic, $p < 0.05$, 1 degree of freedom). The two studies were analyzed separately using ADVAN6. The First-Order Conditional Estimation with Interaction (FOCE-I) method was applied. The structural base model building was performed sequentially for each study; linear one-, two- and three-compartment models were tested. Different absorption models, such as zero-order, first-order or mixed parallel zero- and first-order absorption processes were evaluated. Absorption lag was tested using a lag time or transit compartments. Saturable processes on absorption rates as well as on clearance were evaluated using Michaelis-Menten kinetics.

Based on the structural base model, IIVs were modelled exponentially and evaluated univariately. IIVs were added to the model if they improved the model in a statistically significant manner and if the parameter estimates of the model remained stable.

The impact of CYP2D6 phenotype and smoking status as covariates was tested on absorption and clearance parameters of the fluvoxamine PopPK models. CYP2D6 phenotype was analyzed as continuous or as categorical covariate, using the dextromethorphan metabolic ratios as reported for each participant. Smoking status was analyzed as categorical covariate.

4.3 Results

Study population

The population of the study by Spigset et al. 1997¹⁷ consisted of 10 young healthy volunteers, that were categorized by CYP2D6 phenotype. The only female and 4 of the male volunteers were phenotyped as CYP2D6 extensive metabolizers, whereas 5 males were characterized as CYP2D6 poor metabolizers. All subjects were non-smokers. Mean age was 25 years and bodyweight ranged from 55 to 86 kg¹⁷.

The population of the study by Spigset et al. 1995¹⁶ consisted of 24 young healthy volunteers, whereof 12 were non-smokers and 12 were smokers, with 5 females and 7 males in each group. All volunteers were characterized as CYP2D6 extensive metabolizers. Mean age was 36.5 years and bodyweight ranged from 51 to 95 kg¹⁶.

In each study one sample was missing and excluded from analysis. Overall, 139 and 311 fluvoxamine post-dose plasma concentrations were available for analysis, from the studies of Spigset et al. 1997¹⁷ and Spigset et al. 1995¹⁶, respectively.

Population pharmacokinetic model

The pharmacokinetics of fluvoxamine in both studies were best described by a one-compartment model with zero-order absorption and linear elimination from the central compartment. As shown in Table S11, parameter estimates were precise with low to moderate relative standard errors. Diagnostic plots as presented by goodness of fit plots (Figure S11a) and visual predictive checks (Figure S11b) demonstrate that the data is adequately described.

Parameter estimates for both studies are listed in Table S11. Zero-order input time differed slightly between both studies with 1.53 hours and 3.51 hours, respectively. Absorption lag time was estimated at 2.75 hours and 1.79 hours, respectively. The volumes of distribution were estimated at 2610 l/F and 3030 l/F. Fluvoxamine was cleared from the systemic circulation with 147 l/h/F and 133 l/h/F, respectively. IIV was mild to moderate with 29 to 53 %CV on the two different volumes of distribution and 49 %CV for both studies on clearance. Residual variability was best described with a combined error model. Although the additive error is very low, it was necessary to adequately describe the data.

The impact of CYP2D6 phenotype on total clearance of fluvoxamine was best described as a categorical covariate. Volunteers phenotyped as CYP2D6 poor metabolizers had a 22% lower total clearance compared to extensive metabolizers (mean CL = 114 l/h vs. 147 l/h, p-value < 0.001). To evaluate the impact of smoking on total clearance of fluvoxamine, smoking status was incorporated as a categorical covariate. Fluvoxamine total clearance was approximately 28% higher in smokers compared to non-smokers (mean CL = 170 l/h vs. 133 l/h, p-value < 0.001).

Simulations of the fluvoxamine plasma concentrations over time illustrate the differences in fluvoxamine elimination between CYP2D6 extensive and poor metabolizers as well as between non-smokers and smokers (Figure S11c).

Table S11. Parameter estimates of the final population pharmacokinetic models

Parameter	Spigset 1997		Spigset 1995		Description
	Value	RSE [%]	Value	RSE [%]	
Fixed effects					
D (h)	1.53	12	3.51	9	Zero-order input time
ALAG (h)	2.75	1	1.79	6	Absorption lag time
V _{Central} (l/F)	2610	11	3030	12	Volume of distribution over bioavailability
CL (l/h/F)	147	25	133	18	Total clearance over bioavailability
Random effects: Interindividual variability (IIV)					
IIV V _{Central} (%CV)	29	21	53	18	IIV in volume of distribution
IIV CL (%CV)	49	17	49	22	IIV in total clearance
Covariates					
CYP2D6 poor metabolism on CL	0.775	33	N/A	N/A	Impact of CYP2D6 poor metabolism on CL
Smoking on CL	N/A	N/A	1.28	21	Impact of smoking on CL
Residual variability					
Proportional (%)	34	13	49	18	Proportional residual error
Additive (nmol/ml)	(9*10 ⁻¹⁰)	N/A	3*10 ⁻⁶	50	Additive residual error

CL, total clearance; CV, coefficient of variation; RSE, relative standard error; N/A, not applicable. Parameter values in parentheses were fixed.

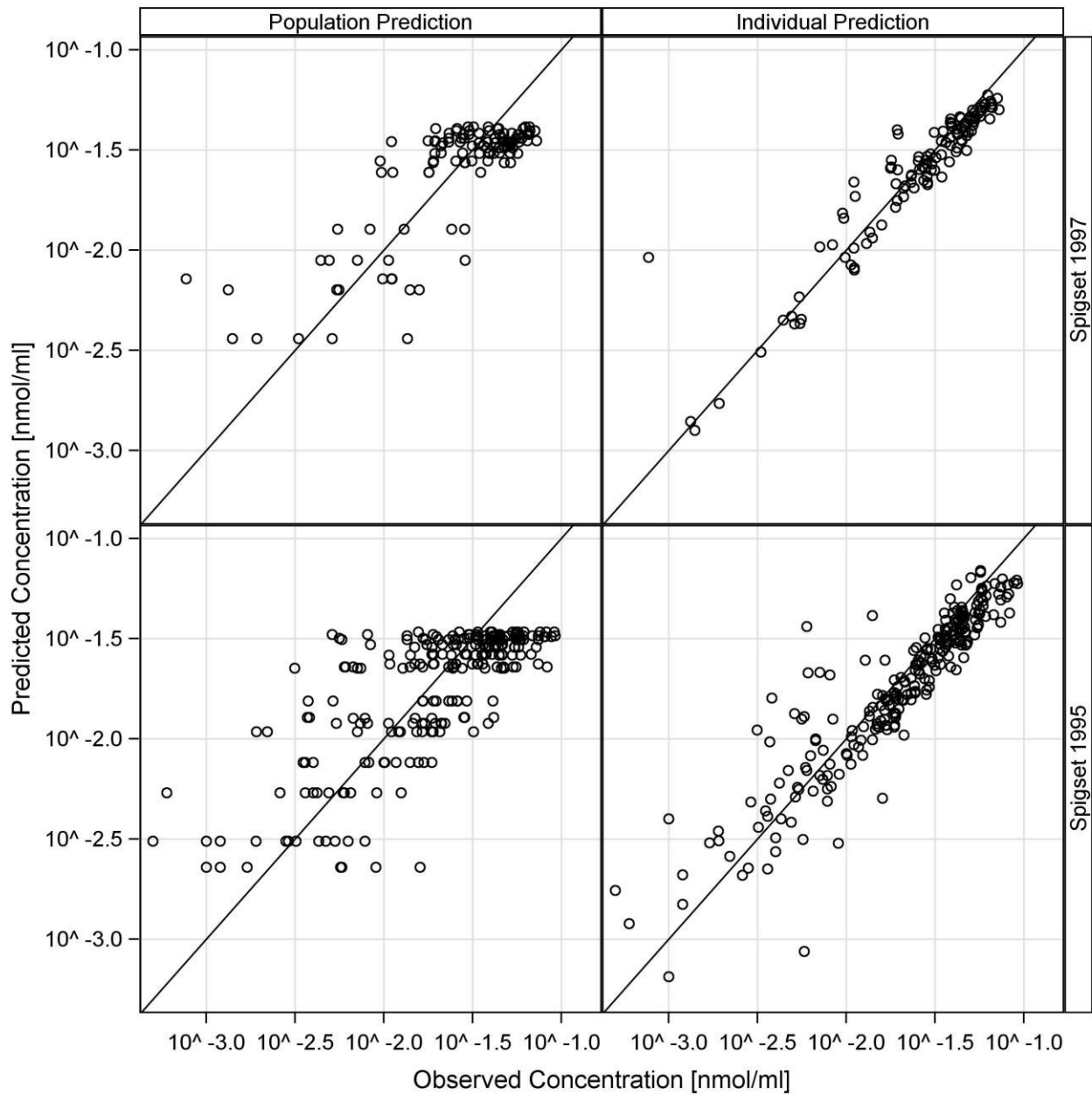


Figure S11a. Goodness of fit plots. Goodness of fit plots of the final population pharmacokinetic models for the studies of Spigset et al. 1997¹⁷ (upper panel) and Spigset et al. 1995¹⁶ (lower panel). Shown are population predictions (left panel) and individual predictions (right panel) versus observed plasma concentrations.

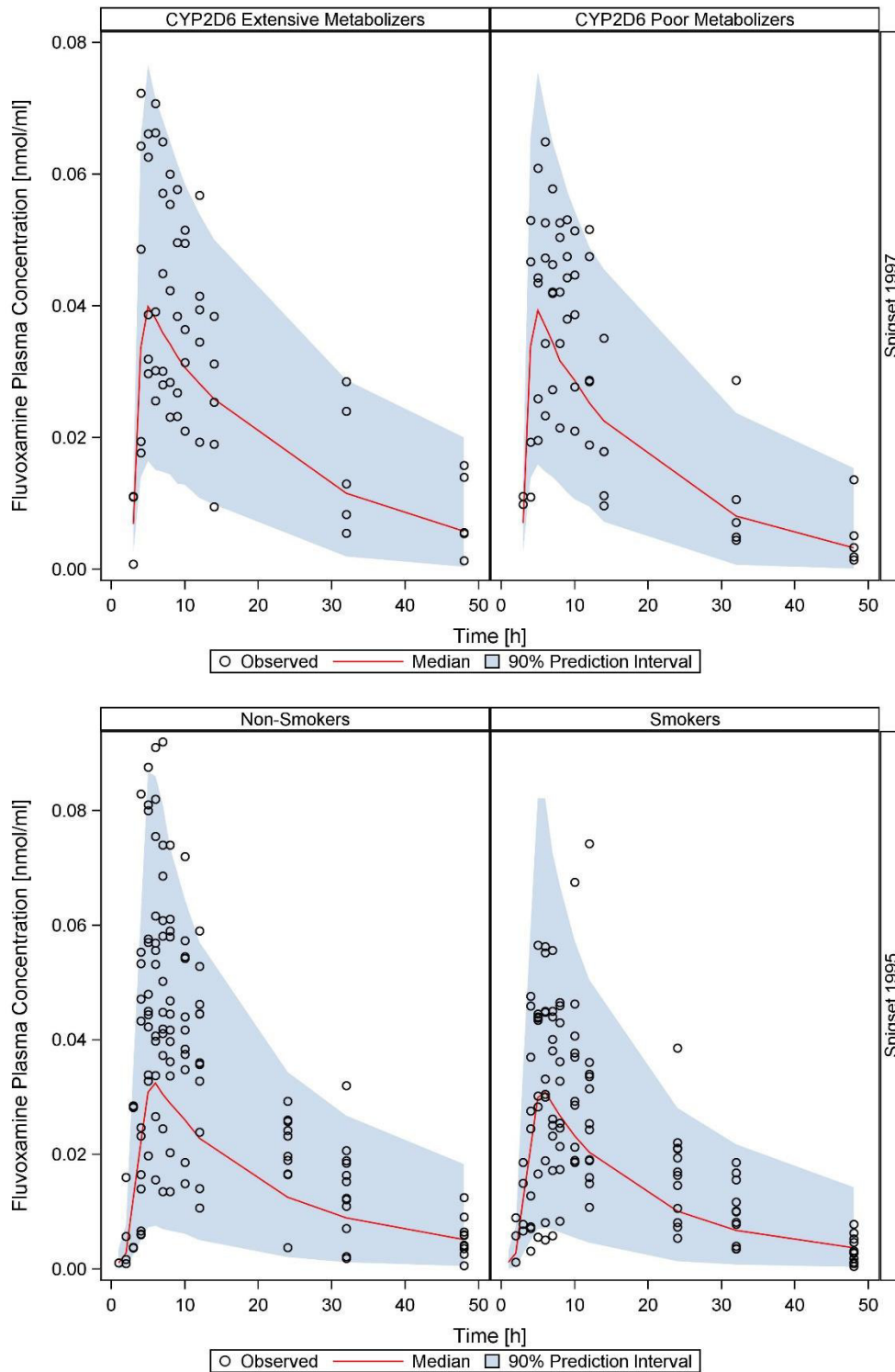


Figure S11b. Visual predictive checks. Visual predictive checks of the final population pharmacokinetic models for the studies of Spigset et al. 1997¹⁷ (upper panel) and Spigset et al. 1995¹⁶ (lower panel). Shown are observed plasma concentrations (open circles), median predicted plasma concentrations (solid red lines) and the 5th to 95th percentiles of simulated plasma concentrations in 1000 simulated subjects (shaded areas).

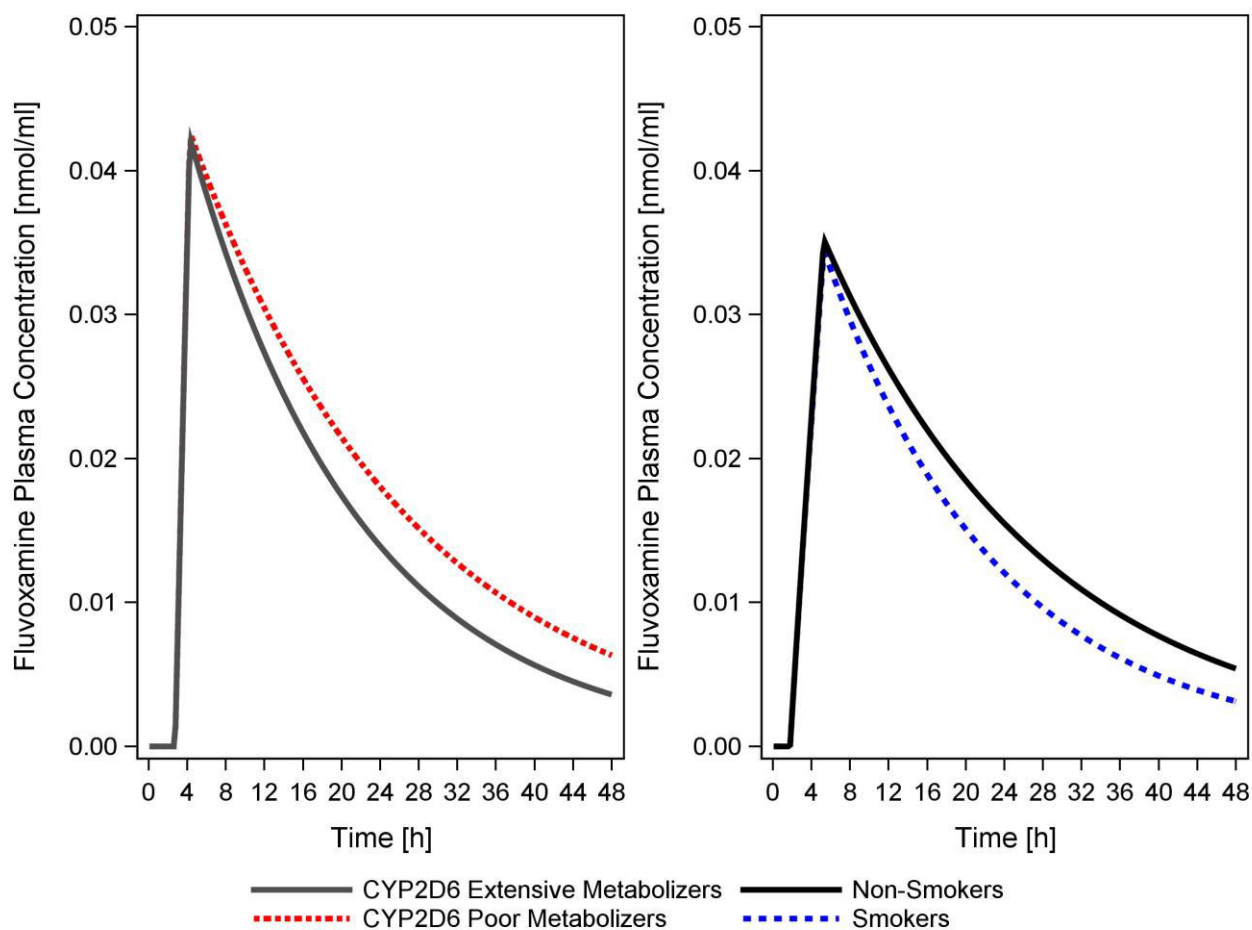


Figure S11c. Impact of CYP2D6 phenotype and smoking on fluvoxamine pharmacokinetics. Simulated plasma concentration-time profiles for single oral doses of 50 mg fluvoxamine using the final population pharmacokinetic models. In the left panel, the solid grey line illustrates the plasma concentrations of CYP2D6 extensive metabolizers; the dashed red line illustrates the simulated fluvoxamine plasma concentrations of CYP2D6 poor metabolizers. In the right panel, the solid black line illustrates the plasma concentrations of non-smokers; the dashed blue line illustrates the simulated fluvoxamine plasma concentrations of smokers.

5 References

1. Open Systems Pharmacology. OSP repository: Caffeine template model. <https://github.com/Open-Systems-Pharmacology/Example_Caffeine/blob/master/Caffeine.pksim5> (2018). Accessed 02 October 2018.
2. Hanke, N. *et al.* PBPK Models for CYP3A4 and P-gp DDI Prediction: A Modeling Network of Rifampicin, Itraconazole, Clarithromycin, Midazolam, Alfentanil, and Digoxin. *CPT Pharmacometrics Syst. Pharmacol.* **7**, 647–59 (2018).
3. Perucca, E., Gatti, G. & Spina, E. Clinical pharmacokinetics of fluvoxamine. *Clin. Pharmacokinet.* **27**, 175–90 (1994).
4. ANI Pharmaceuticals Inc. Fluvoxamine maleate - prescribing information. (2008).
5. Spigset, O., Granberg, K., Hägg, S., Söderström, E. & Dahlqvist, R. Non-linear fluvoxamine disposition. *Br. J. Clin. Pharmacol.* **45**, 257–63 (1998).
6. Miura, M. & Ohkubo, T. Identification of human cytochrome P450 enzymes involved in the major metabolic pathway of fluvoxamine. *Xenobiotica.* **37**, 169–79 (2007).
7. Spigset, O., Axelsson, S., Norström, A., Hägg, S. & Dahlqvist, R. The major fluvoxamine metabolite in urine is formed by CYP2D6. *Eur. J. Clin. Pharmacol.* **57**, 653–8 (2001).
8. DeBree, H., VanderSchoot, J. & Post, L. Fluvoxamine maleate; Disposition in man. *Eur. J. Drug Metab. Pharmacokinet.* **8**, 175–79 (1983).
9. U.S. Food and Drug Administration. Clinical Drug Interaction Studies - Study Design, Data Analysis, Implications for Dosing, and Labeling Recommendations. Draft Guidance for Industry. (2017).
10. Japanese Society of Hospital Pharmacists. 医薬品インタビューフォーム. (2015).
11. Christensen, M. *et al.* Low daily 10-mg and 20-mg doses of fluvoxamine inhibit the metabolism of both caffeine (cytochrome P4501A2) and omeprazole (cytochrome P4502C19). *Clin. Pharmacol. Ther.* **71**, 141–52 (2002).
12. DeVries, M., VanHarten, J., VanBemmel, P. & Raghoobar, M. Single and multiple oral dose fluvoxamine kinetics in young and elderly subjects. *Ther. Drug Monit.* **14**, 493–98 (1992).
13. Fukasawa, T. *et al.* Effects of caffeine on the kinetics of fluvoxamine and its major metabolite in plasma after a single oral dose of the drug. *Ther. Drug Monit.* **28**, 308–11 (2006).
14. Kunii, T. *et al.* Interaction study between enoxacin and fluvoxamine. *Ther. Drug Monit.* **27**, 349–53 (2005).
15. Orlando, R., DeMartin, S., Andrighetto, L., Floreani, M. & Palatini, P. Fluvoxamine pharmacokinetics in healthy elderly subjects and elderly patients with chronic heart failure. *Br. J. Clin. Pharmacol.* **69**, 279–86 (2010).
16. Spigset, O., Carleborg, L., Hedenmalm, K. & Dahlqvist, R. Effect of cigarette smoking on fluvoxamine pharmacokinetics in humans. *Clin. Pharmacol. Ther.* **58**, 399–403 (1995).
17. Spigset, O., Granberg, K., Hägg, S., Norström, A. & Dahlqvist, R. Relationship between fluvoxamine pharmacokinetics and CYP2D6/CYP2C19 phenotype polymorphisms. *Eur. J. Clin. Pharmacol.* **52**, 129–33 (1997).
18. VanHarten, J., VanBemmel, P., Dobrinska, M.R., Ferguson, R.K. & Raghoobar, M. Bioavailability of fluvoxamine given with and without food. *Biopharm. Drug Dispos.* **12**, 571–6 (1991).
19. Bahrami, G. & Mohammadi, B. Rapid and sensitive bioanalytical method for measurement of fluvoxamine in human serum using 4-chloro-7-nitrobenzofurazan as pre-column derivatization agent: application to a human pharmacokinetic study. *J. Chromatogr. B. Analyt. Technol. Biomed. Life Sci.* **857**, 322–6 (2007).
20. Labellarte, M. *et al.* Multiple-dose pharmacokinetics of fluvoxamine in children and adolescents. *J. Am. Acad. Child Adolesc. Psychiatry* **43**, 1497–505 (2004).
21. Fleishaker, J. & Hulst, L. A pharmacokinetic and pharmacodynamic evaluation of the

- combined administration of alprazolam and fluvoxamine. *Eur. J. Clin. Pharmacol.* **46**, 35–9 (1994).
22. Hallifax, D. & Houston, J.B. Saturable uptake of lipophilic amine drugs into isolated hepatocytes: mechanisms and consequences for quantitative clearance prediction. *Drug Metab. Dispos.* **35**, 1325–32 (2007).
 23. Claassen, V. Review of the animal pharmacology and pharmacokinetics of fluvoxamine. *Br. J. Clin. Pharmacol.* **15**, 349S–355S (1983).
 24. Crews, K.R. *et al.* Clinical Pharmacogenetics Implementation Consortium guidelines for cytochrome P450 2D6 genotype and codeine therapy: 2014 update. *Clin. Pharmacol. Ther.* **95**, 376–82 (2014).
 25. Karjalainen, M.J., Neuvonen, P.J. & Backman, J.T. In vitro inhibition of CYP1A2 by model inhibitors, anti-inflammatory analgesics and female sex steroids: predictability of in vivo interactions. *Basic Clin. Pharmacol. Toxicol.* **103**, 157–65 (2008).
 26. Yao, C. *et al.* Fluvoxamine-theophylline interaction: gap between in vitro and in vivo inhibition constants toward cytochrome P4501A2. *Clin. Pharmacol. Ther.* **70**, 415–24 (2001).
 27. Olesen, O.V. & Linnet, K. Fluvoxamine-Clozapine drug interaction: inhibition in vitro of five cytochrome P450 isoforms involved in clozapine metabolism. *J. Clin. Psychopharmacol.* **20**, 35–42 (2000).
 28. Open Systems Pharmacology Suite Community. Open Systems Pharmacology Suite Manual, Version 7.0.0. (2017).
 29. Schmitt, W. General approach for the calculation of tissue to plasma partition coefficients. *Toxicol. In Vitro* **22**, 457–67 (2008).
 30. Kawai, R. *et al.* Physiologically based pharmacokinetic study on a cyclosporin derivative, SDZ IMM 125. *J. Pharmacokinet. Biopharm.* **22**, 327–365 (1994).
 31. Hospira Inc. Aminophylline - aminophylline injection, solution. (2018).
 32. ratiopharm GmbH. Fachinformation: Theophyllin retard-ratiopharm® 125 mg/- 250 mg/- 375 mg/- 500 mg Retardkapseln. (2014).
 33. Zhang, Z. & Kaminsky, L.S. Characterization of human cytochromes P450 involved in theophylline 8-hydroxylation. *Biochem. Pharmacol.* **50**, 205–11 (1995).
 34. Karjalainen, M.J., Neuvonen, P.J. & Backman, J.T. Rofecoxib is a potent, metabolism-dependent inhibitor of CYP1A2: implications for in vitro prediction of drug interactions. *Drug Metab. Dispos.* **34**, 2091–6 (2006).
 35. Lu, P. *et al.* Mechanism-based inhibition of human liver microsomal cytochrome P450 1A2 by zileuton, a 5-lipoxygenase inhibitor. *Drug Metab. Dispos.* **31**, 1352–60 (2003).
 36. Macias, W.L. *et al.* Lack of effect of olanzapine on the pharmacokinetics of a single aminophylline dose in healthy men. *Pharmacotherapy* **18**, 1237–48 (1998).
 37. Rovei, V., Chanoine, F. & Strolin Benedetti, M. Pharmacokinetics of theophylline: a dose-range study. *Br. J. Clin. Pharmacol.* **14**, 769–78 (1982).
 38. U.S. Food and Drug Administration. Drug development and drug interactions: table of substrates, inhibitors and inducers. <<https://www.fda.gov/Drugs/DevelopmentApprovalProcess/DevelopmentResources/DrugInteractionsLabeling/ucm093664.htm>> (2017). Accessed 02 October 2018.
 39. Mckinnon, R.S. *et al.* Studies on the mechanisms of action of activated charcoal on theophylline pharmacokinetics. *J. Pharm. Pharmacol.* **39**, 522–5 (1987).
 40. Jonkman, J.H. *et al.* Effects of alpha-interferon on theophylline pharmacokinetics and metabolism. *Br. J. Clin. Pharmacol.* **27**, 795–802 (1989).
 41. Miyazawa, Y. *et al.* Effects of the concomitant administration of tamsulosin (0.8 mg/day) on the pharmacokinetic and safety profile of theophylline (5 mg/kg): A placebo-controlled evaluation. *J. Int. Med. Res.* **30**, 34–43 (2002).

42. Lin, J.H., Chremos, A.N., Chiou, R., Yeh, K.C. & Williams, R. Comparative effect of famotidine and cimetidine on the pharmacokinetics of theophylline in normal volunteers. *Br. J. Clin. Pharmacol.* **24**, 669–72 (1987).
43. Ko, J.W. *et al.* Theophylline pharmacokinetics are not altered by lansoprazole in CYP2C19 poor metabolizers. *Clin. Pharmacol. Ther.* **65**, 606–14 (1999).
44. Schneider, D., Gannon, R., Sweeney, K. & Shore, E. Theophylline and antiparasitic drug interactions. A case report and study of the influence of thiabendazole and mebendazole on theophylline pharmacokinetics in adults. *Chest* **97**, 84–7 (1990).
45. Prince, R.A. *et al.* Effect of quinolone antimicrobials on theophylline pharmacokinetics. *J Clin Pharmacol* **29**, 650–4 (1989).
46. Nix, D.E., Norman, A. & Schentag, J.J. Effect of lomefloxacin on theophylline pharmacokinetics. *Antimicrob. Agents Chemother.* **33**, 1006–8 (1989).
47. Cusack, B., Kelly, J.G., Lavan, J., Noel, J. & O'Malley, K. Theophylline kinetics in relation to age: the importance of smoking. *Br. J. Clin. Pharmacol.* **10**, 109–14 (1980).
48. Sörgel, F. *et al.* Effects of 2 quinolone antibacterials, temafloxacin and enoxacin, on theophylline pharmacokinetics. *Clin. Pharmacokinet.* **22 Suppl 1**, 65–74 (1992).
49. Charles, B., Schneider, J., Norris, R. & Ravenscroft, P. Temelastine does not affect theophylline pharmacokinetics in normal subjects. *Br. J. Clin. Pharmacol.* **24**, 673–75 (1987).
50. Jonkman, J.H., VanderBoon, W.J., Schoenmaker, R., Holtkamp, A.H. & Hempenius, J. Lack of influence of co-trimoxazole on theophylline pharmacokinetics. *J. Pharm. Sci.* **74**, 1103–4 (1985).
51. Sips, A.P., Edelbroek, P.M., Kulstad, S., DeWolff, F.A. & Dijkman, J.H. Food does not effect in bioavailability of theophylline from Theolin Retard®. *Eur. J. Clin. Pharmacol.* **26**, 405–7 (1984).
52. Oosterhuis, B., Jonkman, J.H., Andersson, T. & Zuiderwijk, P.B. No influence of single intravenous doses of omeprazole on theophylline elimination kinetics. *J. Clin. Pharmacol.* **32**, 470–5 (1992).
53. Jonkman, J.H., VanderBoon, W.J., Balant, L.P., Schoenmaker, R. & Holtkamp, A. Chronopharmacokinetics of theophylline after sustained release and intravenous administration to adults. *Eur. J. Clin. Pharmacol.* **26**, 215–22 (1984).
54. Tornatore, K.M. *et al.* Effect of chronic oral contraceptive steroids on theophylline disposition. *Eur. J. Clin. Pharmacol.* **23**, 129–34 (1982).
55. Batty, K.T., Davis, T.M., Ilett, K.F., Dusci, L.J. & Langton, S.R. The effect of ciprofloxacin on theophylline pharmacokinetics in healthy subjects. *Br. J. Clin. Pharmacol.* **39**, 305–11 (1995).
56. Colli, A. *et al.* Ticlopidine-theophylline interaction. *Clin. Pharmacol. Ther.* **41**, 358–62 (1987).
57. Manfredi, R.L. & Vesell, E.S. Inhibition of theophylline metabolism by long-term allopurinol administration. *Clin. Pharmacol. Ther.* **29**, 224–9 (1981).
58. Kwon, J. *et al.* Effect of cimetidine on pharmacokinetics of theophylline in healthy korean volunteers. *Korean J. Clin. Pharm.* **17**, 13–8 (2007).
59. Peng, W.X., Li, H.D. & Zhou, H.H. Effect of daidzein on CYP1A2 activity and pharmacokinetics of theophylline in healthy volunteers. *Eur. J. Clin. Pharmacol.* **59**, 237–41 (2003).
60. Bowles, S.K., Popovski, Z., Rybak, M.J., Beckman, H.B. & Edwards, D.J. Effect of norfloxacin on theophylline pharmacokinetics at steady state. *Antimicrob. Agents Chemother.* **32**, 510–2 (1988).
61. Upton, R.A. *et al.* Intraindividual variability in theophylline pharmacokinetics: statistical verification in 39 of 60 healthy young adults. *J. Pharmacokinet. Biopharm.* **10**, 123–34 (1982).
62. Trembath, P.W. & Boobois, S.W. Pharmacokinetics of a sustained-release theophylline formulation. *Br. J. Clin. Pharmacol.* **9**, 365–9 (1980).
63. Antal, E.J., Kramer, P.A., Mercik, S.A., Chapron, D.J. & Lawson, I.R. Theophylline pharmacokinetics in advanced age. *Br. J. Clin. Pharmacol.* **12**, 637–45 (1981).

64. Fourtillan, J.B. *et al.* Pharmacokinetics of ofloxacin and theophylline alone and in combination. *Infection* **14 Suppl 1**, S67-9 (1986).
65. Meyer, M.C. *et al.* Bioequivalence of immediate-release theophylline capsules. *Biopharm. Drug Dispos.* **20**, 417–9 (1999).
66. Brion, N., Naline, E., Beaumont, D., Pays, M. & Advenier, C. Lack of effect of terfenadine on theophylline pharmacokinetics and metabolism in normal subjects. *Br. J. Clin. Pharmacol.* **27**, 391–5 (1989).
67. Jonkman, J., VanderBoon, W., Balant, L. & Cotonnec, Jyl. Food reduces the rate but not the extent of the absorption of theophylline from an aqueous solution. *Eur. J. Clin. Pharmacol.* **28**, 225–27 (1985).
68. Karim, A. Effects of food on the bioavailability of theophylline from controlled-release products in adults. *J. Allergy Clin. Immunol.* **78**, 695–703 (1986).
69. O’Neil, M.J. *et al.* *The Merck Index: An Encyclopedia of Chemicals, Drugs, and Biologicals* 14th edn. (Merck Research Laboratories, Whitehouse Station, NJ, USA, 2006).
70. Simons, K.J., Simons, F.E., Briggs, C.J. & Lo, L. Theophylline protein binding in humans. *J. Pharm. Sci.* **68**, 252–3 (1979).
71. Vallner, J.J., Speir, W.A., Kolbeck, R.C., Harrison, G.N. & Bransome, E.D. Effect of pH on the binding of theophylline to serum proteins. *Am. Rev. Respir. Dis.* **120**, 83–6 (1979).
72. Fleetham, J.A., Bird, C.E., Nakatsu, K., Wigle, R.D. & Munt, P.W. Dose-dependency of theophylline clearance and protein binding. *Thorax* **36**, 382–6 (1981).
73. Buss, D., Leopold, D., Smith, A.P. & Routledge, P.A. Determinants of the plasma protein binding of theophylline in health. *Br. J. Clin. Pharmacol.* **15**, 399–405 (1983).
74. Ha, H.R., Chen, J., Freiburghaus, A.U. & Follath, F. Metabolism of theophylline by cDNA-expressed human cytochromes P-450. *Br. J. Clin. Pharmacol.* **39**, 321–6 (1995).
75. Fukami, T., Nakajima, M., Sakai, H., Katoh, M. & Yokoi, T. CYP2A13 metabolizes the substrates of human CYP1A2, phenacetin, and theophylline. *Drug Metab. Dispos.* **35**, 335–9 (2007).
76. Lelo, A., Birkett, D., Robson, R. & Miners, J. Comparative pharmacokinetics of caffeine and its primary demethylated metabolites paraxanthine, theobromine and theophylline in man. *Br. J. Clin. Pharmacol.* **22**, 177–182 (1986).
77. Birkett, D.J. & Miners, J.O. Caffeine renal clearance and urine caffeine concentrations during steady state dosing. Implications for monitoring caffeine intake during sports events. *Br. J. Clin. Pharmacol.* **31**, 405–8 (1991).
78. Baneyx, G., Parrott, N., Meille, C., Iliadis, A. & Lavé, T. Physiologically based pharmacokinetic modeling of CYP3A4 induction by rifampicin in human: influence of time between substrate and inducer administration. *Eur. J. Pharm. Sci.* **56**, 1–15 (2014).
79. Panchagnula, R., Gulati, I., Varma, M. & Raj, Y.A. Dissolution methodology for evaluation of rifampicin-containing fixed-dose combinations using biopharmaceutic classification system based approach. *Clin. Res. Regul. Aff.* **24**, 61–76 (2007).
80. Agrawal, S. & Panchagnula, R. Implication of biopharmaceutics and pharmacokinetics of rifampicin in variable bioavailability from solid oral dosage forms. *Biopharm. Drug Dispos.* **26**, 321–34 (2005).
81. Boman, G. & Ringberger, V.A. Binding of rifampicin by human plasma proteins. *Eur. J. Clin. Pharmacol.* **7**, 369–73 (1974).
82. Wishart, D.S. *et al.* DrugBank: a comprehensive resource for in silico drug discovery and exploration. *Nucleic Acids Res.* **34**, D668-72 (2006).
83. Templeton, I.E., Houston, J.B. & Galetin, A. Predictive utility of in vitro rifampin induction data generated in fresh and cryopreserved human hepatocytes, Fa2N-4, and HepaRG cells. *Drug Metab. Dispos.* **39**, 1921–9 (2011).
84. Shou, M. *et al.* Modeling, prediction, and in vitro in vivo correlation of CYP3A4 induction. *Drug*

- Metab. Dispos.* **36**, 2355–70 (2008).
85. Loos, U. *et al.* Pharmacokinetics of oral and intravenous rifampicin during chronic administration. *Klin. Wochenschr.* **63**, 1205–11 (1985).
 86. Tirona, R.G., Leake, B.F., Wolkoff, A.W. & Kim, R.B. Human organic anion transporting polypeptide-C (SLC21A6) is a major determinant of rifampin-mediated pregnane X receptor activation. *J. Pharmacol. Exp. Ther.* **304**, 223–8 (2003).
 87. Nakajima, A. *et al.* Human arylacetamide deacetylase is responsible for deacetylation of rifamycins: rifampicin, rifabutin, and rifapentine. *Biochem. Pharmacol.* **82**, 1747–56 (2011).
 88. Collett, A., Tanianis-Hughes, J., Hallifax, D. & Warhurst, G. Predicting P-glycoprotein effects on oral absorption: correlation of transport in Caco-2 with drug pharmacokinetics in wild-type and *mdr1a*(-/-) mice *in vivo*. *Pharm. Res.* **21**, 819–26 (2004).
 89. Greiner, B. *et al.* The role of intestinal P-glycoprotein in the interaction of digoxin and rifampin. *J. Clin. Invest.* **104**, 147–53 (1999).
 90. Chen, Y., Liu, L., Laille, E., Kumar, G. & Surapaneni, S. *In vitro* assessment of cytochrome P450 inhibition and induction potential of azacitidine. *Cancer Chemother. Pharmacol.* **65**, 995–1000 (2010).
 91. Rae, J.M., Johnson, M.D., Lippman, M.E. & Flockhart, D.A. Rifampin is a selective, pleiotropic inducer of drug metabolism genes in human hepatocytes: studies with cDNA and oligonucleotide expression arrays. *J. Pharmacol. Exp. Ther.* **299**, 849–57 (2001).
 92. Reitman, M.L. *et al.* Rifampin's acute inhibitory and chronic inductive drug interactions: experimental and model-based approaches to drug-drug interaction trial design. *Clin. Pharmacol. Ther.* **89**, 234–42 (2011).
 93. Kajosaari, L.I., Laitila, J., Neuvonen, P.J. & Backman, J.T. Metabolism of repaglinide by CYP2C8 and CYP3A4 *in vitro*: effect of fibrates and rifampicin. *Basic Clin. Pharmacol. Toxicol.* **97**, 249–56 (2005).
 94. Kawai, R. *et al.* Physiologically based pharmacokinetic study on a cyclosporin derivative, SDZ IMM 125. *J. Pharmacokinet. Biopharm.* **22**, 327–65 (1994).
 95. Rodgers, T., Leahy, D. & Rowland, M. Physiologically based pharmacokinetic modeling 1: Predicting the tissue distribution of moderate-to strong bases. *J. Pharm. Sci.* **94**, 1259–76 (2005).
 96. Taylor, M.J., Tanna, S. & Sahota, T. *In vivo* study of a polymeric glucose-sensitive insulin delivery system using a rat model. *J. Pharm. Sci.* **99**, 4215–27 (2010).
 97. Walser, A. *et al.* Quinazolines and 1,4-benzodiazepines. 84. Synthesis and reactions of imidazo[1,5-a][1,4]benzodiazepines. *J. Org. Chem.* **43**, 936–44 (1978).
 98. Heikkinen, A.T., Baneyx, G., Caruso, A. & Parrott, N. Application of PBPK modeling to predict human intestinal metabolism of CYP3A substrates - an evaluation and case study using GastroPlus. *Eur. J. Pharm. Sci.* **47**, 375–86 (2012).
 99. Vossen, M. *et al.* Dynamically simulating the interaction of midazolam and the CYP3A4 inhibitor itraconazole using individual coupled whole-body physiologically-based pharmacokinetic (WB-PBPK) models. *Theor. Biol. Med. Model.* **4**, 13 (2007).
 100. Lemaitre, F. *et al.* Propofol, midazolam, vancomycin and cyclosporine therapeutic drug monitoring in extracorporeal membrane oxygenation circuits primed with whole human blood. *Crit. Care* **19**, 40 (2015).
 101. Björkman, S., Wada, D.R., Berling, B.M. & Benoni, G. Prediction of the disposition of midazolam in surgical patients by a physiologically based pharmacokinetic model. *J. Pharm. Sci.* **90**, 1226–41 (2001).
 102. Patki, K.C., Moltke, L.L. Von & Greenblatt, D.J. *In vitro* metabolism of midazolam, triazolam, nifedipine, and testosterone by human liver microsomes and recombinant cytochromes p450: role of *cyp3a4* and *cyp3a5*. *Drug Metab. Dispos.* **31**, 938–44 (2003).

103. Meyer, M., Schneckener, S., Ludewig, B., Kuepfer, L. & Lippert, J. Using expression data for quantification of active processes in physiologically based pharmacokinetic modeling. *Drug Metab. Dispos.* **40**, 892–901 (2012).
104. Nishimura, M. & Naito, S. Tissue-specific mRNA expression profiles of human phase I metabolizing enzymes except for cytochrome P450 and phase II metabolizing enzymes. *Drug Metab. Pharmacokinet.* **21**, 357–74 (2006).
105. Rodrigues, A.D. Integrated cytochrome P450 reaction phenotyping: attempting to bridge the gap between cDNA-expressed cytochromes P450 and native human liver microsomes. *Biochem. Pharmacol.* **57**, 465–80 (1999).
106. PK-Sim® Ontogeny Database Documentation, Version 7.3. (2017).
107. Nishimura, M., Yaguti, H., Yoshitsugu, H., Naito, S. & Satoh, T. Tissue distribution of mRNA expression of human cytochrome P450 isoforms assessed by high-sensitivity real-time reverse transcription PCR. *J. Pharm. Soc. Japan* **123**, 369–75 (2003).
108. Rowland Yeo, K., Walsky, R.L., Jamei, M., Rostami-Hodjegan, A. & Tucker, G.T. Prediction of time-dependent CYP3A4 drug-drug interactions by physiologically based pharmacokinetic modelling: Impact of inactivation parameters and enzyme turnover. *Eur. J. Pharm. Sci.* **43**, 160–73 (2011).
109. Greenblatt, D.J. *et al.* Time course of recovery of cytochrome P450 3A function after single doses of grapefruit juice. *Clin. Pharmacol. Ther.* **74**, 121–29 (2003).
110. Prasad, B. *et al.* Interindividual variability in hepatic organic anion - transporting polypeptides and P-glycoprotein (ABCB1) protein expression: quantification by liquid chromatography tandem mass spectroscopy and influence of genotype, age, and sex. *Drug Metab. Dispos.* **42**, 78–88 (2014).
111. Nishimura, M. & Naito, S. Tissue-specific mRNA expression profiles of human ATP-binding cassette and solute carrier transporter superfamilies. *Drug Metab. Pharmacokinet.* **20**, 452–77 (2005).
112. European Medicines Agency. Guideline on the investigation of drug interactions. (2015).
113. European Medicines Agency. Draft guideline on the qualification and reporting of physiologically based pharmacokinetic (PBPK) modelling and simulation. (2016).
114. U.S. Food and Drug Administration. Physiologically Based Pharmacokinetic Analyses - Format and Content. Guidance for Industry. (2018).
115. Shimada, T., Yamazaki, H., Mimura, M., Inui, Y. & Guengerich, F.P. Interindividual Variations in Human Liver Cytochrome-P-450 Enzymes Involved in the Oxidation of Drugs, Carcinogens and Toxic-Chemicals - Studies With Liver-Microsomes of 30 Japanese and 30 Caucasians. *J. Pharmacol. Exp. Ther.* **270**, 414–23 (1994).
116. Sachse, C., Brockmüller, J., Bauer, S. & Roots, I. Functional significance of a C→A polymorphism in intron 1 of the cytochrome P450 CYP1A2 gene tested with caffeine. *Br. J. Clin. Pharmacol.* **47**, 445–9 (1999).
117. Nakajima, M. *et al.* Genetic polymorphism in the 5'-flanking region of human CYP1A2 gene: effect on the CYP1A2 inducibility in humans. *J. Biochem.* **125**, 803–8 (1999).
118. Nordmark, A., Lundgren, S., Ask, B., Granath, F. & Rane, A. The effect of the CYP1A2 *1F mutation on CYP1A2 inducibility in pregnant women. *Br. J. Clin. Pharmacol.* **54**, 504–10 (2002).
119. Takata, K. *et al.* Phenotype-genotype analysis of CYP1A2 in Japanese patients receiving oral theophylline therapy. *Eur. J. Clin. Pharmacol.* **62**, 23–8 (2006).
120. Kalow, W. & Tang, B. The use of caffeine for enzyme assays: A critical appraisal. *Clin. Pharmacol. Ther.* **53**, 503–14 (1993).
121. Ozdemir, V. *et al.* Evaluation of the genetic component of variability in CYP3A4 activity: a repeated drug administration method. *Pharmacogenetics* **10**, 373–88 (2000).

122. Watkins, P.B. Noninvasive tests of CYP3A enzymes. *Pharmacogenetics* **4**, 171–84 (1994).
123. Rasmussen, B.B., Jeppesen, U., Gaist, D. & Brøsen, K. Griseofulvin and fluvoxamine interactions with the metabolism of theophylline. *Ther. Drug Monit.* **19**, 56–62 (1997).
124. Orlando, R. *et al.* Liver dysfunction markedly decreases the inhibition of cytochrome P450 1A2-mediated theophylline metabolism by fluvoxamine. *Clin. Pharmacol. Ther.* **79**, 489–99 (2006).
125. Guest, E.J., Aarons, L., Houston, J.B., Rostami-Hodjegan, A. & Galetin, A. Critique of the two-fold measure of prediction success for ratios: application for the assessment of drug-drug interactions. *Drug Metab. Dispos.* **39**, 170–3 (2011).
126. Boyce, E.G. The effect of rifampin on theophylline pharmacokinetic parameters (following intravenous aminophylline) in normal volunteers. (1984).
127. Powell-Jackson, P.R., Jamieson, A.P., Gray, B.J., Moxham, J. & Williams, R. Effect of rifampicin administration on theophylline pharmacokinetics in humans. *Am. Rev. Respir. Dis.* **131**, 939–40 (1985).
128. Thelen, K., Coboeken, K., Willmann, S., Dressman, J.B. & Lippert, J. Evolution of a detailed physiological model to simulate the gastrointestinal transit and absorption process in humans, part II: extension to describe performance of solid dosage forms. *J. Pharm. Sci.* **101**, 1267–80 (2012).
129. Jeppesen, U., Loft, S., Poulsen, H.E. & Brøsen, K. A fluvoxamine-caffeine interaction study. *Pharmacogenetics* **6**, 213–22 (1996).
130. Culm-Merdek, K.E., Moltke, L.L. von, Harmatz, J.S. & Greenblatt, D.J. Fluvoxamine impairs single-dose caffeine clearance without altering caffeine pharmacodynamics. *Br. J. Clin. Pharmacol.* **60**, 486–93 (2005).
131. Lam, Y.W.F., Alfaro, C.L., Ereshefsky, L. & Miller, M. Pharmacokinetic and pharmacodynamic interactions of oral midazolam with ketoconazole, fluoxetine, fluvoxamine, and nefazodone. *J. Clin. Pharmacol.* **43**, 1274–82 (2003).